

**Enhanced analysis of stratified climate archives through
upgrade of Laser Ablation Inductively Coupled Plasma
Quadrupole to Time of Flight Mass Spectrometry?**

Dissertation zur Erlangung des Grades

Dr. rer. nat.

vorgelegt dem

Fachbereich Geowissenschaften (FB5)

der Universität Bremen

vorgelegt von

Dorothee Wilhelms-Dick

Bremen, Mai 2008

Gutachter

Prof. Dr. H. Miller

PD Dr. S. Kasten

Prüfer

Prof. Dr. W. Bach

Dr. M. Kriews

Promotionslolloquium

Am 24.07.2008

Preface

This work is submitted as a dissertation, instructed by Dr. Michael Kriews and supervisor Prof. Dr. Heinrich Miller.

The cumulative thesis includes five manuscripts (2 published, 1 in press, 1 submitted and 1 in preparation for submission) to which a general introduction is prefixed in Chapter 1. There, the thesis is linked to the overarching scientific background, a general overview of related analytical methods in the Geosciences is given, which concludes with a focus on inorganic mass-spectrometric methods, particularly on time of flight-mass spectrometers (TOF-MS). The thesis's objectives are summarized in Chapter 1.1. In Chapter 2, a short summary of my own contributions is given for each of the five manuscripts. Chapter 3 describes the recently developed inductively coupled plasma (ICP)-TOF-MS, which I assessed within this study for the analysis of frozen and liquid ice core samples. In Chapter 4 and 5 performance studies of the ICP-TOF-MS system are presented and discussed. Conclusions and scientific perspectives follow in Chapter 6. Chapter 7 compiles the references for Chapters 1–6. I lead-author the Publications I, III and IV on the application of the analytical method developed by Reinhardt (2002) to different sample matrices. Finally, in future our studies aim for improved matching of different ice cores and climatic archives, which refines on the basis for studies on couplings in the global climate system, as *e.g.* undertaken in Publication II. Three different mass spectrometer systems, including the ICP-TOF-MS system, are compared in Publication V with respect to the analysis of low concentrated rare earth elements (REE) in Antarctic ice core samples. References in the manuscripts are respectively included.

Contents

Preface	i
Tables	iv
Figures	vi
Abbreviations	ix
Summary	1
Zusammenfassung	4
1 Introduction	7
1.1 Objectives.....	12
2 List of Publication submitted for the thesis	13
3 Materials, Instrumentations and Methods	15
3.1 Inductively Coupled Plasma Mass Spectrometry.....	15
3.1.1 ICP-TOF-MS.....	16
3.1.2 Inductively Coupled Plasma.....	17
3.1.3 Interface.....	20
3.1.4 Ion optic.....	20
3.1.5 Ion repeller and mass analyzer.....	21
3.1.6 Detection system.....	23
3.1.7 Interferences.....	24
3.1.8 Sample introduction systems for liquid samples.....	26
3.2 Laser ablation as sample introduction system for solid samples.....	28
3.2.1 Absorption characteristics of ice.....	29
3.3 Calibration standards.....	30
3.3.1 Multi-element solutions for calibration standards.....	30
3.3.2 Preparation of multi-element calibration standards.....	31
3.3.3 Particulate matter for calibration standards with embedded particles.....	32
3.3.4 Improvement of the preparation of calibration standards with embedded particles.....	33
4 Performance study of the ICP-TOF-MS system for the analysis of liquid samples	37
4.1 Comparison of different sample introduction systems.....	37
4.2 Parameter study: Aridus II-ICP-TOF-MS.....	40
4.2.1 ICP parameter.....	41
4.2.2 Aridus II parameter.....	43
4.2.3 Day to day signal variations.....	43
4.3 Interference studies.....	44
4.4 Instrumental detection limits, spectral resolution and the dynamic range of the ICP-TOF-MS system.....	44
4.5 Analysis of reference materials.....	47

5	Performance study of the LA-ICP-TOF-MS system for the analysis of solid samples	49
5.1	Parameter study: LA-ICP-TOF-MS	50
5.1.1	Plasma jittering during the LA process	52
5.2	Parameter study: LA-Aridus II-ICP-TOF-MS	52
5.2.1	ICP parameter	53
5.2.2	Aridus II parameter	53
5.3	Influence of helium as transport gas	56
5.4	Internal standardisation for ice core analysis	57
5.5	Reasons for low ICP-TOF-MS signals	59
5.5.1	Duty cycle	59
5.5.2	Components of the ion optics	59
5.5.3	Radio-frequency generator	60
5.5.4	Shielding of the plasma	61
5.5.5	Polymers close to the plasma torch	62
5.5.6	Pulsed aerosol introduction	63
5.5.7	Laser shot frequency	63
5.5.8	Size of the sample chamber	64
6	Conclusions and Outlook	65
7	References	68
	Publications	
	Publication I	79
	Publication II	103
	Publication III	109
	Publication IV	119
	Publication V	129
	Acknowledgement	151
	Appendix	153
A1	Utility Model	153
A2	Publication Bunsen Magazin	163
A3	Element concentrations along EDML meter 270	171
A4	Element concentrations of subsections of EDML meter 270 obtained by LA-ICP-Q-MS and ICP-Q-MS analysis of acidified and digested samples	175
A5	Relative element intensities in bivalves obtained by LA-ICP-Q-MS analysis	176
A6	Program (IDL®) for the evaluation of ICP-TOF-MS data	177
A7	Concentration data of reference materials analysed by Aridus II-ICP-TOF-MS	182
A8	Concentration data of Intercomparison samples analysed by Aridus II-ICP-TOF-MS	184

Tables

Table 1:	Preparation of calibration standards for Quadrupole (Q) and Time of Flight (TOF) ICP-MS systems using solutions A-C and F –H (see text, chapter 3.3.1).	32
Table 2:	Preparation of calibration ice standards with defined amounts of particulate matter (standard reference material NIST 1648) for laser ablation ICP-MS analysis. Moreover, the concentration of each certified and noncertified (grey shaded) element in each standard is calculated.	33
Table 3:	LA-ICP-Q-MS calibration data of ice standards with embedded particles (standard reference material NIST 1648). The number of standards used for calibration (inclusive blank), the lowest and highest concentrated standard defining the linear calibration range, the associated RSD of replicate analysis (n=40), the correlation coefficient and the detection limit (DL) are given.....	36
Table 4:	Instrumental settings for the ICP-TOF-MS system coupled to three different nebulizer systems: Cross flow nebulizer (CFN), concentric nebulizer with cyclonic spray chamber and microconcentric nebulizer with desolvation unit (Aridus II).	37
Table 5:	Signal intensities in cps ($\mu\text{g L}^{-1}$) ⁻¹ with RSD (10 replicates), background signals (Bkgd) for m/z ratios 8 and 220 and the degree of M ²⁺ and MO ⁺ formation in % of a 1 $\mu\text{g L}^{-1}$ DP standard analysed by ICP-TOF-MS using different nebulization systems (CFN, concentric nebulizer with cyclonic spray chamber, Aridus II (microconcentric nebulizer with desolvation unit)).	40
Table 6:	Lowest and highest concentrated calibration standard defining the linear calibration range for each analysed isotope. Further the table shows the IDL in ng L ⁻¹ , signal intensities for a 1 $\mu\text{g L}^{-1}$ standard and the calculated spectral resolution using the Aridus II as sample introduction system for the ICP-TOF-MS system.....	46
Table 7:	Signal intensities in cps ($\mu\text{g L}^{-1}$) ⁻¹ with RSD (10 replicates), background signals (Bkgd) for m/z ratios 8 and 220 and the degree of MO ⁺ and M ²⁺ formation in % obtained by Aridus II-ICP-TOF-MS and Aridus II-ICP-Q-MS analysis of a liquid 1 $\mu\text{g L}^{-1}$ DP standard.	49
Table 8:	Calibration data in cps of ²³ Na, ²⁴ Mg, ²⁷ Al, ⁵⁷ Fe, ⁵⁹ Co, ¹³⁸ Ba, ¹⁴⁰ Ce and ²⁰⁸ Pb for a Blank (0), 1-, 10- and 100 $\mu\text{g kg}^{-1}$ multi-element standard obtained by LA-ICP-TOF-MS analysis. The slope and correlation coefficient (r ²) were calculated for each isotope.....	52

Table 9:	Signal intensities in cps ($\mu\text{g kg}^{-1}$) ⁻¹ with RSD (10 replicates), background signals (Bkgd) for m/z ratios 8 and 220 and the degree of MO ⁺ and M ²⁺ formation in % of a frozen 10 $\mu\text{g kg}^{-1}$ DP ice standard obtained by LA-ICP-TOF-MS, LA-Aridus II-ICP-TOF-MS and LA-ICP-Q-MS analysis.....	55
Table 10:	Calibration data in cps of ²³ Na, ²⁴ Mg, ²⁷ Al, ⁵⁷ Fe, ⁵⁹ Co, ¹³⁸ Ba, ¹⁴⁰ Ce and ²⁰⁸ Pb for a Blank (0), 1-, 10- and 100 $\mu\text{g kg}^{-1}$ multi-element ice standard obtained by LA-Aridus II-ICP-TOF-MS analysis. The slope and correlation coefficient (r^2) were calculated for each isotope.	55
Table 11:	Signal intensities in cps ($\mu\text{g kg}^{-1}$) ⁻¹ with RSD (10 replicates), background signals (Bkgd) for m/z ratios 8 and 220 and the degree of MO ⁺ and M ²⁺ formation in % of a frozen 10 $\mu\text{g kg}^{-1}$ DP ice standard obtained by LA-Aridus II-ICP-TOF-MS analysis. Mixing of Ar and He as transport gas according to Figure 23.	57

Figures

Figure 1: Climate archives analysed for the reconstruction of past climate. a) Polar ice core with particle horizons; b) bivalve <i>Laternula elliptica</i> ; c) laminated lake sediment core.	8
Figure 2: General instrumental setup of mass spectrometer systems with an inductively coupled plasma for ion generation.....	15
Figure 3: Experimental setup of the ICP-TOF-MS system developed at the Institute for Analytical Science, supported as a research prototype jointly with Analytik Jena. Principle components are the plasma torch, interface (green), ion optics (blue), ion repeller (yellow), mass analyzer (white) and the detector.....	17
Figure 4: Plasma torch with shield plate, coil and Rf-generator used for plasma generation for the TOF-MS system.	17
Figure 5: The inductively coupled plasma according to Fassel (1978). The sample is ionised within the argon plasma at temperatures of about 10000 K.	19
Figure 6: The Interface of the TOF-MS system used in this study. Pressure differences lead to acceleration of ions from the right to the left side.	20
Figure 7: Ion optics of the ICP-TOF-MS system to diverge incoming ions.	21
Figure 8: Ion repeller and mass analyzer of the TOF-MS system. Incoming ions are redirected by 90° (→ orthogonal acceleration) into the mass analyzer by applying a positive voltage pulse to the repeller plate.	22
Figure 9: Schematic view of isotope separation in ICP-TOF-MS measurements. The flight time of an ion depends on its m/z ratio. Velocity differences of isotopes with one m/z ratio are corrected by redirection of ions at the reflector mirror by 180° (= velocity focusing).	23
Figure 10: Part of an ICP-TOF-MS mass spectrum, to demonstrate the calculation of the resolution of two neighboured isotopes (¹³⁹ La and ¹⁴⁰ Ce).	24
Figure 11: Absorption coefficient of ice for different wavelengths (Warren, 1984). At 1064 nm wavelength the absorption coefficient of ice is two orders of magnitude higher than for 266 nm wavelength.....	29
Figure 12: Schematic of the preparation of calibration standards for the LA-ICP-MS analysis of frozen ice core samples. Multi-element solutions are stepwise frozen in Petri dishes under a clean bench US Class 100 installed in an ice laboratory.....	32

Figure 13: Preparation of calibration standards with homogeneously distributed embedded particles (reference material NIST 1648). The stepwise freezing procedure enables acceptable homogeneity of the calibration standards.	34
Figure 14: Signal variations of replicate analysis of ^{208}Pb of six different ice standards with embedded NIST 1648 particles obtained by LA-ICP-Q-MS analysis. The homogeneity of standards increases with increasing particle concentration which is presented by decreasing RSD values.....	35
Figure 15: Screenshot of ICP-TOF-MS mass spectra with identification of peaks for a $1\ \mu\text{g L}^{-1}$ DP standard using different sample introduction systems: a) CFN, b) concentric nebulizer with cyclonic spray chamber and c) Aridus II. Oxygen based interferences are visible for nebulizer a and b (e.g. $^{16}\text{O}^+$, $^{40}\text{Ar}^{16}\text{O}^+$), nitrogen based interferences are visible for nebulizer c (e.g. $^{40}\text{Ar}^{14}\text{N}^+$, $^{40}\text{Ar}^{14}\text{N}^1\text{H}^+$). The degree of oxide formation decreased significantly for nebulizer c.	39
Figure 16: Sample consumption with SD (3 replicates) in $\mu\text{L min}^{-1}$ as a function of the nebulizer gas flow of the Aridus II sample introduction system.....	41
Figure 17: Signal variation with SD (20 replicates) in counts per second of a $1\ \mu\text{g L}^{-1}$ DP standard containing ^{24}Mg , ^{103}Rh , ^{138}Ba , ^{140}Ce and ^{208}Pb (left side); and changes in the degree of oxide (MO^+) and doubly charged ion (M^{2+}) formation (right side) due to changes in plasma power, nebulizer-, sweep- and nitrogen gas flow obtained by the Aridus II-ICP-TOF-MS system.	42
Figure 18: Day to day signal variations of a $1\ \mu\text{g L}^{-1}$ DP standard obtained by Aridus II-ICP-TOF-MS analysis within the time slice from the 21.07.2007 till the 26.03.2008.....	43
Figure 19: Recovery rates of reference materials (NIST 1640, SLRS-4, SPS-SW1) obtained by Aridus II-ICP-TOF-MS analysis. Most elements show recovery rates between 95% and 105% (dashed lines).	47
Figure 20: Signal variation with SD (20 replicates) in counts per second of a $10\ \mu\text{g kg}^{-1}$ DP standard containing ^{24}Mg , ^{103}Rh , ^{138}Ba , ^{140}Ce and ^{208}Pb (left side); and changes in the degree of oxide (MO^+) and doubly charged ion (M^{2+}) formation (right side) due to changes in plasma power, nebulizer-, plasma- and auxiliary gas obtained by the LA-ICP-TOF-MS system.	51
Figure 21: Schematic of the microconcentric nebulizer with desolvation unit (Aridus II). Either a liquid sample is introduced into the nebulizer or an aerosol produced by LA of frozen samples (Reproduced by permission of Cetac).....	53

Figure 22: Signal variation with SD (20 replicates) in counts per second of a 10 $\mu\text{g kg}^{-1}$ DP standard containing ^{24}Mg , ^{103}Rh , ^{138}Ba , ^{140}Ce and ^{208}Pb (left side); and changes in degree of oxide (MO^+) and doubly charged ion (M^{2+}) formation (right side) due to changes in plasma power, nebulizer-, sweep- and nitrogen gas obtained by the LA-Aridus II-ICP-TOF-MS system.	54
Figure 23: Experimental setup for the use of a mixture of argon (Ar) and helium (He) as transport gas for the LA of frozen ice core samples.	56
Figure 24: Signal intensities of several m/z ratios obtained by LA-ICP-TOF-MS and LA-Aridus II-ICP-TOF-MS of a 10 $\mu\text{g kg}^{-1}$ DP ice standard to validate possible isotopes for internal standardisation.	58
Figure 25: Schematic view of a free-running tube amplifier used for plasma generation in ICP-Q-MS systems (Dzur, 2002). Impedance changes in the load LC-circuit are compensated by small frequency changes in the generator LC-circuit.....	60
Figure 26: Schematic view of a solid state generator used for plasma generation in the ICP-TOF-MS system. The left LC-circuit of the Generator works at constant frequency. Impedance changes in the LC-circuit of the load are compensated by servo driven capacitors in the Match-Box (Reproduced by permission of Advanced Energy).....	61
Figure 27: Shield plate between the coil and the plasma torch to eliminate the pinch effect.	62
Figure 28: Porous polymer (Teflon) close to the plasma torch leads to energy loss in the plasma and therefore in decreasing signal intensities.....	62
Figure 29: Evolution of the intensity of ^{59}Co signal in Nist 610 referenced glass as a function of the laser shot frequency (Gratuze et al., 2001).	63

Abbreviations

aa-ICP-TOF-MS	axial accelerated ICP-TOF-MS
AAS	atomic absorption spectrometry
A.D.	Anno Domini
AC	alternating current
amu	atomic mass unit
Bkgd	Background
b.p.	before present
cps	counts per second
CFN	cross flow nebulizer
CVAFS	cold vapour atomic fluorescence spectrometry
DC	direct current
DL	detection limit
DML	Dronning Maud Land
DP	daily performance
DRC	dynamic reaction cell
EDC	EPICA Dome C
EDML	EPICA DML
EPICA	European Project for Ice Coring in Antarctica
FIA	flow injection analysis
GRIP	Greenland Ice Core Project
ICP-MS	inductively coupled plasma-mass spectrometry
ICP-Q-MS	ICP-Quadrupole-MS
ICP-SF-MS	ICP-Sector Field-MS
ICP-TOF-MS	ICP-Time Of Flight-MS
IDMS	isotope dilution mass spectrometry
INAA	instrumental neutron activation analysis
IDL	instrumental detection limit
IPCC	Intergovernmental Panel on Climate Change
IR	infra red
LA	laser ablation
L.elliptica	Laternula elliptica
M ²⁺	doubly charged ion of element M
MO ⁺	oxide ion of element M
MSA	Methansulfonate
m/z	mass (m) to charge (z) ratio
Nd:YAG	Neodym -Yttrium Aluminium Garnet
oa-ICP-TOF-MS	orthogonal accelerated ICP-TOF-MS
PEEK	Polyetheretherketone

PFA	Polyfluoralkoxy
PIXE	proton induced x-ray emission analysis
ppm	parts per million ($\hat{=}$ mg kg ⁻¹)
ppb	parts per billion ($\hat{=}$ μ g kg ⁻¹)
ppt	parts per trillion ($\hat{=}$ ng kg ⁻¹)
PTFE	Polytetrafluorethylene
RF	radio-frequency
RSD	relative standard deviation
REE	rare earth element
SD	standard deviation
SRM	standard reference material
UV	ultra violet
XRF	X-ray fluorescence

Summary

The analysis of inorganic components of climatic archives provides proxies for climate reconstruction. For many applications commercially available inductively coupled plasma mass spectrometry (ICP-MS) systems, such as ICP-Quadrupole-MS (ICP-Q-MS) or ICP-Sector Field-MS (ICP-SF-MS) systems, are used. One aim of this thesis was to test the laser ablation (LA)-ICP-Q-MS method, as developed by Reinhardt (2002), in respect of its transferability for the analysis of different sample matrices, as well as the adaption of the LA unit to an ICP-Time of Flight-MS (ICP-TOF-MS) system.

An ice core section from the Holocene, drilled in the Atlantic sector of Antarctica, was analysed by LA-ICP-Q-MS in high spatial resolution of about 4 mm (Publication I). Only element concentrations of Na, Mg, Al, K, Mn, Fe, Co, Ni, Zn, Sr, Cd, Ba, La, Ce, Pb and Bi are above the detection limit (DL). All other trace element concentrations in this study exceeded only sporadically the DL. The analysis of sea salt tracers, mineral dust tracers and tracers for other natural or anthropogenic sources revealed in general enhanced element concentrations during winter months. Verification of LA-ICP-Q-MS analysis by ICP-Q-MS analysis of acidified and digested samples as well as by continuous flow analysis (CFA) showed that LA-ICP-Q-MS analysis was better suited to analyse particles embedded in the ice matrix compared to ICP-Q-MS analysis of acidified samples and to CFA. Element concentrations of snow pit samples in the vicinity of the coring site differed by a factor of 1 to 3 compared to our results of the ice core, except Pb which showed 13 times lower concentrations. Compared to deep ice core samples from the Indian sector of Antarctica, our results from the Atlantic sector showed by a factor 1 to 3 decreased concentrations of sea salt components, by a factor 6 to 8 increased concentrations of mineral dust components and by a factor 10 to 40 higher concentrations for other elements.

During the past 10 years, the enhanced input of sediments due to accelerated glacier melting is observed in Potter cove at the Antarctic Peninsula. The analysis of the Antarctic soft shell clam *Laternula elliptica* (Potter Cove, Antarctic Peninsula) by LA-ICP-Q-MS addressed whether the increased sediment input is reflected in the distribution of Fe, and other elements (Al, Mn, Cu, Pb and U) in the ultimate growth bands, which are formed in bivalve umbos (Publication III). In contrast to our hypothesis, element concentrations were highest in the early growth bands formed in the young bivalves and levelled off during the first 6–8 years of bivalve age. After the initial 6–8 years the signal intensities within the growth bands amounted 7.5% for Al, Fe and U, 12% for Mn and Cu, and 18.5% for Pb, compared to the first growth band. Within this period, where the elemental composition does not change significantly, the element ratios Fe/Mn (26.8), Fe/Cu (3.8), Al/Mn (2.8) and Al/Cu (0.4) do neither

resemble the ratios in the surrounding water nor the sediment material in Potter Cove nor the earth crust basal composition.

A frozen lake sediment core from Sacrower See (Potsdam Germany), investigated within this study by LA-ICP-Q-MS, showed annual lamination until a depth of 42.7 cm (Publication IV). This study targeted to settle the question whether the lamination results in varying elemental signature that corresponds to summer and winter layers, with respectively high and low biological activity. The enrichment or depletion of a certain element in a sample relative to the average composition of the Earth's crust is expressed as the enrichment factor (EF). From the increased EF of Ca and Sr in the summer layers, we conclude an increased biological activity. On average, the EF for Ca amounted 81 (minimum: 19; maximum: 677) and the EF for Sr amounted 17 (minimum: 4; maximum: 98). Along the entire sediment core (90 cm), the Pb signature was analysed to detect anthropogenically induced signal variations. Variations in the non-mineral Pb signature for the last 320 years might be assigned to the little ice age, the industrialisation and from the beginning of the 1980's to the reduction of Pb in gasoline.

Often the available sample volume is restricted, which results in a small number of analysed isotopes, due to the sequential mode of the used ICP-Q-MS system. Moreover, the evaluation of results for samples with low element concentrations is problematic and one may face statistical problems. One can infer statistical problems from high relative standard deviations (RSD) of replicate analysis. For example, the analysis of ice core samples exhibited RSD of 20% to 50% for higher concentrated elements (Na, Mg, Al and Fe) compared to 3% to 6% for frozen calibration standards, and RSD between 30% to 70% for low concentrated elements (Mn, Co, Sr, Ba, Ce, Pb, Bi) compared to 4% to 12% in the respective standards. Therefore, inhomogeneities of the samples explain the largest part to the RSD.

The analysis of natural, inhomogeneous samples by LA results in fast changing aerosol composition. The changing aerosol composition as well as the pulsed introduction of ablated sample material by the LA method results in transient signals which are hard to detect with scanning ICP-MS systems.

ICP-TOF-MS systems enable simultaneous analysis of the entire mass spectrum. The applicability of the newly developed ICP-TOF system for ice core analysis in climatic research was explored. After the setup of the instrument, I first studied its accuracy, precision and performance with liquid samples to minimize possible sources of error and to acquaint myself with the new ICP-TOF-MS system. I tested three different sample introduction systems for the analysis of liquid samples by ICP-TOF-MS: A cross flow nebulizer (CFN), concentric nebulizer with cyclonic spray chamber and a microconcentric nebulizer with desolvation unit (Aridus II, Cetac Technologies, Omaha, Nebraska). The analytical performance is defined by the sensitivity, the oxide and doubly charged ion rate, the instrumental detection limits (IDL), the RSDs, the

background noise and the accuracy and the precision. The Aridus II as sample introduction system provided the best results. Compared to an ICP-Q-MS (Elan6000, Perkin/Elmer Sciex) system, the signal intensity was lower by a factor of 2 to 10. The oxide rate amounted to 0.3%, the doubly charged ion rate amounted to 12.7%. Additional low background signals (20 counts per second (cps)) as well as low IDL (0.4 ng L^{-1} to 10 ng L^{-1} for elements exceeding 58 atomic mass units (amu)) enabled the analysis of low concentrated samples. Problems for elements between 23 amu and 72 amu can be explained by complex spectral interferences, mainly based on argon and nitrogen species, and selector impulses to redirect ions to protect the detection system from high ion load. The analysis of reference materials demonstrated that most of the analysed concentrations deviated less than 5% from the certified value with a RSD of 1.5%. Rare earth elements (REE) were of special interest within this study and had a recovery rate of 103% for the reference material SPS-SW1. Due to concentrations in the low ng L^{-1} range, the RSD amounted to 3.4%. The performance of the ICP-TOF-MS system with the Aridus II as sample introduction system enabled the analysis of molten natural ice core samples. The obtained data are in good agreement with ICP-Q-MS and ICP-SF-MS results (Publication V). The ICP-TOF-MS system is able to analyse accurately and precisely REE concentrations exceeding 5 ng L^{-1} and element dependent accuracy and precision between 0.5 and 5 ng L^{-1} .

Based on the experiences with liquid samples, similar experiments were run with the LA unit for the analysis of frozen ice core samples to test whether the new LA-ICP-TOF-MS system conquers the above listed remaining limitations of LA-ICP-Q-MS system. Performance studies showed that replacing argon by a mixture of argon and helium as carrier gas in the sample chamber increased the signal intensity by a factor of 3 to 5. Nevertheless, signal intensities obtained by LA-ICP-TOF-MS were by a factor of 50 to 130 lower compared to LA-ICP-Q-MS analysis. The oxide rate amounted to 17% and the doubly charged ion rate amounted to 31%. Moreover, pressure waves released during the laser ablation process of ice lead to plasma instabilities and often the plasma extinguished after a short time. Additional high background signals (100 cps) do not permit the analysis of low concentrated natural ice core samples at present. Reasons for the distinct signal decrease are the configuration of the generator system, the introduction of pulsed ion packets into the mass analyzer and the use of polymers close to the plasma torch.

Zusammenfassung

Durch die Bestimmung der anorganischen Zusammensetzung von Klimaarchiven erhält man Proxies, die zur Klimarekonstruktion benötigt werden. Häufig werden dazu induktiv gekoppelte Plasma Massenspektrometer (ICP-MS) verwendet, z.B. ICP-Quadrupol-MS (ICP-Q-MS) oder ICP-Sektorfeld-MS (ICP-SF-MS) Systeme. Ein Ziel dieser Arbeit war es, die von Reinhardt (2002) entwickelte Laserablations (LA)-ICP-Q-MS Methode bzgl. der Übertragbarkeit auf verschiedene Probenmaterialien, und eine mögliche Weiterentwicklung dieser Methode durch Kopplung der LA Einheit an ein Flugzeitmassenspektrometer (TOF-MS) zu überprüfen.

Ein Eisbohrkernsegment aus dem Holozän, gebohrt im atlantischen Sektor der Antarktis, wurde mit einer räumlichen Auflösung von 4 mm mittels LA-ICP-Q-MS analysiert (Publikation I). Nur für die Elemente Na, Mg, Al, K, Mn, Fe, Co, Ni, Zn, Sr, Cd, Ba, La, Ce, Pb und Bi wurden Konzentrationen oberhalb der Nachweisgrenze (NWG) erhalten. Alle anderen untersuchten Elemente zeigten nur sporadisch Konzentrationen oberhalb der NWG. Bei der Analyse von Seesalztracern, Mineralstaubtracern und Elementen, die anderen Quellen zugeordnet werden, zeigten fast alle Elemente Konzentrationsmaxima in den Wintermonaten. Ein Vergleich der LA-ICP-Q-MS Methode mit bei Eisbohrkernuntersuchungen gängigen Methoden zeigte, dass für die Untersuchung von im Eis eingeschlossenen Partikeln die LA-ICP-Q-MS Methode besser geeignet ist im Vergleich zur Analyse von angesäuerten flüssigen Proben mittels ICP-Q-MS sowie im Vergleich zur Fluoreszenz Analyse nach kontinuierlichem Schmelzen des Kerns. Elementkonzentrationen in einem Schneeschacht, der in der Nähe des Eisbohrkerns ausgehoben wurde, wichen um den Faktor 1 bis 3 von den analysierten Eisbohrkernkonzentrationen ab. Ausnahme stellte das Pb dar, das im Schneeschacht um den Faktor 13 niedrigere Konzentrationen aufwies. Eisbohrkerne aus dem indischen Sektor der Antarktis mit ähnlichem Alter zeigten um den Faktor 1 bis 3 höhere Konzentrationen für Seesalztracer, um den Faktor 6 bis 8 niedrigere Konzentrationen für Mineralstaubtracer und um den Faktor 10 bis 40 niedrigere Konzentrationen für die restlichen Elemente.

Das zweite Klimaarchiv, das im Rahmen dieser Arbeit untersucht wurde, stellen Muscheln aus der Potter Bucht (Antarktische Halbinsel) dar (Publication III). Hier sollte herausgefunden werden, ob sich das in der Bucht verstärkt eingetragene mineralische Material durch intensivere Gletscherschmelze während der letzten 10 Jahre in den Wachstumsbändern der Muscheln wiederfinden lässt. Dazu wurden die Elemente Fe, Al, Mn, Cu, Pb and U analysiert. Im Gegensatz zu der aufgestellten Hypothese zeigte sich, dass die Elementkonzentrationen innerhalb der ersten 6 bis 8 Jahre auf 7.5% für Al, Fe und U, auf 12% für Mn und Cu und auf 18.5% für Pb, bezogen auf das erste Lebensjahr, abfallen. Nach den ersten 6 bis 8 Lebensjahren ändern sich die Elementkonzentrationen in den Wachstumsbändern der Muscheln kaum noch. In

diesem zweiten Lebensabschnitt ähneln die Elementkonzentrationen Fe/Mn (26.8), Fe/Cu (3.8), Al/Mn (2.8) und Al/Cu (0.4) weder den Elementverhältnissen des umgebenden Wassers noch dem Sediment aus der Bucht und ebenfalls nicht den Elementverhältnissen der oberen Erdkruste.

Das dritte mittels LA-ICP-Q-MS analysierte Klimaarchiv war ein gefrorener Sedimentbohrkern aus dem Sacrower See (Potsdam, Deutschland) (Publikation IV). Dieser war 90 cm lang und zeigte eine stratigraphische Schichtung in den oberen 42.7 cm. Es sollte überprüft werden, ob mit der angewandten Methode diese Schichtung rekonstruiert werden kann. Es war bekannt, dass während der Sommermonate verstärkt biologisches Material in Form von Karbonaten im See sedimentiert. Die An- bzw. Abreicherung von Elementen bzgl. der Zusammensetzung der Erdkruste wird über den Anreicherungsfaktor (AF) ausgedrückt. Untersuchungen zeigten AF Maxima für Ca und Sr während der Sommermonate. Das bedeutet, dass sich die Quelle für diese Elemente in den Sommermonaten geändert hat. Im Durchschnitt betrug der AF für Ca 81 (Minimum: 18; Maximum: 677), für Sr im Durchschnitt 17 (Minimum: 4; Maximum: 98). Entlang des 90 cm langen Sedimentbohrkerns konnten Pb Signaturen der letzten 320 Jahre der kleinen Eiszeit, der Industrialisierung und schließlich der Reduktion von Pb im Benzin zu Beginn der 80er Jahre (20. Jahrhundert) zugeordnet werden. Zuvor wurde der mineralische Anteil aus den Pb Signaturen herausgerechnet.

Oftmals ist die verfügbare Probenmenge zur Bestimmung der anorganischen Zusammensetzung sehr klein, was zu einer niedrigen Anzahl von analysierten Isotopen führt, wenn man mit sequentiell messenden Massenspektrometern arbeitet wie z.B. dem ICP-Q-MS System. Hierbei werden die Elemente nacheinander untersucht. Des Weiteren können bei der Auswertung der Proben mit niedrigen Konzentrationen statistische Probleme auftreten, die anhand der relativen Standardabweichung (RSD) abgeleitet werden können. Die Analyse von Eisbohrkernen zeigte beispielsweise RSD zwischen 20% und 50% für höher konzentrierte Elemente (Na, Mg, Al, Fe), RSD zwischen 30% bis 70% für niedrig konzentrierte Elemente (Mn, Co, Sr, Ba, Ce, Pb, Bi). Die Analyse von gefrorenen Standards mit definierten Konzentrationen zeigte RSD zwischen 3% bis 6% für höher konzentrierte Elemente, zwischen 4% bis 12% für niedrig konzentrierte Elemente. Daran lässt sich ablesen, dass ein Großteil der RSD durch die Inhomogenität der Probe erklärt werden kann.

Durch den gepulsten Eintrag von Probenmaterial während des Ablationsprozesses und zusätzlich durch die Untersuchung von inhomogenen Proben entstehen transiente Signale, die mit sequentiell messenden ICP-MS Systemen nur schwer zu erfassen sind.

Durch die Einführung von TOF-MS Systemen kann das gesamte Elementspektrum simultan erfasst werden. Die Praxistauglichkeit eines neu entwickelten ICP-TOF-MS Systems zur Untersuchung von geschmolzenen und gefrorenen Eisbohrkernen wurde im Rahmen dieser Arbeit überprüft. Nach der Installation dieses Systems im Labor wurden Genauigkeit und Richtigkeit der Analysen bestimmt. Dazu wurden zunächst flüssige

Standards verwendet, um die Anzahl der möglichen Fehlerquellen niedrig zu halten. Das Testen drei verschiedener Probeneinführungssysteme (Cross Flow Zerstäuber, Konzentrischer Zerstäuber mit Cyclonsprühkammer, Mikrokonzentrischer Zerstäuber mit einer Membran zur Trocknung der Probe (Aridus II, Cetac Technologies, Omaha, Nebraska)) ergab, dass nur der Aridus II zur Untersuchung von flüssigen Proben mit niedrigen Elementkonzentrationen geeignet war. Im Vergleich zu einem ICP-Q-MS (Elan6000, Perkin Elmer/Sciex) zeigte das ICP-TOF-MS System um den Faktor 2 bis 10 geringere Signalintensitäten. Die Oxidbildungsrate betrug 0.3%, die Bildungsrate von doppelt geladenen Ionen 12.7%. Niedrige Hintergrundsignale (20 counts pro Sekunde (cps)) sowie niedrige instrumentelle NWG (0.4 ng L^{-1} bis 10 ng L^{-1} für Elemente mit Massen $> 58 \text{ amu}$ (atomare Masseneinheit)) erlauben die Untersuchung von niedrig konzentrierten Proben. Probleme im Massenbereich 23 amu bis 72 amu konnten durch komplexe Störinterferenzen (basierend auf Argon und Stickstoff Spezies) sowie Spannungsimpulse im Messgerät zur Ablenkung von Ionen zum Schutz des Detektors vor hoher Ionenbelastung geklärt werden. Bei der Untersuchung von Standardreferenzmaterialien wichen die meisten Elementkonzentrationen nur weniger als 5% vom zertifizierten Wert ab. Die RSD von Wiederholungsmessungen betrug im Durchschnitt 1.5%. In dieser Arbeit war besonders die Untersuchung von Seltenen Erd Elementen (SEE) von Bedeutung. Bei diesen Elementen betrug die Wiederfindungsrate 103% mit einer Präzision von 3.4% im unteren ng L^{-1} Konzentrationsbereich für den Referenzstandard SPS-SW1. Mit diesen gerätespezifischen Parametern konnten SEE in natürlichen Eisbohrkernproben im flüssigen Zustand untersucht werden. Die erhaltenen Konzentrationen stimmten sehr gut mit Messergebnissen von ICP-Q-MS und ICP-SF-MS Geräten überein (Publikation V). Das neu entwickelte ICP-TOF-MS System misst problemlos SEE Konzentrationen höher als 5 ng L^{-1} . Genauigkeit und Richtigkeit von Konzentrationen zwischen 0.5 ng L^{-1} bis 5 ng L^{-1} sind elementabhängig.

Basierend auf den Parameterstudien der Flüssigproben wurden in einem weiteren Schritt Parameterstudien der LA-ICP-TOF-MS Kopplung durchgeführt. Eine Signalintensitätserhöhung um den Faktor 3 bis 5 konnte für diese Technik erzielt werden, wenn statt Argon als Transportgas eine Mischung aus Helium und Argon verwendet wurde. Dennoch waren die Signalintensitäten um den Faktor 50 bis 130 niedriger im Vergleich zur LA-ICP-Q-MS Kopplung. Die Oxidbildungsrate für die LA-ICP-TOF-MS Kopplung betrug 17%, die Bildungsrate von doppelt geladenen Ionen 31%. Des Weiteren entstanden durch den Laserablationsprozess Druckwellen, die zu Instabilitäten des Plasmas bis hin zur Löschung des Plasmas führten. Zusätzlich hohe Hintergrundsignale (100 cps) lassen es derzeit nicht zu, natürliche Proben niedriger Elementkonzentrationen mit dieser Kopplungstechnik zu untersuchen. Gründe für den deutlichen Signalverlust sind das Generatorsystem zur Plasmaerzeugung, der gepulste Eintrag von Ionenpaketen in den Massenanalysator und die Verwendung von Kunststoffen als Baumaterial im Bereich des Plasmastands.

1 Introduction

Within the international climate research community it is commonly accepted, that climate changes throughout time. It is very likely that anthropogenic activity is responsible for the largest part of climate change. Since 1750 A.D. the CO₂ concentration of the atmosphere increased from 278 ppm to 379 ppm in 2005 A.D. (IPCC, 2007), which is just about the natural amplitude between glacials (180 ppm) and interglacials (250 ppm-300 ppm) over the past 650 kyr (Siegenthaler *et al.*, 2005a). Other greenhouse gas concentrations also increased (Spahni *et al.*, 2005), *e.g.* CH₄, increased since 1750 A.D. from 715 ppb to 1774 ppb in 2005 A.D. and N₂O from 270 to 319 ppb respectively (IPCC, 2007). Moreover, higher air and ocean temperature, widespread melting of snow and ice, and a mean rise of global sea level is observed. The effects are noticeable to humankind, as the environmental changes. Between the years 1950 and 2006 the number of great weather disasters increased by a factor of 3 resulting in an increase of overall loss by about a factor of 36 (Munich RE Group, 2007). To respond to climate change, policymakers need a well founded scientific basis about the causes of climate change, the potential environmental and socio-economic impacts and science based recommendations for adaptation to and mitigation of altered living conditions due to climate change. The Intergovernmental Panel on Climate Change (IPCC) compiles the scientific basis for policy makers.

Present questions in the scientific community are related to the role of greenhouse gases in a warmer and obliquity driven climate, changes in ocean circulation, sea ice extent and atmospheric transport patterns of dust in glacial and interglacial periods. Moreover the role of aerosols in respect to the radiation budget is of interest. Especially the up to a few degrees warmer interglacial periods compared to the Holocene might resemble conditions in a warmer world. Projects to address these questions are presently developed within the international partnerships in ice core sciences (IPICS) (Brook and Wolff, 2006).

To understand climate change and gain information about future climate, paleo-climatic research is undertaken. Since the middle of the 19th century, analytical measurements of meteorological parameters as *e.g.* temperature and air pressure are recorded systematically. This period of “instrumental records” is short compared to the timescales of natural climate variability. Climate proxies stored in various environmental archives provide an estimate for the above mentioned meteorological parameters and extend our information on climate change far beyond the instrumental records. Climate proxies that contain information from the past are obtained by the investigation of climate archives. In this study polar ice core samples, bivalves and frozen lake sediment cores (Figure 1) are looked at more closely.

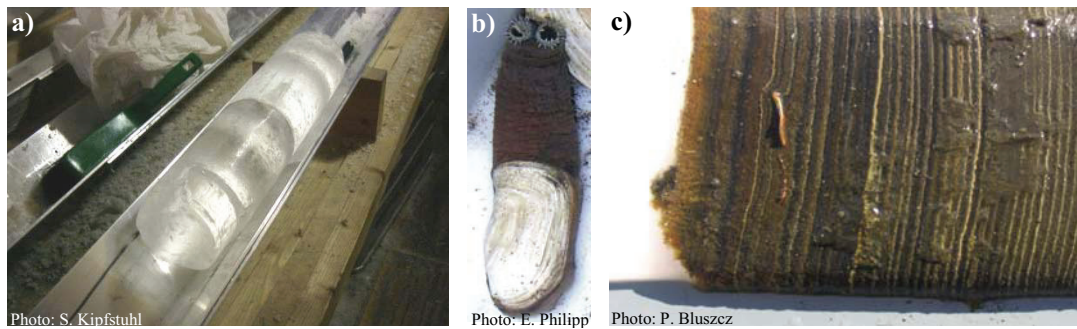


Figure 1: Climate archives analysed for the reconstruction of past climate. a) Polar ice core with particle horizons; b) bivalve *Laternula elliptica*; c) laminated lake sediment core.

Ice cores are the only archives that store a direct sample of ancient air directly from the atmosphere (Petit *et al.*, 1999; North Greenland ice core Project members, 2004; Spahni *et al.*, 2005; Fischer *et al.*, 2008). The time span covered in a certain ice core is mainly determined by the ice thickness, the accumulation rate and the geothermal heat flux at the drilling site and upstream of it. For example, a 3030 m long ice core was drilled at Summit (Position: 72°35'N, 37°38'W, accumulation rate: 210 kg m⁻² yr⁻¹) within the Greenland ice core project (GRIP) (GRIP members, 1993). This ice core represents undisturbed climate information till the last interglacial period (Eemian) (Johnsen *et al.*, 2001). Within the European Project for Ice Coring in Antarctica (EPICA) a 2774.15 m long ice core was drilled at Kohnen station (Dronning Maud Land (DML), Position: 75°00'S, 0°04'E, accumulation rate 64 kg m⁻² yr⁻¹). A 3259.3 m long ice core was drilled at EPICA Dome C (EDC) station (Position: 75°06'S, 123°21'E, accumulation rate 25 kg m⁻² yr⁻¹) (EPICA Community Members 2004, 2006). The EPICA-DML (EDML) ice core stores information of the past 150000 years (Ruth *et al.*, 2007) whereas the EDC ice core covers the last 800000 years (Parrenin *et al.*, 2007). Information about the past temperature on Earth is obtained by analyzing the isotopic composition (hydrogen and oxygen) of ice (EPICA Community Members, 2004). The annual layer thickness stores information about the accumulation rate (Ruth *et al.*, 2007). Air bubbles included in the ice matrix are analysed for trace gases such as CO₂ (Siegenthaler *et al.*, 2005a, 2005b), CH₄ and N₂O (Spahni *et al.*, 2005), which are considered to influence the temperature on Earth. Chemical tracers are one of the best available proxy parameters to perform paleoclimate reconstruction (Legrand and Mayewski, 1997; Wolff *et al.*, 2006; Fischer *et al.*, 2007). Amongst chemical tracers, rare earth elements (REE) and Sr in dust particles are the most prominent tracers to reconstruct the origin of dust (Basile *et al.*, 1997; Delmonte *et al.*, 2004; Gaiero *et al.*, 2004; Revel-Rolland *et al.*, 2006; Gaiero, 2007; Wegner, 2008) and consequently atmospheric circulation patterns of air masses. Due to the geographic isolation of polar regions and therefore the reduced influence of natural and anthropogenic impact, the polar atmosphere is the cleanest atmosphere worldwide. Hence, natural climate variability can be studied more easily.

Bivalves show growth rings similar to tree rings. The species of bivalves defines the available time slice for paleoclimatic research. Typically, bivalves store information of 2 (*Argopecten ventricosus*) to 400 (*Arctica islandica*) years. The incorporation of trace elements into the bivalves' hard structure stores temporal changes in the elemental composition of the marine environment, water temperature as well as the salinity (Rosenberg, 1980). Sr/Ca ratios provide information about past temperatures (Beck *et al.*, 1992). Stable oxygen and carbon isotope and radioisotope analysis allows the reconstruction of the physical and chemical conditions in the bivalve's environment during its growth and thus determines the water depth and temperature, as well as the effect of upwelling and other perturbations on shell growth (Richardson, 2001).

Depending on the sedimentation rate, lake and marine sediment cores archive climate information up to several millions of years. Caution is advised for both types of sediment cores because the upper layers might be destroyed by bioturbation. Information about global climate variations is retrieved by the analysis of marine sediment cores. As example, Emiliani (1955) introduced isotope stratigraphy to paleoceanography. Wefer *et al.* (1999) give a brief overview of marine sediment core proxies analysed to reconstruct the ocean history, *e.g.* temperature estimates from microfossil assemblages and reconstruction of wind transport and conditions on adjacent land areas. Lake sediment cores store information about the environmental change in their catchments areas (Boyle, 2001). These authors report, that the inorganic chemical composition of the mineral material is analysed to describe and quantify the lake's environment. The minerals' fluid inclusions record the temperature at which the crystals formed and provide an opportunity to determine the chemical composition of ambient water (Lowenstein and Brennan, 2001). Carbon ratios ($^{13}\text{C}/^{12}\text{C}$) deliver information about productivity rates, the availability of nutrients and the origin of organic compounds (Meyers and Teranes, 2001). Further anthropogenic induced pollution is stored in lake sediment cores as persistent organic pollutants (POPs) (Blais and Muir, 2001) and fly ash (Rose, 2001).

All the above mentioned archives show stratigraphic layering and have in common, that the inorganic composition of samples represents proxies for climate reconstruction. The thinner the annual layer thickness, the more sophisticated is the sample preparation and analysis if one strives for high-resolution information from the sample. The more information, *e.g.* the inorganic composition, one retrieves from a small sample, the more detailed information about past processes can be accomplished.

Due to the distance of continents to polar regions and shielding circum-Antarctic circulation pattern, several proxies such as mineral dust tracers are very low concentrated in Antarctic ice cores. Several methods for trace element analysis in polar snow and ice are available. Analytical techniques such as *e.g.* atomic absorption spectrometry (AAS) (Candelone *et al.*, 1995; Planchon *et al.*, 2002; Hong *et al.*, 2005) and cold vapour atomic fluorescence spectrometry (CVAFS) (Vandal *et al.*, 1993;

Capelli *et al.*, 1998) are used for single element analysis. Isotope dilution mass spectrometry (IDMS) is used for multi-element analysis (Van de Velde *et al.*, 2005). The continuous melting of ice cores and subsequent analysis by different methods is described in the literature on several occasions. Analysing the molten ice by fluorescence methods delivers information about *e.g.* Na⁺, NH₄⁺ and Methansulfonate (MSA) (Röthlisberger *et al.*, 2000). Coupling the melting device directly to an inductively coupled plasma-mass spectrometer (ICP-MS) system provides multi-element information (Knüsel *et al.*, 2003; Osterberg *et al.*, 2006). Reinhardt *et al.* (2001) and Reinhardt (2002) developed a method that enables high spatial resolution multi-element analysis of frozen ice cores in their solid state by laser ablation ICP-MS (LA-ICP-MS).

Until the mid 1980s the analysis of heavy metal concentrations in bivalve shells was accomplished using instrumental neutron activation analysis (INAA), atomic absorption analysis (AAS) and proton induced x-ray emission analysis (PIXE) (Al-Dabbas *et al.*, 1984; Carriker *et al.*, 1982). Thorn *et al.* (1994) used synchrotron X-Ray Fluorescence (XRF) to analyse element distributions in marine bivalve shells. Since the introduction of ICP-MS at the beginning of the 1980s and the introduction of LA as sample introduction system, it is the preferred method for element analysis of bivalve shells and tissues. LA-ICP-MS was used to analyse Pb, Cu, As, Zn and U in shells of the common cockle *Cerastoderma edule* as indicators for pollution (Price and Pearce, 1997). Mubiana and Blust (2007) used the ICP-MS method to determine the effect of temperature on the accumulation of metals by marine bivalves.

Boyle (2001) reviews several methods for the determination of the inorganic composition of sediment cores in their solid state as well as after total acid digestion of the samples, including *e.g.* INAA, XRF, AAS, atomic emission spectroscopy (AES) and ICP-MS / LA-ICP-MS. Isotope ratio-MS (IR-MS) systems define ¹³C/¹²C ratios (Meyers and Teranes, 2001). POPs are identified by gas chromatography electron capture detector (GC-ECD) and GC-MS (Blais and Muir, 2001).

The appliance of methods for the investigations of the inorganic compositions of natural samples shows, that mass spectrometry has become an established technique for bulk and trace element determination of a variety of different sample matrices. The history of mass spectrometric techniques as well as the design of different mass spectrometric systems is shown by Becker (2007). One of the newer designs used in inorganic mass spectrometry is the time of flight mass spectrometer (TOF-MS) which enables to measure very fast ion intensities of separated ions from the entire mass range (Myers and Hieftje, 1993; Myers *et al.*, 1994; Mahoney *et al.*, 1997; Ray and Hieftje, 2001). These authors reported about ICP-TOF-MS systems with orthogonal accelerated (oa) and axial accelerated (aa) geometry. Since 1993 an oa-ICP-TOF-MS system was brought to the market by GBC Scientific Equipment Pty Ltd (Melbourne, Victoria, Australia). Sturgeon *et al.* (2000) discuss the analytical characteristics of this system.

The same authors report that low background count rates permit low ng L^{-1} detection limits (DL) to be achieved. In literature, this system is used for *e.g.* speciation analysis of tributyltin in aqueous samples (Mester *et al.*, 2001) and the determination of isotope ratio precision for the measurement of transient signals (Willie *et al.*, 2005). In 1998 LECO (St. Joseph, Michigan, USA) introduced an aa-ICP-TOF-MS system. The analytical performance of this system is described by Tian *et al.* (1999). The analysis of isotope ratios constitutes the main field of application of ICP-TOF-MS systems and is described by Vanhaecke *et al.* (1999), Tian *et al.* (2000) and Bankhedda *et al.* (2004). Pelàez *et al.* (2002) compared isotope ratio measurements in elemental speciation obtained by ICP-Quadrupole-MS (ICP-Q-MS) and ICP-TOF-MS systems. Bankhedda *et al.* (2002) describe the flow injection preconcentration with subsequent ICP-TOF-MS analysis for the determination of REE. For these elements the authors obtained DL between 3 and 670 pg L^{-1} . LA-ICP-TOF-MS was conducted for the analysis of tin rich fluid inclusions from the Yankee Lode of the Mole Granite by Bleiner *et al.* (2000). Because of the sensitivity loss of ICP-TOF-MS systems compared to ICP-Q-MS systems (Tian *et al.*, 1999) and therefore lower DL, they do not open up areas for application where quadrupole based MS systems are currently limited.

In the following study, the analysis of different climatic archives by LA-ICP-Q-MS revealed limitations of the method developed by Reinhardt *et al.* (2001) (Publication I, III, IV). Moreover performance studies of a newly developed ICP-TOF-MS system, coupled to a LA system, should overcome the limitations of coupling a LA system to quadrupole based instruments (Chapter 4 and 5, Publication V).

1.1 Objectives

The investigation of different climatic archives, namely polar ice cores, bivalves and frozen lake sediment cores by the LA-ICP-Q-MS method as developed by Reinhardt *et al.* (2002) revealed its methodological limitations. The analysis of inhomogeneous climate archives by LA-ICP-MS results in aerosol formation which composition changes over time. The changing aerosol composition as well as the pulsed introduction of ablated sample material by the LA method result in *transient signals*. Due to the sequential analysing mode of the ICP-Q-MS system the number of analysed isotopes is strongly confined. Analysing as many isotopes as possible is of interest to deduce *e.g.* the corresponding source region of embedded particles in the ice matrix. The *quasi-simultaneous* detection of several isotopes of transient signals is realised in ICP-TOF-MS systems (Myers and Hieftje, 1993; Mahoney *et al.*, 1997). Two ICP-TOF-MS systems for elemental analysis have been on the market for the past 15 years (i) Optimass 8000, GBC, (ii) Renaissance, Leco Inc.. Unfortunately, these two ICP-TOF-MS systems do not fulfil the needs for the analysis of low concentrated samples as *e.g.* ice cores from polar regions.

Therefore, the main objective of this thesis is:

- Setup of an innovative ICP-TOF-MS system, developed at the Institute for Analytical Science in Berlin, supported as a research prototype jointly with Analytik Jena (Hoffmann *et al.* 2002, 2005) in the clean room laboratories of the Alfred Wegener Institute in Bremerhaven.
- Coupling of the LA unit to the ICP-TOF-MS system to localize and analyse impurities in the ice matrix.
- Calculation of element ratios of impurities for source determination.

After the setup of the instrument, its accuracy, precision and performance were studied. Initially, the tests were performed with liquid samples to minimize possible sources of error and to become acquainted with the new ICP-TOF-MS system. As the next step, similar experiments were run with the LA unit for analysis of solid samples to test whether the above listed remaining limitations of LA-ICP-Q-MS method developed by Reinhardt (2002) can be overcome by the new LA-ICP-TOF-MS system. The envisaged analytical developments are expected to enhance our understanding of past circulation patterns in different modes of the climate system.

2 List of Publication submitted for the thesis

In the following a list with publications that has been accepted, submitted or are in preparation for submission is given.

- Publication I

High spatial resolution element analysis of polar ice by Laser Ablation-ICP-MS

D. Dick, H. Reinhardt, U. Ruth, M. Kriews

Submitted to the Journal of Analytical Atomic Spectrometry, 18.04.2008.

Own contribution:

- Elaboration of the concept and the initial idea of the paper together with H. Reinhardt and M. Kriews.
- H. Reinhardt and me prepared and analysed the samples.
- Evaluation and interpretation of LA-ICP-MS data.
- The first draft of the manuscript was written by myself and revised together with all co-authors.

In this context I developed a microtome to decontaminate ice core samples for LA-ICP-MS (Dick *et al.*, 2004; Appendix A1). Further, parts of the results were already shown in the Bunsen-Magazin published by the “Deutsche Bunsengesellschaft für physikalische Chemie” (see Appendix A2). Concentration data of EDML meter 270 obtained by LA-ICP-MS and liquid ICP-MS of molten samples are also given in the Appendix (A3, A4).

- Publication II

One-to-one coupling of glacial climate variability in Greenland and Antarctica

EPICA Community Members (2006)

(A full list of authors is given at the end of Publication II)

Nature, 444, 195-198.

Own contribution:

- participation in the EPICA drilling project in Dronning Maud Land (2005/06)
- processing of ice core samples

- Publication III

Is the umbo matrix of bivalve shells (*Laternula elliptica*) a climate archive?

D. Dick, E. Philipp, M. Kriews, D. Abele (2007)

Aquatic Toxicology, 84, 450-456.

Own contribution:

- The scientific idea for this paper was developed by all authors.
- Samples were analysed by E. Philipp and me.
- Evaluation of the data was done by myself and I interpreted the data with the help of the rest of authors. Data are given in the Appendix (A5).
- I wrote the first manuscript and revised together with all co-authors.

- Publication IV

High spatial resolution analysis of a frozen sediment core by LA-ICP-MS analysis

D. Dick, P. Bluszcz, H. Reinhardt, C. Ohlendorf, B. Zolitschka, M. Kriews

In preparation for submission.

Own contribution:

- The scientific concept of this study was developed by me in cooperation with P. Bluszcz and M. Kriews.
- P. Bluszcz and I analysed the samples.
- Evaluation of the data was done by me.
- The first draft was written by myself and revised with all co-authors.

It is planned to analyse this sediment core segment with X-ray fluorescence spectroscopy to compare these data with LA-ICP-MS data. At the present state this publication has not been reviewed yet.

- Publication V

Rare Earth Elements determined in Antarctic ice by Inductively Coupled Plasma – Time of Flight, Quadrupole and Sector Field-Mass Spectrometry: an inter-comparison study

D. Dick, A. Wegner, P. Gabrielli, U. Ruth, C. Barbante, M. Kriews (2008)

Analytica Chimica Acta, in press.

Own contribution:

- The scientific idea of this publication was elaborated together with M. Kriews.
- I performed the accuracy and precision studies of the ICP-TOF-MS system as well as analyses of natural samples by ICP-Q-MS and ICP-TOF-MS. Concentration data of elements, also of elements which are not discussed in this publication, are given in the Appendix (A8).
- ICP-SF-MS analyses were accomplished by A. Wegner and P. Gabrielli.
- I wrote the first draft of the manuscript and revised together with all co-authors.

3 Materials, Instrumentations and Methods

For this study, analyses were conducted using different kind of sample introduction systems coupled to an ICP-Quadrupole-MS (ICP-Q-MS) and to an ICP-Time of Flight-MS system (ICP-TOF-MS). A microconcentric nebulizer with desolvation unit was conducted for the analysis of liquid samples. A laser ablation (LA) system with a subsequent ICP-MS system enabled the analysis of solid samples.

3.1 Inductively Coupled Plasma Mass Spectrometry

ICP-MS is a powerful technique to analyse the elemental composition and isotope ratios for a diverse range of samples. Figure 2 shows the principle setup. The ICP, the interface, the ion optics and the detection of ions are similar for all kind of MS systems. The mass analyzer, which separates the ions by electrical or magnetic fields, constitutes the main difference.

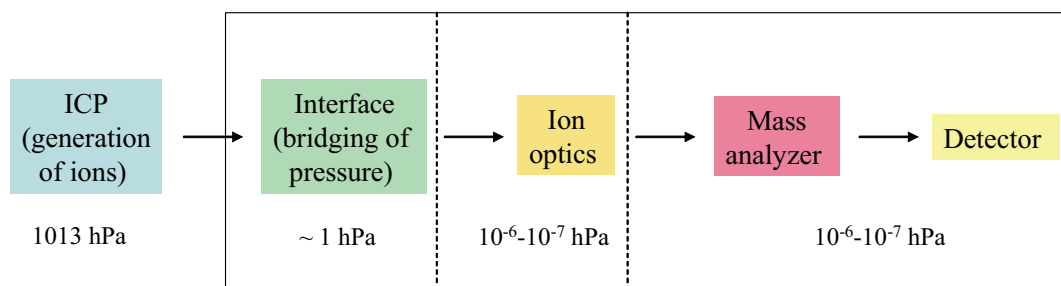


Figure 2: General instrumental setup of mass spectrometer systems with an inductively coupled plasma for ion generation.

Common MS systems for the analysis of elements are: Q-MS-, SF-MS- and TOF-MS systems. Detailed information about the instrumental setup and basic principles of different MS systems is given by Becker (2007).

A quadrupole mass filter consists of four cylindrical or hyperbolic metallic equally long and thick rods, which are excited by connecting a direct current (DC) and a time dependent alternating current (AC) of radio frequency on the respectively opposite pairs of the four rods. The selecting condition for ions with the scanned mass is tuned by adjusting the DC/AC ratio.

Modern SF-MS systems use the double focusing approach. After the sample passed the ICP, the ions are accelerated in the ion optics before they enter the mass analyzer. A magnetic and electric sector field deflect the ions depending on their mass to charge ratio (m/z) and kinetic energy. A complete mass spectrum is scanned by changing the acceleration voltage and magnetic field intensity.

In ICP-TOF-MS systems, pulsed ion packets from a continuous source enter the mass analyzer. After focussing through the ion optics, ions are accelerated, either axial or orthogonal to the sample introduction system, gain kinetic energy and finally enter

the mass analyzer. Resultantly, the velocity of the ions differs dependent on their masses. This principle is used to separate ions of different m/z ratios. With this setup, ions of each packet are simultaneously extracted from the ion source and enter the mass analyser. The *duty cycle* is usually defined as the fraction (percentage) of extracted ions that actually make it into the mass analyzer. Unfortunately, with an ICP-TOF-MS system, this process is not very efficient as in comparison with common ICP-Q-MS systems only 10% of the ions reach the detector (Ray and Hieftje, 2001). In ICP-Q-MS systems and ICP-SF-MS systems, a higher *duty cycle* is obtained by constant ion transfer into the mass analyzer region.

In many applications, sufficient sample amounts are available, so that the material volume is not a limiting factor for the analysis. In contrast, for natural samples the available volumes are on some occasions very limited. These samples require methods, which analyses all isotopes of interest in a very short time to gain all the desired information. Their sequential analysing mode is a disadvantage of common Q-MS and SF-MS systems for elemental analysis. By tuning the electric and/or magnetic fields, only the pre-selected sort of ions reaches the detector. Even though multiple elements can be selected for the analysis by Q-MS or SF-MS, the number of practically measured elements is strongly limited. For example, the dwell time (analysing time for one isotope) amounts 10 ms for Q-MS systems, therefore scanning 230 isotopes takes 2.3 seconds. Instead, 25000 mass spectra per second are taken by the TOF-MS system. The TOF-MS system analyses in the *quasi-simultaneous* mode, where all isotopes are simultaneously extracted from the ion source, but are, depending on their respective m/z ratio, arriving at the detector at different times.

As a major goal, this investigation aims to optimize the prototype of a newly developed ICP-TOF-MS system (Hoffmann *et al.*, 2002; Hoffmann and Lüdke, 2005) for trace element analysis in natural samples. Advantages of an ICP-TOF-MS compared to common MS systems are the simultaneous recording of all elements, fast data logging and few sample uptake. The ICP-TOF-MS system was jointly developed by the Institute for Analytical Science (ISAS) Berlin and Analytik Jena. Now, the ICP-TOF-MS system and principle components of the MS system will be illustrated.

3.1.1 ICP-TOF-MS

The oa-ICP-TOF-MS system used in this study is shown in Figure 3. Parts of this system, the ICP, the interface, ion optics, the ion repeller, the mass analyzer and the detector are described in the following subsections.

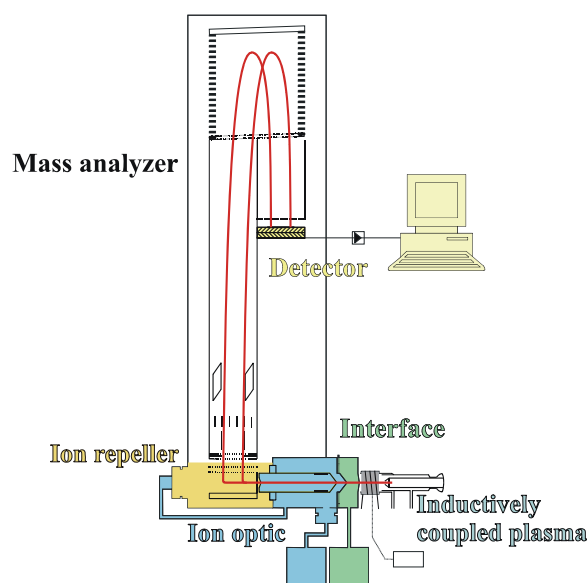


Figure 3: Experimental setup of the ICP-TOF-MS system developed at the Institute for Analytical Science, supported as a research prototype jointly with Analytik Jena. Principle components are the plasma torch, interface (green), ion optics (blue), ion repeller (yellow), mass analyzer (white) and the detector.

3.1.2 Inductively Coupled Plasma

The detection of multiple elements within one sample efforts the separation of elements. This is conducted by electrical or magnetic fields. Therefore elements have to be transferred into ions first. One possibility for ion generation is a thermal plasma. That means a hot (several thousands Kelvin) ionised gas which properties are defined by the ionisation of atoms and molecules. The charge of the plasma is quasi neutral due to the same number of positive charges and the number of electrons on an average.

The generation of a plasma is performed by energy transfer from a high frequent electro-magnetic field onto a constant flowing gas. Mainly argon is used for plasma generation due to its high efficiency for ion generation. Further, the air contains 0.93 % argon; hence, it is the cheapest inert gas. Figure 4 shows the plasma torch.

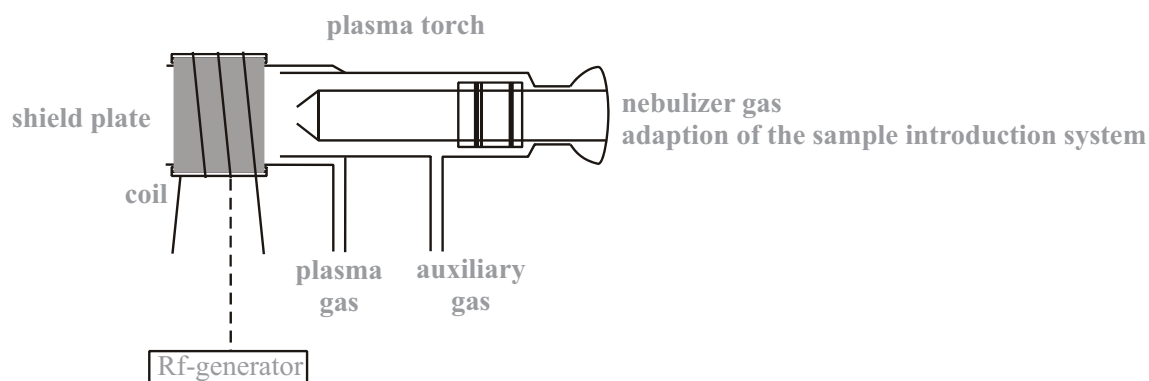


Figure 4: Plasma torch with shield plate, coil and Rf-generator used for plasma generation for the TOF-MS system.

It consists of three concentric quartz tubes and is connected to the sample introduction system by a fitting. The plasma gas is flowing through the outermost tube, the auxiliary gas through the middle tube and the nebulizer gas with sample is flowing through the injector tube.

The plasma gas and auxiliary gas are needed for the plasma and for cooling of the quartz tubes. The high frequency (or radio-frequency RF) power supply drives current through a water cooled copper induction coil. In order to ignite the plasma a high voltage spark is employed in the argon gas. Collision processes lead to further ionization processes according to equation (1):



Further, through the recombination of argon cations with e^{-} , which lead to the formation of excited argon atoms (Ar^{*}), UV light is emitted according to equation 2:



with:

Ar^{+} = argon cation; h = Planck constant; ν = Frequency

Ions are mainly produced by thermal ionisation but also by Penning ionisation and charge transfer (equations 3-6). The energy for ionisation of atoms results from colliding of atoms with atoms or atoms with ions. If an electron absorbed enough energy this electron leaves the atom.



With:

A = analyte atom; A^{+} = analyte ion; X^{*} = meta stable species; X^{+} = ion

M = collision partner (ion, atom, wall)

The grade of ionisation of an element depends on the density of electrons, the temperature and the first ionisation potential and is described by the Saha-equation (equation 7).

$$\frac{n_i \cdot n_e}{n_a} = 2 \cdot \frac{Z_i}{Z_a} \cdot \sqrt{\left(2 \cdot \pi \cdot m \cdot k \cdot \frac{T}{h^2}\right)^3} \cdot e^{-\frac{E_i}{kT}} \quad (7)$$

with:

n_i , n_e , n_a = number of ions i , free electrons e and atoms a

Z_i, Z_a = degeneracy of states for the i -ions

m = mass of an electron ($9.11 \cdot 10^{-28}$ g)

k = Boltzmann constant ($1.38 \cdot 10^{-23}$ J/K)

T = temperature (K)

h = Planck constant ($6.67 \cdot 10^{-27}$ J s)

E_i = is the energy required to remove i electrons from a neutral atom, creating an i -level ion

Date (1975) observed a dependency of the ionization yield on the ionization energy. The alternating electro-magnetic field leads to acceleration of cations and electrons and results in heat energy (Skoog and Larry, 1996). The highest temperature (10000 K) is in height of the coil. These high temperatures demand the plasma and auxiliary gas for cooling. The sample is injected into the plasma through the injector tube. High energy transfer onto the sample and long dwell time of the sample in the plasma lead to drying, combustion, atomising, excitation and ionisation. The time for atomization lies within the ns range, the time for excitation and ionisation is much shorter. According to the Saha–equation (equation 7) the degree of ionisation depends also on the temperature. Figure 5 (Fassel, 1978) illustrates that there are several temperature zones within the plasma; hence to obtain maximum transfer of ions from the plasma into the mass spectrometer system the position of the plasma torch is of importance. For the ICP-TOF-MS system used in this study the optimum positions are: 7 mm distance between the interface and coil and 2 mm between the front of the plasma torch and the coil.

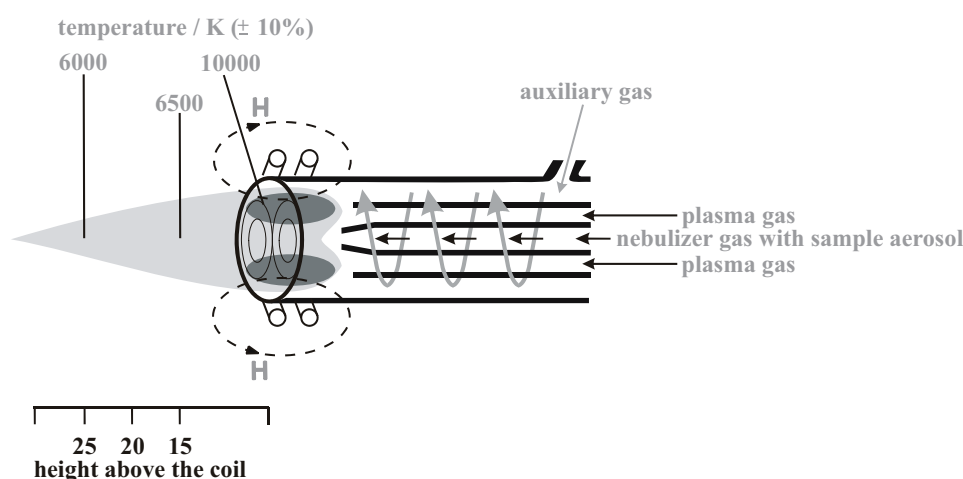


Figure 5: The inductively coupled plasma according to Fassel (1978). The sample is ionised within the argon plasma at temperatures of about 10000 K.

Cations as well as electrons repel each other. To yield a high transport efficiency of ions into the MS system a well defined charge distribution is required. Potential

differences (100–200 V) between the coil and the plasma lead to electrical discharge between the plasma and the skimmer cone from the interface (= pinch effect). This discharge shows itself as arcing. If no care of this problem is taken, further problems such as increasing amount of doubly charged ions or wide spread kinetic energy arise (Douglas and French, 1986). This problem is eliminated in the ICP-TOF-MS system by positioning a grounded shield between the coil and the plasma torch (Sakata and Kawabata, 1994). The position of the shield is of importance and the distance between the front of the plasma torch and the front of the shield plate should be 1.5 mm.

3.1.3 Interface

The interface connects the ionisation system with the mass spectrometer. The role of the interface region, which is shown in Figure 6, is to transport the ions efficiently from the plasma, which is at atmospheric pressure (1013 hPa), to the mass analyzer region at approximately 10^{-6} to 10^{-7} hPa. It is bounded by the sampler cone, skimmer cone and gate valve. The orifice of the sampler cone is 0.8 - 1.2 mm i.d. and the orifice of the skimmer cone, which is generally smaller and more pointed, is 0.4 - 0.8 mm i.d.. A rotary pump creates a pressure of ~ 1 hPa. Through pressure differences ions are sucked through the skimmer cone into the interface and afterwards into the mass analyzer region and are accelerated to about 2500 m s^{-1} for m/z ratios of about ~ 250 to 7000 m s^{-1} for m/z ratios of about ~ 10 (Holland and Tanner, 2001).

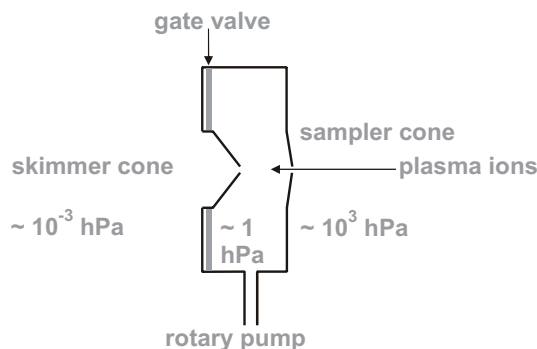


Figure 6: The Interface of the TOF-MS system used in this study. Pressure differences lead to acceleration of ions from the right to the left side.

When the hot plasma is burning, the particle density in front of the sampler cone decreases, therefore the pump system is able to pump down the incoming (diluted) gas to keep the pressure inside the interface. If the plasma is lost, the interface is separated from the ion optics by the gate valve. If the gate valve is closed, the coil and plasma torch can be replaced. This part of the system is water cooled.

3.1.4 Ion optic

The ion optic is needed to focus the divergent ion beam. It consists of an ion extraction skimmer cone, a lens and an entrance slit situated to the repeller region

(Figure 7). Except the lens all components have the same potential. A pressure of $10^{-6/-7}$ hPa is created by a rotary pump and turbomolecular pump.

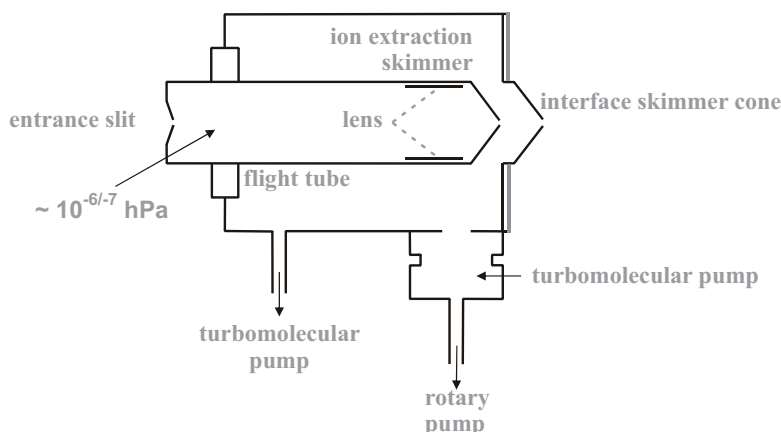


Figure 7: Ion optics of the ICP-TOF-MS system to diverge incoming ions.

3.1.5 Ion repeller and mass analyzer

After passing the entrance slit ions reach the repeller region (Figure 8). It is bounded by the entrance slit, a repeller lens, repeller plate and a repeller grid. During the phase of filling the repeller region with ions, 0 V are applied to the repeller plate and grid, whereby ions are focused and decelerated. A second turbo pump creates a pressure of 10^{-7} hPa when the gate valve is closed and 10^{-6} hPa when the gate valve is open. A voltage pulse of +466 V is applied at 25 kHz rate to the repeller plate, each pulse takes 2 μ s. By passing the potential difference between the repeller plate voltage (+466 V) and the acceleration grid voltage (-1876 V) the ions take up kinetic energy E_{kin} and enter the mass analyzer (Figure 8). The relationship between kinetic energy E_{kin} and velocity v (equation 8-9) of a charged particle is:

$$E_{kin} = \frac{1}{2} \cdot m \cdot v^2 \quad \rightarrow \quad E_{kin} = U \cdot z \quad (8)$$

$$t = \frac{s}{v} = s \cdot \sqrt{\frac{m}{U \cdot z \cdot 2}} \quad (9)$$

E_{kin} = kinetic energy, m = mass, v = velocity of the ion,

U = passed potential difference, z = charge, t = flight time, s = tube length

The flight time t of each ion through the drift tube length s is proportional to the square root of its m/z ratio according to equation 9.

Inside the drift tube (-1876 V) the x-deflectors exist to correct ion trajectories in x direction (direction from plasma to repeller space). After that, 1 mm high and 50 μ m thick metal strips (= selector) are arranged to redirect ions such as *e.g.* O^+ , OH^+ , O^{2+} , Ar^+ from their flight path by applying a different voltage pulse (-1670 V) when these ions are passing in height of the selector. According to equation 9 the times of selected

ions in height of the selector are calculated. If no voltage pulse is applied, the selector voltage is the same as the drift tube voltage (-1876 V). A second deflector (z-deflector) correct ion trajectories in z direction (rectangular to x-direction). The following reflector is bounded by a reflector grid and a reflector mirror with -1100 V applied to the reflector grid and + 466 V applied to the reflector mirror. To homogenize the retarding electrical field in the reflector, metal rings – which are connected by a voltage divider chain – are situated. By reflecting ions in the retarding field of the reflector small velocity differences of ions with one m/z ratio will be compensated (= velocity focussing, Figure 9).

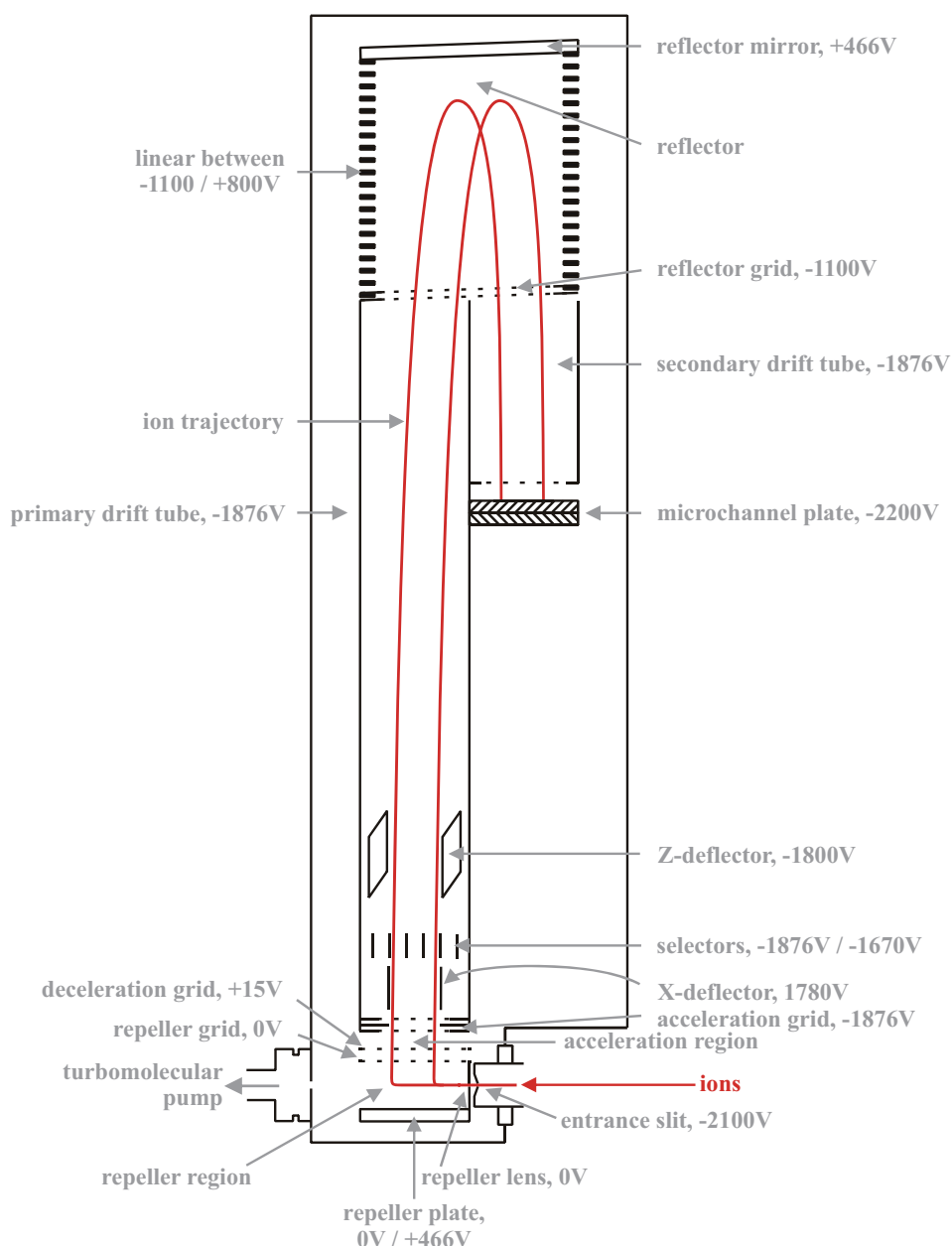


Figure 8: Ion repeller and mass analyzer of the TOF-MS system. Incoming ions are redirected by 90° (→ orthogonal acceleration) into the mass analyzer by applying a positive voltage pulse to the repeller plate.

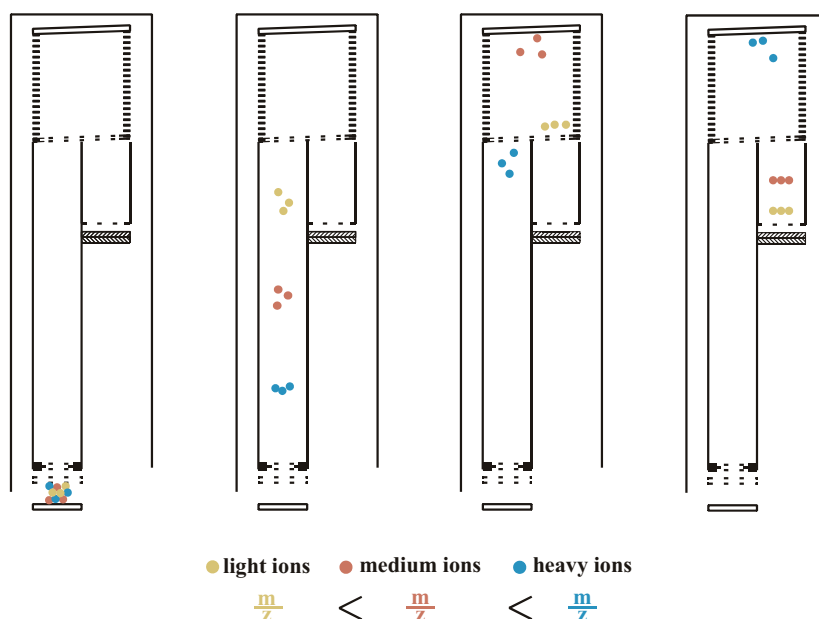


Figure 9: Schematic view of isotope separation in ICP-TOF-MS measurements. The flight time of an ion depends on its m/z ratio. Velocity differences of isotopes with one m/z ratio are corrected by redirection of ions at the reflector mirror by 180° (= velocity focusing).

3.1.6 Detection system

Reflected ions reach the detector through the secondary drift tube. It consists of two micro channel plates in chevron arrangement (Wiza, 1979) (Figure 8). The channel matrix is fabricated from a boron silicate glass treated in such a way that the walls are semiconducting. Parallel electrical contact to each channel is provided by the deposition of a metallic coating, which then serve as input and output electrodes, respectively. Every ion which hits the channel plates' surface releases electrons which are accelerated and creates secondary electrons until finally an electron avalanche reaches the anode surface. Thereby an electrical pulse is released, which is counted after pre-amplifying (detection pulse). The time between repeller pulse (start) and detection pulse (arrival) is the measure for the mass of an ion. The storage of one detection pulse takes 1 ns. In the presented experimental setup the analysis of one complete mass spectrum takes 34 μ s up to mass 285 amu. If each ns data are stored, the spectrum consists of 34000 data points. Each time a channel has to process an incoming ion this channel needs 3 – 4ms to recover (pers. comm. R. Müller, SI Scientific Instr. GmbH, 2008), whereas the flight time of neighbouring isotopes lay within the ns range. This may lead to problems if element concentrations of a sample are high. More detailed information are given by Hoffmann *et al.* (2002, 2005) or can be received by Analytik Jena, the distributor of the ICP-TOF-MS system.

Due to the thermal energy of ions entering the mass analyzer, each m/z ratio creates a signal covering about 27 ns of time at full width at half maximum (FWHM) of the Peak. This peak width defines the spectral resolution of the ICP-TOF-MS system. The spectral resolution is defined by the ratio $R=M/\Delta m$ (Wiley and McLaren, 1955), where

M is the ion mass number and Δm is the mass difference resulting from the temporal half-width Δt of the measurement signal for the mass M. The higher the resolution of the system is, the better it is to separate two isotopes from each other. Figure 10 illustrates a small part from a mass spectrum, which is detected 22.15 μs to 22.40 μs after the repeller pulse is applied, to demonstrate how to calculate the resolution of the ICP-TOF-MS system for a specific m/z ratio (Hoffmann and Lüdke, 2005). The distribution of flight times of a population of isomass ions, and thus the resolution, is greatly affected by the initial temporal, spatial and velocity distributions of the ions within the extraction region. Signal intensities reported in this thesis are related to the peak integral area of isotopes.

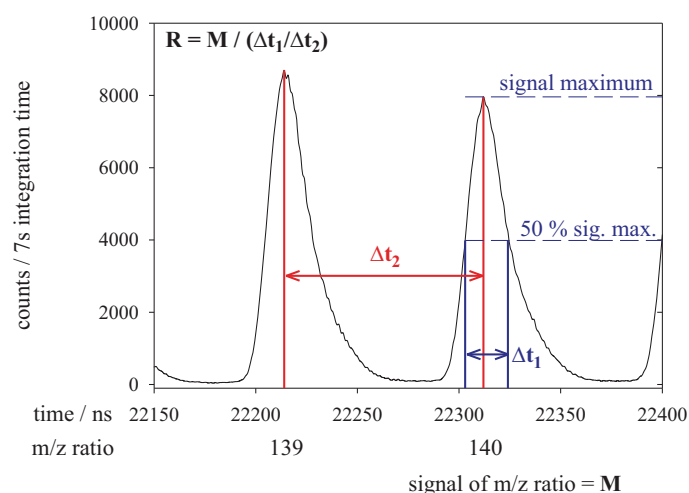


Figure 10: Part of an ICP-TOF-MS mass spectrum, to demonstrate the calculation of the resolution of two neighboured isotopes (^{139}La and ^{140}Ce).

An important advantage of oa-ICP-TOF-MS systems compared to aa-ICP-TOF-MS systems is the minimization of the spread of the initial ion velocities in the beam drift direction (average velocity is zero) which serves to increase the achievable resolving power. On average the resolution for all isotopes analysed for this ICP-TOF-MS system is 620. ICP-Q-MS systems show a resolution of 350 and with ICP-SF-MS systems it is possible to analyse in the low, middle and high resolution mode (400, 4000, 10000).

The ICP-TOF-MS presented here analysis 25000 spectra per second. Therefore this system is best suitable for the detection of *tansient signals* (Benkhedda *et al.*, 2004; Francesconi and Sperling, 2005), such as signals obtained by laser ablation (Hoffmann *et al.*, 2002) or inductively heated vaporization (Lüdke *et al.*, 2005) of solid samples. Further this analysis mode enables precisely analysis of isotope ratio measurements (Peláez *et al.*, 2002; Benkhedda *et al.*, 2004).

3.1.7 Interferences

ICP-MS analysis is limited by interferences. Generally interferences are divided into spectral-, isobaric- and physical based interferences. The first two interferences

have in common that the signal on the m/z ratio of the analysed isotope is composed of the analyte signal plus the signal of the interfering species.

Spectral overlaps are probably the most problematic interferences for ICP-MS. Spectral overlaps include: (i) Polyatomic or molecular interferences, emerging from *e.g.* acids used for sample digestion (HCl, HClO₄) and the plasma gas (argon). During the ionisation process species containing Ar and Cl are formed, *e.g.* Ar⁺, ArAr⁺, ArH⁺, ArO⁺, ArOH⁺, ArCl⁺, ClO⁺, ClN⁺, ClCl⁺. Several combination possibilities results in complex background spectra (Shao and Horlick, 1991; Evans and Giglio, 1993). To avoid these interferences HNO₃ should be used instead of Cl containing acids if possible. But also here, possible interfering species can be formed (*e.g.* NO⁺, NO²⁺). Further it is possible, for elements consisting of more than one isotope, to analyse a less abundant isotope. But then, higher detection limits have to be accepted. (ii) Oxides, hydroxides, hydrides, and doubly charged species produce spectral interferences. Water from the solvent or out of the air provides ¹H⁺, ¹⁶O⁺ and ¹⁶O¹H⁺ to combine with other isotopes in the plasma, especially in the colder part of the plasma (Figure 5). Species such as ⁴⁰Ar¹⁶O⁺ not only interfere with ⁵⁶Fe⁺, but due to all isotopic combinations and any hydride present, also with other isotopes (⁵²Cr, ⁵³Cr, ⁵⁴Cr, ⁵⁴Fe, ⁵⁵Mn, ⁵⁶Fe, ⁵⁷Fe, ⁵⁸Ni and ⁵⁹Co). Moreover, this is a problem which affects particularly the analysis of rare earth or refractory type elements, because many of them form readily molecules (predominantly oxides). All the above mentioned possible interfering species give strong signals in the mass range up to 80 amu. Under fixed working conditions and similar matrices of samples they do not change very much and can be corrected for by subtracting. However they limit DL. Associated with this interference are doubly charged ion spectral interferences. Here, ions are generated with a double positive charge producing an isotope peak at half its mass. These interferences are particular important for elements which have relatively low ionisation potentials.

Isobaric interferences are produced by isotopes with differing atomic number but with the same m/z ratio. For example, the analysis of ¹⁴²Nd⁺ is interfered by ¹⁴²Ce⁺. Simple equations can be used for correction if the concentration of the interfering species is not too high (Krause, 1993).

Physical based interferences influence the transport of ions. High matrix load of the sample influences the transport through the tubing and solid matrix accumulates at the orifices of cones (Douglas and Kerr, 1988). At first the gas flow is influenced and after a given time the orifice is clogged. The droplet size is of the aerosol is also influenced by the matrix.

3.1.7.1 Reduction of Interferences

In general, spectral interferences can be minimized by carefully optimization of the plasma and nebulizer gas as well as the position of the plasma torch. The use of desolvation units reduces the water and acid (HCl) content of the sample depending on

the temperature of the desolvation unit and therefore reduces interferences (for more information see chapter 3.1.8) (Cetac, 2008). So-called cool plasma techniques (at low plasma power (500-800 W) and increased nebulizer gas flow rate (1.5-1.8 L min⁻¹)) reduce argon associated interferences (Jiang *et al.*, 1988; Douglas and Tanner, 1998). Molecular and atomic interferences can be reduced by the dynamic reaction cell technique (DRC) (Perkin Elmer, 1999). This technique works with *e.g.* NH₃, CH₄, He or H₂ as reaction gas (Tanner and Baranov, 1999; Bollinger and Schleismann, 1999). The collision of polyatomic species with the reaction gas results in *e.g.* excited states of the polyatomics or unstable intermediates that subsequently dissociate. Further it was observed that argon ions are neutralized by NH₃. More references on the reduction of interferences are given in a review article of Becker and Dietze (2000).

3.1.8 Sample introduction systems for liquid samples

There are many different sample introduction systems available, but they all basically achieve the same result, and that is to generate a fine aerosol of the sample, so it can be effectively ionized in the plasma. The sample introduction system as well as the ICP are the most critical parts of the ICP-MS system, because most of the sample is lost in these two parts. Normally the sample is pumped into the nebulizer system via a peristaltic pump which enables a constant sample flow into the introduction system. The sample is then broken up into small droplets by a constant gas flow. Besides nebulizing the sample into small droplets, the nebulizing system has to get rid of large droplets (> 10 µm) which influence the plasma performance and which are not ionized. By far, the most common sample introduction systems are the pneumatic nebulizers (Thomas, 2004), which use constant flowing gases to generate fine sample aerosols. For the optimization of the presented ICP-TOF-MS system three different nebulization systems were used.

Usually MS systems are equipped with cross flow nebulizers (CFN). They are generally more tolerant to samples containing higher solids and/or particulate matter. In most cases the liquid sample is pumped into the nebulizer using a peristaltic pump. The argon gas (~1 L min⁻¹) is directed at 90° to the tip of the sample capillary tube. The contact of the fast flowing gas and the liquid causes the generation of the aerosol. Gravity forces larger droplets to exit the nebulizer via a drain tube. The CFN takes up about 1 mL sample per minute. Only 3 to 5% of the sample gets into the ICP.

In concentric nebulizing systems the gas flow is parallel to the sample capillary. The sample is introduced into a low pressure region, generated by fast flowing gas. The low pressure and the flowing gas lead to aerosol formation. To remove large droplets from the aerosol the concentric nebulizer is used in combination with a cyclonic spray chamber. It operates by centrifugal forces. According to the droplet size they are discriminated by means of a vortex produced by the tangential flow of the sample and argon gas flow inside the spray chamber. Large droplets fall out through the drain.

Concentric systems need about 1 mL sample per minute but can give better sensitivity and stability compared to CFN systems. However, the small orifice is susceptible to be plugged by matrix rich samples. About 50 to 60% of the sample reaches the plasma.

Microflow systems are high-efficient nebulizers needing about 20-400 μL of sample per minute which enable the analysis of low volume samples. They operate at higher gas pressure to accommodate the lower sample flow rates. The principle is similar to concentric nebulizing systems, where the gas flows parallel to the sample capillary. Another advantage of these nebulizers is that they are operated in the self aspirating mode. This reduces the signal to noise ratio derived from pumping oscillating. The microflow system made of PFA used in this study (Aridus II, Cetac Technologies, Omaha, Nebraska) is connected to a heated PFA spray chamber (70°C – 100°C), and a heated microporous PTFE membrane (160°C). Solvents of the sample, such as H_2O , HNO_3 and HCl , are removed nearly completely from the aerosol by mean of the membrane. It is impermeable for the sample, except Boron. The removal of the solvent from the sample reduces the generation of interfering species. For example, argon (which is used as plasma gas) and H_2O form ArO^+ (mass 56) in the plasma, which interferes the analysis of $^{56}\text{Fe}^+$. The removal of water through the membrane enables the analysis of the most abundant iron isotope ($^{56}\text{Fe}^+$) which is not possible using the CFN system for nebulization. Further advantage of this system is that the aerosol is much finer compared to aerosols generated by conventional concentric nebulizers. More than 90% of the sample reaches the ICP.

3.1.8.1 Alternate sampling accessories

It is recognized that the above mentioned spray chambers with nebulizers have certain limitations, particular when it comes to complex samples (Thomas, 2004). Depending on the amount of dissolved solids (maximum 0.2%), the washout time of the system can be very long. Dilution steps and the addition of internal standards are labour intensive and the risk for contamination increases. Further the analysis of solids or slurries is very difficult. Therefore alternate sampling accessories were developed. Electrothermal vaporization enables the analysis of liquid and solid samples. The sample is evaporated within a graphite furnace before being introduced into the plasma (Lüdke *et al.*, 1999). The analysis of low volume samples (2-100 μL) is possible. As example, an ultra-low-dead-volume nanoinjection valve was used for nanovolume flow injection determination (Schaumlöffel *et al.*, 2005), where a sample consumption of $7 \mu\text{L min}^{-1}$ enables the preconcentration of even low volume samples. A further technique for the analysis of liquid samples is the flow injection technique (FIA), where the sample is carried into the ICP by means of a carrier stream (Olivas *et al.*, 1995).

For the direct determination of solid samples with respect to trace element concentration, depth, and lateral distribution, several sample introductions are available. An overview of most important ion sources for solid state mass spectrometry (the sputter ion source, the laser ion source, the glow discharge ion source and the laser ablation

system coupled to an ICP-MS) is given by Becker and Dietze (2000). This review contains useful information on the use of different ion sources as well as further literature for detailed information.

3.2 Laser ablation as sample introduction system for solid samples

In the 1980s Gray (1985) reported about the successful coupling of high energy lasers to ICP-MS systems. The principle behind this approach is the use of high powered laser to ablate the surface of a solid sample and to transport the ablated sample into the coupled ICP-MS system (Denoyer *et al.* 1991). Since that time a vast development of the laser ablation (LA)-ICP-MS method took place. Nearly all kind of solid material, *e.g.* metals, rocks, and biological specimen, can be analysed (Price and Pearce, 1997; Eggins, 2003; Pisonero *et al.*, 2007).

Solid state lasers are the most common systems used for LA of solid samples. The first LA system developed for ICP instrumentation was a ruby laser, operating at 694 nm (Gray, 1985). However, this system showed poor stability, low power density and large beam diameter. Solid state lasers using a neodymium-doped yttrium aluminium garnet (Nd:YAG) are commercially distributed since the late 1980s. The Nd:YAG laser system operates at 1064 nm wavelength. This infrared (IR) laser shows complex ablation processes, poor precision, and because of poor laser coupling this wavelength is not suitable for many solid materials (Durrant, 1999). Therefore systems were developed using optical components to double (532 nm), triple (355 nm), quadruple (266 nm) and quintuple (216 nm) the frequency; the ablation efficiency increased (Jeffries *et al.*, 1995; Shuttleworth, 1995). Further, high quality optics enables a homogeneous beam profile providing high energy density to couple with the sample matrix. Moreover, Guillong *et al.* (2003) demonstrated that the usage of a shorter wavelength results in mainly small particles; smaller particles are more efficient converted into ions within the ICP. These wavelengths are used *e.g.* to determine the partitioning of trace elements in mafic minerals (Foley *et al.*, 1996), the analysis of tree rings that reflect the exposure of trees to metal deposition (Watmough *et al.*, 1997) or for the analysis of archaeological materials (Gratuze *et al.*, 2001).

The trend toward shorter wavelength and the improvement in the quality of the optical components lead to the development of UV gas-filled lasers, such as XeCl* (308 nm), KrF* (248 nm) and ArF* (193 nm). The index * shows, that *e.g.* ArF* mainly exists in the excited state. These lasers are called Excimer lasers. The expression comes from “excited dimer” where dimer means a molecule consisting of two identical atoms, whereas “Exciplex” comes from “excited state complex” where the complex consists of different atoms. Nowadays Excimer is used for both systems. The pumping mechanism for such a system is complex compared to Nd:YAG systems (Durrant, 1999) but their wavelengths show better absorption capabilities for UV transparent materials (*e.g.* calcites and silicates). Excimer lasers are used *e.g.* for the analysis of minerals (Bea *et*

al. 1996; Sylvester and Ghaderi, 1997) and the analysis of fluid inclusions in minerals (Günther *et al.* 1998; Bleiner *et al.*, 2000, Wang *et al.*, 2006).

CO₂ lasers are the most powerful lasers. The laser medium consists of a CO₂-N₂-He gas mixture, which is excited by gas discharge. Main excitation process of CO₂ is by collision of CO₂ with metastable N₂, formed during gas discharge. The wavelength of the laser light is 9.6 μm and 10.6 μm depending on the energy level. Kneubühl and Sigrist (1999) give detailed information about the principle of this and the above mentioned laser types. Energies in the continuous mode of 80 kW and of about 100 kJ in the pulse mode as well as the efficiency enable a wide variety of appliance, *e.g.* the analysis of trace gases with tunable CO₂ lasers (Repond and Sigrist, 1996) and CO₂ laser application in alleviating orthodontic pain (Fujiyama *et al.* 2008).

Today laser ablation is a very attractive tool due to its various advantages. Direct analysis of solid samples is possible without labour intensive sample preparation and therefore the risk of sample contamination is considerably reduced. Using UV lasers with high quality optics enables the bulk and micro analysis of geological materials. Further, interferences in the coupled ICP-MS system due to solvents are reduced.

3.2.1 Absorption characteristics of ice

As mentioned above the used wavelength is of importance for the ablation efficiency. Sample materials have different absorption characteristics for different wavelength. Laser ablation of solids showed that UV lasers are more suitable for geological applications compared to IR lasers (Durrant, 1999). Instead, the ablation efficiency of ice is much better using 1064 nm (Nd:YAG laser). Although ice is transparent for the human eye, it is opaque for the IR. Figure 11 illustrates the absorption coefficient of ice depending on the wavelength (Warren, 1984).

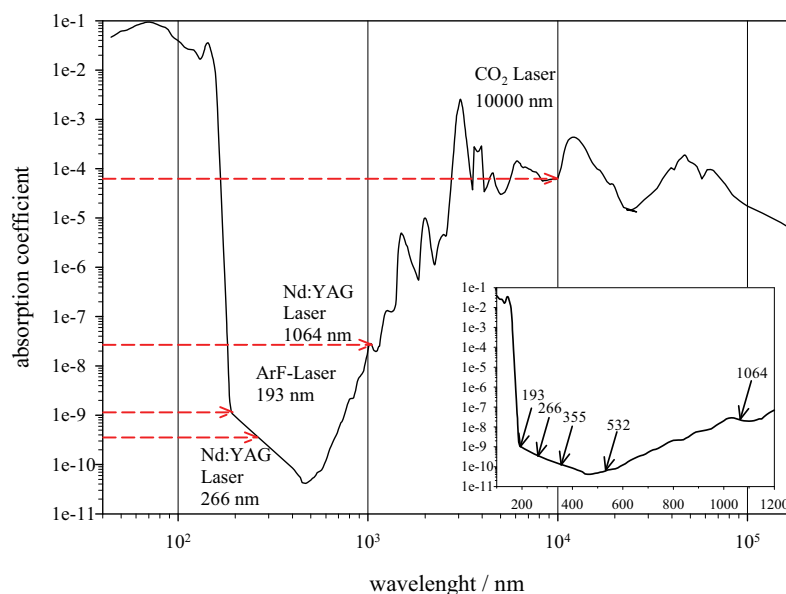


Figure 11: Absorption coefficient of ice for different wavelengths (Warren, 1984). At 1064 nm wavelength the absorption coefficient of ice is two orders of magnitude higher than for 266 nm wavelength.

The higher the coefficient is, the more material is ablated by a given laser pulse power. It can easily be seen that doubling, quadrupling or quintupling the Nd:YAG frequency would result in lower absorption coefficients and consequently higher transparency of UV light. Below 190 nm the absorption coefficient increases again. Working with wavelengths below 190 nm implies that the beamline has to be hermetically sealed, because the air absorbs this laser light.

The ablation efficiency increases by 3 orders of magnitude using a CO₂ laser ablation system, working at 10600 nm. So far it was not possible to test this kind of laser for laser ablation analysis of ice. Presumably the sample would be destroyed by high absorption without using any filter system between the laser rod and sample surface. For this study a Nd:YAG system (1064 nm) was used.

Beside the choice of laser wavelength, the adjusting of laser energy is of importance. The used laser energy depends on the melting and evaporation point of the sample. In the system used for laser ablation of ice, high energy results in intensified blasting of the sample whereas low energy results in reduced ablation efficiency. The optimization of the laser ablation system used for ice core analysis is described in detail by Reinhardt (2002).

3.3 Calibration standards

One question which has to be answered before the analysis can start is: Do I have suitable standards for the calibration of the system? Matrix matching is necessary because the ablation rate (quantity of mass ablated per laser pulse) varies with the sample matrix. For the analysis of geological samples by LA-ICP-MS, where the laser ablation system is mainly applied, meanwhile several standards are commercially available. The analysis of frozen ice by LA-ICP-MS is not widely spread and therefore standards have to be prepared in the laboratory. H₂O is the matrix of ice samples, therefore water-based standards can be used for the calibration. Commercially available ICP-MS multi-element stock solutions (Perkin Elmer) were used for external calibration of the ICP-MS systems for liquid and frozen ice core samples. Moreover, first investigations were accomplished to prepare frozen ice standards with homogeneously embedded particles. For this purpose the NIST 1648 reference material was used.

3.3.1 Multi-element solutions for calibration standards

A: PERKIN ELMER Multi-element Verification Standard

Elements: Ce, Dy, Er, Eu, Gd, Ho, La, Lu, Nd, Pr, Sm, Sc, Tb, Th, Tm, Y, Yb in 5% HNO₃, concentration: 10 mg L⁻¹, PE Nr. N930-0232

B: PERKIN ELMER Multielement Verification Standard

Elements: Ag, Al, As, Ba, Be, Bi, Ca, Cd, Co, Cr, Cs, Cu, Fe, Ga, In, K, Li, Mg, Mn, Na, Ni, Pb, Rb, Se, Sr, Tl, V, U, Zn in 5% HNO₃, concentration: 10 mg L⁻¹, PE Nr. N930-0233

- C: PERKIN ELMER Multielement-Verification-Standard
Elements: Au, Hf, Ir, Pd, Pt, Rh, Ru, Sb, Sn, Te in 10% HCl, concentration: 10 mg L⁻¹, PE Nr. N930-0234
- D: FMS AWI-II, High-Purity standards
Elements: Mg, Rh, Ba, Ce, Pb in 2% HNO₃, concentration: 10 mg L⁻¹
- E: Rh-solution (RhCl₃), MERCK
1000 mg L⁻¹ for ICP-MS, RhCl₃ in 8% HCl, No: K24758650 803
- F: diluted Rh-solution (1 mg L⁻¹)
- 100 µg L⁻¹ solution E
 - 2 mL HCl (30%, suprapure, Merck)
 - filled up to a volume of 100 mL with ultrapure water
- G: diluted multi-element solution 1 (200 µg L⁻¹)
- 2 mL of solution A, B, C
 - 2 mL HNO₃ (distilled 65%, p.a., Merck)
 - filled up to a volume of 100 mL with ultrapure water
- H: diluted multi-element solution 2 (10 µg L⁻¹)
- 100 µL of solution A, B, C
 - 2 mL HNO₃ (distilled 65%, p.a., Merck)
 - filled up to a volume of 100 mL with ultrapure water

3.3.2 Preparation of multi-element calibration standards

All labware which came into contact with samples and standards were run through a special cleaning procedure described elsewhere (Publication V). A reverse osmosis system coupled to a Purelab ultra system (Elga, High Wycombe, U.K.) produced ultrapure water. Steps for standard preparation were carried out under a clean bench US Class 100 installed in a clean room US class 10000. For standard preparation volumetric flasks (PTFE) were used.

Concentrations of calibration standards ranged from 1 ng L⁻¹ to 100 µg L⁻¹. All standards contained 10 µg L⁻¹ Rh for ICP-Q-MS and 1 µg L⁻¹ Rh for ICP-TOF-MS analysis as internal standard. Defined volumes of multi-element solutions were filled into volumetric flasks (PTFE), acidified with HNO₃ (distilled, 65% HNO₃, p.a., Merck) and filled up with ultrapure water. Low concentrated standards were prepared from diluted multi-element solutions. Detailed information about the preparation of multi-element standards used is given in Table 1.

Daily optimization was done to reduce possible interferences and to obtain maximum signal intensity. This was done by analysing the so called Daily Performance (DP) standard, which contained five elements covering the entire mass range:

- 500 µL of solution D for ICP-Q-MS analysis, 50 µL of solution D for ICP-TOF-MS analysis

- 10 mL of HNO₃ (distilled 65% HNO₃, pro analysis, Merck)
- filled up to a volume of 500 mL with ultra pure water

Table 1: Preparation of calibration standards for Quadrupole (Q) and Time of Flight (TOF) ICP-MS systems using solutions A-C and F-H (see text, chapter 3.3.1).

Standard	size of volumetric flask / mL	HNO ₃ [mL] (distilled 65 %, p.a., Merck)	solution F [μL] Q / TOF	X mL from standard Y	solution G [μL]	solution H [μL]	solution A, B, C [μL]
Blank	100	2	1000 / 100	-	-	-	-
1 ng L ⁻¹	100	1.8	900 / 90	10 ml / 10 ng L ⁻¹	-	-	-
10 ng L ⁻¹	100	2	999 / 99	-	-	100	-
20 ng L ⁻¹	100	2	998 / 98	-	-	200	-
50 ng L ⁻¹	100	2	995 / 95	-	-	500	-
0.1 μg L ⁻¹	100	2	990 / 90	-	-	1000	-
0.5 μg L ⁻¹	50	1	950 / 25	-	125	-	-
1 μg L ⁻¹	100	2	900 / 0	-	500	-	-
5 μg L ⁻¹	50	1	500 / 0	-	1250	-	-
10 μg L ⁻¹	50	1	-	-	-	-	50
20 μg L ⁻¹	50	1	-	-	-	-	100
50 μg L ⁻¹	50	1	-	-	-	-	250
100 μg L ⁻¹	100	2	-	-	-	-	1000

For the quantitative determination of trace elements in frozen ice cores a stepwise freezing procedure of calibration standards was developed by Reinhardt (2002) for the calibration of the LA-ICP-MS system. In contrast to freezing the entire volume of standard in one step, this procedure reduces the inhomogeneity of ice standards (the relative standard deviations (RSD) of replicate analysis decrease from 30% to < 10%). 5 mL of the calibration standard solution is transferred into a pre-cleaned Petri dishes under a clean bench US class 100 installed in a cold room at -20°C (Figure 12). This step is repeated 4 times every 30 minutes.

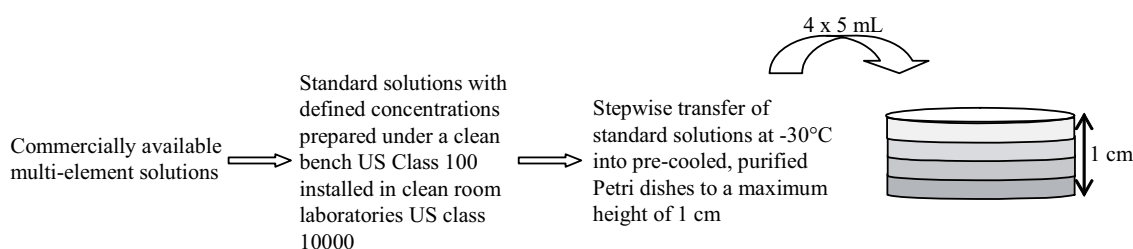


Figure 12: Schematic of the preparation of calibration standards for the LA-ICP-MS analysis of frozen ice core samples. Multi-element solutions are stepwise frozen in Petri dishes under a clean bench US Class 100 installed in an ice laboratory.

3.3.3 Particulate matter for calibration standards with embedded particles

A: National Institute for Standards and Technology: NIST 1648

Certified elements: Al, As, Cd, Cu, Cr, Fe, K, Mn, Na, Ni, Pb, Se, U, V, Zn

Noncertified elements: Ag, Ba, Ce, Cl, Co, Cs, Eu, Hf, I, In, La, Mg, Ru, S, Sb, Sc, Sn, Th, Ti, W

3.3.4 Improvement of the preparation of calibration standards with embedded particles

Due to matrix matching of calibration standards, the analysis of particle horizons in ice cores demands a calibration with ice standards with embedded particles. Therefore, a method to produce standards with homogeneously distributed particles was developed. For test measurements the standard reference material NIST 1648 was used. This is an urban particulate matter.

First, different amounts of reference material NIST 1648 were put into pre-cleaned polyethylene (PE) flasks. A fraction of ultrapure water was added. This mixture was acidified with distilled HNO₃ (65% HNO₃, p.a., Merck) to accord to the laboratory rule of adding the acid to the water. To obtain the standard solution, containing suspended and dissolved NIST 1648, the volumetric flask was filled to its calibration mark with ultrapure water. Detailed information about the preparation of six different NIST 1648 standards is given in Table 2.

Table 2: Preparation of calibration ice standards with defined amounts of particulate matter (standard reference material NIST 1648) for laser ablation ICP-MS analysis. Moreover, the concentration of each certified and noncertified (grey shaded) element in each standard is calculated.

	Standard 1	Standard 2	Standard 3	Standard 4	Standard 5	Standard 6
NIST 1648 / mg			12.3	12.2	24.6	50
x mL from Standard y	0.626 mL from Standard 4	7 mL from Standard 4				
HNO ₃ / mL	2	2	20	10	10	10
final volume / mL	100	100	1000	500	500	500
	$\mu\text{g kg}^{-1}$	$\mu\text{g kg}^{-1}$	$\mu\text{g kg}^{-1}$	$\mu\text{g kg}^{-1}$	$\mu\text{g kg}^{-1}$	$\mu\text{g kg}^{-1}$
Na	0.65	7.26	52.3	104	209	422
Mg	1.22	13.7	98.4	195	394	795
Al	5.22	58.4	421	834	1683	3399
K	1.60	17.9	129	256	517	1044
V	0.02	0.24	1.72	3.42	6.89	13.9
Cr	0.06	0.69	4.96	9.83	19.83	40.06
Mn	0.13	1.47	10.6	21.0	42.3	85.5
Fe	5.97	66.8	481	954	1924	3887
Ni	0.01	0.14	1.01	2.00	4.03	8.15
Co	0.003	0.03	0.22	0.44	0.89	1.79
Cu	0.09	1.04	7.49	14.9	30.0	60.5
Zn	0.73	8.13	58.5	116	234	473
As	0.02	0.20	1.41	2.81	5.66	11.4
Se	0.00	0.05	0.33	0.66	1.33	2.68
Ag	0.001	0.01	0.07	0.15	0.30	0.60
Cd	0.01	0.13	0.92	1.83	3.69	7.46
In	0.0002	0.00	0.01	0.02	0.05	0.10
Ba	0.11	1.26	9.07	18.0	36.3	73.3
La	0.01	0.07	0.52	1.02	2.07	4.17
Ce	0.001	0.01	0.06	0.12	0.25	0.50
Eu	0.000	0.00	0.01	0.02	0.04	0.08
Pb	1.00	11.2	80.6	160	322	651
Th	0.001	0.01	0.09	0.18	0.36	0.74
U	0.001	0.01	0.07	0.13	0.27	0.55

According to the expected element concentrations in polar ice cores with embedded particles, the amount of NIST 1648 used for calibration standard preparation was chosen. As it is shown in Table 2, the used amount of NIST 1648 was always smaller than 100 mg. According to the manufacturer, due to the homogeneity of the standard, a minimum of 100 mg of the dried material should be used for any analytical determination to be related to the certified values of the certificate. Therefore it was expected, that the quality of the calibrations and the RSD of replicate analysis were influenced and that the correlation coefficients would not be ideal.

The liquid standards with suspended particles were shaken for a minimum time of 30 minutes. The stepwise freezing procedure (Figure 13) was accomplished under a clean bench US Class 100 installed in an ice laboratory. Figure 13 illustrates the developed freezing procedure of the diluted NIST 1648 reference material. One Petri dish (\varnothing 5 cm) was placed upon a smaller Petri dish which was filled with liquid nitrogen. 1 mL of the standard solution was pipetted into the upper Petri dish and liquid nitrogen was used for shock-freezing. The bottle containing the standard solution with suspended NIST 1648 was shaken again and once more 1 mL of the standard solution was pipetted into the upper Petri dish and shock-frozen again. This procedure was repeated several times until the Petri dish was filled up. Nitrogen is used for shock-freezing to avoid coagulation of particles within the standard and hence to increase the homogeneity of the frozen ice standard.

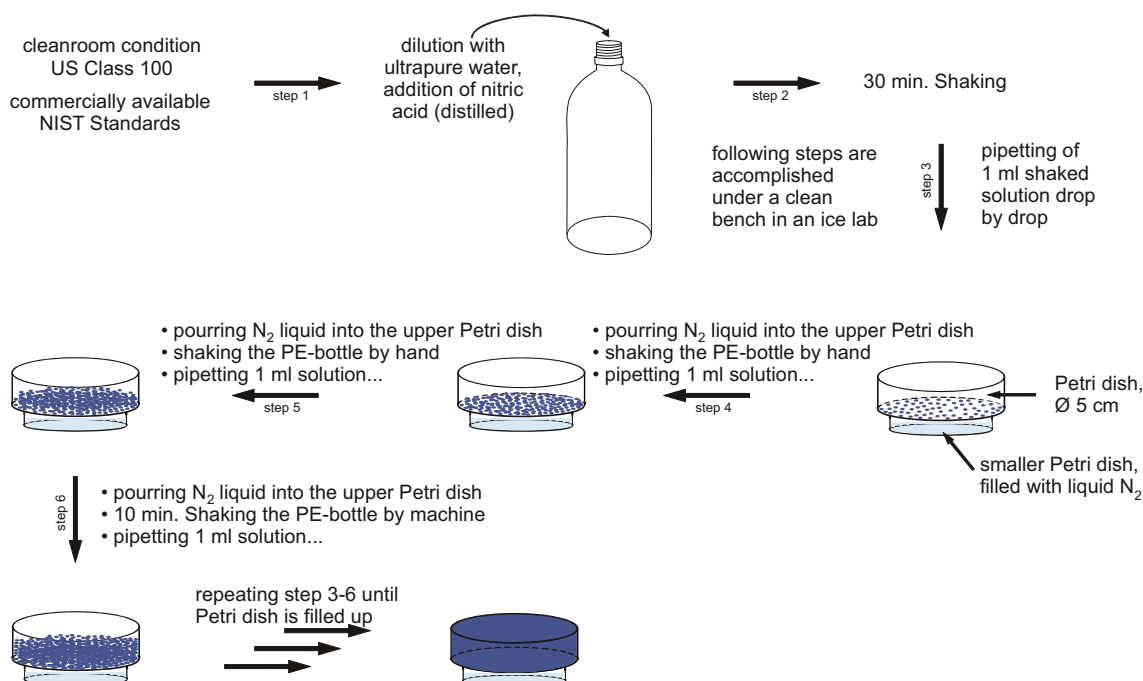


Figure 13: Preparation of calibration standards with homogeneously distributed embedded particles (reference material NIST 1648). The stepwise freezing procedure enables acceptable homogeneity of the calibration standards.

Due to problems with the ICP-TOF-MS system, the analyses of these standards were so far only tested with the LA-ICP-Q-MS system in respect to the linearity of calibration standards. The optimization procedure of the LA-ICP-Q-MS system is presented by Reinhardt (2002). Ideal laser settings in the presented thesis were: Laser energy: 380 mJ; Focus: on the sample surface; Q-Switch: 190 μs . Analysis showed, that the homogeneity of the standards increased with increasing NIST 1648 concentration, which is presented by decreasing RSD of replicate analysis. As example, Figure 14 shows the signal variation of ^{208}Pb , as relative intensity (normalized to ^{17}OH), for different calibration standards. A detailed description for internal standardisation and why it is accomplished is given in chapter 5.4.

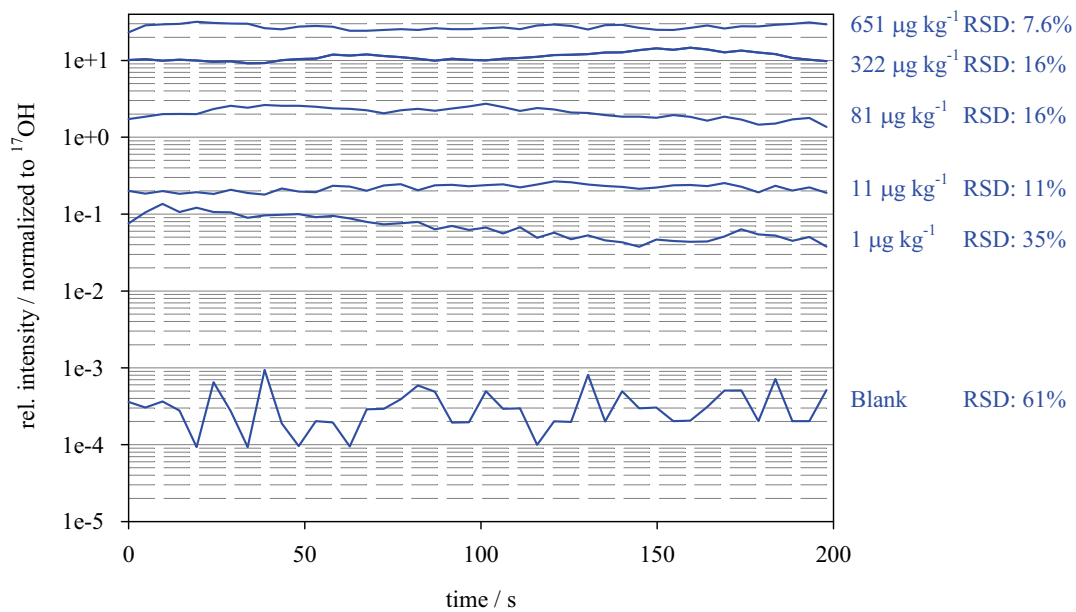


Figure 14: Signal variations of replicate analysis of ^{208}Pb of six different ice standards with embedded NIST 1648 particles obtained by LA-ICP-Q-MS analysis. The homogeneity of standards increases with increasing particle concentration which is presented by decreasing RSD values.

The RSD of ^{208}Pb decreased from 61% for the blank, to 35% for a $1 \mu\text{g kg}^{-1}$ standard and finally to 7.6% for a $651 \mu\text{g kg}^{-1}$ standard. Moreover, Figure 14 shows linear dependency of the signal intensity and the concentration. Linear dependency is also shown for all other elements. Table 3 lists calibration data for elements analysed. The RSD of replicate analysis is anti-correlated to the concentration of elements. For some elements, the calculated DL (3σ criterion of the blank, 10 replicate analyses) is lower than the standard defining the lower limit of linear calibration. Only concentrations of real ice core samples, exceeding both, the lowest calibration standard and the DL, can be evaluated. The calibration studies showed that the presented procedure to be a promising method to quantify particles embedded in frozen ice cores. Due to problems with the ICP-TOF-MS system at the present state it was not possible to test this calibration procedure for the analysis of real ice core samples.

Table 3: LA-ICP-Q-MS calibration data of ice standards with embedded particles (standard reference material NIST 1648). The number of standards used for calibration (inclusive blank), the lowest and highest concentrated standard defining the linear calibration range, the associated RSD of replicate analysis (n=40), the correlation coefficient and the detection limit (DL) are given.

	no. of data points for calib.	concentration range		homogeneity of standards		r^2	DL / $\mu\text{g kg}^{-1}$
		conc. of lowest conc. standard / $\mu\text{g kg}^{-1}$	conc. of highest conc. standard / $\mu\text{g kg}^{-1}$	RSD of lowest conc. Standard / %	RSD of highest conc. Standard / %		
²³ Na	4	104	422	12.5	16.4	0.9791	0.134
²⁴ Mg	6	1.22	795	26.8	8.6	0.9865	0.173
²⁷ Al	6	5.22	3399	30.9	15.6	0.9473	4.46
³⁹ K	6	17.9	1044	17.1	20.4	0.9022	2.43
⁵² Cr	6	0.688	40.1	22.3	21.3	0.9921	0.697
⁵⁵ Mn	6	1.47	85.5	21.0	9.2	0.9794	0.216
⁵⁷ Fe	7	5.97	3887	46.9	12.3	0.9993	8.81
⁵⁹ Co	5	0.221	1.79	15.3	17.2	0.9970	0.077
⁶³ Cu	7	0.093	60.5	39.5	9.7	0.9496	0.214
⁶⁴ Zn	6	8.13	473	27.3	11.1	0.9735	0.325
¹¹⁴ Cd	5	0.923	7.46	22.4	9.8	0.9712	0.092
¹⁴⁰ Ce	7	0.001	0.497	55.9	10.9	0.9549	0.001
²⁰⁸ Pb	6	1.00	651	35.2	7.6	0.9952	0.017
²³⁸ U	5	0.068	0.547	30.5	17.8	0.9932	0.007

4 Performance study of the ICP-TOF-MS system for the analysis of liquid samples

The use of simultaneously analysing systems allows the analysis of all isotopes of interest in a short time (*e.g.* 25000 spectra per second). Therefore the new ICP-TOF-MS system was setup. Investigations should clarify the benefit of this system for the analysis of ultra low concentrations in liquid and solid samples.

Evaluation of the data was done using the *interactive data language* (IDL[®]) as programming software. A program written by myself enabled fast data acquisition of ICP-TOF-MS raw data (see Appendix, A6). Out of each spectrum, consisting of 34000 single data (see chapter 3.1.6), the peak integral areas (= signal intensities) of isotopes of interest were extracted. These signal intensities were processed using Microsoft Excel.

Analysis showed that signal intensities increased during the day by about 20%. This might be explained by thermal effects. Further, sometimes parts of the spectrum showed extremely high intensities which could not be proven by replicate analysis. Therefore peak integral area data of extracted isotopes were controlled for each spectrum to see whether there is some kind of irregularity or not.

4.1 Comparison of different sample introduction systems

Three different nebulizer systems were tested for performance studies of the ICP-TOF-MS system: the CFN, a cyclonic spray chamber with concentric nebulizer and a microconcentric nebulizer with desolvation unit (Aridus II). Each sample introduction system needs specific instrumental settings (Table 4).

Table 4: Instrumental settings for the ICP-TOF-MS system coupled to three different nebulizer systems: Cross flow nebulizer (CFN), concentric nebulizer with cyclonic spray chamber and microconcentric nebulizer with desolvation unit (Aridus II).

Nebulizer	CFN	conc. nebulizer with cyclonic spray chamber	Aridus II
Detector / V	2230	2230	2230
Sweeps	175000	175000	175000
replicates	200	200	200
Plasma / W	1050	1100	1050
Nebulizer gas / L min ⁻¹	1.05	1.2	0.98
Auxiliary gas / L min ⁻¹	1.2	1.5	1.4
Plasma gas / L min ⁻¹	15	15	14.5
peristaltic pump /rpm	30	30	
Sweep Gas / L min ⁻¹			5.1
N ₂ / mL min ⁻¹			22
spray chamber /°C			110
Membrane /°C			160

Constant instrumental settings such as the detector voltage, sweeps (= number of analyses per replicate), replicates and the parameter for the peristaltic pump (for not self aspirating nebulizers) enabled the comparison of the different nebulizing systems. All experiments were carried out analysing a $1 \mu\text{g L}^{-1}$ DP standard. Regarding to the analysis of natural ice core samples instrumental characteristics were set to achieve highest signal sensitivities for REE. Ce, included in the analysed DP standard, and other REE are important elements for climate research.

Figure 15 shows mass spectra using the above mentioned sample introduction systems. Lowest signal intensities for ^{24}Mg , ^{103}Rh , ^{138}Ba , ^{140}Ce and ^{208}Pb are obtained by CFA-ICP-TOF-MS analysis and highest signal intensities are obtained by Aridus II-ICP-TOF-MS analysis. In all three mass spectra interferences by $^{40}\text{Ar}^+$ ions are visible. Interferences based on oxygen species are present using the CFN and concentric nebulizer with cyclonic spray chamber as sample introduction system. The addition of nitrogen when using the Aridus II is reflected in nitrogen based interferences. The removal of water by the Aridus II system leads to distinct reduction of the oxide species of ^{140}Ce .

Table 5 lists all signal intensities in counts per second (cps) as well as other parameters for different sample introduction systems obtained for a $1 \mu\text{g L}^{-1}$ DP standard. The signal intensities are expressed as cps. These studies showed low signal intensities for the CFN system. Compared to well establish systems, *e.g.* coupling the CFN to an ICP-Q-MS (Elan6000, Perkin/Elmer Sciex) system, the signal intensity of the CFN-ICP-TOF-MS technique was lower by a factor of 400. Further, high RSD (about 4%) as well as an extremely high degree of oxide formation (MO^+) and doubly charged ion formation (M^{2+}) (74% and 14% respectively) demanded an alternative sample introduction system. In contrast to the CFN system, the cyclonic spray chamber with concentric nebulizer resulted in a signal increase by a factor of 2 and a reduction of the degree of M^{2+} and MO^+ formation by a factor of 2. But still, such high MO^+ intensities disabled the analysis of REE at low concentrations. The RSD increased to a median value of 6%. The Aridus II as sample introduction system provided the best results. Compared to the conventional CFN system it showed on average increased sensitivity by a factor of 10 and specifically a factor of 50 for Ce. The degree of M^{2+} formation was similar for the CFN and the Aridus II sample introduction systems and the formation of MO^+ decreased significantly from 74% (CFN) to 0.3% (Aridus II). In addition, the Aridus II system lead to lower background signals (20 cps) compared to the CFN system (90 cps) and concentric nebulizer with cyclonic spray chamber (100 cps).

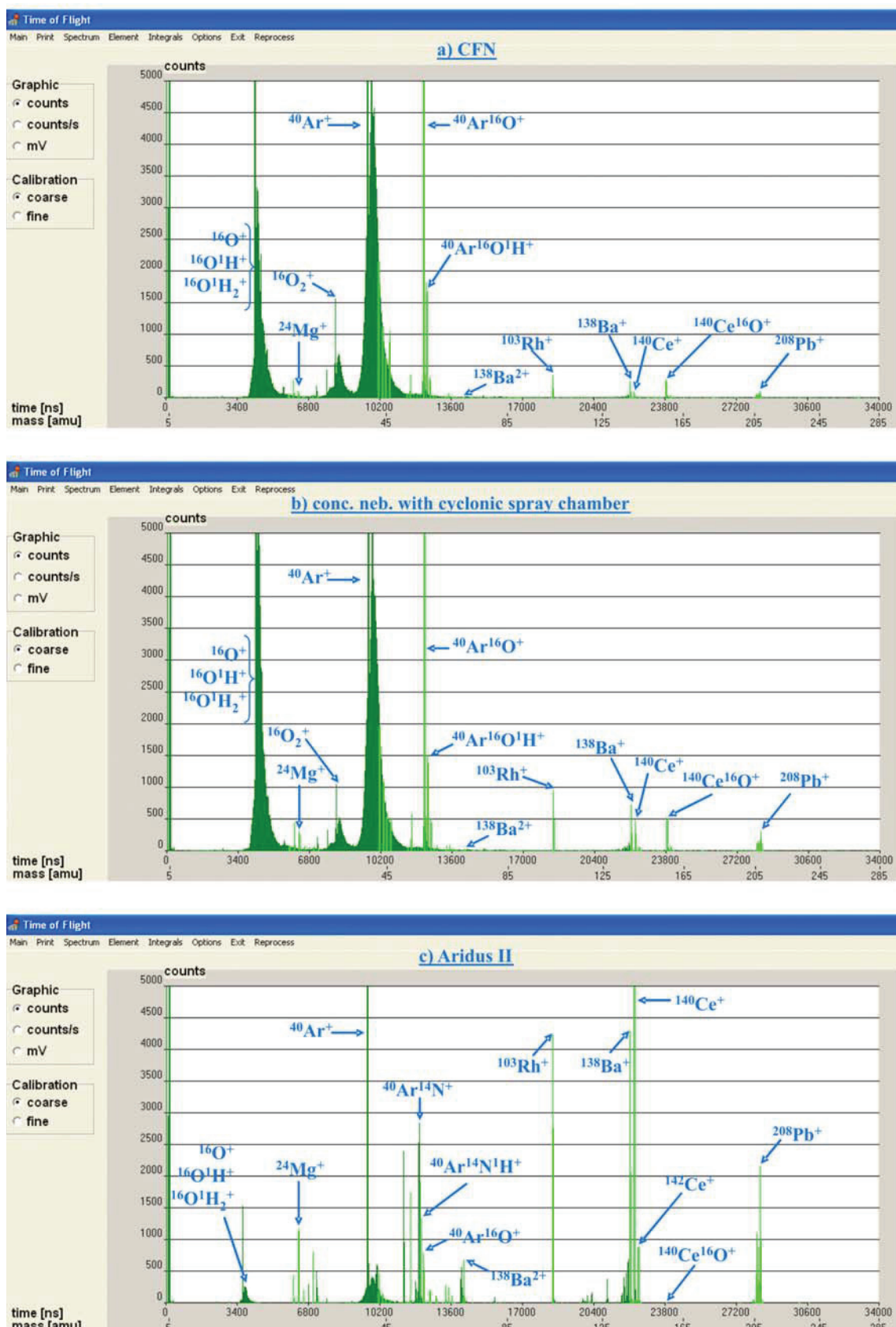


Figure 15: Screenshot of ICP-TOF-MS mass spectra with identification of peaks for a $1 \mu\text{g L}^{-1}$ DP standard using different sample introduction systems: a) CFN, b) concentric nebulizer with cyclonic spray chamber and c) Aridus II. Oxygen based interferences are visible for nebulizer a and b (e.g. $^{16}\text{O}^+$, $^{40}\text{Ar}^{16}\text{O}^+$), nitrogen based interferences are visible for nebulizer c (e.g. $^{40}\text{Ar}^{14}\text{N}^+$, $^{40}\text{Ar}^{14}\text{N}^{16}\text{H}^+$). The degree of oxide formation decreased significantly for nebulizer c.

Table 5: Signal intensities in cps ($\mu\text{g L}^{-1}$)⁻¹ with RSD (10 replicates), background signals (Bkgd) for m/z ratios 8 and 220 and the degree of M^{2+} and MO^+ formation in % of a $1 \mu\text{g L}^{-1}$ DP standard analysed by ICP-TOF-MS using different nebulization systems (CFN, concentric nebulizer with cyclonic spray chamber, Aridus II (microconcentric nebulizer with desolvation unit)).

	CFN		conc. Neb. with cyclonic spray chamber		Aridus II	
	cps	RSD %	cps	RSD %	cps	RSD %
²⁴ Mg	400	4	800	7	2600	2
²⁵ Mg	200	6	200	6	400	5
¹⁰³ Rh	1400	3	3300	6	13000	2
²⁰⁶ Pb	400	4	800	6	4400	2
²⁰⁷ Pb	300	4	700	6	3900	2
²⁰⁸ Pb	700	3	1600	6	9500	2
⁶⁹ Ba ²⁺	200	5	300	4	2200	2
¹³⁸ Ba	1200	3	3100	6	15000	2
¹⁴⁰ Ce	400	4	2000	2	23000	2
¹⁵⁶ CeO	1200	3	1900	12	69	12
⁸ Bkgd	100	7	120	7	20	15
²²⁰ Bkgd	80	8	80	8	20	15
M^{2+} /%	14.4		7.6		12.7	
MO^+ /%	73.6		48.8		0.3	

These experiments revealed that low concentrations (some ng L^{-1}) of REE and other trace elements as to be expected in ice core samples from polar regions (Gabrielli *et al.*, 2006; Tao *et al.*, 2001) can only be successfully analysed using the Aridus II as sample introduction system. According to Table 5 a 1 ng L^{-1} standard would result in 23 cps for Ce, which is above the background noise of 20 cps. For the CFN as well as the concentric nebulizer system achievable signal intensities for a 1 ng L^{-1} standard (0.4 cps and 2 cps respectively) would be far below to the background noise level and are therefore not detectable.

4.2 Parameter study: Aridus II-ICP-TOF-MS

Before analysing liquid samples, the performance of the Aridus II-ICP-TOF-MS system was checked. Maximum intensities of Mg, Rh, Ba, Ce and Pb of a $1 \mu\text{g L}^{-1}$ DP standard (see chapter 3.3) indicated the right position of the plasma torch.

Figure 17 illustrates the dependency of the signal intensity in counts per second as well as the degree of MO^+ and M^{2+} formation on the plasma power, nebulizer gas-, sweepgas- and nitrogen gas flow. ¹³⁸Ba²⁺ ($m/z = 69$) is taken as doubly charged ion tracer, it interferes the determination of ⁶⁹Ga⁺ ($m/z = 69$). ¹⁴⁰Ce¹⁶O⁺ ($m/z = 156$) interferes the analysis of ¹⁵⁶Gd⁺ and ¹⁵⁶Dy⁺ (both: $m/z = 156$). M^{2+} corresponds to the signal intensity ratio $^{138}\text{Ba}^{2+}/(^{138}\text{Ba}^{2+} + ^{138}\text{Ba}^+)$; MO^+ corresponds to the signal intensity ratio $^{140}\text{Ce}^{16}\text{O}^+/(^{140}\text{Ce}^{16}\text{O}^+ + ^{140}\text{Ce}^+)$. These proxies (M^{2+} and MO^+) must be minimized

to enable the analysis of analyte masses. As shown in Figure 17, for multi-element analysis a compromise, in respect to signal intensity and the degree of M^{2+} and MO^+ formation, must always be made.

4.2.1 ICP parameter

Plasma power: The analyte signal decreased with increasing plasma power. If the plasma power, hence the plasma temperature, increased, the M^{2+} formation increased because there was enough energy for the second ionisation process. However, increasing plasma power resulted in decreasing oxide formation until 1050/1100 W, afterwards the MO^+ rate slightly increased. The ICP-TOF-MS systems shut down several times using a plasma power below 1000 W. For the analysis of samples a plasma power of 1000–1050 W is advised.

Nebulizer gas flow: The introduced sample volume increases with increasing nebulizer gas flow for self aspirating nebulizers. Therefore, the analyte signal is positively correlated with the nebulizer gas flow. At increasing nebulizer gas flow the droplet size decreases and thus the analyte introduction goes up. However this is at the expense of the residence time in the plasma, the plasma temperature and thus also the ionisation. Therefore an increase of the gas flow resulted in decreasing M^{2+} formation. The MO^+ rate decreased up to a nebulizer gas flow of 1.2 L min^{-1} because the effect of increased material input into the plasma outweighed the cooling of the plasma. MO^+ formation steeply increased above a flow of 1.2 L min^{-1} . Figure 16 illustrates the sample consumption of the Aridus II nebulizer system at different nebulizer gas flow rates. Below 0.8 L min^{-1} and above 1.15 L min^{-1} nebulizer gas flows the standard deviation (SD) of sample consumption increased. Considering all parameters the tests showed that a nebulizer gas of $\sim 1 \text{ L min}^{-1}$ is ideal for the analysis.

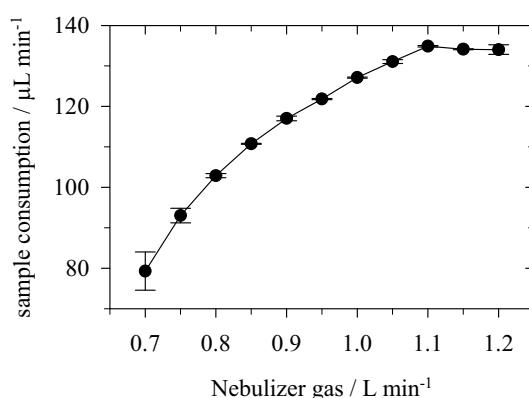


Figure 16: Sample consumption with SD (3 replicates) in $\mu\text{L min}^{-1}$ as a function of the nebulizer gas flow of the Aridus II sample introduction system.

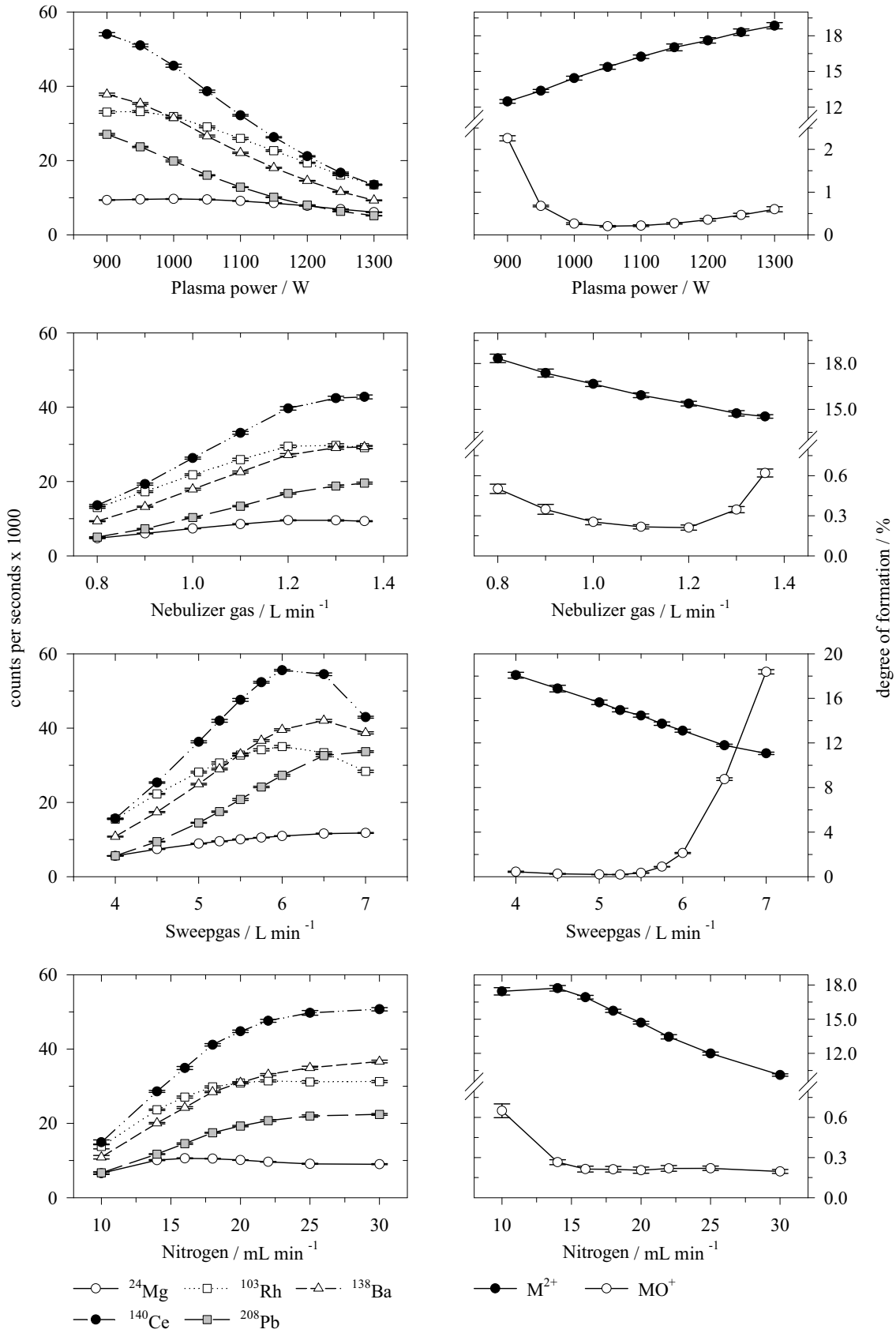


Figure 17: Signal variation with SD (20 replicates) in counts per second of a $1 \mu\text{g L}^{-1}$ DP standard containing ^{24}Mg , ^{103}Rh , ^{138}Ba , ^{140}Ce and ^{208}Pb (left side); and changes in the degree of oxide (MO^+) and doubly charged ion (M^{2+}) formation (right side) due to changes in plasma power, nebulizer-, sweep- and nitrogen gas flow obtained by the Aridus II-ICP-TOF-MS system.

4.2.2 Aridus II parameter

Sweepgas flow: Increasing the sweepgas flow from 4 to 6 L min⁻¹ resulted in an increase of signal intensities by a factor of 2 to 5. Above 6 L min⁻¹ the signal decreased again for Ce. Above 5.5 L min⁻¹ the degree of MO⁺ formation increased rapidly whereas M²⁺ intensities decreased constantly. Further the plasma stability decreased using a sweepgas flow higher 5.5 L min⁻¹. Hence, for the analysis of samples a sweepgas flow of ~5 L min⁻¹ is recommended.

Nitrogen gas flow: At 18 mL min⁻¹ ²⁴Mg showed highest sensitivity whereas the intensities of all other isotopes increased with increasing nitrogen gas flow. Above 15 mL min⁻¹ the MO⁺ rate was nearly constant. The formation of M²⁺ was more or less constant up to 15 mL min⁻¹. Gas flows higher than 15 mL min⁻¹ resulted in decreasing M²⁺ formation. Unfortunately plasma stability got worse above ~25 mL min⁻¹ leading to frequent automatic shut down of the system.

4.2.3 Day to day signal variations

The signal intensities of a 1 µg L⁻¹ DP standard obtained by Aridus II-ICP-TOF-MS changed from day to day (Figure 18). Considering the time slice from the 21.07.2007 till the 26.03.2008, ²⁴Mg signal intensities varied by 54%, ¹⁰³Rh signal intensities by 28%, ¹³⁸Ba signal intensities by 23%, ¹⁴⁰Ce signal intensities by 21% and ²⁰⁸Pb signal intensities by 20%. Therefore, in the Tables presented in this thesis, different signal intensities for a 1 µg L⁻¹ DP standard obtained at different sampling days are shown.

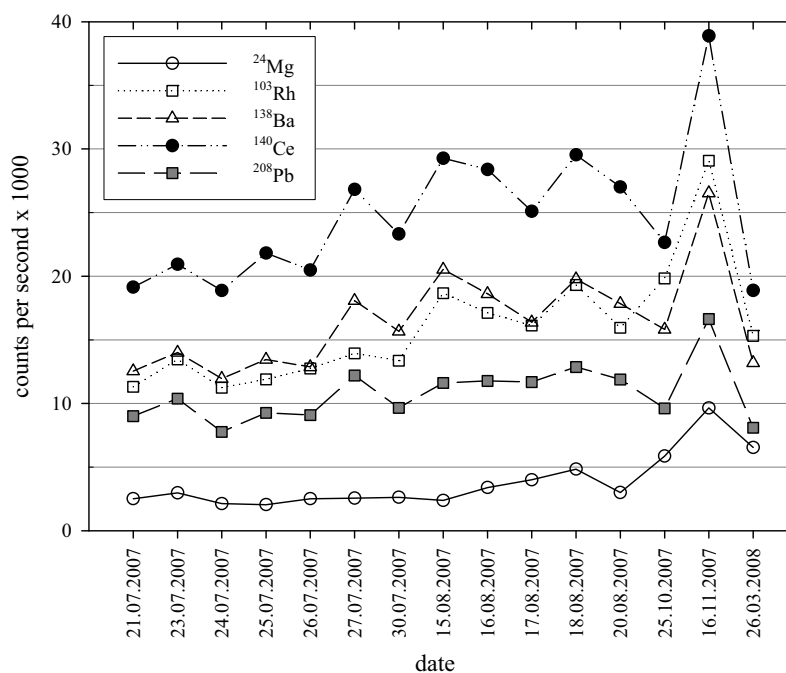


Figure 18: Day to day signal variations of a 1 µg L⁻¹ DP standard obtained by Aridus II-ICP-TOF-MS analysis within the time slice from the 21.07.2007 till the 26.03.2008.

4.3 Interference studies

In chapter 3.1.7 three different types of possible interferences in ICP-MS studies are described. Isobaric interferences and spectral interferences can be considered by equations (10 and 11, respectively), hence the analyte signal can be adequately corrected.

$${}^m X_{corr} = {}^m X - \frac{{}^m Y_A \cdot {}^n Y}{{}^n Y_A} \quad (10)$$

$${}^m X_{corr} = {}^m X - oxide \cdot \frac{{}^{m-16} Y_A \cdot {}^{16} O_A}{{}^n Y_A} \quad (11)$$

with:

${}^m X$ = signal intensity of isotope X with mass m

${}^m Y_A$ = abundance of isotope Y with mass m in %

${}^n Y_A$ = abundance of isotope Y with mass n in %

${}^n Y$ = signal intensity of isotope Y with mass n

$$oxide = \frac{\text{signal intensity of } {}^{140}\text{Ce}^{16}\text{O}^+}{\text{signal intensity of } ({}^{140}\text{Ce}^{16}\text{O}^+ + {}^{140}\text{Ce}^+)}$$

${}^{m-16} Y_A$ = abundance of isotope Y with mass (m-16) in %

${}^{16} O_A$ = abundance of oxygen with mass 16 in %

The evaluation software for the ICP-TOF-MS system included correction equations for isotopes ${}^{58}\text{Ni}$, ${}^{69}\text{Ga}$, ${}^{138}\text{Ba}$, ${}^{142}\text{Nd}$, ${}^{144}\text{Nd}$, ${}^{155}\text{Gd}$, ${}^{157}\text{Gd}$, ${}^{159}\text{Tb}$, ${}^{161}\text{Dy}$, ${}^{163}\text{Dy}$, ${}^{166}\text{Er}$, ${}^{167}\text{Er}$, ${}^{168}\text{Er}$, ${}^{164}\text{Dy}$, ${}^{156}\text{Gd}$, ${}^{158}\text{Gd}$, ${}^{169}\text{Tm}$, ${}^{171}\text{Yb}$, ${}^{172}\text{Yb}$, ${}^{173}\text{Yb}$, ${}^{174}\text{Yb}$, ${}^{175}\text{Lu}$ and ${}^{191}\text{Ir}$ (see Appendix A6). The very good agreement among concentrations obtained by two or more different isotopes suggested that isobaric and spectral interferences were successfully corrected and negligible.

4.4 Instrumental detection limits, spectral resolution and the dynamic range of the ICP-TOF-MS system

The instrumental detection limits (IDL) as well as the spectral resolution of the ICP-TOF-MS system are important device-specific parameters. The difference between the analyte signal and background signal, determine the performance of the analytical technique in the detection of ions. The evaluation of the analyte signal is given if the analyte signal exceeds the IDL, which is defined as three-fold variance (3σ criterion) of the background noise. Calculations of the IDL were accomplished for each calibration using the blank standard (10 replicates). Day to day changes of the IDLs were observed (RSD: 28%). The separation of ions with different m/z ratios is characterized by the spectral resolution. Table 6 shows the IDL and spectral resolution, which were

calculated according to chapter 3.1.6, for isotopes analysed. If several isotopes of one element exist it is possible to calibrate / optimize the system using the sum of these isotope intensities leading to higher sensitivity for the corresponding element. This was generally done for elements whose concentrations in natural samples are expected to be low (Table 6, grey shaded). It was found that the IDLs for the ICP-TOF-MS system are comparable to the IDLs of ICP-Q-MS system. High IDL for ^{43}Ca , ^{46}Ti , ^{53}Cr and ^{54}Fe can be explained by complex background spectra as a result of interfering species (Figure 15 and chapter 3.1.7). Moreover high IDLs of these isotopes and ^{27}Al may result from selector impulses to redirect interfering species (see chapter 3.1.5). Detailed investigations of liquid samples showed that the voltage pulse applied to the selector for the redirection of interfering species affect the analysis of neighboured masses. Moreover, the isotopic abundance of some of the above mentioned isotopes is very low resulting in high IDL. The average spectral resolution of the ICP-TOF-MS system was better compared to ICP-Q-MS systems (620 and 350, respectively).

A further criterion for the assessment of an ICP-MS system is the dynamic range of the detector. It determines the analyzable element concentration range. Table 6 shows the lowest and highest concentrated standard defining the linear calibration range. Data evaluation of ^{23}Na is problematic because only the $1\ \mu\text{g L}^{-1}$ and $5\ \mu\text{g L}^{-1}$ standard show linear dependency. Further, calibration data for m/z ratios of 23 to 72 indicate problems with data evaluation, except ^{59}Co and ^{60}Ni . This can be again explained by complex background spectra as a result of interfering species (Figure 15 and chapter 3.1.7). Ratios exceeding $m/z = 72$ show linear behaviour for an order of magnitude between 10^4 and 10^5 (= dynamic range of the detector). Conventional ICP-MS systems show a dynamic range of an order of magnitude of about 10^9 . Hoffmann and Lüdke (2005) described that for the presented ICP-TOF-MS system the well defined signal measurement becomes limited in the counting mode when the temporal succession of ions hitting the detector is so short that double pulses occur. Therefore, an additional analogue signal acquisition system was installed. The ion signals of the detector are simultaneously collected as in the counting mode, but processed by a fast AD-converter (10 ns). This mode is considerably less sensitive compared with the counting mode but permits an extension of the dynamic range by about two orders of magnitude. Unfortunately, this was not observed for the ICP-TOF-MS installed in AWI laboratories.

Samples with concentrations below the IDL or below or above the standards defining the linear calibration range were rejected and not considered for interpretation.

Table 6: Lowest and highest concentrated calibration standard defining the linear calibration range for each analysed isotope. Further the table shows the IDL in ng L^{-1} , signal intensities for a $1 \mu\text{g L}^{-1}$ standard and the calculated spectral resolution using the Aridus II as sample introduction system for the ICP-TOF-MS system.

Instrumental settings: Plasma Power: 1050 W; Nebulizer gas: 0.98 L min^{-1} ; Sweepgas: 4.9 L min^{-1} ; Nitrogen: 21 mL min^{-1} .

	calibration		IDL / ng L^{-1}	sensitivity $\text{cps} (\mu\text{g L}^{-1})^{-1}$	spectral resolution		calibration		IDL / ng L^{-1}	sensitivity $\text{cps} (\mu\text{g L}^{-1})^{-1}$	spectral resolution
	from / $\mu\text{g L}^{-1}$	to / $\mu\text{g L}^{-1}$					from / $\mu\text{g L}^{-1}$	to / $\mu\text{g L}^{-1}$			
⁷ Li	0.001	5	5.5	2000	238	¹⁴⁵ Nd	0.001	5	2.4	3200	626
²³ Na	1	5	20	6100	456	¹⁴⁶ Nd	0.001	5	0.8	6400	596
²⁴ Mg	0.5	10	37	3000	408	Nd	0.001	0.5	0.8	38000	
²⁵ Mg	0.5	10	64	490	485	¹⁴⁷ Sm	0.001	5	2.4	5200	641
²⁷ Al	1	50	634	2200	616	¹⁴⁹ Sm	0.001	10	1.7	4900	615
⁴³ Ca	10	50	3045	1800	256	¹⁵² Sm	0.001	5	1.3	9900	615
⁴⁴ Ca	5	50	477	1800	387	Sm	0.001	5	0.9	20000	
⁴⁶ Ti	10	50	12855	320	565	¹⁵¹ Eu	0.001	5	0.7	16000	630
⁵¹ V	0.01	5	2.4	11000	594	¹⁵³ Eu	0.001	5	0.5	18000	593
⁵² Cr	0.1	10	82	13000	565	Eu	0.001	5	0.3	34000	
⁵³ Cr	1	50	297	170	816	¹⁵⁵ Gd	0.001	10	2.1	5300	641
⁵⁴ Fe	20	50	95318	250	795	¹⁵⁶ Gd	0.001	10	1.2	7000	674
⁵⁵ Mn	0.5	5	61	11000	588	¹⁵⁷ Gd	0.001	10	2.6	5300	664
⁵⁶ Fe	0.1	5	19	9100	604	¹⁵⁸ Gd	0.001	10	1.0	8400	625
⁵⁷ Fe	0.1	20	136	280	631	Gd	0.001	10	0.7	26000	
Fe	0.1	5	18	9400		¹⁵⁹ Tb	0.001	0.5	0.2	35000	616
⁵⁸ Ni	0.02	5	5.6	6100	621	¹⁶¹ Dy	0.001	10	1.3	120000	610
⁵⁹ Co	0.001	5	2.0	10000	636	¹⁶³ Dy	0.001	5	0.9	8800	611
⁶⁰ Ni	0.02	20	10	2600	643	¹⁶⁴ Dy	0.001	5	0.8	10000	649
⁶² Ni	0.5	20	36	400	708	Dy	0.001	5	0.6	140000	
⁶³ Cu	0.01	1	1.2	3800	466	¹⁶⁵ Ho	0.001	0.5	0.3	32000	601
⁶⁴ Zn	0.5	10	15	4500	619	¹⁶⁶ Er	0.001	5	0.9	12000	623
⁶⁵ Cu	10	50	9.4	1600	585	¹⁶⁷ Er	0.001	5	1.3	8100	578
⁶⁶ Zn	1	10	81	300	706	¹⁶⁸ Er	0.001	5	1.5	9400	605
⁶⁹ Ga	0.05	5	16	8600	542	Er	0.001	5	0.8	29000	
⁷² Ge	0.1	50	105	160	669	¹⁶⁹ Tm	0.001	0.5	0.4	33000	676
⁷⁵ As	0.001	10	7.7	1900	593	¹⁷¹ Yb	0.001	10	2.7	4800	627
⁸⁵ Rb	0.001	5	2.5	11000	630	¹⁷² Yb	0.001	5	0.8	7100	619
⁸⁶ Sr	0.01	10	8.1	1600	602	¹⁷³ Yb	0.001	10	1.4	5300	588
⁸⁸ Sr	0.001	5	5.8	15000	642	¹⁷⁴ Yb	0.001	10	1.0	10000	626
Sr	0.001	5	5.4	17000		Yb	0.001	10	0.5	28000	
⁸⁹ Y	0.001	5	0.5	20000	639	¹⁷⁵ Lu	0.001	0.5	0.5	30000	583
¹⁰⁵ Pd	0.01	20	5.0	3400	665	¹⁹¹ Ir	0.001	10	1.7	6900	613
¹⁰⁷ Ag	0.001	10	3.4	7100	654	¹⁹³ Ir	0.001	5	0.6	12000	620
¹⁰⁹ Ag	0.001	10	2.7	5900	678	Ir	0.001	5	0.7	19000	
Ag	0.001	10	2.7	13000		¹⁹⁴ Pt	0.01	10	5.3	4100	652
¹¹¹ Cd	0.01	20	3.1	2300	765	¹⁹⁵ Pt	0.01	10	3.4	4200	658
¹¹⁴ Cd	0.001	10	2.3	5500	648	Pt	0.01	10	3.6	8400	
¹¹⁵ In	0.001	0.5	0.5	23000	633	¹⁹⁷ Au	0.05	20	4.8	7300	652
¹¹⁹ Sn	0.01	10	13	1800	625	²⁰⁴ Pb	0.01	5	36	450	763
¹²¹ Sb	0.001	10	1.6	6100	641	²⁰⁵ Tl	0.001	0.1	1.4	11000	630
¹³⁷ Ba	0.01	20	6.0	2900	685	²⁰⁶ Pb	0.01	5	3.6	6100	581
¹³⁸ Ba	0.01	5	2.4	19000	627	²⁰⁷ Pb	0.01	5	3.8	5000	671
¹³⁹ La	0.001	0.5	0.5	32000	607	²⁰⁸ Pb	0.01	10	2.9	12000	616
¹⁴⁰ Ce	0.001	1	0.6	29000	653	Pb	0.01	10	2.4	23000	
¹⁴¹ Pr	0.001	1	0.4	36000	607	²⁰⁹ Bi	0.001	5	0.9	19000	597
¹⁴² Nd	0.001	5	0.9	14000	620	²³² Th	0.001	0.5	0.4	34000	585
¹⁴³ Nd	0.001	5	2.3	4500	694	²³⁸ U	0.001	5	0.4	34000	621
¹⁴⁴ Nd	0.001	5	1.4	9700	635						

4.5 Analysis of reference materials

The validation of the ICP-TOF-MS system is performed by analysing commercially available standard reference materials (SRM). Several SRM are available for the analysis of different kind of sample matrices with varying element concentrations to ensure accurate and precise analysis. In this study three reference materials were used to validate the quality of the ICP-TOF-MS measurements:

NIST 1640: National Institute for Standards and Technology, Trace Elements in Natural Water

SLRS-4: National Research Council Canada, River Water Reference Materials for Trace Metals

SPS-SW1: Spectrapure Standards AS, Reference Material for measurements of Elements in Surface Waters

Replicate analysis of diluted samples, according to the calibration range of isotopes (Table 6), showed median RSD values (which is a measure of precision) of 1.5%. Figure 19 shows recovery rates, which are a measure of accuracy, of the certified elements for the three SRM. The ratio of analysed concentrations to certified concentrations defines the recovery rate. 58% of all analysed concentrations showed recovery rates between $100 \pm 5\%$. 82% of all samples deviated by maximal 20% from the certified concentrations. All elements showed recovery rates between 95% and 105% for at least one analysed SRM, except Ca and Zn. All evaluated concentrations of SRM are given as supplementary material in the Appendix (A7).

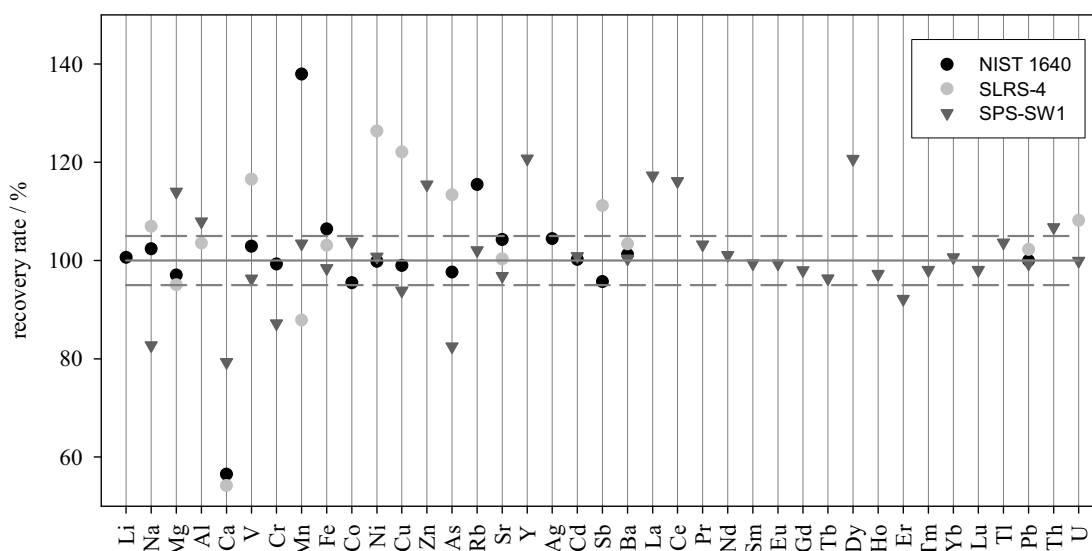


Figure 19: Recovery rates of reference materials (NIST 1640, SLRS-4, SPS-SW1) obtained by Aridus II-ICP-TOF-MS analysis. Most elements show recovery rates between 95% and 105% (dashed lines).

High Background noise levels above $m/z = 40$ to about $m/z = 72$, due to large amounts of argon and nitrogen species, influence the analysis of isotopes within this range (Leach and Hieftje, 2001). By the insertion of a collision / reaction cell in ICP-MS systems the amount of interfering species can be minimized (see chapter 3.1.7.1). Moreover, it is possible to use cool plasma conditions (see chapter 3.1.7.1) to reduce argon based interferences (Jiang *et al.*, 1988). Unfortunately performance studies showed that this technique is not possible for the ICP-TOF-MS system due to automatic shut down of the system. A detailed description of the analysis of REE in SRM and in natural ice core samples is given in Publication V.

5 Performance study of the LA-ICP-TOF-MS system for the analysis of solid samples

Information about the element pattern of ice core samples (e.g. including particle horizons in frozen ice core samples) as well as the localization of impurities in the ice matrix demand coupling the LA unit as sample introduction system to the ICP-TOF-MS system. In the supplementary material of Publication I (Figure S2) the experimental setup of the LA system is shown. Investigations of a liquid $1 \mu\text{g L}^{-1}$ DP standard by Aridus II-ICP-Q-MS and Aridus II-ICP-TOF-MS clarified the expected signal intensity for the analysis of frozen ice standards by LA-ICP-TOF-MS. Table 7 shows signal intensities with RSD of several elements, the background signal for m/z ratios of 8 and 220, as well as information about the degree of M^{2+} and MO^+ formation obtained by the mentioned systems for the analysis of liquid DP standards. Depending on the analysed isotope, the signals for the Aridus II-ICP-TOF-MS system were about a factor 2 to 10 lower than the signals for the Aridus II-ICP-Q-MS system. The formation of MO^+ was 10 times higher and the generation of M^{2+} as well as the RSD of replicate analysis was 2 times higher for the ICP-TOF-MS systems. It was expected that these ratios could be achieved by LA-ICP-TOF-MS compared to LA-ICP-Q-MS.

Table 7: Signal intensities in cps ($\mu\text{g L}^{-1}$)⁻¹ with RSD (10 replicates), background signals (Bkgd) for m/z ratios 8 and 220 and the degree of MO^+ and M^{2+} formation in % obtained by Aridus II-ICP-TOF-MS and Aridus II-ICP-Q-MS analysis of a liquid $1 \mu\text{g L}^{-1}$ DP standard.

Instrumental settings: a) Aridus II-ICP-TOF-MS: Plasma Power: 1050 W; Nebulizer gas: 0.98 L min^{-1} ; Sweepgas: 4.9 L min^{-1} ; Nitrogen: 21 mL min^{-1} ; b) Aridus II-ICP-Q-MS: Plasma Power: 1300 W; Nebulizer gas: 1.0 L min^{-1} ; Sweepgas: 2.9 L min^{-1} ; Nitrogen: 9 mL min^{-1} .

	Aridus II-ICP-TOF-MS		Aridus II-ICP-Q-MS	
	cps ($\mu\text{g L}^{-1}$) ⁻¹	RSD / %	cps ($\mu\text{g L}^{-1}$) ⁻¹	RSD / %
²⁴ Mg	2100	2	22000	1
¹⁰³ Rh	11000	2	48000	1
²⁰⁸ Pb	7800	2	51000	1
⁶⁹ Ba ²⁺	2100	2		
¹³⁸ Ba	12000	2	34000	1
¹⁴⁰ Ce	19000	2	45000	1
¹⁵⁶ CeO	50	9		
⁸ Bkgd	20	14	70	7
²²⁰ Bkgd	20	15	60	8
M^{2+} /%	15		6	
MO^+ /%	0.3		0.04	

Signal intensities for the Aridus II-ICP-TOF-MS system presented in Table 5 and Table 6 are higher than signal intensities in Table 7. In chapter 4.2.3, day to day variations of signal intensities obtained for a $1 \mu\text{g L}^{-1}$ DP standard are shown. The data for each Table shown in this thesis were taken at different days; hence the presented signal intensities diverge from each other.

5.1 Parameter study: LA-ICP-TOF-MS

Reinhardt (2002) described the optimization of the LA system. Ideal LA settings in the presented study were: Laser energy: 380 mJ; Focus: on the sample surface; Q-Switch: 190 μ s.

Parameter studies of the LA-ICP-TOF-MS system were accomplished analysing a 10 μ g kg⁻¹ DP ice standard (see chapter 3.3.2). Maximum signal intensities of Mg, Rh, Ba, Ce and Pb defined the plasma torch position. Figure 20 shows the signal intensities of Mg, Rh, Ba, Ce and Pb and the degree of MO⁺ and M²⁺ formation in dependency on plasma power, nebulizer-, plasma- and auxiliary gas variations.

Plasma power: Between 900 W and 1000 W the signal intensity did not show any trend, above 1000 W the signal intensities decreased with increasing plasma power. Below 1000 W the ICP-TOF-MS systems shut down several times. The MO⁺ as well as the M²⁺ formation increased by a factor of 2 with increasing plasma power from 900 W to 1200 W. According to Figure 20 a plasma power of 1000 W is recommended for the LA-ICP-TOF-MS system.

Nebulizer gas flow: Increasing the nebulizer gas flow from 0.5 L min⁻¹ to 0.9 L min⁻¹ resulted in an increase of signal intensities by a factor of 2. As shown by Reinhardt (2002), gas flows above 0.9 L min⁻¹ cause turbulent gas flows inside the sample chamber and therefore variations of signals increase. The MO⁺ as well as the M²⁺ formation decreased with increasing nebulizer gas flow. Low RSD values of signal intensities commend a nebulizer gas flow of 0.8 L min⁻¹.

Plasma gas flow: Varying the plasma gas flow between 14 and 17 L min⁻¹ showed maximum signal intensities as well as minimal M²⁺ and MO⁺ forming rates at 16 L min⁻¹ but the RSD of signal intensities were high (\varnothing 50%).

Auxiliary gas flow: Compared to other parameters, auxiliary gas flow variations had a negligible influence. The signal variations did not show any trend. It seems that between 1.5 L min⁻¹ and 1.6 L min⁻¹ the signal reached maximum intensities and lowest M²⁺ and MO⁺ forming rates.

In general signal intensities obtained by Aridus II-ICP-TOF-MS (Figure 17) were higher by a factor about 35 to 270 than those obtained by coupling the LA system to the ICP-TOF-MS system (Figure 20). Furthermore, the degree of M²⁺ and MO⁺ formation increased to 31% and 17% for LA-ICP-TOF-MS, respectively (Aridus II-ICP-TOF-MS: M²⁺: 12.7%; MO⁺: 0.3%). Table 8 shows calibration data obtained by the LA-ICP-TOF-MS system with optimized instrumental settings.

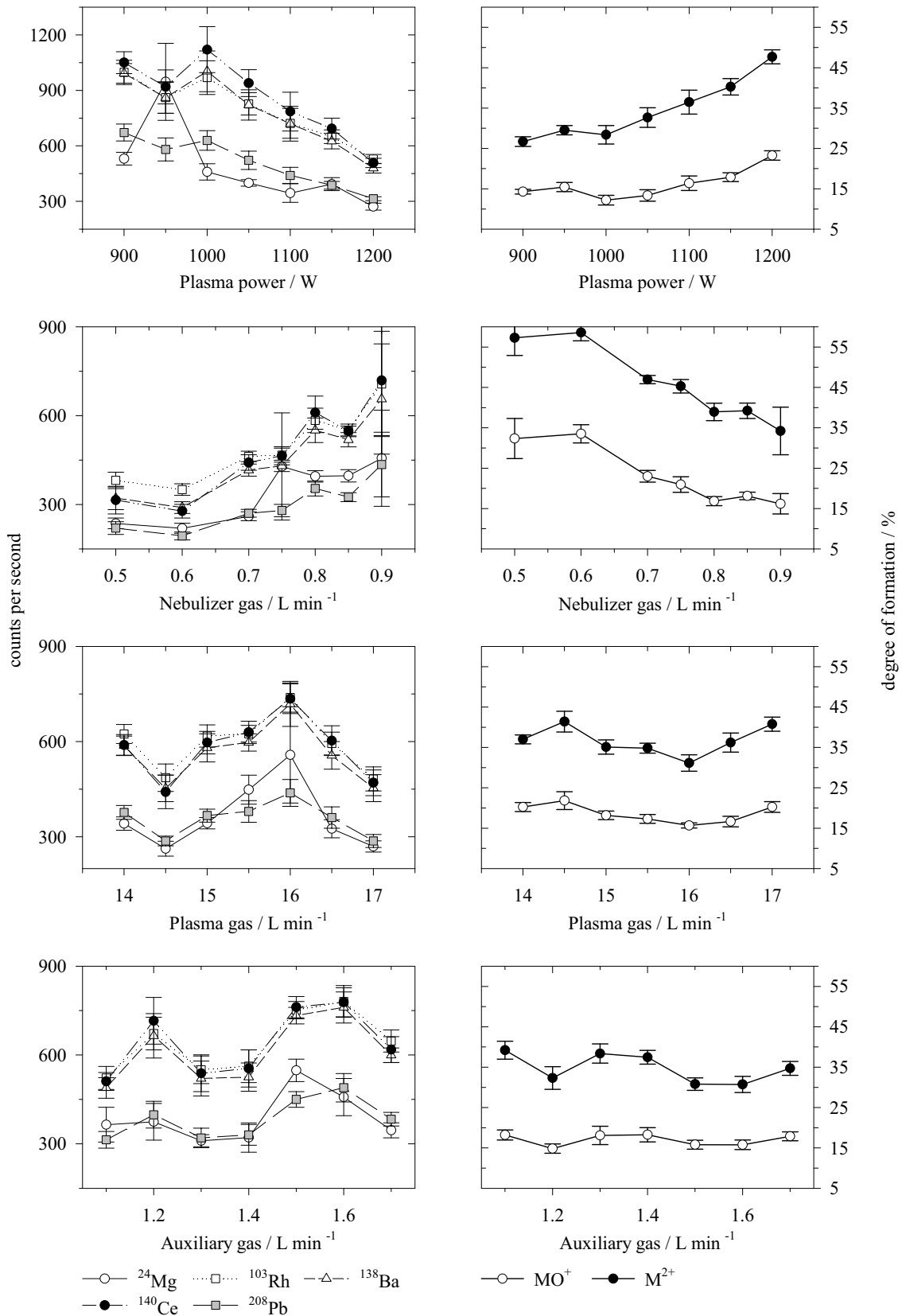


Figure 20: Signal variation with SD (20 replicates) in counts per second of a $10 \mu\text{g kg}^{-1}$ DP standard containing ^{24}Mg , ^{103}Rh , ^{138}Ba , ^{140}Ce and ^{208}Pb (left side); and changes in the degree of oxide (MO^+) and doubly charged ion (M^{2+}) formation (right side) due to changes in plasma power, nebulizer-, plasma- and auxiliary gas obtained by the LA-ICP-TOF-MS system.

Table 8: Calibration data in cps of ^{23}Na , ^{24}Mg , ^{27}Al , ^{57}Fe , ^{59}Co , ^{138}Ba , ^{140}Ce and ^{208}Pb for a Blank (0), 1-, 10- and 100 $\mu\text{g kg}^{-1}$ multi-element standard obtained by LA-ICP-TOF-MS analysis. The slope and correlation coefficient (r^2) were calculated for each isotope.

standard concentration / $\mu\text{g kg}^{-1}$	^{23}Na / cps	^{24}Mg / cps	^{27}Al / cps	^{57}Fe / cps	^{59}Co / cps	^{138}Ba / cps	^{140}Ce / cps	^{208}Pb / cps
0	14000	680	460	590	410	160	110	140
1	6700	580	450	980	540	320	230	300
10	8700	1000	2100	610	1500	1800	1400	1600
100	10000	4800	2900	690	11000	17000	14000	13000
slope	3	42	21	0	108	173	144	126
r^2	0.0023	0.9992	0.6947	0.0182	1.0000	1.0000	0.9999	0.9997

Light masses (^{23}Na , ^{24}Mg , ^{27}Al) exhibited high blank contributions. It seems that ^{23}Na and ^{57}Fe can not be evaluated at all. Only ^{24}Mg , representing light masses, showed linear dependency of the signal intensity on the concentration of the standard above $10 \mu\text{g kg}^{-1}$. Estimates indicate the possibility to analyse samples with concentrations exceeding 20 ng kg^{-1} for m/z ratios of 59, 138, 140 and 208. However, this is clearly above the expected concentration range to be expected in polar ice core samples.

5.1.1 Plasma jittering during the LA process

During the LA process the plasma jittered at 10 Hz, which is the frequency of the laser shots. This effect was also observed when other sample matrices were analysed (e.g. bivalves) and also when the tube, connecting the sample chamber with the plasma torch was elongated from 50 cm to 5 m. Obviously the pulsed ablation of the sample release pressure waves which influence the stability of the plasma. It was observed several times that the ICP-TOF-MS system shut down due to plasma jittering.

5.2 Parameter study: LA-Aridus II-ICP-TOF-MS

Reinhardt (2002) used $^{16}\text{O}^1\text{H}^+$ as internal standard for LA-ICP-Q-MS analysis of ice cores as water is the main component of the sample matrix, to eliminate variations in e.g. plasma power, nebulizer gas flow and in the sample ablation and transport process (see also chapter 5.4). Coupling the Aridus II between the LA and ICP-TOF-MS system implies that the water from the sample is extracted; therefore it is not possible to use $^{16}\text{O}^1\text{H}^+$ as internal standard. But in order to circumvent problems with low signal intensities as well as plasma instability using the LA as the only sample introduction system, I coupled the Aridus II system between the LA unit and the ICP-TOF-MS system (Figure 21). The upward tilted installation of the heated PFA spray chamber enables droplets to leave the chamber by a pump drain. Advantage of this installation compared to on axis systems is that large droplets ($> 10 \mu\text{m}$) do not reach the membrane and therefore the signal stability increases.

As for the Aridus II-ICP-TOF-MS (chapter 4.2), the signal intensities, the degree of MO^+ and M^{2+} formation, which depends on plasma power, nebulizer-, sweep- and nitrogen gas flows, were monitored (Figure 22).

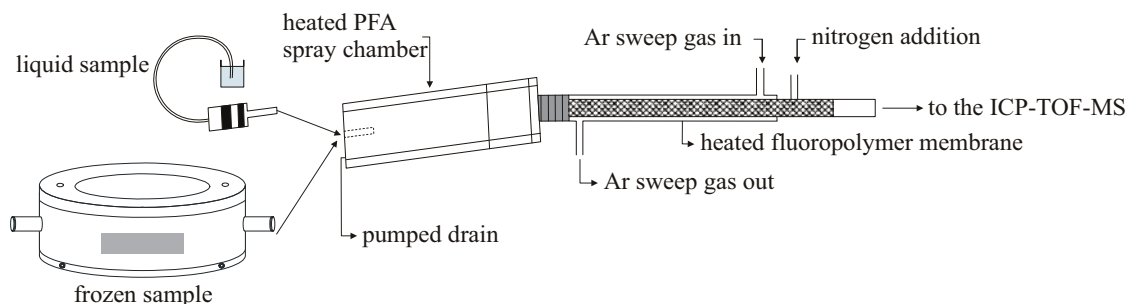


Figure 21: Schematic of the microconcentric nebulizer with desolvation unit (Aridus II). Either a liquid sample is introduced into the nebulizer or an aerosol produced by LA of frozen samples (Reproduced by permission of Cetac).

5.2.1 ICP parameter

Plasma power: Increasing the plasma power from 1000 W to 1200 W resulted in lower signal intensities by a factor of 2 to 5. Again, the MO^+ and M^{2+} formation increased along with increasing plasma power. Below 1000 W, analysis was not possible due to instabilities in the plasma region and subsequent automatic shut down of the system.

Nebulizer gas flow: The nebulizer gas flow varied between 0.5 L min^{-1} and 0.9 L min^{-1} . Low M^{2+} concentrations accompanied maximal signal intensities at 0.8 L min^{-1} . The MO^+ generation did not vary much and increased from 0.6% at 0.5 L min^{-1} to 1.2% at 0.9 L min^{-1} nebulizer gas flow.

5.2.2 Aridus II parameter

Sweepgas flow: Clear signal intensity maxima were observed at 6 L min^{-1} sweep gas flow. The MO^+ formation increased with increasing sweepgas flow, the M^{2+} formation showed no clear tendency.

Nitrogen gas flow: A nitrogen gas flow of 23 mL showed maximum signal intensities, except ^{24}Mg , which intensities decreased from 3200 cps at 9 mL min^{-1} to 1600 cps at 27 mL min^{-1} . Between 13 mL min^{-1} and 23 mL min^{-1} nitrogen gas flow, the MO^+ rate did not vary, while at 23 mL min^{-1} minimum M^{2+} values were obtained. Below 13 mL min^{-1} and above 23 mL min^{-1} the degree of MO^+ formation increased.

The implementation of the Aridus II system improved the plasma stability considerably by repressing the pressure wave released during the ablation process of the sample. Extracting the water from the sample resulted in few water molecules entering the plasma, hence the plasma temperatures increased and the degree of oxide formation decreased.

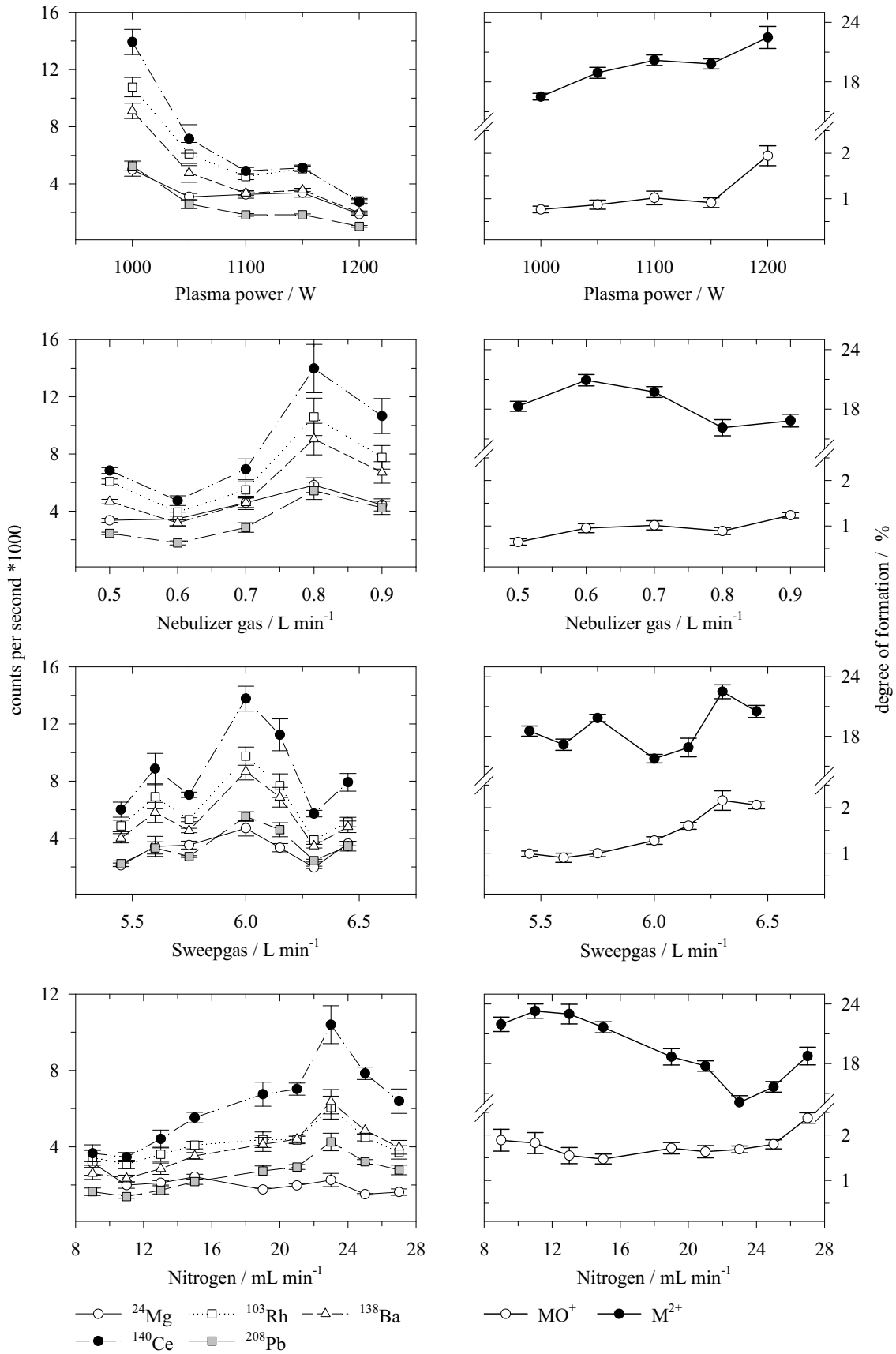


Figure 22: Signal variation with SD (20 replicates) in counts per second of a $10 \mu\text{g kg}^{-1}$ DP standard containing ^{24}Mg , ^{103}Rh , ^{138}Ba , ^{140}Ce and ^{208}Pb (left side); and changes in degree of oxide (MO^+) and doubly charged ion (M^{2+}) formation (right side) due to changes in plasma power, nebulizer-, sweep- and nitrogen gas obtained by the LA-Aridus II-ICP-TOF-MS system.

Compared to LA-ICP-TOF-MS analysis, signal intensities increased by a factor of 4 to 10 using the LA-Aridus II-ICP-TOF-MS system (Table 9). The RSD for ^{24}Mg was considerably reduced. As expected, the degree of MO^+ formation was much lower when employing the Aridus II nebulizer. LA-ICP-TOF-MS analysis provided on average lower signal intensities by a factor of 50 to 130 compared to LA-ICP-Q-MS analysis (also shown in Table 9).

Table 9: Signal intensities in cps ($\mu\text{g kg}^{-1}$)⁻¹ with RSD (10 replicates), background signals (Bkgd) for m/z ratios 8 and 220 and the degree of MO^+ and M^{2+} formation in % of a frozen $10 \mu\text{g kg}^{-1}$ DP ice standard obtained by LA-ICP-TOF-MS, LA-Aridus II-ICP-TOF-MS and LA-ICP-Q-MS analysis.

Instrumental settings: Laser energy: 380 mJ; Focus: on sample surface; a) LA-ICP-TOF-MS: Plasma Power: 1000 W; Nebulizer gas: 0.8 L min^{-1} ; b) LA-Aridus II-ICP-TOF-MS: Plasma Power: 1000 W; Nebulizer gas: 0.9 L min^{-1} ; Sweepgas: 6.0 L min^{-1} ; Nitrogen: 17 mL min^{-1} ; c) LA-ICP-Q-MS: Plasma Power: 1400 W; Nebulizer gas: 1.0 L min^{-1} .

	LA-ICP-TOF-MS		LA-Aridus II-ICP-TOF-MS		LA-ICP-Q-MS	
	cps ($\mu\text{g kg}^{-1}$) ⁻¹	RSD / %	cps ($\mu\text{g kg}^{-1}$) ⁻¹	RSD / %	cps ($\mu\text{g kg}^{-1}$) ⁻¹	RSD / %
^{24}Mg	60	59	220	17	3500	9
^{103}Rh	80	13	510	14	2800	8
^{208}Pb	50	14	330	14	6200	10
$^{69}\text{Ba}^{2+}$	30	5	110	7		
^{138}Ba	70	13	490	15	3600	10
^{140}Ce	70	14	800	15	3400	8
^{156}CeO	10	10	14	15		
$^8\text{Bkgd}$	90	8	20	15	8	28
$^{220}\text{Bkgd}$	110	7	20	18	10	27
$\text{M}^{2+} / \%$	31		18		1	
$\text{MO}^+ / \%$	17		2		0.2	

Calibration studies were also performed with the LA-Aridus II-ICP-TOF-MS system (Table 10) and approved the parameter optimization. Several signal intensities were barely above the blank intensities for the $1 \mu\text{g kg}^{-1}$ standard between m/z ratios 23 to 57. Signal intensities for elements above mass 57 show distinct differences from the blank signal.

Table 10: Calibration data in cps of ^{23}Na , ^{24}Mg , ^{27}Al , ^{57}Fe , ^{59}Co , ^{138}Ba , ^{140}Ce and ^{208}Pb for a Blank (0), 1-, 10- and $100 \mu\text{g kg}^{-1}$ multi-element ice standard obtained by LA-Aridus II-ICP-TOF-MS analysis. The slope and correlation coefficient (r^2) were calculated for each isotope.

standard concentration / $\mu\text{g kg}^{-1}$	^{23}Na / cps	^{24}Mg / cps	^{27}Al / cps	^{57}Fe / cps	^{59}Co / cps	^{138}Ba / cps	^{140}Ce / cps	^{208}Pb / cps
0	20000	1500	1100	140	120	160	50	170
1	19000	1900	1900	150	800	1100	1700	750
10	22000	4900	7900	280	6500	9200	15000	6100
100	60000	36000	22000	1800	63000	79000	110000	43000
slope	409.50	340	197	17	627	787	1132	428
r^2	0.9969	1.0000	0.9516	0.9997	1.0000	0.9998	0.9993	0.9988

LA-ICP-Q-MS studies of an Antarctic ice core (from the Holocene) revealed that only Na, Mg, Al, K, Mn, Fe, Co, Ni, Zn, Sr, Ba, La, Ce, Pb and Bi concentrations were higher than the IDL (Publication I). Low signal to noise ratios for a $1 \mu\text{g kg}^{-1}$ standard obtained in this study show that at the present state results obtained by the LA-ICP-Q-MS system can not be achieved by the LA-ICP-TOF-MS system due to much lower signal intensities.

5.3 Influence of helium as transport gas

In literature, the positive effect of the presence of helium gas in the ablation cell is described. According to *e.g.* Russo (1995), Eggins *et al.* (1998), Günther and Heinrich (1999) and Horn and Günther (2003) usage of helium is beneficial concerning the particle size distribution, the aerosol transport, reduced elemental fractionation and the plasma shielding. The addition of helium results in larger laser plasma and the transport into the plasma torch is more efficient. Therefore helium was added into the sample chamber according to Figure 23.

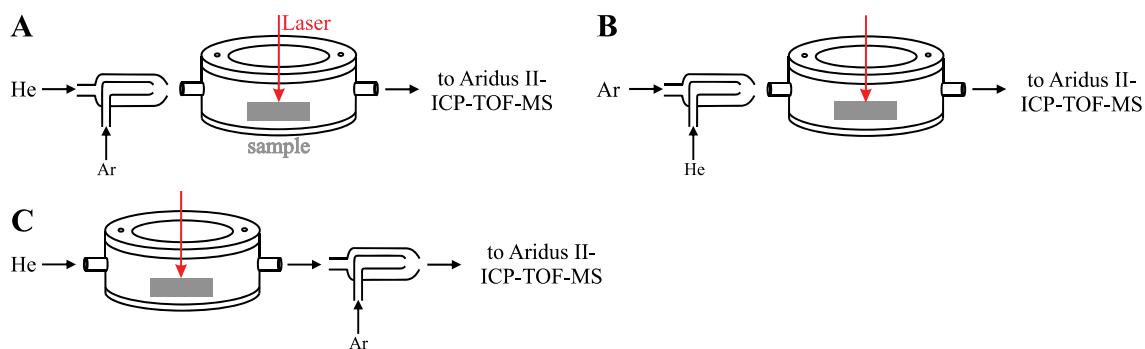


Figure 23: Experimental setup for the use of a mixture of argon (Ar) and helium (He) as transport gas for the LA of frozen ice core samples.

For configurations A and B best signal intensities were achieved using an argon to helium ratio of 7:1 (0.7 L min^{-1} : 0.1 L min^{-1}). For the experimental setup according to Figure 23 C following gas flow rates were used: He: 0.9 L min^{-1} ; Ar: 0.1 L min^{-1} . All other parameters were kept constant (Plasma power: 1100 W ; Plasma gas: 15 L min^{-1} ; Auxiliary gas: 1.4 L min^{-1} ; Sweepgas: 6 L min^{-1} ; Nitrogen: 23 mL min^{-1}). Again, a $10 \mu\text{g kg}^{-1}$ DP ice standard was analysed by LA-Aridus II-ICP-TOF-MS. Table 11 shows signal intensities of isotopes included in the DP ice standard after optimization of the system without and with helium (the column assignment A, B and C refers to Figure 23). Obviously, the addition of helium to the transport gas resulted in a signal increase by a factor of 3 to 5 for the setup A and B. Setup A showed better RSD values for replicate analysis compared to setup B. Setup C showed increased signal intensities by a factor of 2 to 3 and RSD values were similar compared to the setup using only argon as transport gas. The addition of helium to the transport gas resulted in decreasing M^{2+} formation in each experimental setup, while the degree of MO^+ formation slightly increased, especially for setup A.

Table 11: Signal intensities in cps ($\mu\text{g kg}^{-1}$)⁻¹ with RSD (10 replicates), background signals (Bkgd) for m/z ratios 8 and 220 and the degree of MO^+ and M^{2+} formation in % of a frozen $10 \mu\text{g kg}^{-1}$ DP ice standard obtained by LA-Aridus II-ICP-TOF-MS analysis. Mixing of Ar and He as transport gas according to Figure 23.

Instrumental settings: Laser energy: 380 mJ; Focus: on sample surface; Plasma Power: 1100 W; Sweepgas: 6.0 L min^{-1} ; Nitrogen: 23 mL min^{-1} ; Nebulizer gas: A and B) 0.7 L min^{-1} Ar and 0.1 L min^{-1} He; C) 0.9 L min^{-1} He and 0.1 L min^{-1} Ar.

	without He		A		B		C	
	cps ($\mu\text{g kg}^{-1}$) ⁻¹	RSD / %	cps ($\mu\text{g kg}^{-1}$) ⁻¹	RSD / %	cps ($\mu\text{g kg}^{-1}$) ⁻¹	RSD / %	cps ($\mu\text{g kg}^{-1}$) ⁻¹	RSD / %
²⁴ Mg	200	17	600	9	700	11	400	8
¹⁰³ Rh	500	14	1400	7	1500	15	800	18
²⁰⁸ Pb	300	14	1700	8	1400	16	970	17
⁶⁹ Ba ²⁺	100	7	100	7	100	13	90	12
¹³⁸ Ba	500	15	1400	8	1400	16	900	19
¹⁴⁰ Ce	800	15	2200	7	2200	15	1300	18
¹⁵⁶ CeO	10	15	100	10	50	12	30	23
⁸ Bkgd	20	15	20	12	40	11	30	14
²²⁰ Bkgd	20	18	20	19	30	12	20	13
M^{2+} / %	18		8		9		10	
MO^+ / %	2		4		2		3	

For further investigations it is recommended to use the experimental setup shown in Figure 23 A with an argon to helium ratio of 0.7 L min^{-1} : 0.1 L min^{-1} even if the MO^+ concentration increases by a factor of 2.

5.4 Internal standardisation for ice core analysis

Variations within the sample introduction system, in plasma conditions, in the nebulizer gas flow as well as instrumental drifts and matrix effects result in varying signal intensities. To reduce these variations, or rather increase the precision of the analysis, an internal standard is required. For ICP-MS analysis this is represented by an element with a defined concentration. It is compulsory that the concentration of this element is low and therefore negligible in the analysed samples. Hence, in this study all liquid standards and samples were spiked with a defined volume of Rh standard (see chapter 3.3). The Rh signal obtained for standards and samples should be nearly the same. Discrepancies would indicate problems with the *e.g.* plasma conditions, nebulizer gas flow or matrix composition of the sample. Reduction and even elimination of these variations is achieved by element ratio calculation of element signal intensities and Rh signal intensities. This kind of internal standardisation can not be used in case of solid materials such as ice core samples. Internal standardisation in LA-ICP-MS analysis also implies the correction of variations in the sample ablation, the transport process and the position of the laser focus. Reinhardt (2002) used $^{16}\text{O}^1\text{H}^+$ as internal standard as it is the main component of the sample matrix and hence its concentration does not change. In ideal case, signal variations are reduced and the precision of measurements increased which would result in smooth signal intensities along with time. Studies by Reinhardt (2002) showed RSD of replicate analysis after internal standardisation of 3% to 6%. To

clarify which isotopes can be used for internal standardisation for the ICP-TOF-MS system, $^{16}\text{O}^1\text{H}^+$, $^{18}\text{O}^1\text{H}^+$ and isotopes with a m/z ratio of 20 (e.g. $^{18}\text{O}^2\text{H}^+$, $^{18}\text{O}^1\text{H}_2^+$ and neon (contained in argon gas)) were monitored (Figure 24) together with isotopes from a DP ice standard.

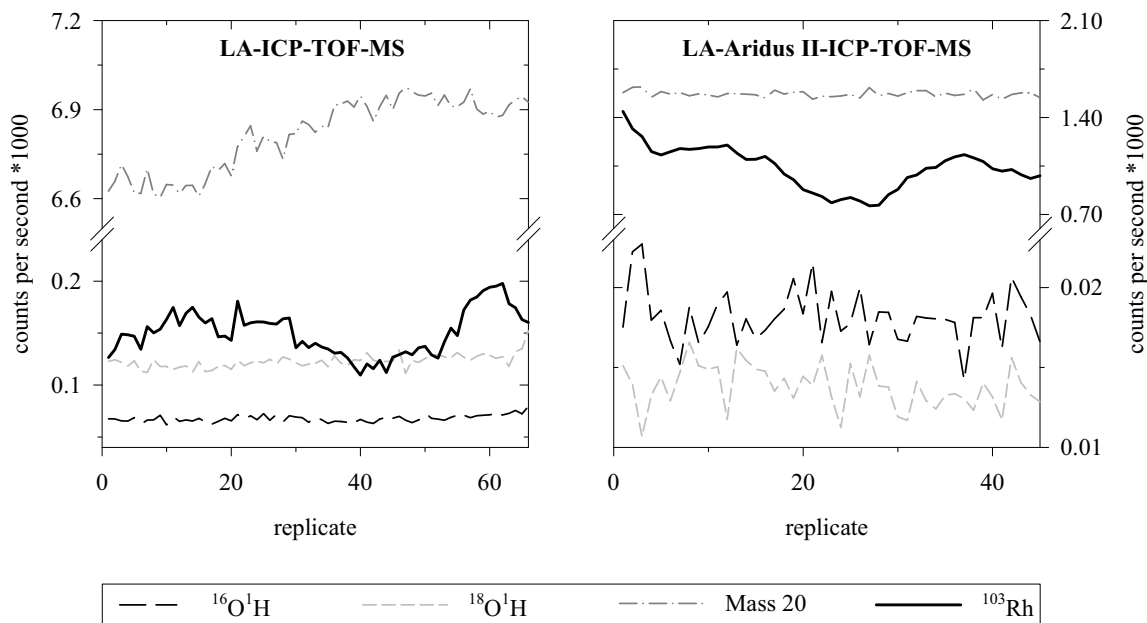


Figure 24: Signal intensities of several m/z ratios obtained by LA-ICP-TOF-MS and LA-Aridus II-ICP-TOF-MS of a $10 \mu\text{g kg}^{-1}$ DP ice standard to validate possible isotopes for internal standardisation.

Replicate analysis showed coincident variations for ^{24}Mg , ^{103}Rh , ^{138}Ba , ^{140}Ce and ^{208}Pb but not for the isotopes proposed for internal standardisation (Figure 24, left side, Rh representing the elements). The isotopes with a m/z ratio of 20 showed varying signals but the pattern looked different compared to the Rh signal. Interestingly, virtually only slight signal variation was observed for $^{16}\text{O}^1\text{H}^+$ and $^{18}\text{O}^1\text{H}^+$. This test was repeated with the Aridus II system coupled between the LA and the ICP-TOF-MS system (Figure 21). As expected signal intensities of $^{16}\text{O}^1\text{H}^+$, $^{18}\text{O}^1\text{H}^+$, and the isotope with a m/z ratio of 20 decreased significantly and did not vary as the Rh signal did (Figure 24, right side). I observed that about 20% of the signal intensity of the m/z ratio 20 resulted from Neon gas by comparing signals obtained before and during the laser ablation process (not shown in Figure 24, right side). The argon used as plasma gas contained traces of krypton and xenon as well. These isotopes and the combination of these isotopes with oxygen were also monitored but did not show a coherent signal variation with ^{24}Mg , ^{103}Rh , ^{138}Ba , ^{140}Ce and ^{208}Pb .

To protect the detector against high ion load related to oxygen and argon species, selector impulses were set to redirect these species from their flight path (see chapter 3.1.5). For the LA-ICP-TOF-MS system $^{16}\text{O}^+$ and $^{16}\text{O}^1\text{H}_2^+$ were redirected. Analysis of liquid samples already showed that the voltage pulses applied to the selector affect the analysis of neighbored masses. Therefore, the analysis of $^{16}\text{O}^1\text{H}^+$ and $^{18}\text{O}^1\text{H}^+$ was

influenced in LA-ICP-TOF-MS studies, which is represented by low signal intensities (Figure 24, left side). Therefore at the present state there is no isotope available for internal standardisation of ice core samples.

Great effort has been done on non matrix-matched quantification for the analysis of glass samples (*e.g.* minerals). Most promising seems to be a quantification strategy based on the transported aerosol particle volume (Kuhn and Günther, 2006). In this approach internal element standardisation has been replaced by measurements of the relative mass of the particles introduced into the ICP-MS using aerosol size distributions and sample bulk density. The authors analysed the particle size distribution by light scattering from a constant aerosol fraction (~1%). This strategy should be tested to verify if this procedure can be transferred on the analysis of frozen ice core samples.

5.5 Reasons for low ICP-TOF-MS signals

The standard equipment for the ICP-TOF-MS system uses the CFN as sample introduction system. The degree of MO^+ formation above 70% (see chapter 4.1) is extremely high compared to results obtained by coupling the CFN to an ICP-Q-MS system (3%). This indicates low energy transfer from the generator system into the ICP. There are several reasons for lower ICP-TOF-MS signal intensities compared to ICP-Q-MS signal intensities (decreased signal intensities by a factor of 2 to 10 for the analysis of liquid samples and by a factor of 50 to 130 for the analysis of solid samples).

5.5.1 Duty cycle

Due to the fact that pulsed ion packets are transferred from the ion optic region into the drift tube of ICP-TOF-MS system (at 25 kHz rate – each pulse taking 2 μs), the extraction rate of ions into the drift tube amounts just 5% compared to ICP-Q-MS and ICP-SF-MS systems for liquid samples (this study).

5.5.2 Components of the ion optics

In ICP-Q-MS systems the first component in the ion optic system is a focus lens. In contrast, an ion extraction skimmer cone is placed in front of the focus lens in the presented ICP-TOF-MS System. Only a small fraction of ions pass the small orifice of this skimmer cone. This extraction skimmer cone is needed for several reasons: (i) to exclude ions and particles which do not have a straight flight paths and therefore collision processes behind this cone are reduced, (ii) ions have to be transferred into the repeller region with low spatial resolution to improve the resolution of the MS system and (iii) due to the voltage applied to this cone the extraction rate of ions increases. The extracted fraction of ions by the skimmer cone is influenced by the applied voltage. Increasing the voltage from 2000 V up to 2500 V results in increasing the ion extraction rate but the lifetime of the skimmer cone decreases rapidly. For common MS systems

analysing in the sequential mode this extraction skimmer cone is not necessary because the voltage applied to the focus lens is tunable.

5.5.3 Radio-frequency generator

High ion production rates in mass spectrometry analysis require constant plasma conditions and sufficient high plasma energy. Hence the plasma generation system is a crucial part of the device. The plasma requires a continuous power feeding of about 1 kW in order to keep the plasma energy high and thus, not to extinguish. The power is injected into the plasma torch using an inductive coupling from an outer coil (Figure 4). For such a high energy transfer via the coil, this coil is operated at an electrical resonant frequency. This is being determined by the load, *i.e.* the state of the plasma depending on the materials inside (either the plasma gas or plasma gas and sample aerosol), and electrical resonant components, being additional capacitors and inductors.

Two plasma generation systems are used for plasma generation in ICP-MS systems, which are both fed by the public main supply. In a first conversion stage the rectified grid voltage is controlled by a DC/DC converter to a constant voltage of 0...50 V. In the following this is represented by the input voltage source of the generator, *i.e.* either the common free-running tube amplifier or the solid state generator.

Commonly free-running tube amplifiers are used for plasma generation in mass spectrometry (Figure 25) operating at 40.68 MHz.

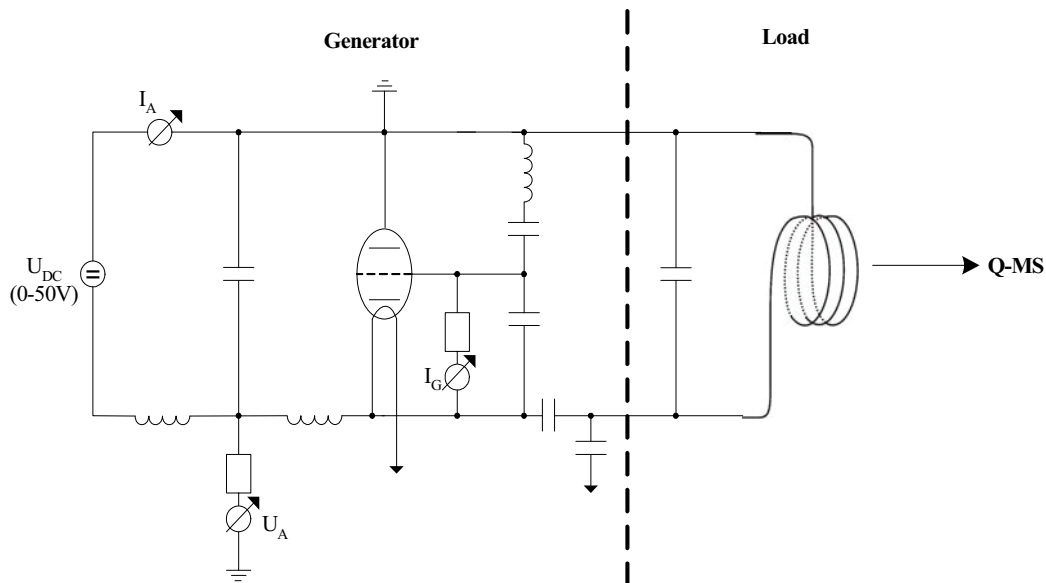


Figure 25: Schematic view of a free-running tube amplifier used for plasma generation in ICP-Q-MS systems (Dzur, 2002). Impedance changes in the load LC-circuit are compensated by small frequency changes in the generator LC-circuit.

The plasma torch is placed within the coil (Figure 5), which is integrated in the LC-circuit on the right side of Figure 25 (load circuit). Within the plasma torch the sample is ionized and afterwards transported into the coupled Q-MS system. As mentioned

above impedance and resonance changes brought about by the sample and / or matrix components are compensated by electronic tuning of the operating frequency to the resonant frequency. This frequency regulation is very fast due to direct connection of the left LC-circuit to the tube, retracing the operating frequency. This well established kind of free-running RF generator allows successful analysis of many sample matrices.

A solid state generator working at 27.12 MHz produces the plasma for the ICP-TOF-MS system installed in the laboratories of the Alfred Wegener Institute. Figure 26 shows the setup of this generator. Due to the topology, the operating frequency is fixed to the design of the generator side. Thus, changes of resonance coming from the load (e.g. plasma jittering, Chapter 5.1.1) cannot be compensated by variation of the operating frequency. As an alternative the resonance frequency is tuned back to the operating frequency by fast servo driven capacitors (within the Match-Box). However, mechanically moved components cannot show such fast responses compared to not moved components. These mechanical devices often failed to compensate rapid impedance changes. The result is either a low energy transfer into the plasma or an extinguished plasma.

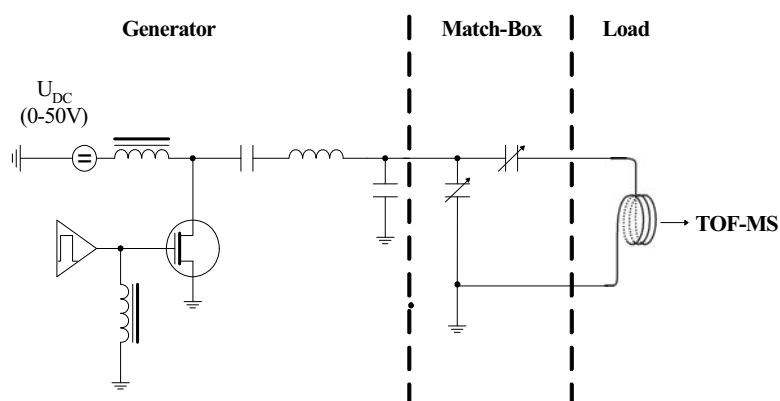


Figure 26: Schematic view of a solid state generator used for plasma generation in the ICP-TOF-MS system. The left LC-circuit of the Generator works at constant frequency. Impedance changes in the LC-circuit of the load are compensated by servo driven capacitors in the Match-Box (Reproduced by permission of Advanced Energy).

5.5.4 Shielding of the plasma

Plasma shielding is necessary to eliminate the so-called pinch effect (see chapter 3.1.2). In the ICP-TOF-MS system this was achieved by the use of a grounded shield between the coil and the plasma torch (Figure 27, left side).

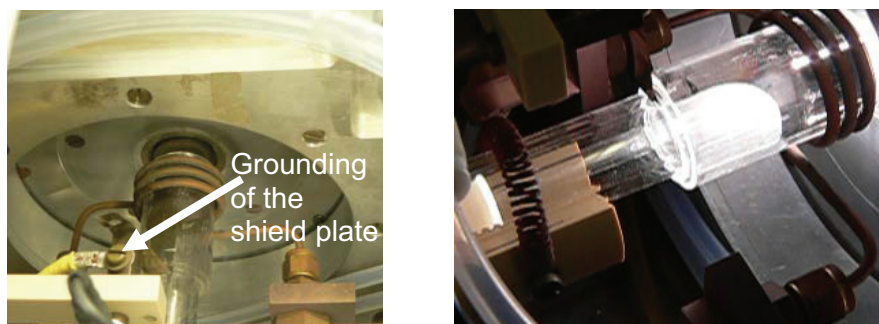


Figure 27: Shield plate between the coil and the plasma torch to eliminate the pinch effect.

The slits in the shield plate (Figure 27, right side) are needed otherwise the shield plate would become too hot due to induced eddy currents. Problems with shielding can result in increasing amounts of doubly charged ions or wide spread kinetic energy (Douglas and French, 1986). Hence the ion extraction rate decreases (Thomas, 2004).

Other ICP-MS suppliers, *e.g.* Perkin-Elmer Sciex, use the PLASMALOK[®] system to eliminate the pinch effect described by Douglas and French (1986). A modified impedance matching network with the ground near the centre of the load coil greatly reduces the voltage differences between plasma and sampler cone, eliminating arcing between these two components. The use of this well established technique should also lead to higher sensitivity of the ICP-TOF-MS system and is highly recommended.

5.5.5 Polymers close to the plasma torch

In regular time intervals the signal intensities obtained by ICP-TOF-MS analysis decreased significantly. Simultaneously, I observed some kind of whiskers in the plasma. Inside the region where the plasma torch is mounted, several polymer components are installed. In search for the reason of the whiskers, defect polymers were found (Figure 28). This defect caused losses of plasma power, visible as whiskers, and is accompanied by worse sample ionisation and therefore signal intensity losses.

Each polymer has its specific electrical properties. Polymers with low permittivity, high contact resistance and dielectric strength are needed close to the plasma torch. Typical polymers used in the ICP-TOF-MS system are Polytetrafluorethylene (PTFE) and Polyetheretherketone (PEEK). According to the above mentioned electrical properties PTFE appears better suited in the plasma torch region compared to PEEK.

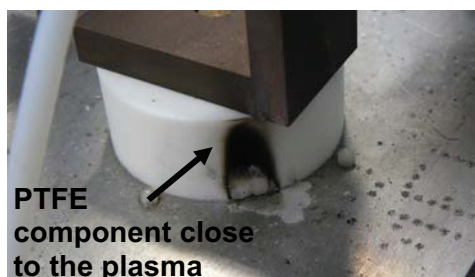


Figure 28: Porous polymer (Teflon) close to the plasma torch leads to energy loss in the plasma and therefore in decreasing signal intensities.

In practice, however, tests showed that the life time was higher for PEEK components. Note that electrical properties refer to normal conditions (20°C and test frequency of 1 MHz). In contrast, the plasma is ignited and maintained by a high frequent electro-magnetic field of 27.12 MHz. This electro-magnetic field as well as the UV light emitted by recombination of Ar^+ cations with e^- (see equation 2) degrade polymers and alter their electrical properties. Once a polymer is defect the plasma power decreases. The use of ceramic components instead of polymers close to the plasma torch should reduce problems with energy losses.

5.5.6 Pulsed aerosol introduction

The pulsed introduction of the sample aerosol by LA affects the signal intensity. The ablation process of the sample releases pressure waves which influence the stability of the plasma and reduces the energy transferred from the generator system onto the plasma (see chapter 5.5.3). Therefore fewer ions are produced.

5.5.7 Laser shot frequency

Gratuze *et al.* (2001) report that the laser shot frequency has an effect on the sensitivity of the ICP-MS system. It is correlated with the frequency of the laser as it is directly related to the amount of material sent to the plasma torch. The authors show the signal intensity pattern of Cobalt in the reference glass standard NIST 610 as a function of the laser shot frequency. These authors worked with a quadrupled Nd:YAG laser at 266 nm. Doubling the laser shot frequency resulted in doubling the signal intensity (Figure 29, blue box). During the ablation process the distance between the laser focus and sample surface increases, therefore the signal intensity decreases along with time.

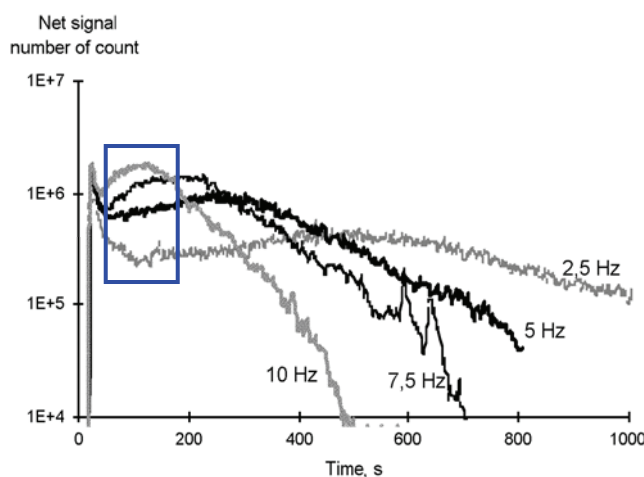


Figure 29: Evolution of the intensity of ^{59}Co signal in Nist 610 referenced glass as a function of the laser shot frequency (Gratuze *et al.*, 2001).

Interestingly, Bleiner and Günther (2001) performed similar studies with a 193 nm ArF* Excimer laser. They applied 50 laser shots on the NIST 610 reference glass standard at repetition rates of 0.1, 1 and 10 Hz. Bleiner and Günther (2001) report that

reduced signal intensities at higher repetition rates were caused by the particle loss of the sample in the transport system (due to particle-particle agglomeration) and subsequent deposition. Moreover they said that changing the repetition rate between 5 and 20 Hz showed a linear dependency on the sensitivity, which indicated constant aerosol transport within this range. Different ablation behaviour reported by these two working groups might be a result of different laser wavelengths used. Future studies in ice core analysis should therefore concentrate on doubling the laser frequency from 10 Hz to 20 Hz to test if the signal intensities increase by a factor of 2 as well.

5.5.8 Size of the sample chamber

Bleiner and Günther (2001) observed that the signal structure modified by reducing the volume of the sample chamber. They analysed the SRM 610 Glass from NIST using a 193 nm ArF* Excimer laser system. These authors report that the peak height of a single laser shot was increased by a factor of 6, and that the signal width was reduced by a factor of 7 when the sample chamber volume was reduced from 63 cm³ to 0.25 cm³. Therefore, for the experimental setup used in this study it should also be tested whether a sample chamber with smaller volume results in increasing signal intensities. But, for the analysis of natural ice core samples it has to be taken into account that replacing the analysed sample by a new sample is very time consuming. In addition, smaller samples effort more sample preparation, in terms of cutting the sample with a bandsaw into smaller pieces, which implies possible sample contamination. Moreover the sample chamber height is strongly confined. During the ablation process water droplets might deposit on the sample chamber window, which restricts further ablation. The deposition of water droplets was already observed using the large sample chamber. When the laser beam couples into these water droplets the window of the sample chamber might be destroyed.

6 Conclusions and Outlook

LA-ICP-Q-MS was successfully applied to the investigation of three different climatic archives with stratigraphic layering (Publication I, III, IV) and will in future support the synchronisation of archives for fundamental studies as *e.g.* in Publication II.

For a section of the EPICA-DML ice core from Antarctica, where the annual layer thickness amounts to about 6.5 cm, 15 analyses per year were performed (Publication I). The concentration of sea salt tracers, mineral dust tracers and tracers for other natural or anthropogenic sources peaks during the winter months. Moreover, the investigation demonstrated that LA-ICP-Q-MS is superior for the analysis of embedded particles in the ice matrix compared to common methods, like *e.g.* liquid ICP-MS of acidified samples or continuous flow analysis. Of special interest was the comparison of LA-ICP-Q-MS analysis of frozen ice cores with other high resolution methods. My results suggest that, depending on the concentration of analysed samples, the coupling of conventional continuous melting devices to ICP-MS systems is most suitable for multi-element analysis of ice cores. My judgement is based on the fact, that the ICP-MS analysis of liquid samples achieves better recovery rates and lower DL compared to LA-ICP-Q-MS analysis. However, the spatially high resolved localization of particles in the ice core-section and the analysis of their elemental composition are solely possible by LA-ICP-MS analysis.

The precise synchronisation of polar ice cores amongst each other and with other climatic archives is the basis for advanced studies of climate processes, as *e.g.* in Publication II. Besides atmospheric trace gases, volcanic tephra layers are analysed for their genetic information to synchronize ice cores with each other (Kohno et al., 2005; Severi et al., 2007) and are considered to synchronise ice cores with other archives, as *e.g.* marine sediment cores. At present, the tephra is mainly characterized by wavelength dispersive electron microprobe. As the DL of REE is sufficient low to characterize the tephra by REE finger-printing, LA-ICP-MS analysis of tephra layers embedded in polar ice cores constitutes an additional method for synchronisation of climatic archives in future.

Annual growth bands of the soft clam shell *Laternula elliptica* (Potter Cove, Antarctic Peninsula) are less than 400 μm thick. In Publication III, we investigated whether the increased mineral input, thus associated with the glacial melting, around Potter Cove results in rising element signals within the latest growth bands of the umbo matrix. We used LA-ICP-Q-MS to determine the annual variation of selected elements across the umbo matrix and proved that the accretion of our investigated elements into the umbo matrix is largely a function of animal ecophysiology and life history rather than of climate change.

By means of LA-ICP-Q-MS we proved the possibility to determine different elemental composition in summer and winter layers of a frozen sediment core from

Sacrower See (Potsdam, Germany; Publication IV), without time consuming sample preparation.

The analysis of bivalves and sediment cores for this study used a Nd:YAG laser, which was initially chosen for its absorption properties in ice. Even though we gained a plentiful of information with the present equipment, for future studies I recommend the use of a frequency quadrupled Nd:YAG laser, due to its better absorption capabilities in mineral material and achievable smaller spot size. The analysis of appropriate reference materials will enable the elemental quantification.

The main limitation of LA-ICP-Q-MS measurements is the number of analysed isotopes, especially for point scan analysis of embedded particles in ice matrices and the analysis of growth bands of bivalves. For scanning MS systems, like *e.g.* quadrupole mass spectrometers, the technically feasible number of studied isotopes depends on the available sample volume, the number of required replicate analysis and the isotope concentration within a sample. Several replicate analyses are needed to avoid counting statistic problems. Moreover, all discussed samples here are inhomogeneous, so that the composition of ablated material could rapidly change during proceeding ablation. The changing aerosol compositions as well as the pulsed introduction of sample material by the LA method result in a transient signal. If one strives for the detection of these variations, *e.g.* for localizing of trace compounds in complex matrices, the analysing time has to be shorter than the characteristic time constant of these variations under given ablation conditions. Scanning one element after another, as it is done in Quadrupole and Sector Field ICP-MS systems, implies that the ion packages for the analyses of different isotopes are not necessarily originating from coherent sample volumes. The resultant element or isotope ratios from incoherent sample volumes, could *e.g.* result in a flawed mineral dust source determination in polar ice cores.

The introduction of time of flight ICP-MS (ICP-TOF-MS) systems for the characterisation of the inorganic composition of samples permits the *quasi-simultaneous* multi-element analysis. Unfortunately, up to now low concentration samples were inaccessible to ICP-TOF-MS analysis without intense concentration, due to the sensitivity loss compared to ICP-Q-MS systems. In Chapter 4 I demonstrated the suitability of the innovative ICP-TOF-MS system for trace element studies by a performance study. The accuracy and precision of this ICP-TOF-MS system compares to well-established ICP-Q-MS systems. The signal sensitivity was 2 to 10 times lower for ICP-TOF-MS analysis. This is however only possible when using a microconcentric nebulizer with desolvation unit (Aridus II) as sample introduction system. Calibration studies as well as the investigation of different SRM showed that the calibration range is limited to an order of magnitude of about 10^4 to 10^5 except for m/z ratios between 23 and 72. Therefore, the analyses of several dilutions are necessary to obtain isotope concentrations in the mass range between 7 amu and 238 amu. The observed minor formation of MO^+ and high signal intensity of Ce, which is representative of REE,

enables the analysis of important tracers in ice cores for climatic research (Publication V). The ICP-TOF-MS system requires much less sample volume for the analysis compared to scanning mass spectrometry systems as the *quasi-simultaneous* analysing mode reduced the analysing time significantly.

In principle, the recording of 25000 spectra per second by LA-ICP-TOF-MS permits to study transient or very short signals. With respect to polar ice cores, the investigation of transient signals is limited by low signal sensitivity (Chapter 5). Switching to a combination of argon and helium as transport gas increased the signal sensitivity by a factor of 3 to 5. The new LA-ICP-TOF-MS system had by a factor of 50 to 130 lower signals, compared to the LA-ICP-Q-MS system. Moreover, internal standardisation to exclude signal variation was not possible as Reinhardt (2002) presented for LA-ICP-Q-MS. The replacement of the internal standard by measurements of the relative mass of the ablated material introduced into the plasma might lead to improvement of the quantification of ice core samples as reported for other sample matrices (Bleiner and Günther, 2001).

Overall, I conclude that for the innovative ICP-TOF-MS system, the analysis of trace elements in natural samples with the present experimental setup is only possible when samples are transferred into the liquid state. This permits the characterisation of mineral dust in ice core samples.

Increasing the signal sensitivity of the ICP-TOF-MS system should be tackled by (i) using a free-running RF generator, (ii) the use of ceramic materials close to the plasma torch, (iii) using a sample chamber with a smaller volume, and by (iv) increasing the repetition rate of the LA system.

I recommend improving the data evaluation by (i) developing a dual detector calibration, which uses the pulse as well as the analogue mode for data evaluation as it is done for the ICP-Q-MS system (Elan6000 Perkin Elmer/Sciex), and (ii) extending the concentration range towards higher concentrations for the analysis by exploring curved calibration graphs as it is done for data evaluation in atomic absorption spectrometry.

7 References

- Al-Dabbas M.A.M., F.H. Hubbard, J. McManus (1984): *The shell of Mytilus as an indicator of zonal variations of water quality within an estuary*. Estuarine Coastal Shelf Sci., **18**, 263–270.
- Basile I., F.E. Grousset, M. Revel, J.-R. Petit, P.E. Biscaye, N.I. Barkov (1997): *Patagonian origin of glacial dust deposited in East Antarctica (Vostok and Dome C) during glacial stages 2, 4 and 6*. Earth Planet. Sci. Lett., **146**, 573–589.
- Bea F., P. Montero, A. Stroh, J. Baasner (1996): *Microanalysis of minerals by Excimer UV-LA-ICP-MS system*. Chem. Geol., **133**, 145–156.
- Beck J.W., L.R. Edwards, E. Ito, F.W. Taylor, J. Recy, F. Rougerie, P. Joannot, C. Henin (1992): *Sea-Surface Temperature from Coral skeletal strontium/calcium ratios*. Science, **257**, 644–647.
- Becker J.S. (2007): *Inorganic Mass Spectrometry; Principles and Applications*. John Wiley & Sons Ltd, The Atrium, Southern Gate, Chichester, West Sussex England.
- Becker J.S., H.J. Dietze (2000): *Inorganic mass spectrometric methods for trace, ultratrace, isotope, and surface analysis*. Intern. J. Mass Spectrom., **197**, 1–35.
- Benkhedda K., H.G. Infante, F.C. Adams (2002): *Inductively coupled plasma mass spectrometry for trace analysis using flow injection on-line preconcentration and time-of-flight mass analyser*. Trends in Anal. Chem., **21**(5), 332–342.
- Benkhedda K., H.G. Infante, F.C. Adams (2004): *Determination of total lead and lead isotope ratios in natural waters by inductively coupled plasma time-of-flight mass spectrometry after flow injection on-line preconcentration*. Anal. Chim. Acta, **506**, 137–144.
- Blais J.M., D.C.G. Muir (2001): *Paleolimnological Methods and Applications for Persistent Organic Pollutants*. In: Tracking Environmental Change using Lake Sediments. Volume **2**, Physical and Geochemical Methods. W.M. Last, J.P. Smol (Eds). Kluwer Academic Publishers, The Netherlands, pp. 271–298.
- Bleiner D., D. Günther (2001): *Theoretical description and experimental observation of aerosol transport processes in laser ablation inductively coupled plasma mass spectrometry*. JAAS, **16**, 449–456.
- Bleiner D., K. Hametner, D. Günther (2000): *Optimization of a laser ablation-inductively coupled plasma „time of flight“ mass spectrometry system for short transient signal acquisition*. Fresenius J. Anal. Chem., **368**, 37–44.
- Bollinger D.S., A.J. Schleisman (1999): *Analysis of High Purity Acids Using a Dynamic Cell Reaction Cell ICP-MS*. At., Spectrosc., **20**, No.2, 60–63.

- Boyle J.F. (2001): *Inorganic Geochemical Methods in Paleolimnology*. In: Tracking Environmental Change using Lake Sediments. Volume 2, Physical and Geochemical Methods. W.M. Last, J.P. Smol (Eds.). Kluwer Academic Publishers, The Netherlands, pp. 83–141.
- Brook E., E. Wolff (2006): *The Future of Ice Core Science*, Eos Trans. AGU, **87**(4), 39, 10.1029/2006EO040004.
- Candelone J.P., S. Hong, C. Pellone, C.F. Boutron (1995): *Post-Industrial Revolution changes in large-scale atmospheric pollution of the northern hemisphere by heavy metals as documented in central Greenland snow and ice*. JGR, **100**(D8), 16605–16616.
- Capelli R., V. Minganti, C. Chiarini, R. De Pellegrini (1998): *Mercury in Snow Layers from the Antarctica*. Int. J. Environ. Anal. Chem., **71**(3-4), 289–296.
- Carriker M.R., C.P. Swann, J.W. Ewart (1982): *An exploratory study with the proton microprobe of the ontogenetic distribution of 16 elements in the shell of living oysters*. Mar. Biol., **69**, 235–246.
- Cetac, <http://www.cetac.com/anotes/archappnotespdf/mcn-6000.pdf>, 14.03.2008.
- Date A.L. (1975): *Mass-spectrometric Analysis of Solutions Using an Atmospheric Pressure Ion Source*. Analyst, **100**, 289–299.
- Delmonte B., I. Basile-Doelsch, J.-R. Petit, V. Maggi, M. Revel-Rolland, A. Michard, E. Jagoutz, F. Grousset (2004): *Comparing the Epica and Vostok dust records during the last 220,000 years: stratigraphical correlation and provenance in glacial periods*. Earth & Science Reviews, **66**, 63–87.
- Dick D., M. Kriews, H. Reinhardt, E. Dunker, M. Littmann (2004): *Vorrichtung zum mechanischen Abtragen der obersten Schicht einer Festkörperprobe*. Utility Model, DE 20 2004 010 599 U1.
- Denoyer E.R., K.J. Fredeen, J.W. Hager (1991): *Laser solid sampling for inductively coupled plasma mass spectrometry*. Anal. Chem., **63**, 445A–457A.
- Douglas D.J., J.B. French (1986): *An improved interface for inductively coupled plasma-mass spectrometry (ICP-MS)*. Spectrochim. Acta, Part B, **41**(3), 197–204.
- Douglas D.J., L.A. Kerr (1988): *Study of solids deposition on inductively coupled plasma mass spectrometry samplers and skimmers*. JAAS, **3**, 749–752.
- Douglas D.J., S.D. Tanner (1998): In *Inductively Coupled Plasma Mass Spectrometry*, A. Montaser (Ed.), Wiley-VCH, New York, pp. 623.
- Durrant S.F. (1999): *Laser ablation inductively coupled plasma mass spectrometry: achievements, problems, prospects*. JAAS, **14**, 1385–1403.

- Dzur B. (2002): *Ein Beitrag zur Anwendung des thermisch-induktiv gekoppelten Hochfrequenz-Plasmas (ICP) zum atmosphärischen Plasmaspritzen oxidkeramischer Werkstoffe*. Dissertation an der Fakultät für Elektrotechnik und Informationstechnik der TU Ilmenau, pp. 50.
- Emiliani C. (1955): *Pleistocene Temperatures*. J. Geol., **63**, 538-578.
- Eggins S.M. (2003): *Laser Ablation ICP-MS Analysis of Geological Materials Prepared as Lithium Borate Glasses*. Geostandards and Geoanalytical Research, **27**(2), 147–162.
- Eggins S.M., L. P. J. Kinsley, J. M. G. (1998): *Shelley Deposition and element fractionation processes during atmospheric pressure laser sampling for analysis by ICP-MS*. Appl. Surf. Sci., **127-129**, 278–286.
- EPICA Community Members (2004): *Eight glacial cycles*. Nature, **429**, 623–628.
- EPICA Community Members (2006): *One-to-one coupling of glacial climate variability in Greenland and Antarctica*. Nature, **444**, 195–198.
- Evans E. H., J. J. Giglio (1993): *Interferences in inductively coupled plasma mass spectrometry- a review*. JAAS, **8**, 1–18.
- Fassel V. A. (1978): *Quantitative elemental analysis by plasma emission spectroscopy*. Science, **202**, 183–191.
- Fischer H., M. Behrens, M. Bock, U. Richter, J. Schmitt, L. Loulergue, J. Chappellaz, R. Spahni, T. Blunier, M. Leuenberger, T.F. Stocker (2008): *Changing boreal methane sources and constant biomass burning during the last termination*. Nature, **452**, 864-867.
- Fischer H., M.-L. Siggard-Andersen, U. Ruth, R. Röthlisberger, E. Wolff (2007): *Glacial/Interglacial Change in Mineral Dust and Sea-Salt Records in Polar Ice Cores: Sources, Transport, and Deposition*. Rev. Geophys., **45**, RG1002.
- Foley S.F., S.E. Jackson, B.J. Fryer, J.D. Greenough, G.A. Jenner (1996): *Trace element partition coefficients for clinopyroxene and phlogopite in an alkaline lamprophyre from Newfoundland by LAM-ICP-MS*. Geochim. Acta, **60**(4), 629-639.
- Francesconi K.A., M. Sperling (2005): *Speciation analysis with HPLC-mass spectrometry: time to take stock*. Analyst, **130**, 998–1001.
- Fujiyama K., T. Deguchi, T. Murakami, A. Fujii, K. Kushima, T. Takano-Yamamoto (2008): *Clinical Effect of CO₂ Laser in Reducing Pain in Orthodontics*. Angle Orthodontist, **78**(2), 299–303.
- Gabrielli P., C. Barbante, C. Turetta, A. Marteel, C. Boutron, G. Cozzi, W. Cairns, C. Ferrari, P. Cescon (2006): *Direct Determination of Rare Earth Elements at the Subpicogram per Gram Level in Antarctic Ice by ICP-SFMS Using a Desolvation System*. Anal. Chem., **78**(6), 1883–1889.

- Gaiero D.M. (2007): *Dust provenance in Antarctic ice during glacial periods: From where in southern South America?* Geophys. Res. Lett., **34**, 1–6.
- Gaiero D.M., P.J. Depetris, J.L. Probst, S.M. Bidart, L. Leleyter (2004): *The signature of river- and wind-borne materials exported from Patagonia to the southern latitudes: a view from REEs and implications for paleoclimatic interpretations.* Earth Planet. Sci. Lett., **219**, 357–376.
- Gratuze B., M. Blet-Lemarquand, J.-N. Barrandon (2001): *Mass spectrometry with laser sampling: A new tool to characterize archaeological materials.* J. Radioanal. Nucl. Chem., **247**(3), 645–656.
- Gray A.L. (1985): *Solid sample introduction by laser ablation for inductively coupled plasma mass spectrometry.* Analyst, **110**, 551–556.
- Greenland Ice Core Project (GRIP) members (1993): *Climate instability during the last interglacial period recorded in the GRIP ice core.* Nature, **364**, 203–207.
- Guillong M., I. Horn, D. Günther (2003): *A comparison of 266 nm, 213 nm and 193 nm produced from a single solid state Nd:YAG laser for laser ablation ICP-MS.* JAAS, **18**, 1224–1230.
- Günther D., A. Audétat, R. Frischknecht, C.A. Heinrich (1998): *Quantitative analysis of major, minor and trace elements in fluid inclusions using laser ablation –inductively coupled plasma-mass spectrometry.* JAAS, **13**, 263–270.
- Günther D., C.A. Heinrich (1999): *Enhanced sensitivity in laser ablation-ICP mass spectrometry using Helium-argon mixtures as aerosol carrier.* JAAS, **14**, 1663–1368.
- Hoffmann E., C. Lüdke (2005): *The ICP-TOF mass spectrometer: an alternative for elemental analysis.* Spectroscopy Europe, **17** No.1, 16–23.
- Hoffmann E., C. Lüdke, J. Skole, H. Stephanowitz, J. Wollbrandt, W. Becker (2002): *New methodical and instrumental developments in laser ablation inductively coupled plasma mass spectrometry.* Spectrochim. Acta, Part B, **57**, 1535–1545.
- Holland G., S. Tanner (2001): *Plasma Source Mass Spectrometry: The new Millennium.* Royal Society of Chemistry, pp. 83.
- Hong S.M., C.F. Boutron, C. Barbante, S.D. Hur, K. Lee, P. Gabrielli, G. Capodaglio, C.P. Ferrari, C. Turetta, J.-R. Petit, V.Y. Lipenkov (2005): *Glacial–interglacial changes in the occurrence of Pb, Cd, Cu and Zn in Vostok Antarctic ice from 240000 to 410000 years BP.* J. Environ. Monit., **7**(12), 1326–1331.
- Horn I., D. Günther (2003): *The influence of ablation carrier gases Ar, He and Ne on the particle size distribution and transport efficiencies of laser ablation-induced aerosols: implications for LA-ICP-MS.* Appl. Surf. Sci., **207**(1-4), 144–157.

- IPCC (2007): Forster, P., V. Ramaswamy, P. Artaxo, T. Berntsen, R. Betts, D.W. Fahey, J. Haywood, J. Lean, D.C. Lowe, G. Myhre, J. Nganga, R. Prinn, G. Raga, M. Schulz and R. Van Dorland, 2007: *Changes in Atmospheric Constituents and in Radiative Forcing*. In: Climate Change 2007: The Physical Science Basis. Contribution of Working Group I to the Fourth Assessment Report of the Intergovernmental Panel on Climate Change [Solomon, S., D. Qin, M. Manning, Z. Chen, M. Marquis, K.B. Averyt, M. Tignor and H.L. Miller (Eds.)]. Cambridge University Press, Cambridge, United Kingdom and New York, NY, USA, pp. 141.
- Jeffries T.E., W.T. Perkins, N.J.G. Pearce (1995): *Comparison of Infrared and Ultraviolet Laser Probe Microanalysis Inductively Coupled Plasma Mass Spectrometry in Mineral Analysis*. Analyst, **120**, 1365–1371.
- Jiang S.J., R.S. Houk, M.A. Stevens (1988): *Alleviation of Overlap Interferences for determination of Potassium Isotope Ratios by Inductively Coupled Plasma Mass Spectrometry*. Anal. Chem., **60**, 1217-1221.
- Johnsen S.J., D. Dahl-Jensen, N. Gundestrup, J.P. Steffensen, H.B. Clausen, H. Miller, V. Masson-Delmotte, A.E. Sveinbjörndottir, J. White (2001): *Oxygen isotope and palaeotemperature records from six Greenland ice-core stations: Camp Century, Dye-3, GRIP, GISP2, Renland and NorthGRIP*, Journal of Quaternary Science, **16** (4), 299–307.
- Kneubühl F.K., M.W. Sigrist (1999): *Laser*. Teubner Studienbücher: Physik, pp. 252–259.
- Knüsel S., D.E. Piguet, M. Schwikowski, H.Q. Gäggler (2003): *Accuracy of Ice-Core Trace-Element Analysis by Inductively Coupled Plasma Sector Field Mass Spectrometry*. Environ. Sci. Technol., **37**, 2267–2273.
- Kohn M., S. Kipfstul, A. Lambrecht, Y. Fuji, A. Kronz (2005): *Tephra study on the EPICA-DML ice core*. Geophysical Research Abstracts, Vol. **7**, 07573.
- Krause P. (1993): *Entwicklung von Anwendungsmöglichkeiten der ICP-MS und der Laser-ICP-MS in der Umweltanalytik*, Dissertation, FB Chemie, Universität Hamburg, in Schriftenreihe Angewandte Analytik, Bd. **17**, W. Dannecker (Hrsg.), Institut für Anorganische und Angewandte Chemie der Universität Hamburg.
- Kuhn H.-R., D. Günther (2006): *A quantification strategy in laser ablation ICP-MS based on the transport aerosol particle volume determined by optical particle size measurement*. JAAS, **21**, 1209-1213.
- Leach A.M., G.M. Hieftje (2001): *Use of an ion guide collision cell to improve the analytical performance of an inductively coupled plasma time-of-flight mass spectrometer*. Int. J. Mass Spectrom., **212**, 49–63.
- Legrand M., P. Mayewski (1997): *Glaciochemistry of polar ice cores: a review*. Rev. Geophys., **35**, 219–243.

- Lowenstein T., S.T. Brennan (2001): *Fluid inclusions in Paleolimnological Studies of Chemical Sediments*. In: Tracking Environmental Change using Lake Sediments. Volume 2, Physical and Geochemical Methods. W.M. Last, J.P. Smol (Eds.). Kluwer Academic Publishers, The Netherlands, pp. 189–216.
- Lüdke C., E. Hoffmann, J. Skole, M. Kriews (1999): *Determination of trace metals in size fractionated particles from arctic air by electrothermal vaporization inductively coupled plasma mass spectrometry*. JAAS, **11**, 1685–1690.
- Lüdke C., J. Skole, K. Taubner, M. Kriews (2005): *Trace metal analysis in arctic aerosols by an inductively coupled plasma-time of flight-mass spectrometer combined with an inductively heated vaporizer*. Spectrochim. Acta, Part B, **60** (11), 1412–1422.
- Mahoney P.P., S.J. Ray, G.M. Hieftje (1997): *Time-of-Flight Mass Spectrometry for Elemental Analysis*. Focal Point, **51**(1), 16A–28A.
- Mester Z., R.E. Sturgeon, J.W. Lam, P.S. Maxwell, L. Péter (2001): *Speciation without chromatography, Part I: Determination of tributyltin in aqueous samples by chloride generation, headspace solid-phase microextraction and inductively coupled plasma time of flight mass spectrometry*. JAAS, **16**, 1313–1316.
- Meyers P.A., J.L. Teranes (2001): *Sediment organic matter*. In: Tracking Environmental Change using Lake Sediments. Volume 2, Physical and Geochemical Methods. W.M. Last, J.P. Smol (Eds.). Kluwer Academic Publishers, The Netherlands, pp. 239–269.
- Mubiana V.K., R. Blust (2007): *Effects of temperature on scope for growth and accumulation of Cd, Co, Cu and Pb by marine bivalve Mytilus edulis*. Mar. Environ. Res., **63**, 219–235.
- Munich RE Group, April 2007, http://www.munichre.com/en/ts/geo_risks/natcatservice/long-term_statistics_since_1950/default.aspx (17.03.2008).
- Myers D. P., G.M. Hieftje (1993): *Preliminary Design Considerations and Characteristics of an Inductively Coupled Plasma-Time-of-Flight-Mass Spectrometer*. Microchem. J., **48**, 259–277.
- Myers D.P., G. Li, P. Yang, G.M. Hieftje (1994): *An Inductively Coupled Plasma-Time-of-Flight Mass Spectrometer for Elemental Analysis. Part I: Optimization and Characteristics*. J. Am. Soc. Mass. Spectrom., **5**, 1008–1016.
- North Greenland ice core Project members (2004): *High-resolution record of the Northern Hemisphere climate extending into the last interglacial period*. Nature, **431**, 147–151.
- Olivas R.M., C.R. Quétel, O.F.X. Donard (1995): *Sensitive determination of selenium by ICP-MS with flow injection and hydride generation in the presence of organic solvents*. JAAS, **10**, 865–870.

- Osterberg E.C., M.J. Handley, S.B. Sneed, P.A. Mayewski, K.J. Kreutz (2006): *Continuous Ice Core Melter System with Discrete Sampling for Major Ion, Trace Element, and Stable Isotope Analysis*. Environ. Sci. Technol., **40**, 3355–3361.
- Parrenin F., J.-M. Barnola, J. Beer, T. Blunier, E. Castellano, J. Chappellaz, G. Dreyfus, H. Fischer, S. Fujita, J. Jouzel, K. Kawamura, B. Lemieux-Dudon, L. Loulergue, V. Masson-Delmotte, B. Narcisi, J.-R. Petit, G. Raisbeck, D. Raynaud, U. Ruth, J. Schwander, M. Severi, R. Spahni, J. P. Steffensen, A. Svensson, R. Udisti, C. Waelbroeck, E. Wolff (2007): *The EDC3 chronology for the EPICA Dome C ice core*. Clim. Past, **3**, 485–497.
- Peláez M.V., J.M. Costa-Fernández, A. Sanz-Medel (2002): *Critical comparison between quadrupole and time-of-flight inductively coupled plasma mass spectrometers for isotope ratio measurements in elemental speciation*. JAAS, **17**, 950–957.
- Perkin Elmer. ELAN DRC Series, product information, Shelton, USA.
- Petit J.-R., J. Jouzel, D. Raynaud, N. I. Barkov, J.-M. Barnola, I. Basile, M. Bender, J. Chappellaz, M. Davisk, G. Delaygue, M. Delmotte, V. M. Kotlyakov, M. Legrand, V. Y. Lipenkov, C. Lorius, L. Pépin, C. Ritz, E. Saltzman, M. Stievenard (1999): *Climate and atmospheric history of the past 420,000 years from the Vostok ice core, Antarctica*. Nature, **399**, 429-436.
- Pisonero J., J. Koch, M. Wälle, W. Hartung, N.D. Spencer, D. Günther (2007): *Capabilities of Femtosecond Laser Ablation Inductively Coupled Plasma Mass Spectrometry for Depth profiling of Thin Metal Coatings*. Anal. Chem., **79**, 2325–2333.
- Planchon F.A.M., C.F. Boutron, C. Barbante, G. Cozzi, V. Gaspari, E.W. Wolff, C.P. Ferrari, P. Cescon (2002): *Short-term variations in the occurrence of heavy metals in Antarctic snow from Coats Land since the 1920s*. Sci. Total Environ., **300**, 129–142.
- Price G.D., N.J.G. Pearce (1997): *Biomonitoring of Pollution by Cerastoderma edule from the British Isles: a Laser Ablation ICP-MS study*. Mar. Pollut. Bull., **34**(12), 1025–1031.
- Ray S.J., G.M. Hieftje (2001): *Mass analyzers for inductively coupled plasma time-of-flight mass spectrometry*. JAAS, **16**, 1206–1216.
- Reinhardt H. (2002): *Entwicklung und Anwendung eines Laserablations-ICP-MS-Verfahrens zur Multielementanalyse von atmosphärischen Einträgen in Eisbohrkernen*. Dissertation, Faculty 2 (Biology / Chemistry) of the University Bremen.

- Reinhardt H., M. Kriews, H. Miller, O. Schrems, C. Lüdke, E. Hoffmann, J. Skole (2001): *Laser ablation inductively coupled plasma mass spectrometry: a new tool for trace element analysis in ice cores*. Fresen. J. Anal. Chem., **370**, 5, 629–636.
- Repond P., M.W. Sigrist (1996): *Photoacoustic spectroscopy on trace gases with continuous tunable CO₂ lasers*. Appl. Opt., **35**(21), 4065–4085.
- Revel-Rolland M., P. De Deckker, B. Delmonte, P.P. Hesse, J.W. Magee, I. Basile-Doelsch, F. Grousset, D. Bosch (2006): *Eastern Australia: a possible source of dust in east Antarctica interglacial ice*. EPSL, **249**, 1–13.
- Richardson C.A. (2001): *Molluscs as archives of environmental change*. Oceanography and Marine Biology: an Annual Review, **39**, 103–164.
- Rose N. (2001): *Fly-Ash Particles*. In: Tracking Environmental Change using Lake Sediments. Volume 2, Physical and Geochemical Methods. W.M. Last, J.P. Smol (Eds.). Kluwer Academic Publishers, The Netherlands, pp. 319–349.
- Rosenberg G.D. (1980): *An ontogenetic approach to the environmental significance of bivalve shell chemistry*. In: Skeletal Growth of Aquatic Organisms. D.C. Rhoads, R.A. Lutz (Eds.), Plenum, New York, pp. 133–168.
- Röthlisberger R., M. Bigler, M. Hutterli, S. Sommer, B. Stauffer (2000): *Technique for Continuous High-Resolution Analysis of Trace Substances in Firn and Ice Cores*. Environ. Sci. Technol., **34**, 338–342.
- Ruth U., J.M. Barnola, J. Beer, M. Bigler, T. Blunier, E. Castellano, H. Fischer, F. Fundel, P. Huybrechts, P. Kaufmann, S. Kipfstuhl, A. Lambrecht, A. Morganti, H. Oerter, F. Parrenin, O. Rybak, M. Severi, R. Udisti, F. Wilhelms, E. Wolff (2007): *"EDML1": a chronology for the EPICA deep ice core from Dronning Maud Land, Antarctica, over the last 150 000 years*. Clim. Past, **3**(3), 475–484.
- Russo R.E. (1995): *Laser Ablation*. Appl. Spectrosc., **49**(9), 14A–28A.
- Sakata K., K. Kawabata (1994): *Reduction of fundamental polyatomic ions in inductively coupled plasma mass spectrometry*. Spectrochim. Acta, Part B, **49**, 1027–1038.
- Schaumlöffel D., P. Giusti, M.V. Zoriy, C. Pickardt, J. Szpunar, R. Lobinski, J. S. Becker (2005): *Ultratrace determination of uranium and plutonium by nano-volume flow injection double-focusing sector field inductively coupled plasma mass spectrometry (nFI-ICP-SFMS)*. JAAS, **20**(1), 17–21.
- Severi M., S. Becagli, E. Castellano, A. Moranti, R. Traversi, R. Udisti, U. Ruth, H. Fischer, P. Huybrechts, E. Wolff, F. Parrenin, P. Kaufmann, F. Lambert, J.P. Steffensen (2007): *Synchronisation of the EDML and EDC ice cores for the last 52 kyr by volcanic signature matching*. Clim. Past, **3**, 367–374.

- Shao Y., G. Horlick (1991): *Recognition of mass-spectral interferences in inductively coupled plasma-mass spectrometry*. Appl. Spectrosc., **45**, 143–147.
- Shuttleworth S. (1995): *Optimisation of laser wavelength in the ablation sampling of glass materials*. Appl. Surf. Sci., **96-98**, 513–517.
- Siegenthaler U., T.F. Stocker, E. Monnin, D. Lüthi, J. Schwander, B. Stauffer, D. Raynaud, J.-M. Barnola, H. Fischer, V. Masse-Delmotte, J. Jouzel (2005a): *Stable Carbon Cycle-Climate Relationship During the Late Pleistocene*. Science, **310**, 1313–1317.
- Siegenthaler U., E. Monnin, K. Kawamura, R. Spahni, J. Schwander, B. Stauffer, T.F. Stocker, J.-M. Barnola, H. Fischer (2005b): *Supporting evidence from the EPICA Dronning Maud Land ice core for atmospheric CO₂ changes during the past millennium*. Tellus, **57B**, 51–57.
- Skoog D.A., J.J. Larry (1996): *Principles of Instrumental Analysis*. 4th Edition, Saunders College Publishing, Orlando, Florida, pp. 255.
- Spahni R., J. Chappellaz, T.F. Stocker, L. Louergue, G. Hausammann, K. Kawamura, J. Flückiger, J. Schwander, D. Raynaud, V. Masson-Delmotte, J. Jouzel (2005): *Atmospheric Methane and Nitrous Oxide of the Late Pleistocene from Antarctic Ice Cores*. Science, **310**, 1317–1321.
- Sturgeon R.E., J.W.H. Lam, A. Saint (2000): *Analytical characteristics of a commercial ICP orthogonal acceleration time-of-flight mass spectrometer (ICP-TOFMS)*. JAAS, **15**, 607-616.
- Sylvester P.J., M. Ghaderi (1997): *Trace element analysis of scheelite by excimer laser ablation-inductively coupled plasma-mass spectrometry (ELA-ICP-MS) using synthetic silicate glass standard*. Chem. Geol., **141**, 49–65.
- Tanner S.D., V.L. Baranov (1999): *Theory, design, and operation of a dynamic reaction cell for ICP-MS*. At. Spectrosc., **20**(2), 45–52.
- Tao G., R. Yamada, Y. Fujikawa, A. Kudo, J. Zheng, D.A. Fisher, R.M. Koerner (2001): *Determination of trace amounts of heavy metals in arctic ice core samples using inductively coupled plasma mass spectrometry*. Talanta, **55**, 765–772.
- Thomas R. (2004): *Practical guide to ICP-MS*. Marcel Dekker, Inc., Monticello, New York, USA.
- Thorn K., R.M. Cerrato, M.L. Rivers (1994): *Elemental Distributions in Marine Bivalve Shells as Measures by Synchrotron X-Ray Fluorescence*. Biol. Bull., **188**, 57–67.
- Tian X., H. Emteborg, F.C. Adams (1999): *Analytical performance of axial inductively coupled plasma time of flight mass spectrometry*. JAAS, **14**, 1807-1814.

- Tian X., H. Emteborg, M. Barbaste, F.C. Adams (2000): *Accuracy and precision of lead isotope ratios in wines measured by axial inductively coupled plasma time of flight mass spectrometry*. JAAS, **15**, 829-835.
- Vandal G.M., W.F. Fitzgerald, C.F. Boutron, J.P. Candelone (1993): *Variations in mercury deposition to Antarctica over the past 34,000 years*. Nature, **362**, 621–623.
- Van de Velde K., P. Vallelonga, J.P. Candelone, K.J.R. Rosman, V. Gaspari, G. Cozzi, C. Barbante, R. Udisti, P. Cescon, C.F. Boutron (2005): *Pb isotope record over one century in snow from Victoria Land, Antarctica*. EPSL, **232**(1-2), 95–108.
- Vanhaecke F., L. Moens, R. Dams, L. Allen, S. Georgitis (1999): *Evaluation of the Isotope Ratio Performance of an Axial Time-of-Flight ICP Mass Spectrometer*. Anal. Chem., **71**(15), 3297-3303.
- Wang L., Y. Wang, J. Wang, D. Günther (2006): *Fluid mineralization of the Dajing Sn-polymetal deposit: Evidence from LA-ICP-MS analysis of individual fluid inclusions*. Chinese Science Bulletin, **51**(22), 2781-2788.
- Warren S.G. (1984): *Optical constants of ice from the ultraviolet to the microwave*. Appl. Optics, **23**, 1206–1225.
- Watmough S.A., T.C. Hutchinson, R.D. Evans (1997): *Application of Laser Ablation Inductively Coupled Plasma-Mass Spectrometry in Dendrochemical Analysis*. Environ. Sci. Technol., **31**, 114-118.
- Wegner A. (2008): *Sources and Transport Characteristics of Mineral Dust in Dronning Maud Land*. Dissertation, Faculty 5 (Geoscience) of the University Bremen.
- Wefer G., W.H. Berger, J. Bijma, G. Fischer (1999): *Clues to Ocean History: a Brief Overview of Proxies*. In: Use of Proxies in Paleoceanography. G. Fischer, G. Wefer (Eds.), Springer Verlag Berlin Heidelberg, pp. 1–68.
- Wiley W.C., I.H. McLaren (1955): *Time-of-Flight Mass Spectrometer with Improved Resolution*. Rev. Sci. Instrum., **26**, 1150–1157.
- Willie S., Z. Mester, R.E. Sturgeon (2005): *Isotope ratio precision with transient sample introduction using ICP orthogonal acceleration time-of-flight mass spectrometry*. JAAS, **20**, 1358-1364.
- Wiza J.L. (1979): *Microchannel Plate Detectors*. Nuclear Instruments and Methods, **162**, 587-601.
- Wolff E., H. Fischer, F. Fundel, U. Ruth, B. Twarloh, G.C. Littot, R. Mulvaney, R. Röthlisberger, M. de Angelis, C.F. Boutron, M. Hansson, U. Jonsell, M.A. Hutterli, F. Lambert, P. Kaufmann, B. Stauffer, T.F. Stocker, J.P. Steffensen, M. Bigler, M.L. Siggaard-Andersen, R. Udisti, S. Becagli, E. Castellano, M. Severi, D. Wagenbach, C. Barbante, P. Gabrielli, V. Gaspari (2006): *Southern Ocean sea-ice extent, productivity and iron flux over the past eight glacial cycles*. Nature, **440**, 491–496.

Publication I

High spatial resolution element analysis of polar ice by Laser Ablation-ICP-MS

D. Dick, H. Reinhardt, U. Ruth, M. Kriews

Submitted to the Journal of Analytical Atomic Spectrometry, 18.04.2008.

High spatial resolution element analysis of polar ice by Laser Ablation-ICP-MS

Dorothee Dick, Heiko Reinhardt[†], Urs Ruth and Michael Kriews^{*}

Alfred Wegener Institute for Polar and Marine Research, Am Handelshafen 12, 27570 Bremerhaven; [†] Hamburger Stadtentwässerung, Köhlbranddeich 1, 20457 Hamburg

Abstract

An ice core section from the Holocene, drilled in the Atlantic sector of Antarctica, was analysed by laser ablation-inductively coupled plasma-mass spectrometry (LA-ICP-MS) in high spatial resolution of about 4 mm. With this method, the concentrations of sea salt tracers (Na, Mg, K, Sr, Ba), mineral dust tracers (Al, Mn, Fe, La and Ce) and tracers for other natural or anthropogenic sources (Co, Ni, Cd, Zn, Pb and Bi) were determined. The analysed ice core, including a visible particle horizon, revealed in general enhanced element concentrations during winter months. After the LA-ICP-MS analysis, samples were molten and split into two parts. Verification of LA-ICP-MS analysis by ICP-MS analysis of acidified and digested samples as well as by continuous flow analysis (CFA) showed that LA-ICP-MS analysis was better suited to analyse particles included in the ice matrix. Element concentrations of snow pit samples in the vicinity of the deep ice coring site differed by a factor of 1 to 3 compared to our results, except Pb which showed 13 times lower concentrations. Compared to deep ice core samples from the Indian sector of Antarctica, our results showed decreased concentrations by a factor of 1 to 3 for sea salt components, increased concentrations by a factor of 6 to 8 for mineral dust components and by a factor of 10 to 40 higher concentrations for other elements.

Keywords: laser ablation, high-resolution analysis, multi-element analysis, climate archives, ice cores

Introduction

The study of trace elements in natural samples (*e.g.* sediment cores, ice cores, corals, bivalves, tree rings) as indicator for environmental pollution and for paleoclimate research has been used extensively during the past decades.^{1,2} Depending on the sample size, the information desired and the physical state, several analytical methods have been employed. Usually samples under investigation have to be dissolved by means of digestion. Laser ablation (LA) is established as an appropriate technique for either the

^{*} Corresponding author tel.: +49-(0)471-4831-1420; fax: +49-(0)471-4831-1149; email: Michael.Kriews@awi.de

examination of solid samples – where only small amounts of sample material are available – or when high resolution sampling is required.^{3,4} Due to the small sample amounts ablated by the laser beam a highly sensitive detection system is required. Advantages of inductively coupled plasma mass spectrometry (ICP-MS) make the coupling of LA and ICP-MS most adequate for major and trace element analysis. Applications and developments in LA are given by Russo *et al.*⁵ and Günther *et al.*⁶, while more information on the investigations of solid and liquid samples by inorganic mass spectrometric methods is given by Becker and Dietze.⁷ In contrast to digestion of samples with subsequent analysis, LA-ICP-MS offers high spatial resolution analysis combined with less handling of hazardous materials, less sample preparation and therefore potentially less sample contamination. In terms of sample preparation, it is a fast method compared to liquid ICP-MS. Therefore, LA-ICP-MS combined with a cooled sample chamber has a great potential for the analysis of frozen environmental and climate archive samples, *e.g.* finely stratified material like ice cores. LA-ICP-MS analysis of polar ice cores constitutes an additional method for ice core analysis and can be used to validate data obtained by other high resolution methods, *e.g.* Continuous Flow Analysis (CFA) in combination with an ICP-MS system.⁸⁻¹¹

Ice cores from Polar Regions are amongst the most suitable archives of global climatic conditions.¹²⁻¹⁴ Gases trapped within the ice cores reflect the atmospheric composition of the past.¹⁵ Air borne trace compounds like mineral dust, sea salt and anthropogenic pollutants are deposited on polar ice caps.^{1,16,17} Especially from the rare earth element (REE) and Sr composition of the mineral dust deposits, the corresponding source region can likely be identified.¹⁷⁻¹⁹ Due to the stratified deposition of snow, these tracers are deposited chronologically and potentially archive climatic changes. Large distances from source areas to the deposition site on the polar ice caps leads to a considerable loss en route. Therefore, a careful sample preparation and a highly sensitive analytical method are required.²⁰⁻²² Within the EPICA (European Project for Ice Coring in Antarctica)¹³ a 2774.15 m long ice core (diameter: 98 mm) was drilled at Kohnen station (Dronning Maud Land (DML), Position: 75°0.10'S, 0°4.07'E). For this study, we investigated exemplarily a 1 m long section between 269 and 270 m depth (EDML metre 270, where EDML = EPICA-DML), which was dated to 3550 – 3567 years before present (yr b.p.),²³ where b.p. refers to “years before 1950”. Most striking in this core segment is a visible 2 mm wide particle horizon at 269.60 m depth (3559.5 yr b.p.). High spatial resolution trace element analysis of this ice core segment was done by LA-ICP-MS. Additionally, for a morphological study of individual particles, Cryo Scanning Electron Microscopy (Cryo-SEM) was performed. After LA-ICP-MS analysis, samples were molten and analysed by conventional ICP-MS. One part of the sample was acidified while for the other part a total acid digestion was applied to assess the reliability of LA-ICP-MS analysis.

Experimental

Standards and labware

At the Alfred Wegener Institute for Polar and Marine Research (AWI) in Bremerhaven, Germany, ultrapure water was produced by coupling a reverse osmosis system with a Purelab ultra system (Elga, High Wycombe, U.K.). Commercially available ICP-MS multi-element stock solutions (Perkin Elmer) were used for external calibration of the LA-ICP-MS and ICP-MS systems. All standards were acidified to pH 1 with subboiled HNO₃ (distilled 65% HNO₃, pro analysis, Merck) and contained 10 µg L⁻¹ Rh (RhCl₃, Merck) as internal standard. Eppendorf pipettes with polypropylene (PP) tips were used for sample and standard preparation. The preparation of ice standards for calibration is described by Reinhardt *et al.*²⁴ Steps for standard preparation for liquid ICP-MS were done under a clean bench US Class 100 installed in a clean room US class 10000. At the AWI, all labware that came into contact with samples and standards was run through a special cleaning procedure described elsewhere.²⁵

Ice core sampling and preparation

Parallel to the core axis, the EDML ice core metre 270 was sawn into smaller stripes for the use of different analytical methods in a cold room at -20°C. For LA analysis, one calotte with a face from the former ice core surface was available. Owing to the dimensions of the sample chamber, this part was split into 13 subsections (~8.0 cm • 3.3 cm • 1.5 cm) with a band saw. Subsection no. 9 included the remarkable particle horizon (Figure S 1). All subsections were fixed on object slides using ultrapure water. To decontaminate the sample surface, the top was cut down to 1 cm with a Molybdenum microtome knife under a clean bench US Class 100 installed in our cold room at -20°C. The operator wore PE gloves and elbow length gloves during the decontamination. Every 2.5 mm the knife was decontaminated with 2% HNO₃ (distilled 65% HNO₃, Merck) and the PE gloves were replaced.

Individual parts (0.5 cm³ volume) of the particle horizon in 269.60 m depth were separated under clean room conditions at -20°C with a pre-cleaned spatula. These parts were fixed on sample carriers for Cryo-SEM investigations with a special glue freezing at low temperatures (Tissue-Tek[®] O.C.T.[™] Compound, Sakura Finetek, USA).

Cryo-SEM

The size distribution and the bulk composition of the particles were determined by Cryo-SEM, a modified SEM coupled with an energy dispersive X-ray analysis (EDXA) system at the Materialprüfungsanstalt Bremen, Germany. A temperature of -130°C inside this device enables the analysis of frozen materials. To intensify the surface conductivity, the sample surface was sputtered with carbon. Analyses were carried out before and after sputtering.

LA-ICP-MS

The frozen polar ice core EDML metre 270 was analysed with LA-ICP-MS (laser source: Quanta-Ray® GCR-11, (Nd:YAG) Spectra Physics 1064 nm; ICP-MS: Elan 6000 Perkin Elmer/Sciex) using a special cryogenic sampling cell.^{26,27} Generally, each matrix has a specific wavelength dependent absorption coefficient. In our case, *i.e.* for glacial ice, 1064 nm is best suitable for LA.²⁸ The absorption coefficient of mineral material at lower wavelength is much higher. Therefore more effective ablation of the sample occur. Hitherto, it was not possible to switch to a lower wavelength for direct ablation of embedded particles. The experimental setup for direct analysis of frozen samples is shown in the supplementary material (Figure S 2). A detailed description is given by Reinhardt *et al.*²⁴ In contrast, we used an optical system with a focal length of 90 mm instead of 75 mm in order to reduce the width of the ablated line from 300 µm to 200 µm. An overview of optimized parameters can be found in Table 1. Details about calibration studies, detection limits and method verification by analysing frozen standard reference materials are described in.^{3,24,29}

High spatial resolution LA analysis perpendicular to the core axis was performed every 4 mm (Figure S 1) on subsections no. 1 to 8 and 10 to 13, and every 3 mm on subsection no. 9. The first and the last centimetre on each subsection were discarded because of potential contamination problems. In total 60 isotopes of 44 elements were determined (Table 1).

ICP-MS

After LA-ICP-MS analysis, samples were separated from the object slides and about 0.5 mm was cut away from all surfaces by a microtome. Afterwards samples were molten and divided into two fractions. One fraction (10 mL) was acidified to pH 1 with subboiled HNO₃ (65% distilled HNO₃, pro analysis, Merck) and concentrated by a factor of 5 with a pressure digestion system (Druckaufschlusssystem DAS, Picotrace GmbH, Germany). The second fraction (10 mL) was transferred into pre-cleaned polyfluor-alkoxy (PFA) vessels, afterwards they were concentrated and digested according to Dick *et al.*²⁵ These samples were analysed by ICP-MS (Elan 6000 Perkin Elmer/Sciex).

Results and discussion

Morphology and bulk composition studies of the particle horizon in EDML metre 270 by Cryo-SEM

Numerous particles are incorporated in the ice matrix. The geometric particle sizes covered a range from 1 to 20 µm. Angular particles indicating mineral dust,³⁰ as well as spherical particles, which are typically formed during high temperature processes (combustion, meteoric impact),³⁰ were detected. With EDXA, the bulk composition of these particles could be clarified. Apart from the main components Ca, Si and Al, which are characteristic for mineral dust, several Au and Pt particles were found as minor

compounds. Scanning electron images of mineral dust, Au, and Pt particles, the bulk composition, as well as EDXA spectra are shown in the supplementary material (Figure S 3). Concerning the remarkable Pt and Au findings, for several reasons we are confident that these particles have not been incorporated into the matrix by contamination: (i) EDXA spectra of the sample before and after sputtering showed no differences. (ii) Analyses were accomplished on freshly generated fracture surfaces. Therefore, contamination sources (i.e. band saw, Molybdenum knife for surface treatment of the ice sample or the spatula) can be excluded.

Annual variations in EDML metre 270

In a next step, LA-ICP-MS analysis was performed on EDML metre 270. On each ablated line, 5 replicate analyses were repeated. Due to inherent inhomogeneity of the sample material, the LA-ICP-MS method entailed considerably higher relative standard deviations (RSD) of the results compared with bulk analyses, e.g. liquid ICP-MS. RSD of elements discussed in this paper are shown in Table 1. Information about the RSD and detection limits (d.l.) of all analysed isotopes is given as supplementary material (Table S 1).

Table 1: Operating conditions and analysed isotopes for the applied laser ablation inductively coupled plasma mass spectrometer system (LA-ICP-MS). Relative standard deviations (RSD) in % for natural ice samples and detection limits (d.l.) in ng kg^{-1} for LA-ICP-MS analysis of ice core samples are also given.

<i>ICP-MS</i>		<i>PerkinElmer Sciex Elan 6000</i>						
Radio frequency power		1400 W						
Plasma gas		14.0 L min ⁻¹						
Auxiliary gas		0.83 L min ⁻¹						
Carrier Gas		1.1 L min ⁻¹						
Dwell time		10 ms						
Sweeps / Replicate		20						
Replicate		5						
<i>laser system</i>		<i>Spectra Physics, Quanta-Ray® GCR-11</i>						
Wavelength		1064 nm						
Mode		Q-Switch						
Q-Switch time		220 μs						
Laser energy		280 mJ						
Pulse Frequency		10 Hz						
Focus		on sample surface						
Laser scan mode		line scan						
position of lines		perpendicular to the core axis						
line length		29 mm						
Line width		200 μm						
spatial resolution		3 - 4 mm						
<i>analysed isotopes</i>								
¹⁷ OH, ⁷ Li, ⁹ Be, ²³ Na, ²⁴ Mg, ²⁵ Mg, ²⁷ Al, ³⁹ K, ⁴³ Ca, ⁴⁴ Ca, ⁵¹ V, ⁵² Cr, ⁵³ Cr, ⁵⁵ Mn, ⁵⁶ Fe, ⁵⁷ Fe, ⁵⁸ Ni, ⁵⁹ Co, ⁶⁰ Ni, ⁶⁴ Zn, ⁶⁶ Zn, ⁸⁵ Rb, ⁸⁶ Sr, ⁸⁸ Sr, ⁸⁹ Y, ¹⁰³ Rh, ¹⁰⁵ Pd, ¹¹¹ Cd, ¹¹⁴ Cd, ¹³⁸ Ba, ¹³⁹ La, ¹⁴⁰ Ce, ¹⁴¹ Pr, ¹⁴² Nd, ¹⁴³ Nd, ¹⁴⁷ Sm, ¹⁴⁹ Sm, ¹⁵¹ Eu, ¹⁵³ Eu, ¹⁵⁸ Gd, ¹⁵⁹ Tb, ¹⁶⁴ Dy, ¹⁶⁵ Ho, ¹⁶⁶ Er, ¹⁶⁹ Tm, ¹⁷⁴ Yb, ¹⁷⁵ Lu, ¹⁹¹ Ir, ¹⁹¹ Ir, ¹⁹⁴ Pt, ¹⁹⁵ Pt, ¹⁹⁷ Au, ²⁰⁴ Pb, ²⁰⁵ Tl, ²⁰⁶ Pb, ²⁰⁷ Pb, ²⁰⁸ Pb, ²⁰⁹ Bi, ²³² Th, ²³⁸ U								
	RSD	d.l.		RSD	d.l.	RSD	d.l.	
	(%)	(ng kg^{-1})		(%)	(ng kg^{-1})	(%)	(ng kg^{-1})	
Na	24	271	Al	48	1960	Co	46	6
Mg	32	249	Mn	50	73	Cd	69	26
Sr	35	23	Fe	37	241	Pb	48	9
Ba	46	3	Ce	35	4	Bi	31	4

Year-round aerosol sampling at Kohnen station showed a seasonal maximum of Na^+ concentrations during winter,³¹ providing us a valuable tracer to identify winter snow layers by Na concentration maxima. Figure 1 shows smoothed element concentrations (gliding Gaussian average, 3 points) of sea salt tracers Na, Mg, Sr, and Ba, mineral dust tracers Al, Mn, Fe, and Ce, as well as tracers for possible other natural or anthropogenic sources or for volcanic events (Co, Cd, Pb and Bi) versus (vs.) the age of the ice core.²³ According to the counted Na concentration maxima derived by continuous flow analysis (CFA), also shown in Figure 1, the segment covered a time slice of 15 years, instead of 17 years obtained by Ruth *et al.*²³ Note that parts of concentration profiles of Mn, Ce, Co, Cd and Bi were below the d.l. Sea salt related components show similar concentration patterns. For Ba however, the signal variability was significantly higher.

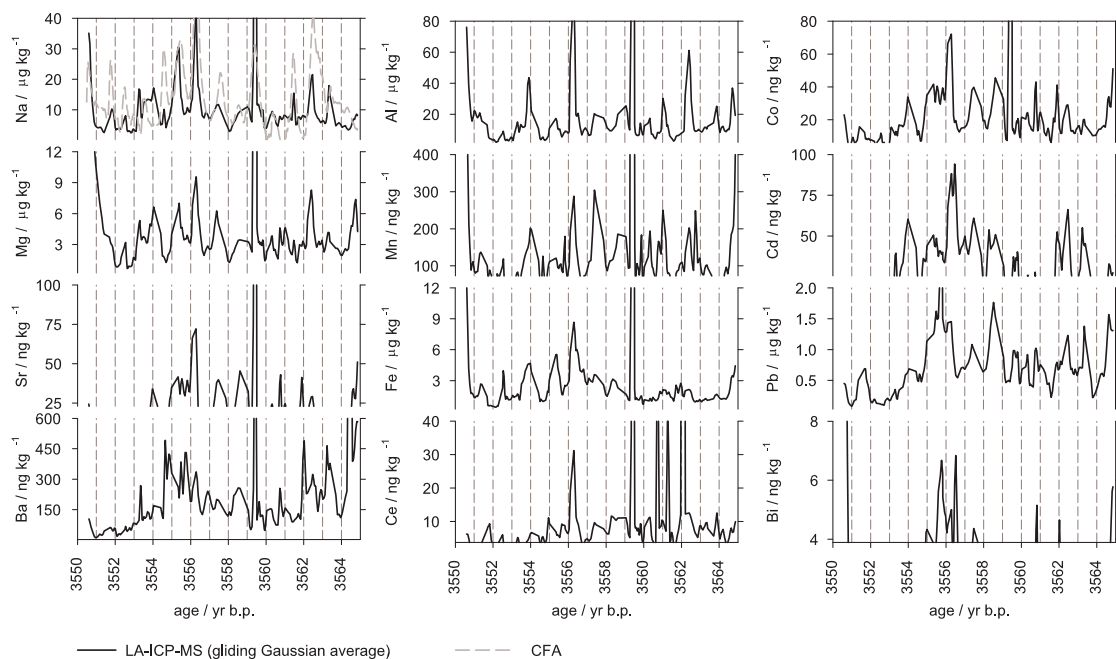


Figure 1: Element concentrations of Na, Mg, Sr, Ba, Al, Mn, Fe, Ce, Co, Cd, Pb and Bi in the Antarctic ice core EDML metre 270 vs depth (black line: gliding Gaussian average (3 points) obtained by LA-ICP-MS. Grey long dashed line: Na concentrations obtained by CFA analysis. Short dashed grey lines perpendicular to the x-axis mark summer months. The beginning of each y-axis corresponds to the d.l.

Notably, EDML metre 270 showed no distinct temporal phase shifting between sea salt (Na) and mineral dust (Al) tracers. Other mineral dust tracers like Mn and Fe showed similar concentration profiles. Minimum concentrations of Ce are close to or below the d.l., but the concentration pattern is comparable to other mineral dust tracers. In summer 3558 yr b.p. Mn concentrations are more pronounced. Between 3560 and 3564 yr b.p. Fe shows only weak signature changes. Phase shifts between mineral dust and sea salt deposition is often a characteristic feature in polar snow pit and polar aerosol studies.^{32,33,34} However, investigations of a snow pit excavated at Kohnen station showed that typical sea salt components have additional mineral dust sources.³⁵

Concentration profiles of Co, Cd, Pb and Bi are highly fluctuating and parts of the concentration profiles of Co, Cd and Bi are below the d.l.. Only Co and Pb show partly similar concentration patterns in relation to sea salt and mineral dust tracers.

Short-term variability of element concentrations within EDML metre 270 is shown in Table 2 and Figure 1. The ratios of maximum element concentrations to minimum element concentrations vary by 10 to 1300. Maximum to minimum concentrations of 12 to 100 are reported by Planchon *et al.*³² and ratios by 40 to 4800 are reported by Kriews *et al.*³⁵

Table 2: Averaged element concentrations with SD of EDML metre 270 (calculated without the particle horizon) analysed with LA-ICP-MS as well as element concentrations with SD of one snow pit dug at Kohlen station and analysed by ICP-MS after acid digestion. Values below the d.l. were set to d.l./2. Element concentrations of ice core sections from two other drilling sites in Antarctica: Dome C and Vostok station are shown for comparison. For the latter two drilling sites samples were analysed after melting and acidifying to pH 1 by ICP-Sector Field-MS (except Na, which was analysed by ion chromatography).

	EDML meter 270	Kohlen ³⁵	Dome C	Dome C	Vostok ³⁷
sample depth / m	269-270 m*	0-1.86 m			126.73 m
time period / yr b.p.	3550-3564	3-13			1640
	$\mu\text{g kg}^{-1}$	$\mu\text{g L}^{-1}$	$\mu\text{g L}^{-1}$	$\mu\text{g L}^{-1}$	$\mu\text{g L}^{-1}$
Na	8.8 ± 6.7	27.3 ± 38.8	22.2 ^{16,a}		
Mg	4.1 ± 5.6	7.9 ± 7.1	13.6 ^{36,b}	5.3 ^{36,c}	
Al	13.4 ± 17	42.6 ± 160			1.8
Mn	0.1 ± 0.1	0.1 ± 0.2	0.048 ^{36,b}	0.008 ^{36,c}	0.014
Fe	2.1 ± 1.8	4.1 ± 6.0	0.299 ^{16,d}	0.328 ^{16,e}	
	ng kg^{-1}	ng L^{-1}	ng L^{-1}	ng L^{-1}	ng L^{-1}
Co	18 ± 14	14 ± 20	2 ^{36,b}	1 ^{36,c}	2
Sr	49 ± 33	50 ± 52			63
Cd	27 ± 20	12 ± 18	0.5 ^{36,b}	1.0 ^{36,c}	
Ba	191 ± 306	438 ± 1590	15 ^{36,b}	4 ^{36,c}	11
La	7 ± 25	7 ± 26	1 ^{20,f}		
Ce	11 ± 57	15 ± 60	3 ^{20,f}		
Pb	683 ± 466	51 ± 76			
Bi	3 ± 2	2 ± 3	0.1 ^{36,b}	0.2 ^{36,c}	

^a Dome C left column: 3559 yr b.p., 133.1 m

^b Dome C left column: 2015 yr b.p., 87 m

^c Dome C right column: 4156 yr b.p., 152 m

^d Dome C left column: 3000 yr b.p.

^e Dome C right column: 5000 yr b.p.

^f Dome C left column: 14204 yr b.p., 405.6 m

*average concentrations were calculated as follows:

210 lines were ablated perpendicular to the core axis. Two lines were ablated along the particle horizon. For average calculations these two lines were not considered.

Element concentrations in EDML metre 270

Table 2 shows element concentrations of EDML metre 270, concentrations of one snow pit dug at Kohnen station,³⁵ and concentrations of ice core sections from two further deep drilling stations in Antarctica; ^{16,20,36,37} the Dome C and Vostok drilling site. Element concentrations from our ice core segment and the investigated snow pit³⁵ are expected to be similar because ice core studies show, that dust concentrations during the Holocene are comparable whereas dust concentrations increase during glacial times.^{38,39} Literature data from the Dome C and Vostok drilling site are shown to scrutinise the order of magnitude of concentrations obtained by LA-ICP-MS for EDML metre 270.

Sea salt tracer.

Snow pit concentrations of Na, Mg, Sr and Ba exceed EDML metre 270 concentrations by a factor of 1 to 3. Concentrations at Dome C and Vostok are higher for Na, Mg and Sr by a factor of 2.5, 2.3 and 1.3 respectively compared to results obtained in this study. Instead, Ba shows higher concentrations in EDML metre 270 by a factor of 26 and in the snow pit by a factor of 54 compared to samples from Dome C and Vostok station. Sodium concentrations as a proxy for sea salt entry were 1.5 times higher at Dome C station compared to the EDML station during the Holocene, where 28% of the Na concentration was attributed to mineral dust sources.³⁹ This is in good agreement with our results.

Mineral dust tracers.

EDML metre 270 showed on average slightly lower concentrations for Al, Mn, Fe, La and Ce by a factor of 1 to 3 compared to snow pit concentrations. Concentrations at Kohnen station are higher by a factor of (X) for Al (8), Mn (8), Fe (8), La (7) and Ce (4) compared to concentrations of Dome C and Vostok samples. Acidified (pH 1) Holocene samples from the EDML ice core analysed by ICP-MS show Al concentrations of $2.8 \mu\text{g L}^{-1}$ (SD: $1.9 \mu\text{g L}^{-1}$)⁴⁰ which is distinctly different from our results. That study⁴⁰ reports Fe concentrations of about $1.5 \mu\text{g L}^{-1}$ (SD: $1.5 \mu\text{g L}^{-1}$),⁴⁰ which is in good agreement with our results ($2.1 \mu\text{g kg}^{-1}$ with a SD of $1.8 \mu\text{g kg}^{-1}$). Increased Ca concentrations, as proxy for mineral dust, by a factor of 6 at EDML station compared to Dome C station during the Holocene was shown by Fischer *et al.*,³⁹ which is again in good agreement with our results. Fischer *et al.*³⁹ report that during the Holocene 24% of the total Ca concentration originates from sea salt.

Unfortunately, most of the REE concentrations are below the d.l. Element ratios of Al/Ce and Al/La obtained in this study (857 and 1520 respectively) fairly agree with element ratios of the upper continental crust (Al/Ce=1179; Al/La=2398),⁴¹ taken into account the inhomogeneous composition of the upper continental crust.

Tracers for natural or anthropogenic sources or for other natural events.

Mean concentrations of tracers indicating possible contamination are similar to concentration measurements by Kriews *et al.*³⁵ except for Pb, which exhibits increased mean concentrations by a factor of 13 in EDML metre 270. Such high Pb concentrations point to sample contamination. Concentrations at Kohnen station are higher by a factor of (X) for Co (12), Cd (40) and Bi (20) compared to concentrations of Dome C and Vostok samples.

Discussion of concentration differences between different deep drilling sites.

Contribution to the concentration differences between our measurement compared to the studies in the Dome C and the Vostok ice core, can be explained by: (i) the accumulation rate at the EDML station is about a factor 2 to 3 higher;³⁸ (ii) the dust flux is three times higher in the Atlantic (EDML ice core) compared to the Indian Ocean Sector (Dome C and Vostok ice core) of the Southern Ocean;³⁹ (iii) Kohnen station is influenced by Atlantic air masses whereas Dome C and Vostok station are influenced by Indian Ocean air masses⁴²; (iv) EDML metre 270 was analysed by LA-ICP-MS. The snow pit samples from Kohnen station were analysed after total acid digestion, and samples from Dome C and Vostok station were analysed after acidifying the samples to pH 1, which may result in different recovery rates.⁴⁰

In the literature, the concentration pattern as a function of the ice core radius is discussed. The concentration of several elements was found to increase by a factor of 15 to 130 within the outermost 2 to 3 cm of polar ice cores drilled from fluid filled holes.³⁶ The EDML metre 270 section available for LA-ICP-MS analysis had one face from the former ice core surface (Figure S 1). According to Gabrielli *et al.*,³⁶ this part of the ice core is contaminated by the drilling fluid and sample processing. However, distinct seasonal variations of several elements (Figure 1) suggest a likely undisturbed measurement, as higher concentrations, as caused by contamination, would exhibit a statistically irregular distribution. Moreover, element concentrations of all ablated lines of EDML metre 270 showed lognormal distribution. This points to natural sources.⁴³ Therefore, generally enhanced element concentrations at the EDML deep drilling site seem to be reliable and are confirmed by Kriews *et al.*³⁵

Summary of the ice core data of EDML meter 270.

Only element concentrations of Na, Mg, Al, K, Mn, Fe, Co, Ni, Zn, Sr, Cd, Ba, La, Ce, Pb and Bi are higher than the d.l. (Table S 1) for Holocene ice core samples from Antarctica. All other trace element concentrations determined in this study exceeded only sporadically the d.l.. However, due to increasing mineral dust concentrations by a factor of 10–15 during glacial times at the EPICA drilling sites (EDML and EDC),^{20,38} the presented LA-ICP-MS system should certainly be able to provide valuable concentration profiles for all isotopes listed in Table 1 in Antarctic ice cores for glacial periods.

Verification of LA-ICP-MS analysis of EDML metre 270 with other methods

To verify results obtained by LA-ICP-MS and to clarify advantages and disadvantages of the presented method, we compare our results with conventional ICP-MS analysis of acidified and digested samples as well as with CFA measurements of EDML metre 270. The particle horizon in 269.6 m depth is compared to the corresponding particle horizon in the Vostok ice core.

LA-ICP-MS vs. ICP-MS after acidification and digestion of the samples.

In a first step the analysed samples were molten and analysed again after acidification and after acid digestion. In order to assess the recovery rates, we assume that results obtained by ICP-MS after total acid digestion represent the total amount (*i.e.* 100%) of a given element. For subsections 1 to 8 plus 10 to 13, the recovery rate of sea salt components was: Na: 38%, Mg: 105%, Sr: 43% and Ba: 57% for LA-ICP-MS and Na: 77%, Mg: 105%, Sr: 91% and Ba: 74% for ICP-MS after acidification of the sample. Except for Ce, 31% (median value) of the total mineral dust components were found by LA-ICP-MS (Al: 90%, Mn: 30%, Fe: 31% and Ce: 217%) while 71% were recovered in acidified samples (Al: 64%, Mn: 78%, Fe: 97% and Ce: 62%). Recovery rates for Al of 45% and for Fe of 30% obtained by ICP-MS analysis of acidified (pH 1) ice core samples from the EDML drilling site were found elsewhere.⁴⁰ Differences of recovery rates of acidified samples can be explained by different time slices investigated by each study. The concentrations of Pb and Bi were only slightly different from the results of digested samples (108%, 100% for LA-ICP-MS; 93%, 103% for ICP-MS after acidification). The recovery rates decreased when the subsection with the particle horizon was considered exclusively, *i.e.* for sea salt tracers to about 40% for LA-ICP-MS (Na: 26%, Mg: 44%, Sr: 43% and Ba: 36%) and to 28% the pH 1 leach with conventional ICP-MS analysis (Na: 29%, Mg: 16%, Sr: 34% and Ba: 26%). This pH 1 leach with conventional ICP-MS analysis showed especially low recovery rates for mineral dust tracers: Al: 24%, Mn: 15%, Fe: 11% and Ce: 20% (LA-ICP-MS: Al: 45%, Mn: 28%, Fe: 12% and Ce: 98%). Recovery rates for Pb and Bi were 103% and 97% for LA-ICP-MS analysis and 53% and 50% for ICP-MS analysis of acidified samples. These data revealed that the recovery rates obtained by LA-ICP-MS analysis were less affected by particles embedded in the ice matrix than the ICP-MS analysis of acidified samples. Concentration differences obtained for LA-ICP-MS analysis compared to ICP-MS analysis of digested samples might result from: (i) particles included in the ice matrix are not evaporated with 100% efficiency, (ii) adsorption of evaporated particles on the surface of the connection tube between the sample chamber and the ICP, (iii) incomplete ionisation of particles in the plasma.

LA-ICP-MS vs. CFA.

The continuous melting of ice cores and subsequent analysis by fluorescence methods is called CFA and delivers information about *e.g.* Na. This method is described by Röthlisberger *et al.*⁴⁴ For CFA, one calotte from the centre of EDML metre 270 (Figure S 1) was available. Figure 1 presents Na concentrations analysed by LA-ICP-MS and CFA vs. age (yr b.p.). In general, LA-ICP-MS values were lower by a factor of about two, but the element distribution pattern coincided. The resolution of CFA analysis is 1 mm whereas the laser ablates material every 3 and 4 mm respectively. Obviously, the different spatial resolution did not significantly influence the shape of the Na profile along EDML metre 270. Apart from the particle horizon, the mean Na concentration was $13.6 \mu\text{g kg}^{-1}$ (SD: $10.4 \mu\text{g kg}^{-1}$) for CFA and $8.8 \mu\text{g kg}^{-1}$ (SD: $6.7 \mu\text{g kg}^{-1}$) for LA-ICP-MS analysis. The recovery rate for Na obtained by CFA (60%) agreed fairly well with that achieved by ICP-MS of acidified samples (77%). In contrast, only 14% of the total Na content were retrieved in the subsection including the particle horizon by CFA, while 26% were found by LA-ICP-MS analysis. This explains lower Na concentrations analysed in the particle horizon by CFA analysis (Figure 1). Further Na concentration differences might be explained by the sample inhomogeneity.

LA-ICP-MS vs. wavelength dispersive X-ray electron microprobe (WDX).

The age of the EDML particle horizon in 269.60 m depth correlates to the age of the tephra in the Vostok ice core (Antarctica) in 103.14 m depth (Kohno, pers. comm., 2006). Basile *et al.*⁴⁵ analysed the 30 mm thick tephra layer in the Vostok ice core for major and trace elements. They report that the maximum particle size amounts to 50 μm . They analysed the major element composition of single particles out of the tephra using wavelength dispersive X-ray electron microprobe (WDX). For minor constituents the tephra was first dried, then digested with HF + HClO₄ + HNO₃ and finally analysed by ICP-MS.

Due to the different drilling locations, one expects different transport pattern and deposition processes of atmospheric particles. Table 3 compares element ratios rather than absolute element concentrations of the particle horizon in EDML metre 270 from this study with element ratios of the corresponding Vostok tephra in 103.14 m depth, analysed by Basile *et al.*⁴⁵.

Table 3: Element ratios with errors from the particle horizon of EDML metre 270 and the corresponding particle horizon of the Vostok ice core.⁴⁵

	EDML 269.6 m	Vostok 103.14 m ⁴⁵
Al/Na	3.4 ± 0.3	3.3 ± 0.1
Al/Mg	4.1 ± 0.1	5.5 ± 0.3
Al/K	84 ± 6	20 ± 1
Al/Mn	47 ± 1	49 ± 7
Al/Fe	6.1 ± 0.2	1.1 ± 0.03
Ba/Sr	0.7 ± 0.04	0.6
Ba/La	31 ± 1	38.0
Ce/La	4.3 ± 0.2	3.2

The authors suggest the subduction volcanoes of the South Sandwich Islands to be the source of this tephra layer. Nearly all element ratios fit to each other except Al/K and Al/Fe. The different maximum particle size, the application of different methods, the distance between the two drilling sites and the different distance to the source region may explain these differences in element ratios. Our data confirm correlation studies from Kohno (pers. comm., 2006). Therefore, we conclude the EDML particle horizon in 269.60 m depth to be a tephra layer.

Comparison of LA-ICP-MS with other high-resolution methods.

The coupling of a continuous ice-core melt-head to an ICP-MS constitutes a further method for high-resolution analysis. An ice core melter was coupled directly to an ICP-MS system.⁸⁻¹⁰ While the study of McConnell *et al.*⁸ suggested the acidification of samples prior to continuous injection into the nebulizer system of the ICP-MS was suitable to detect the combined insoluble and soluble fractions, subsequent work by Knüsel *et al.*¹⁰ could not confirm this result. Their investigations showed serious difficulties for a number of trace elements usually found in natural silicates. Further problems might be adsorption effects from particles at the surface of the tubing. The separation of a continuous melt water stream into homogenized samples for ICP-MS analysis constitutes another approach (resolution < 1 cm).¹¹ Osterberg *et al.*¹¹ acidified the samples after separation and allowed them to react for 24 h before freezing and storing. However, according to our study the recovery rate of all elements obtained by simple acidification should be well below 100%.

An increase in resolution by a factor of 2.5 is obtained by LA-ICP-MS applied in our study compared to the method presented by Osterberg *et al.*¹¹ This is important if seasonal variations of ice with an annual layer thickness of < 4 cm shall be resolved. Problems might occur for samples with inclined annual layers. Ablation of several parallel lines parallel to the core axis rather than perpendicular to the core axis as performed in this study, and the comparison of the obtained element signature of different lines should solve this problem. Further, the crystal structure evolution might result in redistribution of particles with the ice (*e.g.* pinning), which results in destruction of the initial chronology and is a problem for all high-resolution methods. A disadvantage of LA-ICP-MS compared to charging the ICP-MS from a continuous ice melter is the required amount of time for the analysis and processing of the data (approx. 1 week vs. 2 days for a 1 m ice core section for LA-ICP-MS and the method described by Osterberg *et al.*¹¹, respectively).

Conclusions

LA-ICP-MS, CFA and the continuous melting with discrete sampling (CMDS¹¹) for ICP-MS analysis were used for high resolution analysis of ice core samples. All three methods require only little sample preparation and therefore minimize the risk of sample contamination. Table 4 lists most important parameters for methodological comparison as well as parameters for ICP-MS analysis of acidified samples. Recovery rates of CMDS combined with ICP-MS analysis are expected to be comparable to ICP-MS values of acidified samples. Inhomogeneous samples require several replicate analyses for LA-ICP-MS to reduce the signal noise. A major advantage of LA-ICP-MS is the possibility to use the sample after LA analysis for other analytical methods. In other words, LA-ICP-MS is virtually a non-destructive method.

Table 4: Comparison of different high resolution methods (LA-ICP-MS, CFA and CMDS coupled to an ICP-MS) and ICP-MS after melting the of ice core samples.

	LA-ICP-MS	ICP-MS after acidification	CFA	CMDS* ¹¹ (coupled to ICP-MS)
elements	Na, Mg, Al, K, Mn, Fe, Co, Ni, Zn, Sr, Cd, Ba, La, Ce, Pb, Bi	multi-element	NH ₄ , Ca, Na	multi-element
resolution (mm)	3	80	1	< 10
recovery rate (ice / ice including particles) (%) [‡]				
<i>sea salt</i>	50 / 40	84 / 28	60 / 14	
<i>mineral dust</i>	31 / 37	71 / 18		
<i>rest</i>	104 / 100	98 / 52		

* Continuous Melting with discrete sampling

[‡] total content was obtained by ICP-MS analysis of digested samples

Depending on the concentration of analysed samples it seems that the coupling of continuous melting devices to ICP-MS systems is most suitable for multi-element analysis of ice cores. Because, conventional ICP-MS analysis of liquid samples shows better recovery rates and lower d.l.. However, the localization of particles and the analysis of their elemental composition are enabled by LA-ICP-MS analysis.

Acknowledgment

This work is a contribution to the European Project for Ice Coring in Antarctica (EPICA), a joint European Science Foundation/European Commission scientific programme, funded by the EU and by national contributions from Belgium, Denmark, France, Germany, Italy, the Netherlands, Norway, Sweden, Switzerland and the United Kingdom. The main logistical support was provided by IPEV and PNRA (at Dome C) and AWI (at Dronning Maud Land). This is EPICA publication ##. We thank the University of Bern (esp. M. Bigler) for support with the CFA measurements. Moreover,

we would like to thank H. Juling for operating the Cyro-SEM with the coupled EDXA at the Materialprüfungsanstalt Bremen. The authors thank R. Weller, S. Kasten, F. Wilhelms and M. Rutgers v. d. Loeff (all AWI), D. Wagenbach (University of Heidelberg, Germany) and C. Lüdke for discussion and comments that improved the manuscript and H. Fischer (AWI) for supporting information.

Supporting information

Details of the sample structure and LA pattern, the experimental setup of the LA system, scanning electron microscope images with EDXA spectra of the particle horizon in EDML metre 270, the relative standard deviations found for replicate analysis of natural ice core samples and detection limits of all analysed isotopes are given in the supplementary material.

References

- 1 M. Legrand and P. Mayewski, *Rev. Geophys.*, 1997, 35, 219–243.
- 2 M. Revel-Rolland, P. De Deckker, B. Delmonte, P.P. Hesse, J.W. Magee, I. Basile-Doelsch, F. Grousset, D. Bosch, *Earth Planet. Sci. Lett.*, 2006, 249, 1–13.
- 3 H. Reinhardt, M. Kriews, H. Miller, C. Lüdke, E. Hoffmann, J. Skole, *Anal. Bioanal. Chem.*, 2003, 375, 1265–1275.
- 4 E. Hoffmann, C. Lüdke, H. Scholze, H. Stephanowitz, *Fresenius' J. Anal. Chem.*, 1994, 350, 253–259.
- 5 R.E. Russo, X. Mao, H. Liu, J. Gonzalez, S.S. Mao, *Talanta*, 2002, 57, 425–451.
- 6 D. Günther, I. Horn, B. Hattendorf, *Fresenius' J. Anal. Chem.*, 2000, 368, 4–14.
- 7 J. S. Becker, H.J. Dietze, *International Journal of Mass Spectrometry*, 2000, 197, 1–35.
- 8 J.R. McConnell, G.W. Lamorey, S.W. Lambert, K.C. Taylor, *Environ. Sci. Technol.*, 2002, 36, 7–11.
- 9 J.R. McConnell, A.J. Aristarain, J.R. Banta, P.R. Edwards, J.C. Simoes, *Proceeding of the National Academy of Science of the United States of America*, 2007, 104(14), 5743–5748.
- 10 S. Knüsel, D.E. Piguet, M. Schwikowski, H.Q. Gäggler, *Environ. Sci. Technol.*, 2003, 37, 2267–2273.
- 11 E.C. Osterberg, M.J. Handley, S.B. Sneed, P.A. Mayewski, K.J. Kreutz, *Environ. Sci. Technol.*, 2006, 40, 3355–3361.
- 12 EPICA Community Members, *Nature*, 2004, 429, 623–628.
- 13 EPICA Community Members, *Nature*, 2006, 444, 195–198.
- 14 North Greenland Ice core Project Members, *Nature*, 2004, 431, 147–151.
- 15 U. Siegenthaler, E. Monnin, K. Kawamura, R. Spahni, J. Schwander, B. Stauffer, T.F. Stocker, J.-M. Barnola, H. Fischer, *Tellus B*, 2005, 57, 51–57.
- 16 E. Wolff, H. Fischer, F. Fundel, U. Ruth, B. Twarloh, G.C. Littot, R. Mulvaney, R. Röthlisberger, M. de Angelis, C.F. Boutron, M. Hansson, U. Jonsell, M.A. Hutterli, F. Lambert, P. Kaufmann, B. Stauffer, T.F. Stocker, J.P. Steffensen, M. Bigler, M.L. Siggaard-Andersen, R. Udisti, S. Becagli, E. Castellano, M. Severi, D. Wagenbach, C. Barbante, P. Gabrielli, V. Gaspari, *Nature*, 2006, 440, 491–496.
- 17 I. Basile, F.E. Grousset, M. Revel, J.R. Petit, P.E. Biscaye, N.I. Barkov, *Earth Planet. Sci. Lett.*, 1997, 146, 573–589.

- 18 B. Delmonte, I. Basile-Doelsch, J.R. Petit, V. Maggi, M. Revel-Rolland, A. Michard, E. Jagoutz, F. Grousset, *Earth Planet. Sci. Lett.*, 2004, 66, 63–87.
- 19 D.M. Gaiero, P.J. Depetris, J.L. Probst, S.M. Bidart, L. Leleyter, *Earth Planet. Sci. Lett.*, 2004, 219, 357–376.
- 20 P. Gabrielli, C. Barbante, C. Turetta, A. Marteel, C. Boutron, G. Cozzi, W. Cairns, C. Ferrari, P. Cescon, *Anal. Chem.*, 2006, 78, 1883–1889.
- 21 S. Hong, C.F. Boutron, C. Barbante, S. Do Hur, K. Lee, P. Gabrielli, G. Capodaglio, C.P. Ferrari, C. Buretta, J.R. Petit, V. Y. Lipenkov, *J. Environ. Monit.*, 2005, 7, 1326–1331.
- 22 G. Tao, R. Yamada, Y. Fujikawa, A. Kudo, J. Zheng, D.A. Fisher, R.M. Koerner, *Talanta*, 2001, 55, 765–772.
- 23 U. Ruth, J.-M. Barnola, J. Beer, M. Bigler, T. Blunier, E. Castellano, H. Fischer, F. Fundel, P. Huybrechts, P. Kaufmann, S. Kipfstuhl, A. Lambrecht, A. Morganti, F. Parrenin, O. Rybak, M. Severi, R. Udisti, F. Wilhelms, E. Wolff, *Climate of the Past*, 2007, 3, 475–484.
- 24 H. Reinhardt, M. Kriews, H. Miller, O. Schrems, C. Lüdke, E. Hoffmann, J. Skole, *Fresenius' J. Anal. Chem.*, 2001, 370, 5, 629–636.
- 25 D. Dick, A. Wegner, P. Gabrielli, U. Ruth, C. Barbante, M. Kriews, *Anal. Chim. Acta*, in press.
- 26 M. Kriews, H. Reinhardt, E. Dunker, I. Beninga, W. Ruhe, *Utility Model*, 2004, DE 20 2004 005 991.6.
- 27 M. Kriews, H. Reinhardt, E. Dunker, E. Hoffmann, C. Lüdtkke, I. Beninga, *Patent*, 2004, EP-DE 501 05 651.3-08.
- 28 S.G. Warren, *Appl. Opt.*, 1984, 23, 1206–1225.
- 29 H. Reinhardt, M. Kriews, O. Schrems, C. Lüdke, E. Hoffmann, J. Skole, in: *Plasma Source Mass Spectrometry: The New Millenium*, ed. G. Holland, D. Tanner, The Royal Society of Chemistry, Cambridge, 2001, pp. 185–194.
- 30 K. R. Spurny, Ellis Horwood, Chichester, 1986, p. 31–39.
- 31 R. Weller, D. Wagenbach, *Tellus B*, 2007, 59, 755–765.
- 32 F. Planchon, C.F. Boutron, C. Barbante, G. Cozzi, V. Gaspari, E.W. Wolff, C.P. Ferrari, P. Cescon, *Sci. Total Environ.*, 2002, 300, 129–142.
- 33 R. Weller, J. Wöltjen, C. Piel, R. Resenberg, D. Wagenbach, G. König-Langlo, M. Kriews, *Tellus B*, submitted.
- 34 G. Tuncel, N.K. Aras, W.H. Zoller, *J. Geophys. Res.*, 1989, 94(D10), 13025–13038.

- 35 M. Kriews, S. Dietrich, D. Dick, I. Stölting, A. Wegner, H. Miller, Colloquium Analytische Atomspektrometrie 2007. hdl:[10013/epic.26505.d001](https://nbn-resolving.org/urn:nbn:de:epic:26505-d001)
- 36 P. Gabrielli, C. Barbante, C. Boutron, G. Cozzi, V. Gaspari, F. Planchon, C. Ferrari, C. Buretta, S. Hong, P. Cescon, Atmos. Environ., 2005, 39, 6420–6429.
- 37 P. Gabrielli, F.A.M. Planchon, S. Hong, K.H. Lee, S.D. Hur, C. Barbante, C. Ferrari, J.R. Petit, V.Y. Lipenkov, P. Cescon, C.F. Boutron, Earth Planet. Sci. Lett., 2005, 234, 249–259.
- 38 H. Fischer, M.-L. Siggard-Andersen, U. Ruth, R. Röthlisberger, E. Wolff, Rev. Geophys., 2007, 45, 1–26.
- 39 H. Fischer, F. Fundel, U. Ruth, B. Twarloh, A. Wegner, R. Udisti, S. Becagli, E. Castellano, A. Morganti, M. Severi, E. Wolff, G. Littot, R. Röthlisberger, R. Mulvaney, M.A. Hutterli, P. Kaufmann, U. Federer, F. Lambert, M. Bigler, M. Hansson, U. Jonsell, M. de Angelis, C. Boutron, M.L. Siggard-Andersen, J.P. Steffensen, C. Barbante, V. Gaspari, P. Gabrielli, D. Wagenbach, Earth Planet. Sci. Lett., 2007, 260, 340–354.
- 40 U. Ruth, C. Barbante, M. Bigler, B. Delmonte, H. Fischer, P. Gabrielli, V. Gaspari, P. Kaufmann, F. Lambert, V. Maggi, F. Marino, J.R. Petit, J.P. Steffensen, R. Udisti, D. Wagenbach, A. Wegner, E. Wolff, Environ. Sci. Technol., submitted.
- 41 K.H. Wedepohl, Geochim. Cosmochim. Acta, 1995, 59, No.7, 1217–1232.
- 42 C.H. Reijmer, M.R. Van den Broeke, M.P. Scheele, J. Clim., 2002, 15, 1957–1968.
- 43 M. Kriews, Schriftenreihe Angewandte Analytik, Universität Hamburg, 1992.
- 44 R. Röthlisberger, M. Bigler, M. Hutterli, S. Sommer, B. Stauffer, Environ. Sci. Technol., 2000, 34, 338–342.
- 45 I. Basile, J.R. Petit, S. Touron, F.E. Grousset, N. Barkov, J. Geophys. Res., 2001, 106, 31915–31931.

Supplementary material

High spatial resolution element analysis of polar ice by Laser Ablation-ICP-MS

Dorothee Dick, Heiko Reinhardt[‡], Urs Ruth and Michael Kriews^{*}

Alfred Wegener Institute for Polar and Marine Research, Am Handelshafen 12, 27570
Bremerhaven

[‡] Hamburger Stadtentwässerung, Köhlbranddeich 1, 20457 Hamburg

Number of figures: 3

Number of tables: 1

^{*} Corresponding author tel.: +49-(0)471-4831-1420; fax: +49-(0)471-4831-1149; email: Michael.Kriews@awi.de

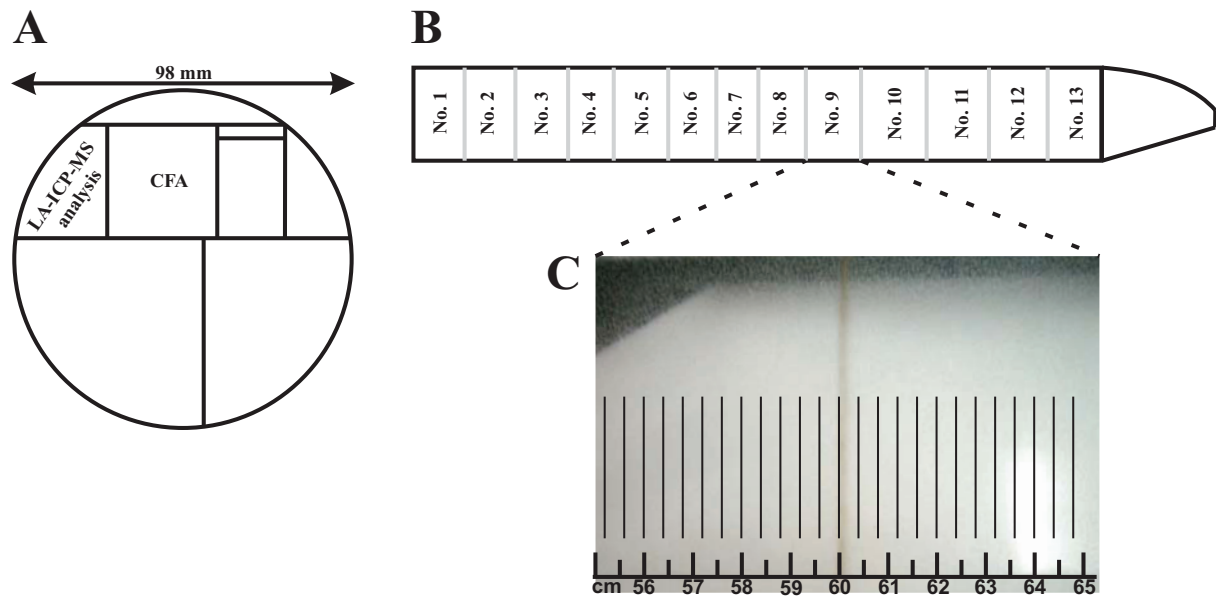


Figure S 1: A: Top view of an ice core with depicted calottes. One calotte was available for LA-ICP-MS analysis and one for continuous flow analysis (CFA). B: Calotte for LA-ICP-MS (1 m long) analysis separated into 13 subsections. C: Part of the EDML metre 270 ice core with the exceptional visible particle horizon at 269.6 m depth. On subsections 1 to 8 and 10 to 13 every 4 mm lines perpendicular to the core axis were ablated (long black lines), on subsection no. 9 every 3 mm.

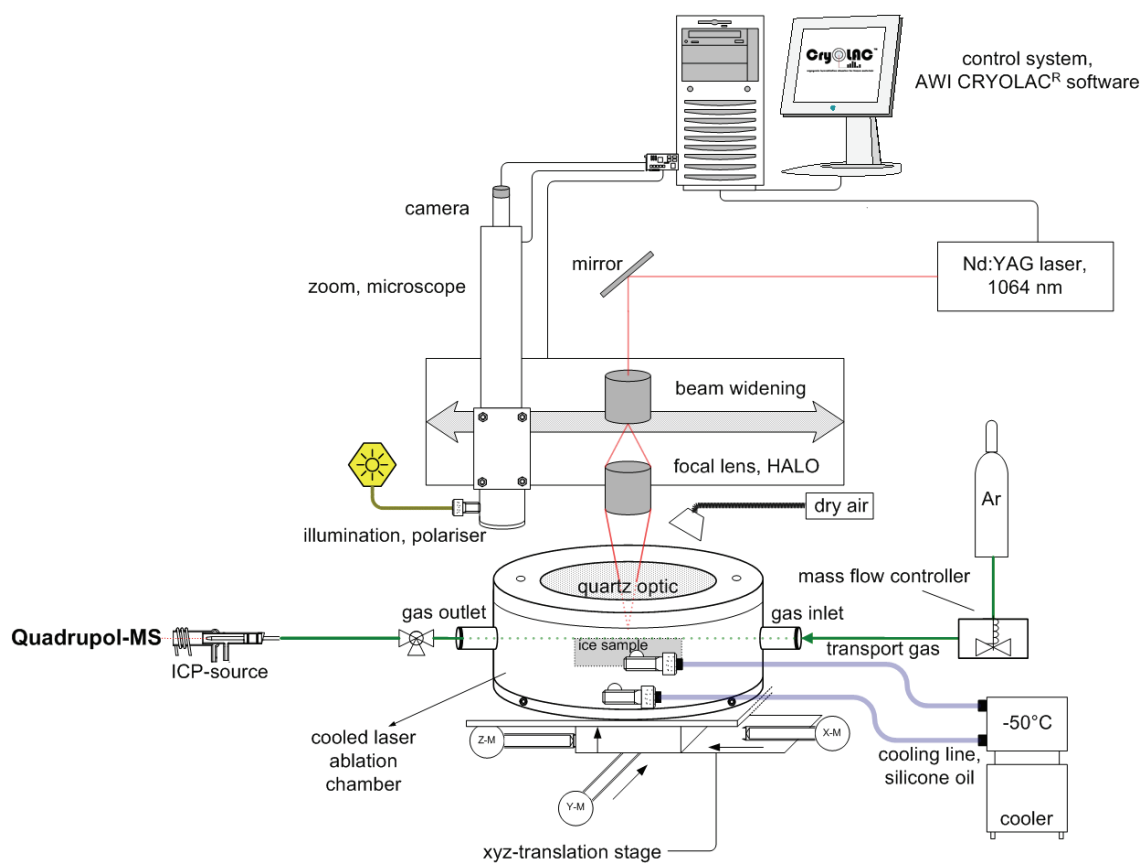


Figure S 2: Experimental setup for LA-ICP-MS analysis of frozen samples.

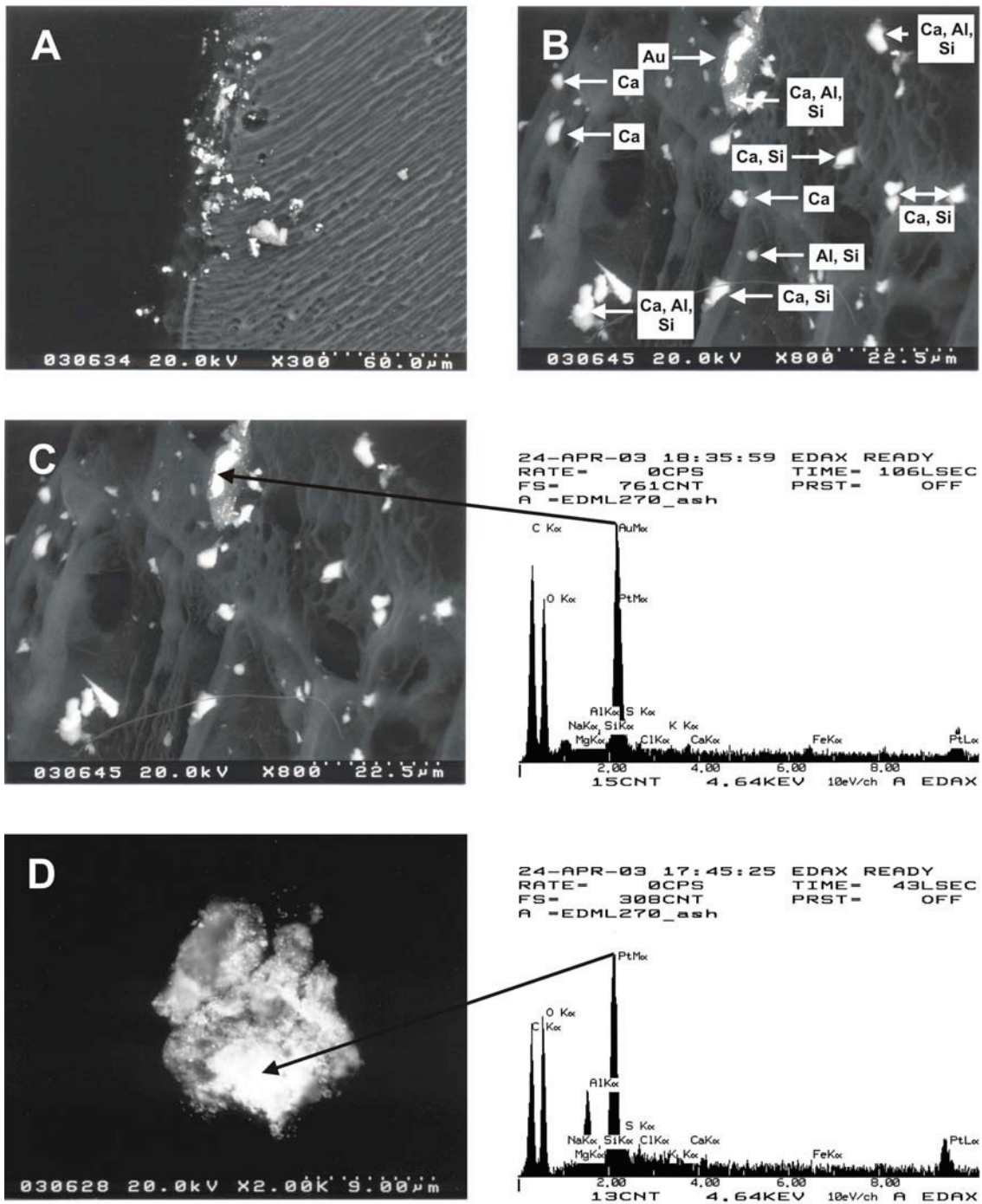


Figure S 3: Scanning electron microscope images of particles incorporated in the particle horizon of the Antarctic ice core EDML metre 270. A: overview of the horizon; B: Main composition of particles; C: Au particle (left) with energy dispersive X-ray analysis (EDXA) spectrum (right); D: Pt particle (left) with EDXA spectrum (right).

Table S 1: Detection limits (d.l.) in ng kg⁻¹ for all analysed isotopes and relative standard deviations (RSD) for LA-ICP-MS analysis obtained by replicate measurements of ice core samples.

Isotope	d.l. (ng L ⁻¹)	RSD (%) (n=5)	Isotope	d.l. (ng L ⁻¹)	RSD (%) (n=5)	Isotope	d.l. (ng L ⁻¹)	RSD (%) (n=5)
⁷ Li	75	244	⁸⁵ Rb	77	58	¹⁶⁴ Dy	6	105
⁹ Be	982	77	⁸⁶ Sr	76	56	¹⁶⁵ Ho	2	71
²³ Na*	0.3	24	⁸⁸ Sr	23	35	¹⁶⁶ Er	5	103
²⁴ Mg*	0.2	32	⁸⁹ Y	89	69	¹⁶⁹ Tm	2	59
²⁵ Mg*	4.4	36	¹⁰³ Rh	12	65	¹⁷⁴ Yb	4	101
²⁷ Al*	2.0	48	¹⁰⁵ Pd	51	105	¹⁷⁵ Lu	2	60
³⁹ K*	0.6	31	¹¹¹ Cd	26	69	¹⁹¹ Ir	10	129
⁴³ Ca*	6.2	16	¹¹⁴ Cd	36	47	¹⁹³ Ir	4	110
⁴⁴ Ca*	5.0	26	¹³⁸ Ba	3	46	¹⁹⁴ Pt	25	69
⁵¹ V	82	60	¹³⁹ La	7	73	¹⁹⁵ Pt	7	91
⁵² Cr*	8.3	19	¹⁴⁰ Ce	4	49	¹⁹⁷ Au	17	39
⁵³ Cr*	1.3	67	¹⁴¹ Pr	3	63	²⁰⁵ Tl	9	30
⁵⁵ Mn	73	50	¹⁴² Nd	11	83	²⁰⁶ Pb	4	40
⁵⁶ Fe*	3.3	37	¹⁴³ Nd	32	97	²⁰⁷ Pb	9	38
⁵⁷ Fe*	0.2	51	¹⁴⁷ Sm	14	160	²⁰⁸ Pb	3	31
⁵⁸ Ni	93	40	¹⁴⁹ Sm	10	125	²⁰⁹ Bi	4	66
⁵⁹ Co	6	62	¹⁵¹ Eu	3	92	²³² Th	2	49
⁶⁰ Ni	83	42	¹⁵³ Eu	5	78	²³⁸ U	4	62
⁶⁴ Zn*	0.2	36	¹⁵⁸ Gd	7	137	¹⁷ OH		
⁶⁶ Zn*	0.1	34	¹⁵⁹ Tb	4	72	²²⁰ Bg		

* concentrations in µg kg⁻¹

Publication II

One-to-one coupling of glacial climate variability in Greenland and Antarctica

EPICA Community Members (listed in alphabetical order): C. Barbante, J.-M. Barnola, S. Becagli, J. Beer, M. Bigler, C. Boutron, T. Blunier, E. Castellano, O. Cattani, J. Chappellaz, D. Dahl-Jensen, M. Debret, B. Delmonte, D. Dick, S. Falourd, S. Faria, U. Federer, H. Fischer, J. Freitag, A. Frenzel, D. Fritzsche, F. Fundel, P. Gabrielli, V. Gaspari, R. Gersonde, W. Graf, D. Grigoriev, I. Hamann, M. Hansson, G. Hoffmann, M. A. Hutterli, P. Huybrechts, E. Isaksson, S. Johnsen, J. Jouze, M. Kaczmarska, T. Karlin, P. Kaufmann, S. Kipfstuhl, M. Kohno, F. Lambert, Anja Lambrecht, Astrid Lambrecht, A. Landais, G. Lawer, M. Leuenberger, G. Littot, L. Loulergue, D. Lüthi, V. Maggi, F. Marino, V. Masson-Delmotte, H. Meyer, H. Miller, R. Mulvaney, B. Narcisi, J. Oerlemans, H. Oerter, F. Parrenin, J.-R. Petit, G. Raisbeck, D. Raynaud, R. Röthlisberger, U. Ruth, O. Rybak, M. Severi, J. Schmitt, J. Schwander, U. Siegenthaler, M.-L. Siggaard-Andersen, R. Spahni, J. P. Steffensen, B. Stenni, T. F. Stocker, J.-L. Tison, R. Traversi, R. Udisti, F. Valero-Delgado, M. R. van den Broeke, R. S.W. van de Wal, D. Wagenbach, A. Wegner, K. Weiler, F. Wilhelms, J.-G. Winther, E. Wolff

Nature, 2006, 444, 195-198.

LETTERS

One-to-one coupling of glacial climate variability in Greenland and Antarctica

EPICA Community Members*

Precise knowledge of the phase relationship between climate changes in the two hemispheres is a key for understanding the Earth's climate dynamics. For the last glacial period, ice core studies^{1,2} have revealed strong coupling of the largest millennial-scale warm events in Antarctica with the longest Dansgaard–Oeschger events in Greenland^{3–5} through the Atlantic meridional overturning circulation^{6–8}. It has been unclear, however, whether the shorter Dansgaard–Oeschger events have counterparts in the shorter and less prominent Antarctic temperature variations, and whether these events are linked by the same mechanism. Here we present a glacial climate record derived from an ice core from Dronning Maud Land, Antarctica, which represents South Atlantic climate at a resolution comparable with the Greenland ice core records. After methane synchronization with an ice core from North Greenland⁹, the oxygen isotope record from the Dronning Maud Land ice core shows a one-to-one coupling between all Antarctic warm events and Greenland Dansgaard–Oeschger events by the bipolar seesaw⁶. The amplitude of the Antarctic warm events is found to be linearly dependent on the duration of the concurrent stadial in the North, suggesting that they all result from a similar reduction in the meridional overturning circulation.

The glacial climate in the North Atlantic region is characterized by rapid shifts from cold stadial to warmer interstadial conditions^{3,4,9}. Greenland temperatures during these Dansgaard–Oeschger (D–O) events rise by 8–16 °C (refs 10, 11) within a few decades followed by a less rapid temperature decline back to stadial conditions. In contrast, glacial climate in the circum-Antarctic region exhibits slower millennial changes with smaller temperature amplitudes of only 1–3 °C (refs 1, 12, 13). After synchronization of Greenland and Antarctic ice core records^{1,2} using the global atmospheric change in CH₄ concentrations, a conspicuous phase relationship between the largest Antarctic warmings (A1–A7; ref. 1) and the longest D–O events was observed with the south warming during the stadial conditions in the north, and starting to cool as soon as the D–O warming set in. This bipolar seesaw pattern was explained by changes in the heat and freshwater flux connected to the Atlantic Meridional Overturning Circulation (MOC), where a stronger MOC leads to increased drainage of heat from the Southern Ocean heat reservoir^{6,7}.

In principle, an interhemispheric climate coupling by the bipolar seesaw should also apply for all the short D–O events. However, to what extent this concept is also able to explain the higher-frequency climate variability in Antarctic ice cores remained unclear (as discussed for example, in ref. 14 and references therein). Here we report

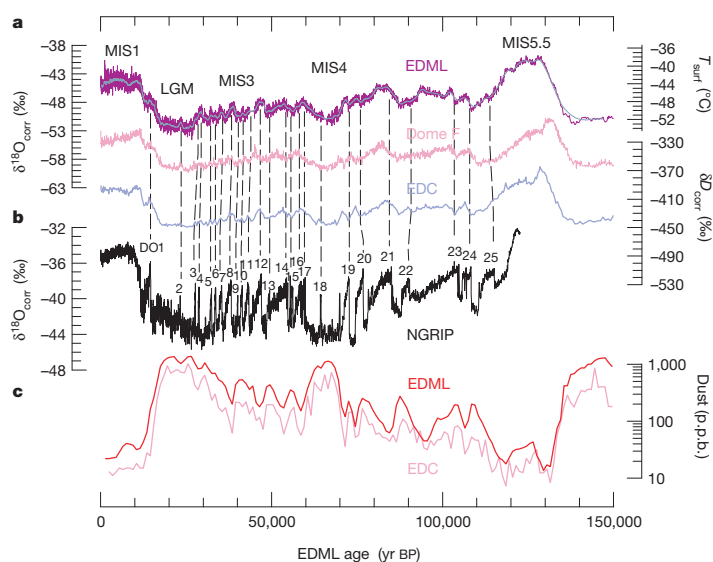


Figure 1 | Antarctic stable isotope records show synchronous millennial variations during the last glacial, whereas rapid variations are encountered in Greenland. a, EDML $\delta^{18}\text{O}$ record (purple, 0.5-m resolution; grey, 15-m running mean) after sea level and upstream correction (see Supplementary Information) over the past 150 kyr. The record shows features similar to those of the EDC¹² (blue) and the Dome F¹³ (pink) isotope records but with more fine structure during MIS3 and MIS4. We note that EDML and EDC are plotted on the new common EDC3 timescale (see Supplementary Information) while Dome F is plotted on its individual timescale. The temperature axis on the right side indicates approximate surface temperatures at EDML as derived from the spatial $\delta^{18}\text{O}$ /temperature gradient (see Supplementary Information). **b**, $\delta^{18}\text{O}$ record of the NGRIP ice core (grey)⁹. **c**, Mineral dust records of the EDML (red) and EDC¹² (pink) ice cores at 1,000-yr resolution; these dust records were used for synchronization of the cores.

*A full list of authors and their affiliations appears at the end of the paper.

on the climate record over the last glacial cycle from a new ice core drilled within the European Project for Ice Coring in Antarctica (EPICA) in the interior of Dronning Maud Land, hence denoted EDML, at 75° S, 0° E, 2,892 m.a.s.l. (metres above sea level), with a recent accumulation rate of 6.4 cm water equivalent (w.e.) per year¹⁵. This site was chosen to complement the long EPICA Dome C (EDC, 75° S, 123° E, 3,233 m.a.s.l., 2.5 cm w.e. yr⁻¹) record¹², because EDML is the first deep ice core in the Atlantic sector of the Southern Ocean region¹⁶ and thus located near the southern end of the bipolar seesaw. The snow accumulation at EDML is two to three times higher than at other deep drilling sites on the East Antarctic plateau, so higher-resolution atmosphere and climate records can be obtained for the last glacial period, making the EDML core especially suitable for studying decadal-to-millennial climate variations in Antarctica.

In Fig. 1 the EDML $\delta^{18}\text{O}$ record as proxy for local temperature on the ice sheet is shown in 0.5-m resolution (equivalent to 15–30 yr during the marine isotope stage MIS3 and 100–150 yr during MIS5) after correction for upstream and glacial–interglacial ice sheet altitude effects (see Supplementary Information). The overall pattern closely resembles that recorded in most Antarctic ice cores previously covering this time period^{12,13,17}. Also, very similar dust profiles (Fig. 1) are encountered at EDML and EDC, related to parallel changes in climate conditions in the Patagonian dust source region common to both cores¹⁸. Despite the high correlation of the EDML $\delta^{18}\text{O}$ and the EDC δD record over the last 150,000 yr ($r^2 = 0.94$ for 250-yr averages) some distinct differences exist. In the penultimate warm period (MIS5.5) the EDML $\delta^{18}\text{O}$ record indicates temperatures about 4–5 °C higher than those of the Holocene, in line with other ice cores from the East Antarctic plateau^{12,13,17}. However, $\delta^{18}\text{O}$ at EDML exhibits persistently higher $\delta^{18}\text{O}$ values over the entire duration of MIS5.5 while other ice cores on the East Antarctic plateau show a substantial drop after an initial climate optimum^{12,13}. We note that this difference is not due to the altitude corrections applied to the EDML $\delta^{18}\text{O}$ record (see Supplementary Information), because a similar temporal evolution during MIS5.5 is also seen in the uncorrected data. Instead, a smaller cooling at EDML in the course of MIS5.5 compared to EDC and Dome Fuji is consistent with marine sediment records from the Atlantic sector of the Southern Ocean revealing persistently warmer summer sea surface temperatures

and a reduced winter sea ice cover throughout MIS5.5 (ref. 19). This suggests that there were regional differences in temperature and sea ice evolution during this period for the Atlantic and Indian Ocean sector.

The most outstanding feature of the high-resolution EDML record is the pronounced millennial variability during the glacial. As indicated by the dashed lines in Fig. 1 each of the warming episodes in Antarctica can be related to a corresponding D–O event, but only synchronization of the age scales allows us to assign them unambiguously and to pinpoint the phase relationship between climate changes in Greenland and Antarctica. To do this, the EDML core has been synchronized (see Supplementary Information) to the layer counted NGRIP ice core^{20,21} over MIS3, using high-resolution CH₄ profiles over the last 55 kyr from the NGRIP, GRIP and GISP2 ice cores¹¹. The synchronized $\delta^{18}\text{O}$ records are shown in Fig. 2. Also plotted is the CH₄ synchronized $\delta^{18}\text{O}$ record from the Byrd ice core¹ and new high-resolution δD data from EDC²² which closely resemble the temperature variability found at EDML during MIS3 and support an Antarctic-wide interpretation of these fluctuations. The higher glacial snow accumulation at EDML (~3 cm w.e. yr⁻¹) compared to that at EDC, Dome Fuji or Vostok (~1.4 cm w.e. yr⁻¹) implies a CH₄ synchronization two to three times better than at those sites. The synchronization uncertainty for MIS3 ranges from 400 to 800 yr for all events in the EDML record, making the synchronization error for EDML always much smaller than the duration of the events themselves.

This is important, because this allows an unequivocal one-to-one assignment not only of the well-known large warm events in Antarctica (A1, A2 and so on) but of each single isotope maximum indicated in Fig. 2 with a corresponding D–O event in the north. Although the exact timing of the temperature maxima relative to the stadial/interstadial transitions cannot be discerned more precisely than the synchronization error, it is evident that each Antarctic warming starts significantly before the respective D–O event. In addition, a synchronization of the stable water isotope records of the GRIP and EDC ice cores using the ¹⁰Be production anomaly around 41,000 yr BP, which constrains the in-phase relationship of the onset of D–O 10 and the respective Antarctic δD maximum to better than 200 yr (ref. 23), supports our CH₄ match. Accordingly, we suggest a new Antarctic Isotope Maximum (AIM) nomenclature in Fig. 2

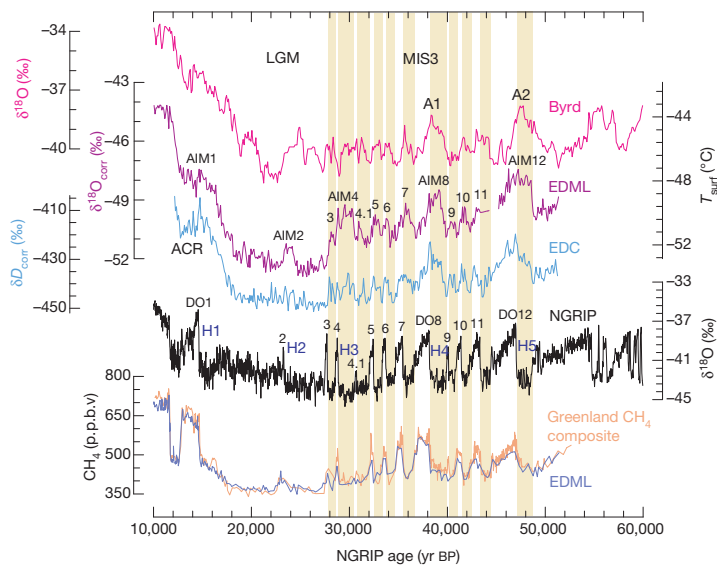


Figure 2 | Methane synchronization of the EDML and the NGRIP records reveals a one-to-one assignment of each Antarctic warming with a corresponding stadial in Greenland. Displayed are 100-yr averages during MIS3 in the EDML, EDC²⁶ and Byrd¹ ice core for the time interval 10–60 kyr BP in comparison with the NGRIP $\delta^{18}\text{O}$ record from Northern Greenland²¹. All records are CH₄ synchronized and given on the new GICC05 age scale for the NGRIP ice core, which has been derived by counting annual layers down to 41 kyr and by a flow model for older ages^{9,21}. Yellow bars indicate the Greenland stadial periods that we relate to respective Antarctic temperature increases. The approximate timing of Heinrich layers in North Atlantic sediments is indicated as well²⁷. The y axis on the right side indicates approximate temperature changes at EDML based on the modern spatial gradient between $\delta^{18}\text{O}$ and temperature.

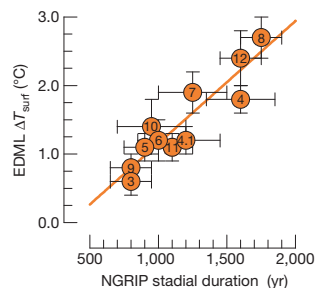


Figure 3 | Amplitudes of Antarctic warmings show a linear relationship ($r^2 = 0.85$) with the duration of the accompanying stadial in Greenland during MIS3. The amplitude was determined from the Antarctic $\delta^{18}\text{O}$ maximum to the preceding minimum of each event; the stadal duration is defined by the interval between the midpoint of the stepwise temperature change at the start and end of a stadial on the extended GICC05 age scale^{9,21}. Error bars reflect the estimated uncertainty in the definition of the maxima and minima in $\delta^{18}\text{O}$ at EDML and in the duration of the concurrent stadial period. Numbers indicate the corresponding AIMs and D–O events.

which reflects the connection of southern warming to reduced oceanic heat transport into the North Atlantic during stadials. The timing and duration of the AIMs relative to D–O events is also indirectly supported by the comparison of changes in deep-water masses linked to Antarctic Bottom Water formation and Atlantic surface water changes, as archived in sediment records offshore of Portugal²⁴.

Most striking is the varying amplitude of the AIMs, which is linearly dependent on the duration of stadials in the north, as shown in Fig. 3. The only significant deviation from this linear relationship during MIS3 is AIM4, in which the error in the stadal duration estimate is quite large. We conclude that the duration of a reduced MOC—and, hence, the duration of the warming period in the Southern Ocean—determines the amount of heat accumulated in the Southern Ocean heat reservoir, strongly supporting the general applicability of the thermal bipolar seesaw⁶ concept within the range of stadial events encountered during MIS3. We note that for longer cessations of the MOC a new equilibrium temperature in the Southern Ocean would be reached and the warming would eventually have to cease. This linear relationship also implies that the Antarctic warming rate—and thus the heat flux from the Southern Ocean to the Atlantic—is similar for all warming events during MIS3. If we assume the same spatial configuration of the overturning cell for cold intervals in MIS3, this would suggest that the strength of the MOC is approximately constant for all stadials, challenging the notion of different overturning rates²⁵ for stadials in which massive iceberg discharges into the North Atlantic (the so-called Heinrich events in Fig. 2: H1–H5) occurred compared to stadials without Heinrich events. Note however, that the stadials before D–O 8 and D–O 12 in which Heinrich events occurred were the longest and the related Antarctic warmings the largest. This may be due to the longer time needed to mix away the large freshwater anomalies during Heinrich events. There is, however, a less clear relationship for other Heinrich events. Comparison of the millennial climate variability during MIS3 at EDML and EDC shows no significant difference in the amplitude of the isotopic change in the Atlantic and Indian Ocean sectors of the Southern Ocean. This implies a uniform ocean heat reservoir controlling temperature changes at both sites and reflects the rapid mixing of the Southern Ocean by the Antarctic Circumpolar Current.

In the EDML $\delta^{18}\text{O}$ record a major warm event (AIM2, connected to D–O 2) is seen during the Last Glacial Maximum, which cannot be clearly identified in the EDC core but is present in the Dome F record (Fig. 1). AIM2 also shows a decrease in high-resolution mineral dust concentrations at EDC, as do all the other AIMs²⁶. We therefore

conclude that AIM2 is a warm event comparable to the other AIMs in MIS3 but is not sufficiently resolved in the EDC record owing to its lower accumulation. The corresponding D–O 2 event in the North Atlantic is preceded by the longest cold period in the NGRIP record (Fig. 2) and accordingly, a higher temperature amplitude of AIM2 is to be expected if the same bipolar seesaw concept holds as for D–O events during MIS3. However, sea level and temperature conditions were significantly different during the Last Glacial Maximum, potentially affecting the spatial configuration and strength of the overturning cell in the North Atlantic. The fact that AIM2 is only 2,000 yr long suggests that the strength of the MOC was not significantly reduced for the entire cold period in the North, but collapsed only about 1,000 yr before D–O 2, which would be in line with significant iceberg discharge depositing ice-rafted debris in the North Atlantic during H2 (ref. 27).

In summary, a strong interhemispheric coupling of all bipolar climate variations during MIS3 via the MOC is supported by the new high-resolution $\delta^{18}\text{O}$ record from EDML indicating that Antarctic warming rates and potentially also overturning rates have been similar for all events in MIS3. The question of what triggers the switch from stadial to interstadial conditions remains. Transitions in the strength of the MOC and its effect on the Atlantic Southern Ocean heat exchange are simulated in response to changes in the North Atlantic freshwater balance^{7,8}; however, the origin of such variations in freshwater input are still not ascertained for all individual D–O events. In addition, large iceberg discharge from the Laurentide ice sheet does not systematically coincide with either the onset or the end of stadials^{27,28}. Recently, the potential role of a change in Southern Ocean sea-ice cover for reinstalling a stronger MOC has been identified for the onset of the Bølling/Allerød warming^{29,30}. The intrinsic feedback of a reduced sea-ice cover in the Southern Ocean during AIMs, followed by a delayed onset of deep-water formation in the North, could potentially explain the interhemispheric climate coupling seen in our records during MIS3.

Received 26 May; accepted 22 September 2006.

- Blunier, T. & Brook, E. J. Timing of millennial-scale climate change in Antarctica and Greenland during the last glacial period. *Science* **291**, 109–112 (2001).
- Blunier, T. et al. Asynchrony of Antarctic and Greenland climate change during the last glacial period. *Nature* **394**, 739–743 (1998).
- Johnsen, S. J. et al. Irregular glacial interstadials recorded in a new Greenland ice core. *Nature* **359**, 311–313 (1992).
- Bond, G. et al. Correlations between records from North Atlantic sediments and Greenland ice. *Nature* **365**, 143–147 (1993).
- McManus, J. F., Oppo, D. W. & Cullen, J. L. A 0.5-million-year record of millennial climate variability in the North Atlantic. *Science* **283**, 971–975 (1999).
- Stocker, T. F. & Johnsen, S. J. A minimum thermodynamic model of the bipolar seesaw. *Paleoceanography* **18**, art. no. 1087 (2003).
- Knutti, R., Flückiger, J., Stocker, T. F. & Timmermann, A. Strong hemispheric coupling of glacial climate through freshwater discharge and ocean circulation. *Nature* **430**, 851–856 (2004).
- Ganopolski, A. & Rahmstorf, S. Rapid changes of glacial climate simulated in a coupled climate model. *Nature* **409**, 153–158 (2001).
- North Greenland Ice Core Project members. High resolution climate record of the northern hemisphere reaching into the last interglacial period. *Nature* **431**, 147–151 (2004).
- Landais, A. et al. Quantification of rapid temperature change during DO event 12 and phasing with methane inferred from air isotopic measurements. *Earth Planet. Sci. Lett.* **225**, 221–232 (2004).
- Huber, C. et al. Isotope calibrated Greenland temperature record over Marine Isotope Stage 3 and its relation to CH_4 . *Earth Planet. Sci. Lett.* **245**, 504–519 (2006).
- EPICA community members. Eight glacial cycles from an Antarctic ice core. *Nature* **429**, 623–628 (2004).
- Watanabe, O. et al. Homogeneous climate variability across East Antarctica over the past three glacial cycles. *Nature* **422**, 509–512 (2003).
- Roe, G. H. & Steig, E. J. Characterization of millennial-scale climate variability. *J. Clim.* **17**, 1929–1944 (2004).
- Oerter, H. et al. Accumulation rates in Dronning Maud Land, Antarctica, as revealed by dielectric-profiling measurements of shallow firn cores. *Ann. Glaciol.* **30**, 27–34 (2000).
- Reijmer, C. H., van den Broeke, M. R. & Scheele, M. P. Air parcel trajectories to five deep drilling locations on Antarctica, based on the ERA-15 data set. *J. Clim.* **15**, 1957–1968 (2002).

17. Petit, J. R. *et al.* Climate and atmospheric history of the past 420,000 years from the Vostok ice core, Antarctica. *Nature* **399**, 429–436 (1999).
18. Basile, I. *et al.* Patagonian origin of glacial dust deposited in East Antarctica (Vostok and Dome C) during glacial stages 2, 4 and 6. *Earth Planet. Sci. Lett.* **146**, 573–589 (1997).
19. Bianchi, C. & Gersonde, R. The Southern Ocean surface between Marine Isotope Stage 6 and 5d: Shape and timing of climate changes. *Palaeogeogr. Palaeoclimatol. Palaeoecol.* **187**, 151–177 (2002).
20. Rasmussen, S. O. *et al.* A new Greenland ice core chronology for the last glacial termination. *J. Geophys. Res.* **111**, D06102 (2006).
21. Andersen, K. K. *et al.* The Greenland ice core chronology 2005, 15–42 kyr. Part 1: Constructing the time scale. *Quat. Sci. Rev.* (in the press).
22. Stenni, B. *et al.* A late-glacial high-resolution site and source temperature record derived from the EPICA Dome C isotope records (East Antarctica). *Earth Planet. Sci. Lett.* **217**, 183–195 (2003).
23. Raisbeck, G., Yiou, F. & Jouzel, J. Cosmogenic ¹⁰Be as a high resolution correlation tool for climate records. *Geochim. Cosmochim. Acta* **66**, abstr. A623 (2002).
24. Shackleton, N. J., Hall, M. A. & Vincent, E. Phase relationships between millennial-scale events 64,000–24,000 years ago. *Paleoceanography* **15**, 565–569 (2000).
25. Rahmstorf, S. Ocean circulation and climate during the past 120,000 years. *Nature* **419**, 207–214 (2002).
26. Röthlisberger, R. *et al.* Dust and sea-salt variability in central East Antarctica (Dome C) over the last 45 kys and its implications for southern high-latitude climate. *Geophys. Res. Lett.* **29**, article no. 1963 (2002).
27. Bond, G. & Lotti, R. Iceberg discharges into the North Atlantic on millennial time scales during the last glaciation. *Science* **267**, 1005–1010 (1995).
28. de Abreu, L., Shackleton, N. J., Joachim Schönfeld, J., Hall, M. & Chapman, M. Millennial-scale oceanic climate variability off the Western Iberian margin during the last two glacial periods. *Mar. Geol.* **196**, 1–20 (2003).
29. Knorr, G. & Lohmann, G. Southern Ocean origin for the resumption of Atlantic thermohaline circulation during deglaciation. *Nature* **424**, 532–536 (2003).
30. Stocker, T. F. & Wright, D. G. Rapid transitions of the ocean's deep circulation induced by changes in surface water fluxes. *Nature* **351**, 729–732 (1991).

Supplementary Information is linked to the online version of the paper at www.nature.com/nature.

Acknowledgements This work is a contribution to the European Project for Ice Coring in Antarctica (EPICA), a joint European Science Foundation/European Commission scientific programme, funded by the EU (EPICA-MIS) and by national contributions from Belgium, Denmark, France, Germany, Italy, the Netherlands, Norway, Sweden, Switzerland and the UK. The main logistic support was provided by IPEV and PNRA (at Dome C) and AWI (at Dronning Maud Land).

Author Information Reprints and permissions information is available at www.nature.com/reprints. The authors declare no competing financial interests. Correspondence and requests for materials should be addressed to H. F. (hufischer@awi-bremerhaven.de).

EPICA Community Members (listed in alphabetical order): C. Barbante^{1,2}, J.-M. Barnola³, S. Becagli⁴, J. Beer⁵, M. Bigler^{6,7}, C. Boutron³, T. Blunier⁶, E. Castellano⁴, O. Cattani⁸, J. Chappellaz³, D. Dahl-Jensen⁷, M. Debret³, B. Delmonte⁹, D. Dick¹⁰, S. Falourd⁸, S. Faria^{10,11}, U. Federer⁶, H. Fischer¹⁰, J. Freitag¹⁰, A. Frenzel¹⁰, D. Fritzsche¹², F. Fundel¹⁰, P. Gabrielli^{2,3}, V. Gaspari¹, R. Gersonde¹⁰, W. Graf¹³, D. Grigoriev¹⁴, I. Hamann¹⁰, M. Hansson¹⁵, G. Hoffmann⁸, M. A. Hutterli^{6,16}, P. Huybrechts^{10,17}, E. Isaksson¹⁸, S. Johnsen⁷, J. Jouzel⁸, M. Kaczmarek¹⁸, T. Karlin¹⁵, P. Kaufmann⁶, S. Kipfstuhl¹⁰, M. Kohno¹⁰, F. Lambert⁶, Anja Lambrecht¹⁰, Astrid Lambrecht¹⁰, A. Landais⁸, G. Lawer¹⁰, M. Leuenberger⁶, G. Littot¹⁶, L. Loulergue³, D. Lüthi¹⁶, V. Maggi⁹, F. Marino⁹, V. Masson-Delmotte⁹, H. Meyer¹², H. Miller¹⁰, R. Mulvaney¹⁶, B. Narcisi¹⁹, J. Oerlemans²⁰, H. Oerter¹⁰, F. Parrenin³, J.-R. Petit³, G. Raisbeck²¹, D. Raynaud³, R. Röthlisberger¹⁶, U. Ruth¹⁰, O. Rybak¹⁰, M. Severi⁴, J. Schmitt¹⁰, J. Schwander⁶, U. Siegenthaler⁶, M.-L. Siggaard-Andersen⁷, R. Spahni⁶, J. P. Steffensen⁷, B. Stenni²², T. F. Stocker⁶, J.-L. Tison²³, R. Traversi⁴, F. Valero-Delgado¹⁰, M. R. van den Broeke²⁰, R. S. W. van de Wal²⁰, D. Wagenbach²⁴, A. Wegner¹⁰, K. Weiler⁶, F. Wilhelms¹⁰, J.-G. Winther¹⁸ & E. Wolff¹⁶

¹Department of Environmental Sciences, University Ca' Foscari of Venice, ²Institute for the Dynamics of Environmental Processes-CNR, Dorsoduro 2137, 30123 Venice, Italy. ³Laboratoire de Glaciologie et Géophysique de l'Environnement (LGGE), CNRS-UJF, BP96 38402 Saint-Martin-d'Hères cedex, France. ⁴Department of Chemistry, University of Florence, Via della Lastruccia 3, 50019 Sesto Fiorentino, Florence, Italy. ⁵EAWAG, PO Box 611, 8600 Dübendorf, Switzerland. ⁶Climate and Environmental Physics, Physics Institute, University of Bern, Sidlerstrasse 5, 3012 Bern, Switzerland. ⁷Niels Bohr Institute, University of Copenhagen, Juliane Maries Vej 30, 2100 Copenhagen OE, Denmark. ⁸Laboratoire des Sciences du Climat et de l'Environnement (LSCE/IPSL), CEA-CNRS-UVSQ, CE Saclay 91191, Gif sur Yvette, France. ⁹Environmental Sciences Department, University of Milano Bicocca, Piazza della Scienza 1, 20126 Milano, Italy. ¹⁰Alfred-Wegener-Institute for Polar and Marine Research, Columbusstrasse, D-27568 Bremerhaven, Germany. ¹¹Max Planck Institute for Mathematics in the Sciences, Inselstrasse 22, 04103 Leipzig, Germany. ¹²Alfred Wegener Institute for Polar and Marine Research, Research Unit Potsdam, Telegrafenberg A 43, 14473 Potsdam, Germany. ¹³GSF National Center for Environment and Health, Ingolstädter Landstrasse 1, 85764 Neuherberg, Germany. ¹⁴University College London, Gower Street, London WC1E 6BT, UK. ¹⁵Department of Physical Geography and Quaternary Geology, Stockholm University, 106 91 Stockholm, Sweden. ¹⁶British Antarctic Survey, High Cross, Madingley Road, Cambridge CB3 0ET, UK. ¹⁷Departement Geografie, Vrije Universiteit Brussel, Pleinlaan 2, 1050 Brussel, Belgium. ¹⁸Norwegian Polar Institute, 9296 Tromsø, Norway. ¹⁹ENEA, C. R. Casaccia, Via Anguillarese 301, 00060 Roma, Italy. ²⁰Utrecht University, Institute for Marine and Atmospheric Research, PO Box 80005, 3508 TA Utrecht, The Netherlands. ²¹CNSM/IN2P3/CNRS, Bat. 108, 91405 Orsay, France. ²²Department of Geological, Environmental and Marine Sciences, University of Trieste, Via E. Weiss 2, 34127 Trieste, Italy. ²³Département des Sciences de la Terre, Université Libre de Bruxelles, CP160/03, 1050 Brussels, Belgium. ²⁴Institute for Environmental Physics, University of Heidelberg, INF229, 69120 Heidelberg, Germany.

Publication III

Is the umbo matrix of bivalve shells (*Laternula elliptica*) a climate archive?

D. Dick, E. Philipp, M. Kriews, D. Abele

Aquatic Toxicology, 2007, 84, 450-456.



Is the umbo matrix of bivalve shells (*Laternula elliptica*) a climate archive?

D. Dick, E. Philipp, M. Kriews, D. Abele*

Alfred Wegener Institute for Polar and Marine Research, Am Handelshafen 12, 27570 Bremerhaven, Germany

Received 12 June 2007; received in revised form 16 July 2007; accepted 16 July 2007

Abstract

Heavy metal accumulation into bivalve soft tissues has received increasing interest in recent years with respect to biomonitoring of environmental change including pollution. To a lesser extent, accretion of elements from the environment into bivalve hard structures (shells) has been investigated, although the importance of the shells as environmental archives has been acknowledged. Here we report element distribution within consecutive growth bands in the shells of the Antarctic soft shell clam *Laternula elliptica*, which is currently exposed to vast environmental change in Antarctic Peninsula coastal environments that undergo rapid climate warming. We performed a high spatial resolution analysis for Al, Fe, Mn, Cu, Pb and U in the shell umbo, by means of laser ablation inductively coupled plasma mass spectrometry (LA-ICP-MS). Element ratios within the umbo did not resemble either the ratios in the surrounding seawater, the sedimenting material in Potter Cove, or even the Earth's crust basal composition. Mn and Cu were preferentially incorporated into the umbo. A strong decrease of element accretion with time could be related to lifetime respiration mass (R) of the animals. This indicates element accretion into the umbo and shell matrix to be largely a function of animal ecophysiology and life history, and these effects need to be considered in the context of potential usefulness of *L. elliptica* shells as environmental archives.
© 2007 Elsevier B.V. All rights reserved.

Keywords: Trace metals; Bivalve shell archives; Laser ablation

1. Introduction

The analysis of the element composition of bivalve shells has gained importance in recent years with respect to environmental monitoring. Bivalves are filter feeders and accumulate inorganic elements and organic compounds from the water column through ingestion of sediment particles (Jing et al., 2006). It is tempting to assume that the rates at which molluscs incorporate ingested elements into newly grown shell should linearly depend on the element composition of the surrounding water over the years (Carriker et al., 1982). For that matter, many publications demonstrate exposure to elevated dissolved or complexed heavy metals to cause increased soft tissues concentrations in aquatic animals including bivalves (e.g.: Yap et al., 2003 for Cd, Cu, Pb, Zn; Jing et al., 2006 for Cu; Bagnyukova et al., 2006 for iron uptake in goldfish). However, uptake of heavy metals into aquatic organisms, especially of the biologically essential metals like Cu, underlies complex physiological regulation by the

animals. Moreover, the uptake may be modified by environmental parameters like water temperature, pH and oxygenation, and modifications can differentially affect different metals. Thus, Huanxin et al. (2000) did not find a simple linear relationship between the concentration of heavy metals in oyster tissue and shells and the environment. Instead, Cu and Zn were greatly enriched in oyster tissue, which the authors attributed to the absolute physiological requirement for these elements. Further, Cd was enriched in the shell presumably due to the easy substitution of Ca by Cd (ionic radius Ca 9.7 and Cd 9.8 nm). Mubiana and Blust (2007) examined the effects of temperature on accumulation of various metals by the blue mussel *Mytilus edulis*. Sequestration of non-essential metals like Cd and Pb correlated positively with temperature, whereas uptake of other species like Co did not show temperature dependency. However, the concentrations of all investigated elements declined in *M. edulis* soft tissue over time when animals were kept in metal-free artificial seawater, which was prepared with high purity salts, indicating that the outside concentrations still have a major impact on the uptake and release of metals into blue mussel soft tissues.

Metals, sequestered into bivalve tissues are translocated to the mantle, the tissue surrounding the animals' soft body. From the

* Corresponding author.

E-mail address: Doris.Abele@awi.de (D. Abele).

outside epidermis of the mantle the elements are released into the extrapallial fluid, located between mantle and clam shell. From this extrapallial fluid the ions are incorporated into the inner surface of the newly forming calcium carbonate skeleton (Tynan et al., 2005). Therefore, once knowing how the specific physiological requirements and adaptations of a species modify element uptake into soft tissues, it might be possible to deduce past environmental metal concentrations from the shell archive of yearly forming growth bands (Price and Pearce, 1997; Richardson et al., 2001).

The use of mollusc shells as proxies for environmental change including pollution events creates the necessity to analyse single year bands within the shell. A variety of techniques to detect minor and trace elements in the shells are described by Richardson (2001). Laser ablation inductively coupled plasma mass spectrometry (LA-ICP-MS) is one of the newer techniques, enabling analysis of a wide range of elements in shellfish (Raith et al., 1996; Richardson et al., 2001). LA-ICP-MS offers high spatial resolution analysis, less sample preparation and, therefore, reduces possibilities for sample contamination. Considering sample preparation and analysis it is a fast method compared to liquid ICP-MS.

The present study analyses metal (Al, Fe, Mn, Cu, Pb, U) variations in *Laternula elliptica* shells (Antarctic soft shell clam) to see how accretion of elements in bivalve hard structures changes over time in successively deposited growth bands. Samples were taken in Potter Cove on King George Island, Antarctica, fronting the Collins glacier. High loads of particulate and dissolved iron are transported into Potter Cove during the austral summer season with glacier melt water run-off (Schloss et al., 2007; Abele et al., 2007), creating an interest in the idea that bivalve shells might be useful archives of long-term changes of environmental iron load under conditions of climate-induced glaciers melting in the Antarctic Peninsula region (Dierssen et al., 2002).

2. Materials and methods

2.1. Bivalve shell sampling

Live specimens of the Antarctic soft shell clam, *L. elliptica*, were collected in 2003 at 10 m water depth in Potter Cove in front of the Argentinean Jubany station on King George's Island (Position: 62°14'S, 58°40'W). The Antarctic bivalve (*L. elliptica*) has a maximum lifespan of >36 years (Philipp et al., 2005) and is a major circum-Antarctic biomass component, colonizing muddy sediments in coastal environments. It is a key species of the Antarctic benthic-pelagic carbon flux (Momo et al., 2002).

Shells of the four oldest animals were cut through the umbo with a diamond saw (Buehler, Isometh, Germany) and wet polished with sandpaper (400 and 600 grain size, see Philipp et al., 2005). The age determination by annual deposited rings within the shell umbo (Brey and Mackensen, 1997) showed that three animals were 23 years old (*1980), and one 21 years old (*1982). Fig. 1 shows an example of a cut and polished umbo of *L. elliptica* after laser ablation with clearly visible annual growth bands.

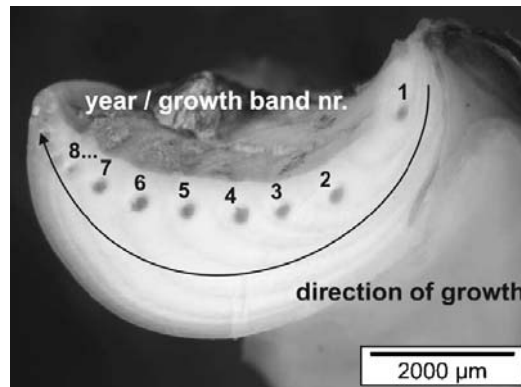


Fig. 1. Cut and polished umbo of *Laternula elliptica* after laser ablation with clearly visible annual growth bands. Photo by K. Beyer.

2.2. Laser ablation analysis

Annual growth bands, visible within the umbo, were analyzed for Al, Mn, Fe, Pb and U with laser ablation inductively coupled plasma mass spectrometry (LA-ICP-MS; Quanta-Ray® GCR-11 Spectra Physics 1064 nm; Elan 6000 Perkin-Elmer/Sciex). An overview of the optimized operation condition parameters used is given in Table 1. The experimental setup for the direct analysis of solid samples is shown by Reinhardt et al. (2001) and Kriews et al. (2004a, 2004b). We used a 1064 nm Nd:YAG laser (Nd-doped Y–Al garnet). The focused laser beam targets the sample inside the cryogenic chamber and ablates the sample surface. Spot sizes of approximately 200 μm were achieved (Fig. 1). At the front side of the chamber the carrier gas argon passes through the ablation cell and transports the ablated material into the connected ICP-Quadrupol MS, where the elements from the sample are ionised, separated, and isotopes detected.

Table 1

Operating conditions for the laser ablation inductively coupled plasma mass spectrometer system (LA-ICP-MS)

Inductively coupled plasma mass spectrometer		Perkin-Elmer Sciex Elan 6000
Radio frequency power		1400 W
Plasma gas		14.0 L min ⁻¹
Auxiliary gas		0.8 L min ⁻¹
Carrier gas		1.0 L min ⁻¹
Dwell time		10 ms
Sweeps/replicate		20
Replicate		5
Laser system		Quanta-Ray® GCR-11 Spectra Physics
Wavelength		1064 nm
Mode		Q-switch
Q-switch time		220 μs
Excitation lamp energy		50 J
Laser energy		200 mJ
Pulse frequency		10 Hz
Laser scan mode		Point scan
Focus		On sample surface
Spot size		200 μm

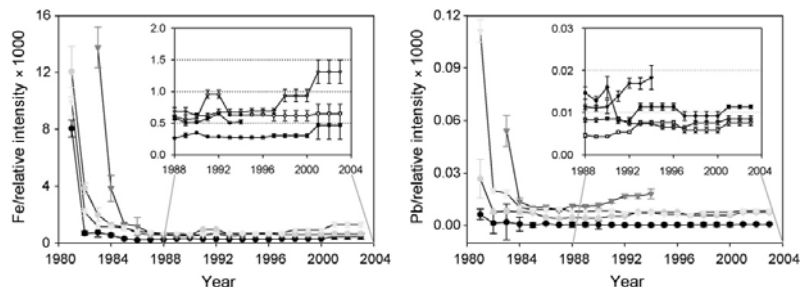


Fig. 2. Relative intensities \pm S.D. ($\times 1000$) of iron and lead in annual growth bands of four different *L. elliptica* between 1980 and 2003. Small diagrams show a magnification of the time course from 1988 to 2003. Yearly resolution was obtained until an age of 12. After this age mean values for groups of up to 4-year bands were calculated, due to the spot size of the laser crater. The same weighted value was assigned to each year in a group.

An integrated microscope was used to target the laser beam to different growth bands of the sample shells. In case the diameter of the laser crater exceeded growth band thickness, mean values of more than one growth band were derived. As matrix matched standards were not available, no element concentrations are provided in this paper. Instead, normalized element signatures are shown.

Each matrix has its specific absorption coefficient at different wavelengths. The 1064 nm wavelength is best suitable for laser ablation of ice cores, which is usually performed in our laboratory. The energy is sufficiently high for intrusion into the ice core, resulting in efficient sample ablation, a process called photoablation (Pearce et al., 2004). If the wavelength is not optimal for a sample matrix, material is removed by small superjacent plasma which forms in the Ar carrier gas owing to high energy density in the focus of the laser beam. This process was termed plasma erosion by Abell (1991). In future investigations of bivalve shells, wavelength of 266 or 213 nm should be used, which are better suitable for the shell matrix to achieve crater diameter smaller than 20 μm . This was, however, not yet available in the laboratory when these analyses were performed.

All data are given as relative intensities, normalized to the Ca signal, or as weighted means (m_w) and weighted standard deviations (s_w) of relative intensities of the analyzed bivalves according to formula (1) (Barlow, 1989). Ca is homogeneously distributed throughout the shell and therefore adequate as an internal standard. In doing so, effects of variations in sample surface texture, laser energy, and plasma energy could be excluded. The sensitivity of the detector system is different for each of the analyzed isotopes, and signals were corrected according to known intensities of isotopes of interest. Calculations were done for comparability of element ratios to literature data.

$$m_w = \frac{\sum(m_i/s_i^2)}{\sum(1/s_i^2)}, \quad s_w = \sqrt{\frac{1}{\sum(1/s_i^2)}} \quad (1)$$

with m_w = weighted mean; s_w = weighted standard deviation; m_i = mean values of each umbo and year; s_i = standard deviation of each umbo and year.

3. Results

Fig. 2 presents the relative intensities of Fe as tracer for glacial sediment ablation and Pb as tracer for anthropogenic compounds versus years.

Both element signatures show a rapid decline within the first years of bivalve life (large diagrams), but in the time span from 1988 to 2003 no common trend was visible in either the iron or lead signatures in the four bivalve shells. In fact, no trend was visible for any of the measured elements (data not shown).

In a next step, weighted average values with weighted standard deviations of the four *L. elliptica* umbos were calculated for each element over bivalve lifetime (Eq. (1), Barlow, 1989). Graphs in Fig. 3 depict intensity means and standard deviations. All element signatures show a rapid decrease within the first 6–8 years of bivalve life. Yearly resolution was obtained until an age of 12. After this age mean values for groups of up to 4-year bands were calculated, due to the spot size of the laser crater. The same weighted value was assigned to each year in a group.

Table 2 gives the weighted means of relative intensities of trace elements in growth bands of four *L. elliptica* shells from 9–23 years of age in % of the value in the first year segment.

Table 2
Weighted means of relative intensities of trace elements in growth bands of four *Laernula elliptica* shells from 9 to 23 years of age in % of the value in the first year segment, and element ratios calculated on the basis of the means of the relative element intensities in annual growth bands between 1990 and 2003

	% of first year	Ratio
Al	9.4 \pm 0.6	
Mn	13.4 \pm 0.8	
Fe	5.9 \pm 0.3	
Cu	11.4 \pm 0.4	
Pb	18.5 \pm 1.2	
U	6.9 \pm 0.5	
Fe/Mn		26.8 \pm 9.4
Fe/Cu		3.8 \pm 1.7
Al/Mn		2.8 \pm 0.3
Al/Cu		0.4 \pm 0.1

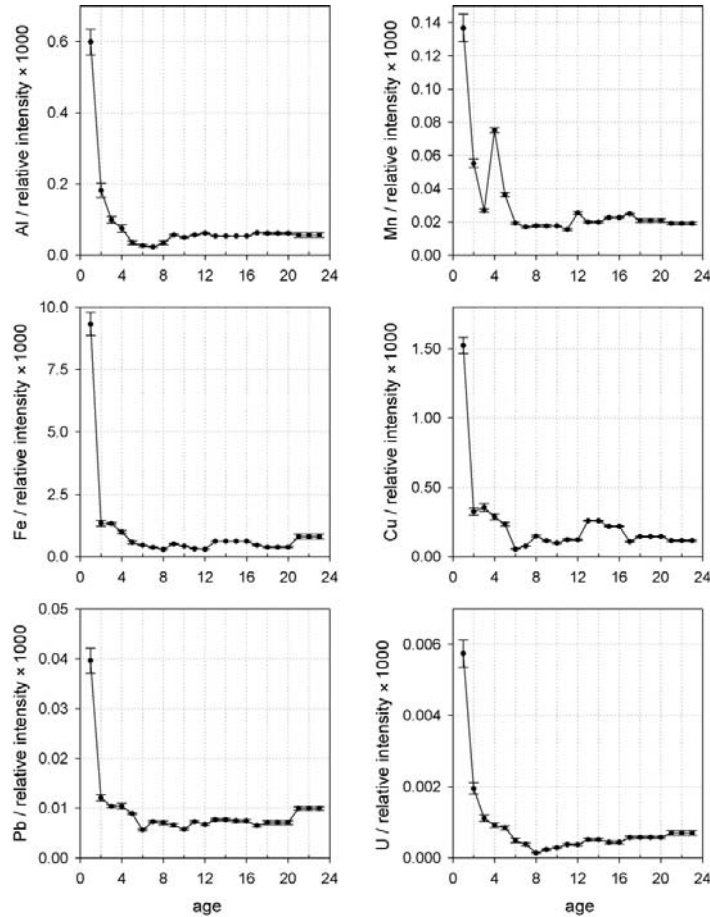


Fig. 3. Weighted means of Al, Mn, Fe, Cu, Pb and U normalized to Ca signal (relative intensities) \pm S.D. ($\times 1000$) in annual growth bands of *L. elliptica*. Yearly resolution was obtained until an age of 12. After this age mean values for groups of up to 4-year bands were calculated, due to the spot size of the laser crater. The same weighted value was assigned to each year in a group.

Relative accretion intensity of Al, Fe and U decreased to $\sim 7.5\%$ compared to the first growth band. Mn and Cu decrease to $\sim 12.5\%$, whereas Pb decreases to 18.5% of the concentration in the first growth band. Element ratios calculated on the basis of the means of the relative element intensities in annual growth bands between 1990 and 2003 were Fe/Mn: 26.8, Fe/Cu: 3.8, Al/Mn: 2.8, Al/Cu: 0.4. There is no correlation visible either between the relative intensities and growth process, or between the element ratios and growth process.

4. Discussion

4.1. Can bivalve shells be used as environmental archives?

The present study was designed to investigate, whether accelerated glacier melting observed over the past 10 years in Potter cove (see Abele et al., 2007; Schloss et al., 2007; Dierssen et

al., 2002) might have caused an increase in Fe and of other elements, contained in ablated sediments and dust minerals, in the ultimate growth bands formed in bivalve umbos from the impacted region. Contrary to our hypothesis, element concentrations were highest in the early growth bands formed in the young bivalves and levelled off during the first 6–8 years of bivalve age. Following this initial life phase, the averaged element concentrations in the growth bands for 9 years and older animals remained constant, without signs of an increase in the most recent years.

Thus, neither did the intensified human activity at Jubany station within the last 15 years result in elevated Pb concentrations, nor could we find an increased iron signal from a potential increase of iron import from the ongoing glacial abrasion. Thus, glacial rock ablation may not have led to a measurable enrichment, because the iron from this natural source is always abundant in this coastal system and the animals may be capable

of controlling the iron uptake. Still, we found iron to be 3–10-fold higher concentrated in digestive gland of soft shell clams from the Potter Cove environment compared to soft shell clams (*Mya arenaria*) from the German Wadden Sea, where also the environmental concentrations are 10-fold lower (Estevez et al., 2002). Thus, the increase of iron from glacial ablation may be too marginal to be detected in bivalve shell archives against a huge environmental background at the present state. Richardson et al. (2001) compared trace element concentrations in growth bands of shells of the bivalve *Modiolus modiolus* from polluted and non-contaminated sites in the North Sea, using LA-ICP-MS. The sewage sludge contained elevated concentrations of Cu, Pb and Zn. Shells of bivalves from polluted sites turned out to be slightly higher loaded with metals than shells from non-polluted sites, except for events in 1972 and 1975, when Zn and Pb concentrations increased by a factor of 4–8 in the shells. In the study of Richardson and colleagues, only Pb showed decreasing concentrations in shell growth bands within the first 7 years of animal age. Cu and Zn accumulation remained constant during animal lifetime. Price and Pearce (1997) found concentration peaks of Pb, As, Cu, Zn and U in shells of the cockle *Cerastoderma edule* (British Isles) collected at four sampling sites. All cockles are characterized by a sudden increase in metal content due to extreme anthropogenic pollution events, in particular Zn and Cu. Only animals from one sampling location showed a synchronized pattern of increasing element concentrations immediately after the winter growth band.

4.2. What is the reason for the decay of signal in the first years?

The strong decay of element accretion in the first 8 years of bivalve age can be related to respiration mass (*R*) data, obtained for the Jubany soft shell clam population by Philipp et al. (2005). The respiration mass index is defined as the product of whole animal respiration and body wet mass. The change of the index over animal lifetime is described by Eq. (2) (Von Bertalanffy, 1934). *R* relates exponentially to body mass (*M*), and the change in body mass over time (growth) depends exponentially on animal size (*S*) at a given age.

$$\log R = a \log M - b, \quad \log M = c \log S - d, \\ S_t = S_\infty(1 - e^{k(t+t_0)}) \quad (2)$$

with *R*=respiration mass in $J d^{-1}$; *M*=growth in body mass in $mm mg^{-1}$; *S_t*=growth in size in $mm a^{-1}$; *t*=time.

Parameter values for *L. elliptica* obtained from Philipp et al. (2005) are: *a*=0.888, *b*=2.067, *c*=3.074, *d*=2.531; *S_∞*=asymptotic maximum size (=91.55 mm); *k*=growth constant (=0.108); *t₀*=age at which lengths would be zero (=−1.598)

Plotting the curve for respiration mass (dashed line) and its first (dotted line) and second (solid line) derivative over animal life time (Fig. 4) results in an inflection point at an age of 7.9 years in the 2nd derivate. This point marks a change in the increase of *R* (1st derivate), which means a progressive slowing of the increase in age-dependent whole animal metabolic rate.

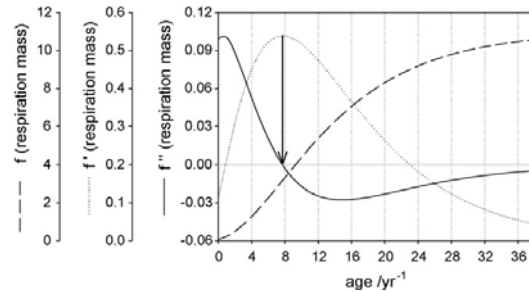


Fig. 4. Respiration mass (—) and its 1st (···) and 2nd (—) derivative of *L. elliptica* ($\log R = a \times \log M - b$, Philipp et al., 2005) vs. age year^{−1}. Inflection point (arrow) at an age of 7.9, indicating progressive slow down in the increase in age-dependent metabolic rate.

Moreover, it coincides with the end of the decrease in element accretion in the umbo between 6 and 8 years of bivalve age. Obviously, young, fast growing and intensely respiring bivalves accumulate heavy metals at higher rates into the shell matrix than older animals. Importantly, the higher accumulation does not reflect a denser packing of the umbo matrix in young animals, because the calculated intensities were Ca-normalized. This speaks for high uptake of heavy metals and less discrimination between wanted and unwanted material in younger than older specimens.

The importance of the analyzed elements for bivalve physiology is variable and complex, but it seems unlikely that any of these elements could be physiologically limiting under Antarctic coastal conditions. Iron and copper are both essential micronutrients as well as active Fenton chemicals, which must be bound to storage and transport proteins in invertebrate tissues, to prevent oxygen radical formation (Abele and Puntarulo, 2004). To see, whether the animals discriminate between different elements, ratios in shell material of *L. elliptica* were compared to the ratios in seawater, sedimenting particles (Abele et al., 2007) and basal ratios from the Earth's crust (Wedepohl, 1995) (Table 3). Water samples and sedimenting particles in Potter Cove were taken in December 2002 and are representative of the two possible uptake mechanisms of heavy metals into the bivalve tissue from the dissolved metal pool or through particle ingestion. Lower ratios (Fe/Mn and Fe/Cu) in *L. elliptica* shell material indicate preferential incorporation of Cu and Mn over Fe into the umbo matrix. Indeed, both metals can substitute Ca²⁺ ions in the calcium carbonate crystals (Tynan et al., 2005). Recent investigations of *L. elliptica* tissue concentrations show that Cu appears to be concentrated in digestive gland (Fe/Cu = 13–21) and gill tissues (Fe/Cu = 15) (Ahn et al., 2001), indicating increased demand for Cu in the Antarctic soft shell clam. For that matter, Cu-containing hemocyanin is the most common oxygen-binding pigment in non-hemoglobin-containing molluscs (Winzerling and Law, 1997) and, although not reported heretofore, it seems possible that copper containing respiratory proteins could exist in *L. elliptica*. Moreover, Cu is the catalytic ion in Fe-oxidases that oxidise ferrous Fe(II) to ferric Fe(III) for the binding to Fe transport and storage proteins (Winzerling and Law, 1997

Table 3

Element ratios in water samples (30 m depth, January 2004) and sediment trap material in Potter Cove (22 December 2002), the Earth's crust and in the umbo matrix of four *L. elliptica* (average \pm S.D.) calculated on the basis of the means of the relative element intensities in annual growth bands between 1990 and 2003

	Fe/Mn	Fe/Cu	Al/Mn	Al/Cu
Water sample (30 m depth) (Abele et al., 2007)	50.5 \pm 3.0	133 \pm 52.3		
Sediment trap sample (Abele et al., 2007)	55.8 \pm 4.7	323 \pm 172		
Earth's crust (Wedepohl, 1995)	58.6	2160	147	5415
<i>L. elliptica</i> (umbo)	26.8 \pm 9.4	3.8 \pm 1.7	2.8 \pm 0.3	0.4 \pm 0.1

for review). It looks like the animals are able to discriminate against the uptake of the relatively toxic element Fe, which is a more efficient Fenton catalyst than Cu and induces formation of reactive oxygen species (ROS) in animal tissues, including very aggressive hydroxyl radicals (OH^{*}) (Estevez et al., 2002). Comparing Fe/Mn and Fe/Cu to Al/Mn and Al/Cu (Table 3), Al is even more discriminated than iron. The Fe/Mn ratio in *L. elliptica* is 2.2 times lower than the ratio in the Earth's crust, where Al is the most highly concentrated metal. Al/Mn amounts to 2.8 in the shells, 53 times lower than in the Earth crust. Pathophysiology of Al in humans involves oxidative stress in the brain and, moreover, bone diseases, because Al competes with elements like Mg and Ca of similar atomic size and electric charge (<http://www.emedicine.com/med/topic113.htm>). It is presently unknown what effects Al can have in bivalve physiology, however, possibly, this element can be highly toxic if not excluded by the animals. Interestingly, aluminium is not measured or referred to in any of the available surveys of metal accumulation in bivalve shells or soft tissues that we are aware of.

4.3. Conclusions and outlook

We could clearly show that the incorporation of elements into the umbo matrix of *L. elliptica* is primarily coupled to respiration mass. No change due to global warming or anthropogenic activity could so far be discerned. However, it may well be possible that with increased accuracy and technical refinement, which improve spatial resolution, further analyses of bivalve shell material may enable to obtain higher time resolute information. The use of a laser ablation (LA) system with a wavelength of 266 nm should be more applicable to achieve higher sensitivity and smaller crater diameter. More information on other elements in bivalve umbo matrices will be gained, by coupling an inductively coupled plasma time of flight mass spectrometer (ICP-TOF-MS) to the LA-System. Also, higher numbers of animals have to be analyzed for final conclusions.

Acknowledgements

We thank Lic Adrian Atencio, Instituto Antartico, Buenos Aires, for collaboration on the environmental iron concentrations in Jubany and Ilse Stölting for invaluable technical support. Thanks to Tom Brey for lively and competent discussions of the shell archive topic. Moreover, we received all necessary support on Jubany Base and especially from the 2003 Argentinean diving team, who collected *L. elliptica* in Potter Cove. We

would also like to thank two anonymous referees for constructive comments.

References

- Abele, D., Puntarulo, S., 2004. Formation of reactive species and induction of antioxidant defence systems in polar and temperate marine invertebrates and fish. *Comp. Biochem. Physiol. Part A* 138, 405–415.
- Abele, D., Atencio, A., Dick, D., Gonzales, O., Kriewis, M., Meyer, S., Philipp, E., Stölting, I., 2007. Iron, copper and manganese discharge from glacial melting into Potter Cove and metal concentrations in *Laternula elliptica* shells. In: Wiencke, C., Ferreyra, G., Abele, D., Marensi, S. (eds.), *The Potter Cove coastal ecosystem, Antarctica. Synopsis of research performed 1999–2006 at the Dallmann Laboratory and Jubany Station, King George Island (Isla 25 de Mayo)*. Rep. Polar Mar. Res., in press.
- Abell, I.D., 1991. Performance benefits of optimisation of laser ablation sampling for ICP-MS. In: Holland, J.G., Eaton, A.N. (Eds.), *Application of Plasma Source Mass Spectrometry*. Royal Society of Chemistry, pp. 209–271.
- Ahn, I.-Y., Kang, J., Kim, K.-W., 2001. The effect of body size on metal accumulations in the bivalve *Laternula elliptica*. *Ant. Sci.* 13 (4), 355–362.
- Bagnyukova, T.V., Chahrak, O.I., Lushchak, V.I., 2006. Coordinated response of goldfish antioxidant defenses to environmental stress. *Aquat. Toxicol.* 78, 325–331.
- Barlow, R., 1989. *Statistics: A Guide to the Use of Statistical Methods in the Physical Science*. The Manchester Physics Series. Wiley, New York, p. 54.
- Brey, T., Mackensen, A., 1997. Stable isotopes prove shell growth bands in the Antarctic bivalve *Laternula elliptica* to be formed annually. *Polar Biol.* 17, 465–468.
- Carriker, M.R., Swann, C.P., Ewart, J.W., 1982. An exploratory study with the proton microprobe of the ontogenetic distribution of 16 elements in the shell of living oyster. *Mar. Biol.* 69, 234–246.
- Dierssen, H.M., Smith, R.C., Vernet, M., 2002. Glacial meltwater dynamics in coastal waters west of Antarctic Peninsula. *Proc. Natl. Acad. Sci.* 99, 1790–1795.
- Estevez, M.S., Abele, D., Puntarulo, S., 2002. Lipid radical generation in polar (*Laternula elliptica*) and temperate (*Mya arenaria*) bivalves. *Comp. Biochem. Physiol., Part B* 132, 729–737.
- Huanxin, W., Lejun, Z., Presley, B.J., 2000. Bioaccumulation of heavy metals in oyster (*Crassostrea virginica*) tissue and shell. *Environ. Geol.* 38, 1216–1226.
- Jing, G., Li, Y., Xie, L., Zhang, R., 2006. Metal accumulation and enzyme activities in gills and digestive gland of pearl oyster (*Pinctada fucata*) exposed to copper. *Comp. Biochem. Physiol., Part C* 144, 184–190.
- Kriewis, M., Reinhard, H., Dunker, E., Beninga, I., Ruhe, W., 2004a. An analytical system for the detection of spatial patterns of trace element distribution in frozen samples. Utility Patent, DE 20 2004 005 991.6.
- Kriewis, M., Reinhard, H., Dunker, E., Hoffmann, E., Lüdtke, C., Beninga, I., 2004b. Analytical procedure for the detection of trace element distribution patterns in solid samples. Patent, EP-DE 501 05 651.3-08.
- Momo, F., Kowalke, J., Schloss, I., Mercuri, G., Ferreyra, G.A., 2002. The role of (*Laternula elliptica*) in the energy budget of Potter Cove (King George Island, Antarctica). *Ecol. Model.* 155, 43–51.

- Mubiana, V.K., Blust, R., 2007. Effects of temperature on scope for growth and accumulation of Cd, Co, Cu and Pb of the marine bivalve *Mytilus edulis*. *Mar. Environ. Res.* 63, 219–235.
- Philipp, E., Brey, T., Pörtner, H.O., Abele, D., 2005. Chronological and physiological ageing in a polar and a temperate mud clam. *Mech. Ageing Dev.* 126, 598–609.
- Pearce, N.J.G., Westgate, J.A., Perkins, W.T., Preece, S.J., 2004. The application of ICP-MS methods to tephrochronological problems. *Appl. Geochem.* 19, 289–322.
- Price, G.D., Pearce, N.J.G., 1997. Biomonitoring of pollution by *Cerastoderma edule* from the British Isles: a laser ablation ICP-MS study. *Mar. Pollut. Bull.* 34 (12), 1025–1031.
- Raith, A., Perkins, W.T., Pearce, N.J.G., Jeffries, T.E., 1996. Environmental monitoring on shellfish using UV laser ablation ICP-MS. *Fresenius J. Anal. Chem.* 355, 789–792.
- Reinhardt, H., Kriews, M., Miller, H., Schrems, O., Lüdke, C., Hoffmann, E., Skole, J., 2001. Laser ablation inductively coupled plasma mass spectrometry: a new tool for trace element analysis in ice cores. *Fresenius J. Anal. Chem.* 370, 629–636.
- Richardson, C.A., Chenery, S.R.N., Cook, J.M., 2001. Assessing the history of trace metal (Cu, Zn and Pb) contamination in the North Sea through laser ablation ICP-MS of horse mussel, *Modiolus modiolus* shells. *Mar. Ecol. Prog. Ser.* 121, 157–167.
- Richardson, C.A., 2001. Molluscs as archive of environmental change. *Oceanogr. Mar. Biol.* 39, 103–164.
- Schloss, I.R., Ferreyra, G. A., González, O., Atencio, A., Fuentes, V., Tosonotto, G., Mercuri, G., Sahade, R., Tatián, M., Abele, D., 2007. Long term hydrographic conditions and climate trends in Potter Cove. In: Wiencke, C., Ferreyra, G., Abele, D., Marensi, S. (eds.), *The Potter Cove Coastal Ecosystem, Antarctica. Synopsis of research performed 1999–2006 at the Dallmann Laboratory and Jubany Station, King George Island (Isla 25 de Mayo)*. Rep. Polar Mar. Res., in press.
- Tynan, S., Eggins, S., Kinsley, L., Welch, S.A., Kirste, D., 2005. Mussel shells as environmental tracers: an example from the Loveday Basin. In: Roach, I.C. (Ed.), *Regolith 2005—Ten Years of CRC LEME*. CRC LEME, pp. 314–317.
- Von Bertalanffy, L., 1934. Untersuchungen über die Gesetzmäßigkeit des Wachstums. *Arch. F. Entwicklungsmechanik d. Organismen* 131, 613–652.
- Wedepohl, K.H., 1995. The composition of the continental crust. *Geochim. Cosmochim. Acta* 59 (7), 1217–1232.
- Winzerling, J.J., Law, J.H., 1997. Comparative nutrition of iron and copper. *Annu. Rev. Nutr.* 17, 501–526.
- Yap, C.K., Ismail, A., Tan, S.G., 2003. Background concentrations of Cd, Cu, Pb and Zn in the green-lipped mussel *Perna viridis* (Linnaeus) from Peninsular Malaysia. *Mar. Poll. Bull.* 46, 1035–1048.

Publication IV

High spatial resolution analysis of a frozen sediment core by LA-ICP-MS analysis

D. Dick, P. Bluszcz, H. Reinhardt, C. Ohlendorf, B. Zolitschka, M. Kriews

In preparation for submission.

It is planned to analyse this sediment core segment with X-ray fluorescence spectroscopy to compare these data with LA-ICP-MS data. At the present state this publication has not been reviewed yet.

High spatial resolution analysis of a frozen sediment core by LA-ICP-MS analysis

D. Dick, P. Bluszcz⁺, H. Reinhardt[‡], C. Ohlendorf⁺, B. Zolitschka⁺, M. Kriews¹
Alfred Wegener Institute for Polar and Marine Research, Am Handelshafen 12,
27570 Bremerhaven

⁺ Institute of Geography, University of Bremen, Celsiusstr. FVG-M, 28359 Bremen

[‡] Hamburger Stadtentwässerung, Köhlbranddeich 1, 20457 Hamburg

Abstract

High spatial resolution analysis of samples forming natural or climate archives has received increasing interest in recent years. Here we report about element distributions within one frozen lacustrine sediment cores (spatial resolution 1.5 mm) obtained by laser ablation inductively coupled plasma mass spectrometry (LA-ICP-MS). Seasonal variations of Ca and Al were detected, with Ca maxima during summer and Al maxima during winter. Variations in the non-mineral Pb signature for the last 320 years could be assigned to the little ice age, the industrialisation and finally to the reduction of Pb in gasoline at the beginning of the 1980's.

Introduction

Annually laminated sediments are valuable archives for reconstruction of the environmental and climate history of lakes and their catchment areas (Zolitschka *et al.*, 1996, 2006). With common methods (digestion of samples and spectroscopic analysis) it is impossible to gain annual or even subannual information about chemical compounds from laminated varved sediments with less than 1 mm layer thickness, because the required sample volumes for analysis usually exceed 1 cm³ (Zolitschka *et al.*, 1996). In October 2003 the 90 cm long sediment core SAC 03-3A was taken from Sacrower See, located between Berlin and Potsdam in the state of Brandenburg (NE-Germany) (29.5 m a.s.l., 13.06°E, 52.27°N). For this study it was of interest to clarify whether the formation of laminations resulted in variations of the elemental signature that correspond to summer and winter layers. To circumvent problems with sample preparation, investigation of element signatures in frozen sediments of Sacrower See by LA-ICP-MS analysis has been conducted.

¹ Correspondance author tel.: +49-(0)471-4831-1420; fax: +49-(0)471-4831-1149; email: Michael.Kriews@awi.de

Methods

The frozen annually laminated sediment core SAC 03-3A was analysed with LA-ICP-MS (laser source: Quanta-Ray® GCR-11, (Nd:YAG) Spectra Physics 1064 nm; ICP-MS: Elan 6000 Perkin Elmer/Sciex) using a cryogenic sampling cell (Kriews *et al.*, 2004a, 2004b). The experimental setup for the direct analysis of frozen samples is shown elsewhere (Dick *et al.*, 2008 submitted). A detailed description is given by (Reinhardt *et al.*, 2001). An overview of optimized parameters can be found in Table 1.

Table 1: Instrumental settings for the LA-ICP-Q-MS analysis of frozen sediment cores from Sacrower lake.

ICP-MS	PerkinElmer Sciex, Elan 6000	laser system	Spectra Physics, Quanta-Ray® GCR-11
Radio frequency power	1400 W	Wavelength	1064 nm
Plasma gas	14.0 L min ⁻¹	Mode	Q-Switch
Auxiliary gas	0.8 L min ⁻¹	Q-Switch time	220 µs
Carrier Gas	1.0 L min ⁻¹	Laser energy	220 mJ
Dwell time	10 ms	Pulse Frequency	10 Hz
Sweeps / Replicate	20	Focus	on sample surface
Replicate	5 / 120	Laser scan mode	line scan
		position of lines	vertical / horizontal to the core axis
		line length	14 mm / ~ 71 mm
		Line width	100 µm
		spatial resolution	1.5 mm

Each matrix has its specific absorption coefficient at different wavelengths. The 1064 nm wavelength is best suitable for laser ablation of ice cores which is usually done in our laboratories. The energy is sufficiently high for intrusion into the ice to cause photoablation of the sample (Pearce *et al.*, 2004). If the wavelength is not optimal for a sample matrix, material is removed by a small plasma which forms in the Ar carrier gas due to the high energy density in the focus of the laser beam (plasma erosion) (Abell, 1991). The water content in the sediment core was found constant ($89.79 \pm 3.33\%$) by freeze drying. Therefore, the used laser wavelength should also be suitable for the conducted investigations.

Lake sediment core sampling and analysis

To recover the annual lamination and the sediment-water interface in best possible condition we used the Niederreiter Freeze-Corer (Kulbe *et al.*, 2003). The sediment was frozen in-situ at -90 °C and afterwards stored in a special box at -20 °C. In a cold room (-20 °C) one half of the core SAC 03-3A was sawed into 13 overlapping subsections for thin section preparation and LA-ICP-MS analysis. The sediment consists of light and dark coloured layers (Figure 1); one couplet constitutes one year (varve). Visible continuous lamination is only given from the top of the core to a depth of about 42.7 cm (1879 Anno Domini (A.D.)). Below that depth dating was done by extrapolating the sedimentation rate ($2.2 \pm 0.2 \text{ mm a}^{-1}$; (Lüder *et al.*, 2006)). The sediment core dates back to approximately 1674 AD. On all 13 overlapping pieces line scans longitudinally to the core axis were performed to analyse signal variations from 1674 AD to 2003 AD

(Figure 1). Down to a depth of 42.7 cm additionally short lines perpendicular to the core axis, i.e. parallel to the bedding, were ablated in light and dark layers, with a median distance of 1.5 mm (Figure 1) to detect differences between summer and winter layers.

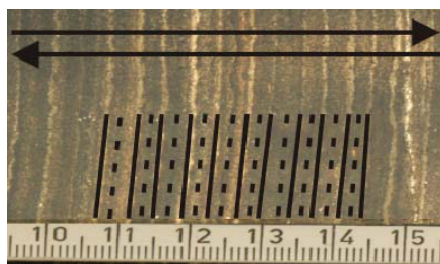


Figure 1: Part of the sediment core (Sacrower See) with the ablation pattern. Two lines parallel to the core axis (indicated by black lines with arrows) and lines perpendicular to the core axis (parallel to the bedding) (——— summer; - - - - winter) were ablated.

13 isotopes of 10 elements were analysed with both scan types. For both scan types relative standard deviation (RSD) were: Na: 10%, Mg; 8.4%, Al: 8.4%. Ca: 8.6%, Sr: 8.8%. Cd: 12%, La: 13.2%, Ce: 13.3%, Pb: 8.8%, U: 12%. Information about the elemental signatures that correspond to summer and winter layers can be collected without any prior external calibration. However internal normalization is necessary to exclude effects caused by variations in sample surface texture, laser energy, and plasma energy. Due to the constant water content of the sediment core, ^{17}OH , representing water, was taken as internal standard for LA-ICP-MS. The sensitivity of the detector system is different for each isotope. Calculations were done for comparability of element ratios to literature data according equation 1.

$$EI_{sed_corr} = EI_{sed} \cdot \frac{100}{E_A} \cdot \frac{UI_s}{EI_s} \quad (1)$$

with:

EI_{sed} = signal intensity of element E in the sediment core in counts per seconds (cps)

E_A = isotope abundance of element E in %

UI_s = signal intensity of uran (U) in a $100 \mu\text{g kg}^{-1}$ standard, as the detector is most sensitive for this element

EI_s = signal intensity of element E in a $100 \mu\text{g kg}^{-1}$ standard

Results and Discussion

Biological activity induced signal variation in the lake sediment core

Climate variations which influence e.g. biological activity in lakes can be examined with lake sediment cores (Ito, 2001). Relative intensities obtained by laser ablation analysis show distinct signal maxima of Ca, Mg and Sr in the sediment record of Sacrower See during summer. The lighter layers, which are formed in spring and

summer, contain a large amount of CaCO₃ which is precipitated in the water column of the lake due to strong photosynthetic CO₂ uptake and sedimentation of centric diatom frustules (Bluszcz *et al.*, 2008). The darker layers formed during autumn and winter are dominated by organic material and pennate diatoms (Figure 1). Mg²⁺ and Sr²⁺ can substitute Ca²⁺ ions in calcium carbonate crystals. Therefore, they show a similar behaviour like Ca. Calcite precipitation starts in late spring and lasts until September (Bluszcz *et al.*, 2008). The amount of Ca and Sr related to mineral dust sources is expressed by the enrichment factor (EF) relative to the Earth's crust (Wedepohl, 1995) and is shown in Figure 2 a and b for the time period 1880-1930. This enrichment factor is calculated according to equation 2.

$$EF_{Earth's_crust} = \frac{(M / Al)_{sample}}{(M / Al)_{Earth's_crust}} \quad (2)$$

where: M = element of interest

High EF for Ca and Sr are observed in the summer layers. Results presented in this graph were obtained by laser ablation perpendicular to the core axis. Alternating analysis of light and dark layers was accomplished. Low EF values < 10 indicate a dominating mineral source, values <<1 and >10 indicate non mineral sources.

Mineral influx variation in the lake sediment core

Figure 2 c shows the Al and Mg signal (normalized to ¹⁷OH) of the sediment core. The EF of Mg ranges between 2 to 12 (3.89 average value). Temperature variations (Osborn *et al.*, 2006) during the period 1880-1930 are also included in Figure 2 c. Osborn *et al.* (2006) report about the analysis of synchronous anomalies of a variety of independent temperature proxies. The authors collected proxy data sets from 14 different regions of the Northern Hemisphere. In this work the data set from the Netherlands / Belgium is of interest due to its proximity to Potsdam (Germany). Temperature proxy data were smoothed and normalized (Osborn *et al.*, 2006). Warmer and colder periods differ by ~1.5 °C.

When temperature is low, higher Al and Mg intensities are observed. This anti-correlation shows a cyclic behaviour. The total sediment accumulation rate amounts to 8.6 mg cm⁻² season⁻¹ (October to March) and increases to 9.7 mg cm⁻² season⁻¹ (April to September) (Bluszcz *et al.*, 2008), whereas the mineral accumulation rate remains almost constant (2.49 mg cm⁻² season⁻¹ from October to March, 2.44 mg cm⁻² season⁻¹ from April to September) (unpublished data). Consequently, increasing biological activity results in dilution of mineral particles correlating with minima in Al signals during warm conditions.

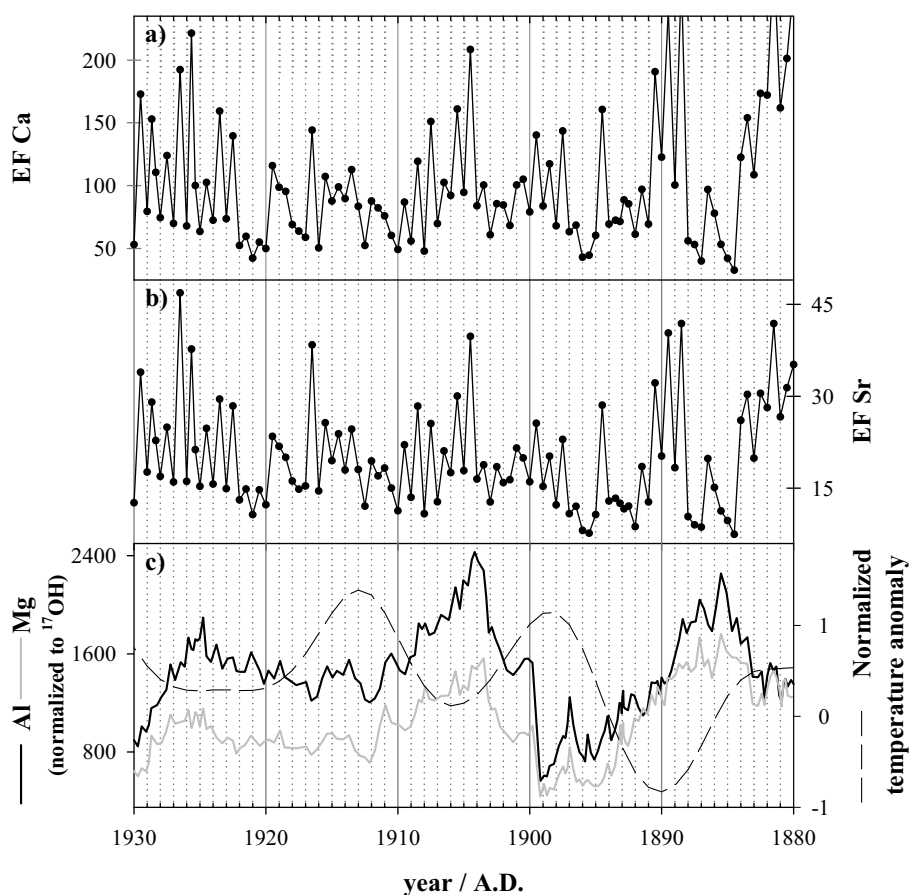


Figure 2: a+b) Enrichment factor (EF) of Ca and Sr relative to the Earth's crust vs. time in the sediment core SAC03-3A measured alternatively in summer and winter layers as identified from visual stratigraphy. Maximum values (peaks) correspond to summer layers. Dotted vertical lines match to winter months. On average the RSD amounts 8.6 % for Ca and 8.8 % for Sr. c) Relative intensities of Al and Mg (normalized to ^{17}OH) vs. time in the sediment core SAC03-3A. Filtered and normalized temperature proxy records (from the Netherlands / Belgium, Osborn *et al.*, 2006) vs. time. When temperature is low, higher Al and Mg intensities are observed.

Anthropogenic influence on the sediment record

Sacrower See is connected to the River Havel in the South. Thus there is a proximity to Berlin which was densely populated during the period of investigation and anthropogenic contamination of Sacrower See is documented (Lüder *et al.*, 2006). To evaluate the anthropogenic contamination, the anthropogenic fraction of Pb was calculated according to equation 3.

$$Pb_{anthr.} = Pb_{sample} - Al_{sample} \cdot \left(\frac{Pb}{Al} \right)_{crust} \quad (3)$$

Figure 3 shows non-mineral Pb along the whole sediment core (1680-2003 A.D.) normalized to ^{17}OH . Data acquisition was problematic for subsections 1, 2 and 4, where LA-ICP-MS analysis obtained high ^{17}OH values or rather low Pb values. For subsection no. 1 and 2 signals of Pb and ^{17}OH (these signals are not shown here) developed into the same direction but more or less pronounced. The signal increased from subsection 1 to subsection 2 by a factor of 10 for Pb and was nearly constant for ^{17}OH . Signals for subsection 2 were 1.5 and 5 times higher compared to subsection 3 for Pb and ^{17}OH

respectively. Interestingly signals developed into different directions on subsection 4. Pb showed decreased signals compared to subsections 3 and 5 whereas ^{17}OH showed increased signals compared to subsections 3 and 5. It is not clear whether problems occurred for Pb data acquisition or ^{17}OH data acquisition. The resulting signal shifts are not incorporated in the interpretation, but the signal progression within these shifts is considered. The little ice age (LIA) lasted from the 15th to the middle of the 19th century. Before the industrialization started, Pb was introduced into the lake only by mineral material. Temperature variations during the LIA resulted in small changes of the Pb signal. In 1815 the industrialization started in Germany. Within a short time period population growth, railway and heavy industries, increasing use of coal and other fuels lead to high input of anthropogenic components (e.g. Pb) into the atmosphere, River Havel and thus Sacrower See. Less Pb input around 1840-1850 might be attributed to the agriculture crisis. Whereas the 1st World War influenced the input of anthropogenic components only slightly, while the 2nd World War resulted in a distinctive decrease of Pb until 1955. After 1945 the economy recovered and around 1955 Germany experienced a period of strong economic activity. Two oil crises (1973 and 1979), the stepwise reduction of Pb from 400 mg L⁻¹ (1972) to 150 mg L⁻¹ (1976) in gasoline (Benzinbleigesetz (BzBIG) of August 5th, 1971) and the launch of unleaded gasoline at the beginning of the 1980's are closely related to decreasing Pb deposition.

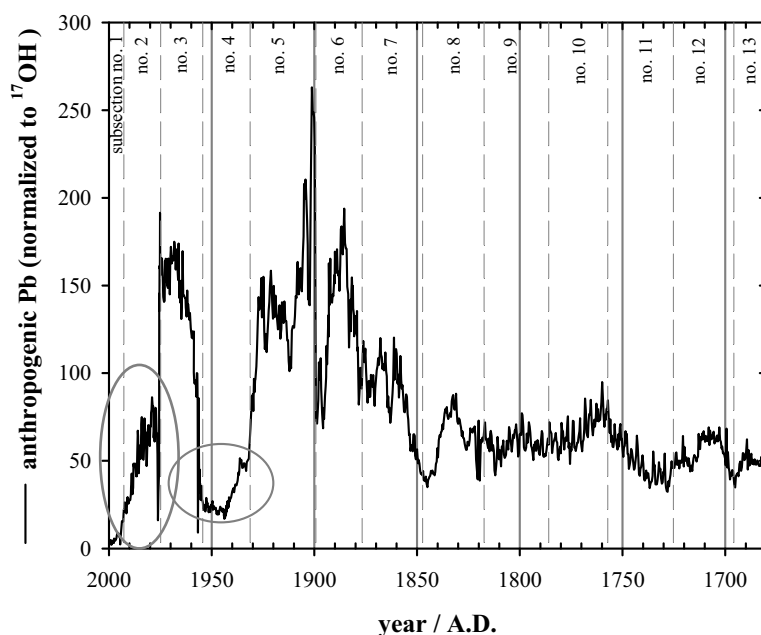


Figure 3: Relative intensity of non-minerogenic Pb fraction in the sediment core SAC03-3A. The analysis of 3 parts of the sediment core (2003-1974: subsection 1 and 2; 1953-1933: subsection 4) resulted in very low Pb/ ^{17}OH ratios. We assume problems with data acquisition of ^{17}OH for these 3 parts that still needs to be explained.

Conclusion and Outlook

First studies showed that it is possible to distinguish summer from winter layers in laminated sediment cores by LA-ICP-MS. As mentioned above, the 1064 nm wavelength is not ideal for mineral material. A frequency quadrupled Nd:YAG laser (266 nm) would improve the absorption efficiency of sediment, therefore more effective ablation of the mineral material would occur. Further, quadrupling the frequency would result in smaller crater diameter and line width which positively affects the possibility to analyse laminated sediments with even smaller annual layer thicknesses.

Appropriate standards for calibration are needed and have to be tested. Given a quantitative signal, evaluation of LA-ICP-MS data along with XRF data, the method which is commonly used for the investigation of sediment cores, is possible.

References

- Abell I.D. (1991): *Performance benefits of optimisation of laser ablation sampling for ICP-MS*. In: Holland, J.G., Eaton, A.N. (Eds.), *Application of Plasma Source Mass Spectrometry*. RSC, pp. 209-271.
- Bluszcz P., E. Kirilova, C. Ohlendorf, A.F. Lotter, B. Zolitschka (2008). Global radiation and onset of stratification as forcing factors of seasonal carbonate and organic matter flux dynamics in a hypertrophic hardwater lake (Sacrower See, northeastern Germany). *Aquatic Geochemistry*, **14**, 73-98.
- Ito E. (2001): *Application of Stable Isotope Techniques to Inorganic and Biogenic Carbonates*. In: *Tracking Environmental Change using Lake Sediments. Volume 2, Physical and Geochemical Methods*. W.M. Last, J.P. Smol (eds). Kluwer Academic Publishers, The Netherlands, pp 351-371.
- Kriews M., H. Reinhard, E. Dunker, I. Beninga, W. Ruhe (2004a): An analytical system for the detection of spatial patterns of trace element distribution in frozen samples. Utility Patent, DE 20 2004 005 991.6.
- Kriews M., H. Reinhardt, E. Dunker, E. Hoffmann, C. Lütke, I. Beninga (2004b): *Analytical procedure for the detection of trace element distribution patterns in solid samples*. Patent, EP-DE 501 05 651.3-08.
- Kulbe T., R. Niederreiter (2003): Freeze coring of soft sediments at a water depth of several hundred meters. *J. Paleolimnol.*, **29**, 257-263.
- Lüder B., G. Kirchner, A. Lücke, B. Zolitschka (2006): Paleoenvironmental reconstructions based on geochemical parameters from annually laminated sediments of Sacrower See (northeastern Germany) since the 17th century. *J. Paleolimnol.*, **35**, 897-912.
- Osborn T.J., K.R. Briffa (2006): The spatial extent of the 20th century warmth in the context of the past 1200 years. *Science*, **311**, 841-844.

- Pearce N.J.G., J.A. Westgate, W.T. Perkins, S.J. Preece (2004): *The application of ICP-MS methods to tephrochronological problems*. Appl. Geochem., **19**, 289-322.
- Reinhardt H., M. Kriews, H. Miller, O. Schrems, C. Lüdke, E. Hoffmann, J. Skole (2001): *Laser ablation inductively coupled plasma mass spectrometry: a new tool for trace element analysis in ice cores*. Fresen. J. Anal. Chem., **370**, 5, 629-636.
- Wedepohl K.H. (1995): *The composition of the continental crust*. Geochim. Cosmochim. Acta **59**(7), 1217-1232.
- Zolitschka B. (1996): High Resolution Lacustrine Sediments and their Potential for Palaeoclimatic Reconstruction. In: NATO ASI Series I, **41**, 454-478.
- Zolitschka B. (2006): *Varved lake sediments*. In: S.A. Elias (ed.). Encyclopedia of Quaternary Science, Elsevier; Amsterdam: 3105-3114.

Publication V

Rare Earth Elements determined in Antarctic ice by Inductively Coupled Plasma – Time of Flight, Quadrupole and Sector Field-Mass Spectrometry: an inter-comparison study

D. Dick, A. Wegner, P. Gabrielli, U. Ruth, C. Barbante, M. Kriews

Analytica Chimica Acta, in press.

Rare Earth Elements determined in Antarctic ice by Inductively Coupled Plasma – Time of Flight, Quadrupole and Sector Field-Mass Spectrometry: an inter-comparison study

D. Dick, A. Wegner, P. Gabrielli^{+,‡}, U. Ruth, C. Barbante^{+,Δ}, M. Kriews^{*}
Alfred Wegener Institute for Polar and Marine Research, Am Handelshafen 12, 27570
Bremerhaven, Germany

⁺Institute for the Dynamics of Environmental Processes – CNR, 30123 Venice, Italy

^ΔDepartment of Environmental Sciences, University of Venice, Ca' Foscari, 30123
Venice, Italy

[‡]School of Earth Science and Byrd Polar Research Center, Ohio State University,
Columbus, OH 43210-1002, USA

Abstract

Inductively coupled plasma mass spectrometry (ICP-MS) is a suitable tool for multi-element analysis at low concentration levels. Rare earth element (REE) determinations in standard reference materials and small volumes of molten ice core samples from Antarctica have been performed with an ICP-Time of Flight-MS (ICP-TOF-MS) system. Recovery rates for REE in e.g. SPS-SW1 amounted to ~103%, and the relative standard deviations were 3.4% for replicate analysis at REE concentrations in the lower ng L⁻¹ range. Analyses of REE concentrations in Antarctic ice core samples showed that the ICP-TOF-MS technique meets the demands of restricted sample mass. The data obtained are in good agreement with ICP-Quadrupole-MS (ICP-Q-MS) and ICP-Sector Field-MS (ICP-SF-MS) results. The ICP-TOF-MS system determines accurately and precisely REE concentrations exceeding 5 ng L⁻¹ while between 0.5 and 5 ng L⁻¹ accuracy and precision are element dependent.

Keywords: ultra trace element analysis, ICP-TOF-MS, rare earth elements, Antarctic ice

Introduction

Inductively coupled plasma mass spectrometry (ICP-MS) is a powerful technique for analysis of the elemental composition and isotope ratios for diverse kinds of samples (environmental, geological and biological samples). Various techniques for mass selection are used in ICP-MS. Sector Field mass spectrometers (SF-MS) [1] and Quadrupole mass spectrometers (Q-MS) [2] have been the most common MS types used for the analysis of natural samples so far. Both instruments scan one element after

* Corresponding author tel.: +49-(0)471-4831-1420; fax: +49-(0)471-4831-1149; email: Michael.Kriews@awi.de

another, which is called sequential analysis. Often the number of isotopes analysed is limited owing to small sample volumes and thus short analysis times. In contrast to the sequential MS systems, the Time of Flight-MS (TOF-MS) analyses in a quasi simultaneous mode [3] as all isotopes are simultaneously extracted from the ion source. This increases the precision and the accuracy of the analysis, which is a particular benefit for isotope ratio measurements [4-6]. Major advantages of such a system are: No limitations on the number of isotopes analysed and fast data acquisition. This latter is important when using sample introduction systems like laser ablation [7] or an inductively coupled heated vaporizer [8] and allows obtaining numerous replicate analyses. In contrast to MS systems analyzing in the sequential mode, for ICP-TOF-MS systems the detection capability is independent of the number of isotopes determined [6]. A brief overview of the application of TOF-MS is provided elsewhere [9]. Until now, only few studies on the use of ICP-TOF-MS for element analysis have been published [7-8, 10-14]. In particular the determination of extreme ultra traces of rare earth elements (REE) has so far been described only rarely [15-16] and only for samples after concentration by a factor of 15 to 22 and by a factor of 500, respectively.

Studies of trace elements in natural samples (*e.g.* ice cores from polar regions) as indicator of environmental pollution and for paleoclimate research have been performed [17-20]. Owing to large distances between Antarctica and its surrounding continents (South America – Antarctica (~1100 km), South Africa – Antarctica (~4000 km) and New Zealand / Australia - Antarctica (~2500 km, ~3000 km)) and because of the shielding circum-Antarctic circulation pattern, Antarctica is the remotest area in the world. This results in very low trace element concentrations. Thus demands are high on sampling of snow and ice cores, on sample preparation and finally on the analysis of low concentrations in limited sample volumes [1-2, 21].

The aim of this work is to assess the accuracy and precision of an ICP-TOF-MS system [7, 12] in determining REE at ultra low concentration levels. The ICP-TOF-MS system was developed at the Institute for Analytical Science in Berlin, supported as a research prototype jointly with Analytik Jena. Reference materials SPS-SW1 and SLRS-4 were analysed. Instrumental detection limits (IDL), the recovery rate and precision, the sample consumption and analysing time are presented. For inter-comparison studies of different MS systems and laboratories, ice core samples drilled within the European Project for Ice Coring in Antarctica (EPICA) [22, 23] were analysed by ICP-TOF-MS, ICP-Q-MS and ICP-SF-MS.

Experimental

Standards and Labware

At the Alfred Wegener Institute (AWI) in Bremerhaven, Germany, ultrapure water was produced by coupling a reverse osmosis system with a Purelab Ultra system (Elga, High Wycombe, U.K.). Commercially available ICP-MS multi-element stock solutions

(10 mg L⁻¹; Perkin Elmer) were used for external calibration of the ICP-TOF-MS and ICP-Q-MS systems. At the Institute for the Dynamics of Environmental Processes (IDPA) in Venice, Italy, where inter-comparison studies with the ICP-SF-MS were conducted, the ultrapure water was produced by coupling a Milli-Q (Millipore, Bedford, MA) water system with a Purelab Ultra system (Elga, High Wycombe, U.K.). Matrix matched calibration was performed at IDPA by spiking different amounts of multi-element standard to a melted surface snow sample. At AWI, all standards were acidified to pH 1 with sub-boiled HNO₃ (distilled 65% HNO₃, pro analysis, Merck) and they were spiked with 1 µg L⁻¹ Rh (RhCl₃, Merck) as internal standard. Eppendorf pipettes with polypropylene (PP) tips were used for sample and standard preparation. Steps for standard preparation were carried out under a clean bench US Class 100 installed in a clean room US class 10000. At AWI, all labware to which samples and standards were exposed were run through a special cleaning procedure (see supplementary material). The cleaning procedure performed at IDPA is described elsewhere [1].

Sample collection and preparation

Reference material

Two reference materials were used to validate the quality of the ICP-TOF-MS as well as the ICP-Q-MS measurements: 1) SPS-SW1: Spectrapure Standards AS, Reference Material for measurements of Elements in Surface Waters, 2) SLRS-4: National Research Council Canada, River Water Reference Materials for Trace Metals.

For applicability to the low REE concentrations expected in Antarctic ice the SPS-SW1 standard was diluted by 1:100. REE from La to Nd in SLRS-4 were determined using a 1:10 dilution, while all other REE were determined without any dilution.

Antarctic Ice Core samples

Within the EPICA two deep ice cores were drilled. One at Kohnen station in Dronning Maud Land (DML) and one at Dome C station (DC). Nine samples from the EPICA-DML (EDML) ice core and eleven samples from EPICA-DC (EDC) were chosen for REE analysis. Sample ages from 14.2 kyr before present (b.p., where present is defined as 1950) to 48.7 kyr b.p. [24-25], i.e. all samples originate from the ultimate glacial period. For each sample a section from the inner part of the ice core was obtained for REE determinations to avoid contamination by the drilling fluid (see supplementary material).

At AWI, samples were melted and transferred into pre-cleaned polyfluor alkoxy (PFA) vessels under a clean bench US Class 100 installed in a clean room laboratory US Class 10000. The polystyrene (PS)-vials used for sample storage were rinsed with 10 mL sub-boiled HNO₃ (1 Mol L⁻¹) which was added into the PFA vessels. Samples were concentrated to 0.5 to 2 mL with a pressure digestion system (Druckaufschlusssystem DAS, Picotrace GmbH, Germany; Figure S2, left side) and digested using 2 mL sub-boiled HNO₃ (distilled 65%, p.a., Merck), 1 mL sub-boiled HF (40%, suprapure,

Merck) and 2 mL H₂O₂ (30%, suprapure, Merck) with the same DAS system by changing the top part (Figure S2, right side). Subsequently, samples were concentrated to a maximum volume of 1.75 mL. Detailed information about the concentration and digestion of samples is given as supplementary material (Figure S2, Table S1). Finally, samples were transferred into polypropylene (PP) vials, Rh was added (1 µg L⁻¹) and the vials were filled up to a volume of 2 mL with sub-boiled HNO₃ (1 Mol L⁻¹). On average, samples were concentrated by a factor of 4. Using these 2 mL samples, REE determinations by ICP-TOF-MS, ICP-Q-MS and ICP-SF-MS were accomplished. Ten blanks (2 mL sub-boiled HNO₃, 1 mL HF and 2 mL H₂O₂) were processed in the same way to test the digestion quality.

Instrumentation

The analytical measurements were conducted at AWI by ICP-TOF-MS (Analytik Jena, Jena, Germany) and ICP-Q-MS (Elan 6000, Perkin Elmer/Sciex, Waltham, Massachusetts). Analyses by ICP-SF-MS (Element2, Thermo Finnigan, Bremen, Germany) were performed at IDPA. The experimental setup for the ICP-TOF-MS is shown elsewhere [12]. The ICP-TOF-MS and the ICP-Q-MS were situated in clean room laboratories, US Class 10000; the ICP-SF-MS is equipped with a US Class 100 clean bench as a clean sample introduction area.

To minimize spectral interference and oxide-formation, microflow nebulization systems with desolvating units were used (Aridus II (for ICP-TOF-MS), MCN6000 (for ICP-Q-MS), Aridus I (for ICP-SF-MS); all: Cetac Technologies, Omaha, Nebraska). These three systems were equipped with a 100 µL min⁻¹ PFA nebulizer, a heated PFA spray chamber, and a heated microporous PTFE membrane. Besides reducing the oxide formation, the signal intensities increased by a factor of ~10 when compared to analysis with cross flow nebulization for ICP-TOF-MS and ICP-Q-MS and by a factor of ~5 for ICP-SF-MS. The instrument settings (Table 1) and the oxide-forming rates of all systems were optimized daily by tuning with a Ce solution.

The main difference between the three sample introduction systems consists in the installation of the spray chamber with respect to the installation of the membrane. Due to vertically installation of the spray chamber in the MCN6000 and slightly downward tilted position in the Aridus I system, larger droplets might pass towards the membrane leading to less stable signals, when the sample flow is not adjusted carefully. In contrast, the spray chamber is slightly upward tilted in the Aridus II system to disable larger droplets to pass towards the membrane, leading to more stable signals. Moreover, in the Aridus II system the nebulizer and spray chamber are shielded to reduce electrostatic effects. Even if different sample introduction systems were used it was expected that only the relative standard deviation (RSD) of replicate analysis was influenced.

Table 1: Instrument settings and measurement parameters for the ICP-TOF-MS, ICP-Q-MS and ICP-SF-MS systems and desolvation units.

	Analytik Jena ICP-TOF-MS	Perkin Elmer/Sciex Elan6000	Thermo Finnigan, Element2
<i>ICP-MS</i>			
RF Power (W)	1050	1350	1250
Plasma gas (L min ⁻¹)	14.5	15	15.5
Auxiliary gas (L min ⁻¹)	1.4	0.8	1.8
Nebulizer gas (L min ⁻¹)	0.98	0.62	0.8-1.1
resolution adopted (m Δm^{-1})	620	350	~400
<i>Nebulizer (with desolvatisation)</i>			
	Aridus II	MCN 6000	Aridus I
Sweep gas (L min ⁻¹)	4.6 - 5.0	2.35	3.40-4.15
Nitrogen (mL min ⁻¹)	21 - 22	12	1 - 18
T (spray chamber) (°C)	110	110	95
T (desolvating unit) (°C)	160	160	175
Sample uptake ($\mu\text{L min}^{-1}$)	130	100	100
<i>Data acquisition</i>			
	from mass		
Isotopes analysed	7 to 238	40	19
Replicates	6	3	40
Integration time (s)	7	0.1 (each isotope)	0.01 (each isotope)
Sweeps	175000	20	30
Measuring time per sample (min)	1.5	7	8
Oxides (%)	0.2 - 0.5	0.03	0.2
Double charged ions (%)	14 - 15	5 - 7	3
<i>miscellaneous</i>			
analyzing mode	simultaneous	sequential	sequential
dynamic range	4	9	9
background cps (REE)	0.5 - 1	3 - 30	0.2
sensitivity 1 $\mu\text{g L}^{-1}$ Indium (cps)	23000	83000	~ 3x10 ⁶
RSD for Nd (%) (conc. 4-50 ng L ⁻¹)	3.2	11.5	7.1
TOF: n=6; Q: n=3; SF: n=40			
IDL of REE (ng L ⁻¹)	0.3 - 1	1 - 3	0.001 - 0.03

Results and discussion

Performance of the ICP-TOF-MS system

To counteract sensitivity drifts, three calibrations were run every day. The linearity of calibration curves was checked by analysing standards at the end of an analysis cycle. Linearity was ascertained from 1 ng L⁻¹ to 5 $\mu\text{g L}^{-1}$. Seven calibration standards ranging from 1 ng L⁻¹ to 500 ng L⁻¹ were analysed ten times per calibration. The calibration range was chosen according to the concentrations expected in the Antarctic ice samples. Table 2 shows averaged calibration data from five calibrations over two days.

Using the Aridus II as the sample introduction system the sensitivity of the tuned ICP-TOF-MS system ranged between 16000 and 32000 counts per second (cps) and $\mu\text{g L}^{-1}$ depending on the REE (see slope in Table 2), which corresponds to 242 cps and 485 cps ng⁻¹ at a sample consumption of 15.2 μL per replicate analysis (175000 Sweeps). A low calibration intercept was obtained for all REE (-121 cps to 92 cps). Generally the standard deviation (SD) for the intercept was high due to counting statistics which decrease with decreasing element concentrations. The resulting correlation coefficients for REE are higher than 0.9980. No IDL was higher than 1 ng L⁻¹ (3 σ criterion of the

blank). For ice samples analyses all signals were first normalized to the internal standard and afterwards the normalized blank value was subtracted.

Table 2: ICP-TOF-MS calibration data for the investigations of intercomparison samples. Values were calculated on the basis of 5 different calibrations. Each standard was analysed 10 times per calibration. The slope with its SD in cps (ng L^{-1})⁻¹, the intercept with its SD in cps, the blank and 50 ng L^{-1} signal with their SD in cps, the correlation coefficient (r^2) and the instrumental detection limit (IDL) in ng L^{-1} are given. Additionally REE concentrations of digested blank samples (in ng L^{-1}) are shown. For calculating element concentration in samples, calibration signals were first normalized to ¹⁰³Rh and afterwards the normalized blank signals were subtracted.

	No. of data points	slope \pm SD (cps ($\mu\text{g L}^{-1}$) ⁻¹)	intercept \pm SD (cps)	blank \pm SD (cps)	50 ng L^{-1} \pm SD (cps)	r^2	IDL (ng L^{-1})	conc. digested blank samples (ng L^{-1})
La	6	27948 \pm 1087	5 \pm 19	31 \pm 6	1363 \pm 101	0.9988	0.6	0.9 \pm 0.03
Ce	7	30553 \pm 2294	-121 \pm 47	38 \pm 9	1260 \pm 122	0.9989	0.6	3.4 \pm 0.1
Pr	6	31525 \pm 1277	0 \pm 24	24 \pm 6	1542 \pm 137	0.9989	0.5	0.7 \pm 0.01
Nd	5	27248 \pm 1425	92 \pm 18	103 \pm 12	1462 \pm 106	0.9980	0.8	1.9 \pm 0.1
Sm	6	16958 \pm 987	56 \pm 10	61 \pm 7	892 \pm 69	0.9987	0.9	0.4 \pm 0.04
Eu	5	29882 \pm 1632	38 \pm 13	46 \pm 7	1539 \pm 126	0.9985	0.5	0.1 \pm 0.01
Gd	5	21286 \pm 955	70 \pm 13	78 \pm 8	1140 \pm 71	0.9984	0.7	0.5 \pm 0.03
Tb	6	31998 \pm 737	-3 \pm 21	25 \pm 4	1544 \pm 102	0.9988	0.3	0.1 \pm 0.01
Dy	5	21299 \pm 1222	53 \pm 11	59 \pm 7	1122 \pm 80	0.9987	0.7	0.7 \pm 0.01
Ho	5	28628 \pm 1585	13 \pm 11	23 \pm 4	1449 \pm 100	0.9986	0.3	0.1 \pm 0.01
Er	5	16880 \pm 1152	32 \pm 6	37 \pm 5	881 \pm 70	0.9988	0.7	0.3 \pm 0.02
Tm	5	28658 \pm 1794	15 \pm 10	23 \pm 4	1455 \pm 112	0.9988	0.3	0.1 \pm 0.01
Yb	5	23954 \pm 1343	70 \pm 14	77 \pm 7	1271 \pm 92	0.9984	0.7	0.6 \pm 0.04
Lu	6	27593 \pm 1240	5 \pm 16	24 \pm 4	1348 \pm 102	0.9992	0.4	0.2 \pm 0.00
Rh*				12572 \pm 719	12926 \pm 810			

* unit: cps ($\mu\text{g L}^{-1}$)⁻¹

Accuracy and Precision of the ICP-TOF-MS and ICP-Q-MS

Two reference materials, SPS-SW1 and SLRS-4, were analysed. Certified REE concentrations are only available for SPS-SW1, each concentration amount being 500 ng L^{-1} . Table 3 summarizes all REE concentrations obtained by ICP-TOF-MS and ICP-Q-MS, the certified values for SPS-SW1 as well as the literature data available for SLRS-4 [26]. For SPS-SW1 the concentrations found do not differ significantly from the certified values except for La, Ce, and Dy. Both MS systems showed distinct differences for Dy to the certified values. The concentrations for La and Ce obtained by ICP-TOF-MS were also significantly increased for SLRS-4. For ICP-TOF-MS analysis it was noted that Ba concentrations exceeding 1 $\mu\text{g L}^{-1}$ (~18000 cps) affect the determination of La and Ce. SPS-SW1 contains 50 $\mu\text{g L}^{-1}$ of Ba or, in a 1:100 dilution, only 0.5 $\mu\text{g L}^{-1}$. The influence of this high Ba content should be clarified in further investigations. SLRS-4 contains 12.2 $\mu\text{g L}^{-1}$ of Ba (1.22 $\mu\text{g L}^{-1}$ in a 1:10 dilution) and La and Ce analysis are also influenced although not as severely as in SPS-SW1. In general, REE concentrations of SLRS-4 obtained by ICP-TOF-MS, ICP-Q-MS and literature data [26] agree well. In most cases, no significant differences were estimated at the 99% level of confidence. The RSD of 10 replicate analyses were similar for the two MS systems. Median values were 3.5% for ICP-TOF-MS analysis (e.g. Ce: 3.4%, Gd: 2.8%, Yb: 5.8) and 2.5% for ICP-Q-MS analysis (e.g. Ce: 1.3%, Gd: 4.7%, Yb: 4.2%) in a concentration range of 2 ng L^{-1} to 60 ng L^{-1} .

Table 3: REE concentrations in ng L^{-1} with SD (10 replicate measurements) in reference materials SPS-SW1 and SLRS-4 obtained by ICP-TOF-MS and ICP-Q-MS. Recovery rates in % for reference material SPS-SW1 are shown in brackets below the concentrations obtained by ICP-TOF-MS and ICP-Q-MS. Concentrations of reference materials SPS-SW1 were derived by analysing a 1:100 dilution. REE from La to Nd in SLRS-4 were analysed out of a 1:10 dilution, all other REE were analysed without any dilution.

	certified	SPS-SW1 (ng L^{-1})		SLRS-4 (ng L^{-1})		reference [26]
		ICP-TOF-MS (recovery rate (%))	ICP-Q-MS	ICP-TOF-MS	ICP-Q-MS	
La	500 ± 10	586 ± 10 (117.3)	495 ± 16 (98.9)	304 ± 4	278 ± 4	287 ± 7
Ce	500 ± 10	581 ± 22 (116.1)	516 ± 10 (103.3)	411 ± 12	361 ± 2	360 ± 11
Pr	500 ± 10	516 ± 17 (103.2)	510 ± 8 (101.9)	77 ± 1	67 ± 2	69 ± 2
Nd	500 ± 10	505 ± 37 (101.1)	510 ± 8 (102.0)	260 ± 10	262 ± 10	269 ± 13
Sm	500 ± 10	497 ± 17 (99.4)	497 ± 1 (99.4)	64 ± 2	57 ± 3	57 ± 2
Eu	500 ± 10	497 ± 14 (99.4)	510 ± 8 (102.1)	12 ± 0.3	11 ± 1	8 ± 0.5
Gd	500 ± 10	490 ± 10 (98.0)	513 ± 8 (102.6)	37 ± 1	40 ± 3	34 ± 2
Tb	500 ± 10	482 ± 13 (96.3)	506 ± 6 (101.1)	4 ± 0.2	5 ± 0.4	4 ± 0.3
Dy	500 ± 10	603 ± 5 (120.7)	852 ± 21 (170.4)	22 ± 1.9	24 ± 0.4	24 ± 1.4
Ho	500 ± 10	486 ± 17 (97.3)	519 ± 13 (103.8)	5 ± 0.2	4 ± 0.5	5 ± 0.3
Er	500 ± 10	461 ± 36 (92.2)	498 ± 5 (99.6)	12 ± 0.4	16 ± 0.9	13 ± 0.5
Tm	500 ± 10	490 ± 20 (98.0)	510 ± 5 (102.0)	2 ± 0.1	2 ± 0.3	2 ± 0.1
Yb	500 ± 10	503 ± 28 (100.7)	503 ± 16 (100.6)	11 ± 0.7	11 ± 0.6	12 ± 0.3
Lu	500 ± 10	490 ± 22 (98.1)	517 ± 3 (103.3)	3 ± 0.1	2 ± 0.2	2 ± 0.1

Interference studies

To reduce problems with spectral interferences in ICP-TOF-MS, for REE mainly represented by oxides, the described desolvation unit was used. Additionally, equations were compiled to calculate the residual fractions of the interfering species. Equation 1, for example, can be used to correct isobaric interferences of ^{142}Nd by ^{142}Ce , while the correction of the ^{155}Gd signal in equation 2, is shown as an example for the correction of the spectral interferences:

$$^{142}\text{Nd}_{\text{corr}} = ^{142}\text{Nd} - \frac{11.08}{88.48} \cdot ^{140}\text{Ce} \quad (1)$$

$$^{155}\text{Gd}_{\text{corr}} = ^{155}\text{Gd} - 0.9967 \cdot ^{139}\text{La} \cdot \text{MO}^+ \quad (2)$$

Isobaric interferences are present for isotopes such as ^{142}Nd (^{142}Ce , 11.08%), ^{144}Nd (^{144}Sm , 3.1%) and ^{164}Dy (^{164}Er , 1.61%). Corrections due to oxide formation must be applied (equation 2) for isotopes exceeding a mass of 154. Tests showed in fact that BaO^+ species are not present and therefore oxide corrections for masses between 146 and 154 can be neglected. Table S2 shows the analysed isotopes with their natural abundances and potential interfering species. When possible, several isotopes of one element were determined to check the efficacy of the corrections. The very good agreement among concentrations obtained by two or more different isotopes suggests

that isobaric and spectral interferences were successfully corrected or rendered negligible.

Ba concentrations exceeding $1 \mu\text{g L}^{-1}$ lead to high background signals (10 cps; usually 0.5 – 1 cps) in the ICP-TOF-MS for mass 139 (La) and 140 (Ce). Therefore, in the majority of cases, La and Ce concentrations were obtained from the diluted samples. Successfully tested equations are integrated within the evaluation system of the ICP-Q-MS systems. REE interference studies of the ICP-SF-MS system used at IDPA are reported in [1].

Long term stability of the ICP-TOF-MS

Two hundred measurements, each with 7 s integration time and 5.4 s relaxation time amounting to a total of 41.3 minutes, have been conducted for long term stability tests of the ICP-TOF-MS system. Several standards were tested and showed very good long term stability. For example, the RSD of Er, the REE with the lowest signal sensitivity, was: 12.9% for a blank standard (37 cps), 11.7% for a 1 ng L^{-1} standard (52 cps), 5.9% for a 10 ng L^{-1} standard (180 cps), 3.4% for a $0.1 \mu\text{g L}^{-1}$ standard (1675 cps), 1.0% for a $0.5 \mu\text{g L}^{-1}$ standard (9450 cps) and 0.8% for a $1 \mu\text{g L}^{-1}$ standard (20230 cps). This is in a good agreement with data obtained by coupling the Aridus II to a Quadrupole ICP-MS system [27].

Concentrations in Antarctic ice core samples

An inter-comparison exercise between three different ICP-MS systems was carried out to illustrate the performance of the ICP-TOF-MS. Figure 1 shows correlation diagrams for REE concentrations obtained by the three different MS systems. For the linear fit function the uncertainties linked to each REE concentration were taken as weighting parameters ($error = SD/\sqrt{n}$, n = number of replicate analysis). The intercept was assumed to be zero. Table S3 lists all concentration data. All concentrations of Antarctic samples were calculated accounting for concentration after digestion (on average a factor of 4) and after subtracting blank.

In general SDs obtained by ICP-Q-MS were much higher compared to the other two MS systems. However, ICP-Q-MS data agreed very well with ICP-SF-MS results. ICP-TOF-MS data were on average slightly higher than concentrations obtained by ICP-Q-MS and on average slightly lower when compared to ICP-SF-MS. Diagrams illustrating ICP-TOF-MS data show on average stronger deviation from the linear fit curve at lower concentrations than the correlation diagrams comparing ICP-SF-MS and ICP-Q-MS data.

For interpretation of correlation diagrams the concentration factor has to be taken into account. Concentrations analysed were about a factor of four higher than concentrations shown in Figure 1 and Table S3. Calculated concentrations range between 0.6 to 260 ng L^{-1} for light REE (LREE: La – Sm) and between 0.08 to 35 ng L^{-1} for heavy REE (HREE: Eu – Lu). Concentrations of glacial samples from the EDC ice core samples analysed previously [1] agree very well with data obtained in this study.

The lowest La concentrations analysed in this study amount to 30 ng L^{-1} (Figure 1A). La concentrations below 40 ng L^{-1} showed strong deviation from the linear fit function in the correlation diagrams illustrating ICP-TOF-MS data. La concentrations obtained by the ICP-TOF-MS system for EDML samples from 904 m, 953 m and 1202 m depth and the EDC sample from 460.9 m depth were higher than for the other systems, whereas lower concentrations were obtained for one EDML sample (1403 m depth) and one EDC sample (411.4 m depth). La concentrations differed from each other for the EDML sample from 1102 m depth for all MS systems. In general, Eu concentrations obtained by ICP-TOF-MS measurements seem to be overestimated, as shown by low slope values ($m < 0.7$, Figure 1 F). The ICP-TOF-MS system yielded values of Pr, Nd, Sm and Eu which were a factor of 2 higher for the EDC sample from 405.9 m depth and a factor of 2 up to 10 higher for Sm, Eu, Gd and Tb for the EDC sample from 422.4 m depth. Concentrations obtained by the ICP-Q-MS system were higher by a factor of 2 up to 3 for the EDML sample from 1302 m depth and shows higher values for all elements for the EDC samples from 442.2 m and 451.6 m depth. Higher concentrations were found by ICP-SF-MS for the EDML sample from 1102 m depth.

The Student T-Test was used to compare REE concentrations for all 20 samples (99% significance level). Comparison of ICP-TOF-MS concentrations with ICP-Q-MS concentrations showed that most of the calculated REE concentrations were not significantly different. However, the conformity between the ICP-Q-MS and ICP-SF-MS systems is better than between the ICP-TOF-MS and ICP-SF-MS systems. The reason for these differences might be that Ba concentrations influence the ICP-TOF-MS determination of La and Ce and that very low HREE concentrations were analysed.

All REE concentrations shown in Figure 1 and Table S3 were about a factor of 5 up to 90 higher than in the digested blank samples. For Antarctic ice core samples the results from the ICP-TOF-MS system were similar to those of the ICP-Q-MS and ICP-SF-MS for concentration levels down to: La: 40 ng L^{-1} , Ce: 40 ng L^{-1} , Pr: 7 ng L^{-1} , Nd: 20 ng L^{-1} , Sm: 4 ng L^{-1} , Gd: 3 ng L^{-1} , Tb: 1 ng L^{-1} , Dy: 3 ng L^{-1} , Ho: 1.5 ng L^{-1} , Er: 2 ng L^{-1} , Tm: 0.8 ng L^{-1} , Yb: 2 ng L^{-1} and Lu 0.5 ng L^{-1} . Eu concentrations obtained by the ICP-TOF-MS system deviated systematically from concentrations obtained by the other systems.

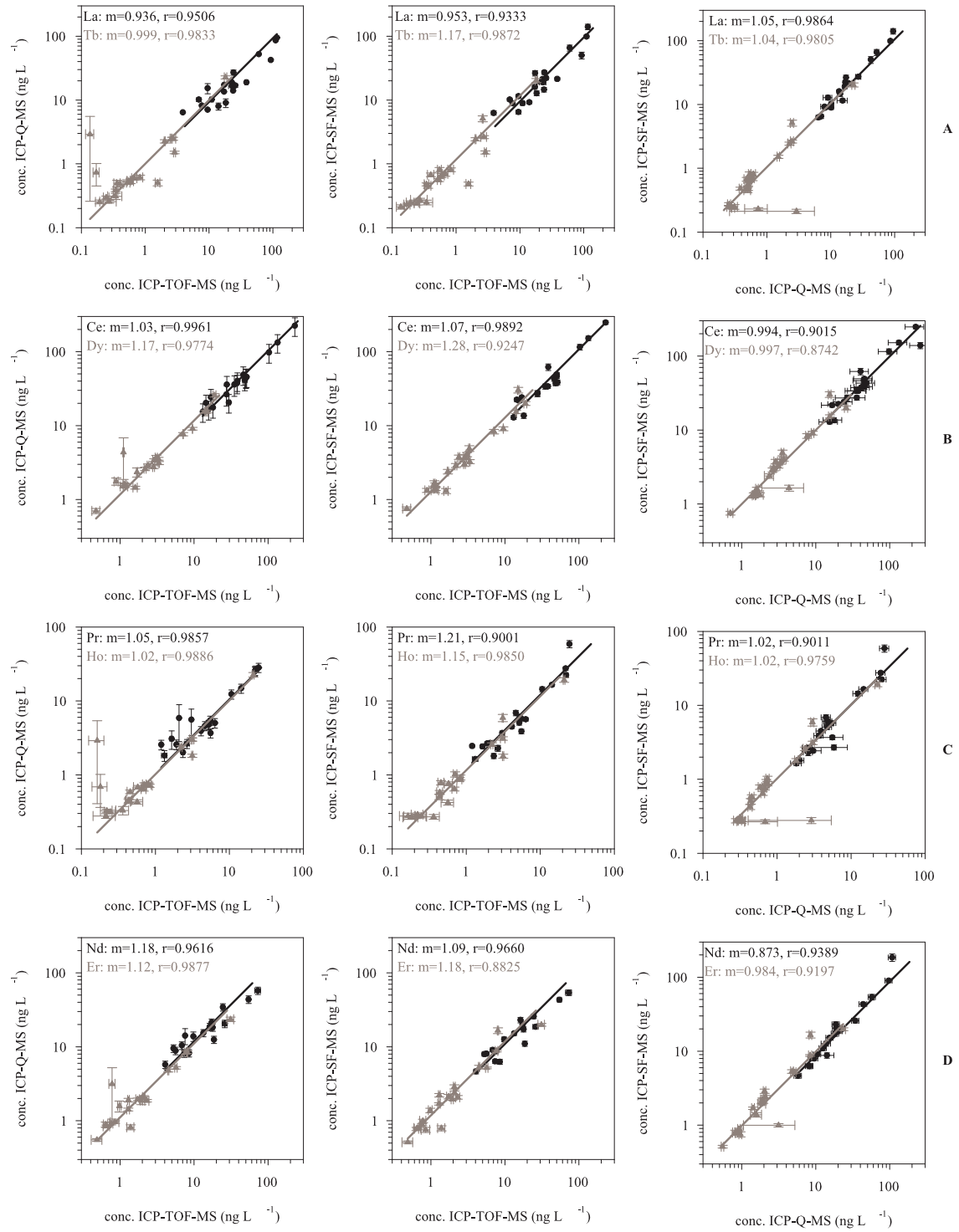


Figure 1: REE concentrations with SD in ng L⁻¹ in Antarctic ice core samples plotted as ICP-Q-MS concentrations vs. ICP-TOF-MS concentrations, ICP-SF-MS concentrations vs. ICP-TOF-MS concentrations and ICP-SF-MS concentrations vs. ICP-Q-MS concentrations with associated parameters for a linear fit ($y=m \cdot x$, Assumption: intercept=0). Errors of each measurement were taken as weighting parameters ($error = SD / \sqrt{n}$, $n = replicate\ analysis$).

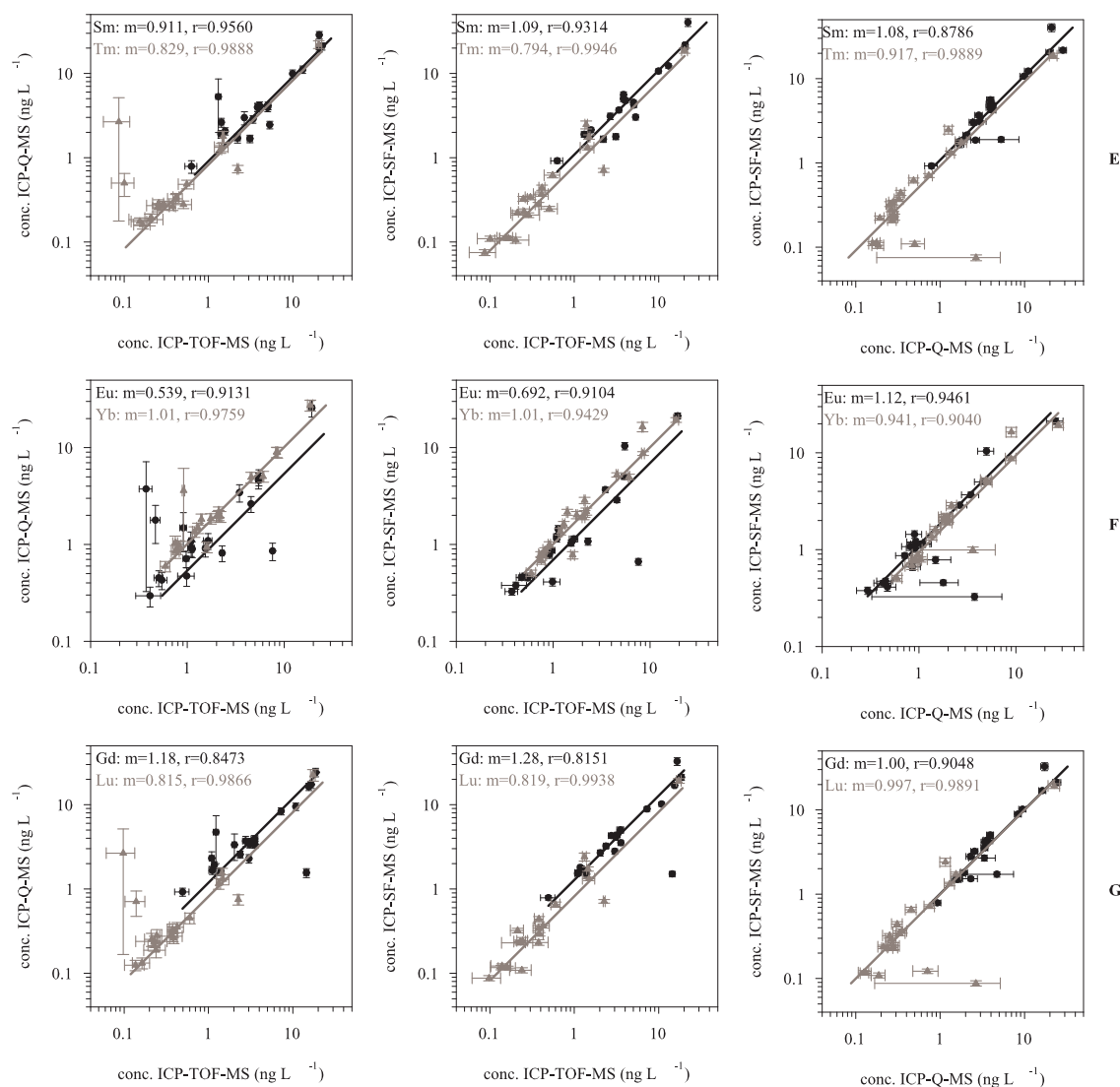


Figure 1: continued

Comparison of ICP-MS systems

Table 1 shows the most important parameters for the ICP-TOF-MS, ICP-Q-MS and ICP-SF-MS systems used in this study. The simultaneous analysing mode of the ICP-TOF-MS leads to several advantages including (i) no limitation on the number of analysed isotopes and (ii) its analysis time when compared to other ICP-MS techniques. While the ICP-TOF-MS system needs 1.5 minutes per sample to analyse the mass range from ${}^7\text{Li}$ to ${}^{238}\text{U}$ (6-fold analysis, 175000 sweeps), the ICP-Q-MS needs 7 minutes for 40 isotopes (3-fold analysis, 20 sweeps) and the ICP-SF-MS needs 8 minutes for 19 isotopes (40-fold analysis, 30 sweeps). Hence the ICP-TOF-MS system requires the lowest sample consumption. However, for the ICP-SF-MS system background signals below 0.2 cps and high sensitivity lead to very low IDL ($0.001 - 0.03 \text{ ng L}^{-1}$). The signal to noise ratio for ICP-TOF-MS and ICP-Q-MS is much lower (31000 and 4900, respectively), consequently higher IDL are observed ($0.3 - 1 \text{ ng L}^{-1}$; $1 - 3 \text{ ng L}^{-1}$).

Conclusions

REE analysis of standard reference materials showed that the ICP-TOF-MS system is best suited for the determination of trace elements with concentrations up to 500 ng L⁻¹. The accuracy and precision found for the reference standard SPS-SW1 are very good. The study of reference materials and inter-comparison exercise between ICP-TOF-MS (Analytik Jena AG), ICP-Q-MS (Elan6000 PerkinElmer/Sciex) and ICP-SF-MS (Element 2, Thermo Finnigan) systems showed that the ICP-TOF-MS system determines accurately and precisely REE concentrations exceeding 5 ng L⁻¹ and that the accuracy and precision between 0.5 and 5 ng L⁻¹ is element dependent. The data indicate that the ICP part of the system is not ideal. It is therefore expected that with improved plasma conditions the ICP-TOF-MS technique may become a very attractive alternative to the ICP-Q-MS and ICP-SF-MS techniques. In general, the expected REE concentrations and the available sample volume can define the kind of ICP-MS to be chosen for analysis. The ICP-SF-MS is the most sensitive method for REE determination and therefore it is recommended when the concentration range is unknown or the sample amount is very small. However, in practical analysis the IDL, resolution on interferences, sample throughput, sample consumption, analytical stability and cost are also important parameters which influence the choice of the ICP-MS system.

Acknowledgement

This work is a contribution to the European Project for Ice Coring in Antarctica (EPICA), a joint European Science Foundation/European Commission scientific programme, funded by the EU and by national contributions from Belgium, Denmark, France, Germany, Italy, the Netherlands, Norway, Sweden, Switzerland and the United Kingdom. The main logistical support was provided by IPEV and PNRA (at Dome C) and AWI (at Dronning Maud Land). This is EPICA publication 200. Special thanks to J-R. Petit, B. Delmonte, M. Bigler and F. Lambert for sample preparation (Antarctic ice cores). The authors would like to thank G. Schlemmer, E. Thamm (both Analytik Jena), F. Wilhelms, J. Schwarz (both AWI) and C. Lüdke for discussion and comments that improved the manuscript. We thank the two anonymous reviewers for constructive criticism.

Supplementary Material

In the supplementary material information about the cleaning procedure of labware at AWI, the EPICA ice core samples and the separation of the samples used for ICP-MS analysis from the inner part of the ice cores are provided. The concentration and digestion of Antarctic ice core samples is shown in Figure S1 and Table S1. Table S2 shows the determined REE isotopes with natural abundances and potential interference species, which are taken into account for evaluating ICP-TOF-MS data. Table S3 lists

all concentration data, with SD, of Antarctic ice core samples obtained by ICP-TOF-MS, ICP-Q-MS and ICP-SF-MS analysis.

Reference

- [1] P. Gabrielli, C. Barbante, C. Turetta, A. Marteel, C. Boutron, G. Cozzi, W. Cairns, C. Ferrari, P. Cescon, *Anal. Chem.*, 78 (2006) 1883.
- [2] G. Tao, R. Yamada, Y. Fujikawa, A. Kudo, J. Zheng, D.A. Fisher, R.M. Koerner, *Talanta*, 55 (2001) 765.
- [3] P.P. Mahoney, S.J. Ray, G.M. Hieftje, *Focal Point*, 51 (1) (1997) 16A.
- [4] K. Benkhedda, H.G. Infante, F.C. Adams, *Anal. Chim. Acta*, 506 (2004) 137.
- [5] X. Tian, H. Emteborg., M. Barbaste, F.C. Adams, *JAAS*, 15 (2000) 829.
- [6] M.V. Peláez, J.M. Costa-Fernández, A. Sanz-Medel, *JAAS*, 17 (2002) 950.
- [7] E. Hoffmann, C. Lüdke, J. Skole, H. Stephanowitz, J. Wollbrandt, W. Becker, *Spectrochim. Acta Part B*, 57 (10) (2002) 1535.
- [8] C. Lüdke, J. Skole, K. Taubner, M. Kriews, *Spectrochim. Acta Part B*, 60 (11) (2005) 1412.
- [9] M. Balcerzak, *Anal. Sci.*, 19 (2003) 979.
- [10] N.H. Bings, J.M. Costa-Fernandez, J.P. Guzowski, A.M. Leach, G.M. Hieftje, *Spectrochim. Acta Part B*, 55 (7) (2000) 767.
- [11] N.H. Bings, *Nachrichten aus der Chemie*, 49(9) (2001) 1069.
- [12] E. Hoffmann, C. Lüdke, *Spectrosc. Eur.*, 17 (No.1) (2005) 20.
- [13] X. Tian, H. Emteborg, F.C. Adams, *JAAS*, 14 (1999) 1807.
- [14] R.E. Sturgeon, J.W.H. Lam, A. Saint, *JAAS*, 15 (2000) 607.
- [15] K. Benkhedda, H.G. Infante, F.C. Adams, *Trends in analytical Chemistry*, 21 (5) (2002) 332.
- [16] S.N. Willie, R.E. Sturgeon, *Spectrochim. Acta*, **56B** (2001) 1707.
- [17] M. Revel-Rolland, P. De Deckker, B. Delmonte, P.P. Hesse, J.W. Magee, I. Basile-Doelsch, F. Grousset, D. Bosch, *EPSL*, 249 (2006) 1.
- [18] M. Legrand, P. Mayewski, *Rev. Geophys.*, 35 (1997) 219.
- [19] E. Wolff, H. Fischer, F. Fundel, U. Ruth, B. Twarloh, G.C. Littot, R. Mulvaney, R. Röthlisberger, M. de Angelis, C.F. Boutron, M. Hansson, U. Jonsell, M.A. Hutterli, F. Lambert, P. Kaufmann, B. Stauffer, T.F. Stocker, J.P. Steffensen, M. Bigler, M.L. Siggaard-Andersen, R. Udisti, S. Becagli, E. Castellano, M. Severi, D. Wagenbach, C. Barbante, P. Gabrielli, V. Gaspari, *Nature*, 440 (2006) 491.

- [20] I. Basile, F.E. Grousset, M. Revel, J.R. Petit, P.E. Biscaye, N.I. Barkov, EPSL, 146 (1996) 573.
- [21] S. Hong, J.P. Candelone, C. Turetta, C.F. Boutron, EPSL, 143 (1996) 233.
- [22] EPICA Community Members, Nature, 444 (2006) 195.
- [23] EPICA Community Members, Nature, 429 (2004) 623.
- [24] U. Ruth, J.M. Barnola, J. Beer, M. Bigler, T. Blunier, E. Castellano, H. Fischer, F. Fundel, P. Huybrechts, P. Kaufmann, S. Kipfstuhl, A. Lambrecht, A. Morganti, H. Oerter, F. Parrenin, O. Rybak, M. Severi, R. Udisti, F. Wilhelms, E. Wolff, Clim. Past, 3 (2007) 475.
- [25] L. Augustin, J. Jouzel, PANGAEA, doi:10.1594/PANGAEA.198743, http://store.pangaea.de/Projects/EPICA/EDC_descr.pdf (2004).
- [26] D. Yeghicheyan, J. Carignan, M. Valladon, M. B. Le Coz, F. Le Cornec, M. Castrec-Rouelle, M. Robert, L. Aquilina, E. Aubry, C. Churlaud, A. Dia, S. Deberdt, B. Dupré, R. Freydier, G. Gruau, O. Hénin, A.M. de Kersabiec, J. Macé, L. Marin, N. Morin, P. Petitjean, E. Serrat, Geostand. Geoanal. Res., 25 (2-3) (2001) 465.
- [27] CETAC, http://www.cetac.com/pdfs/Tech%20Note01_Aridus%20II.pdf (08.05.2008).

Supplementary Material

Cleaning procedure of labware performed at the AWI

At AWI, all labware to which samples and standards were exposed were run through a special cleaning procedure

- 1 week treatment with 3% Mucosol solution (Merck) to degrease all labware, followed by rinsing of all parts with ultrapure water
- 1 week treatment with 1:4 diluted HCl (30%, suprapure, Merck), followed by rinsing of all parts with ultrapure water
- 1 week treatment with 1:4 diluted HNO₃ (distilled 65%, p.a., Merck), followed by rinsing of all parts with ultrapure water
- 1 week treatment with 1:10 diluted HNO₃ (65%, suprapure, Merck), followed by rinsing of all parts with ultrapure water
- Drying of all parts in a clean room US Class 10000 under a clean bench, US Class 100
- Packing of all parts in 2 polyethylene (PE) bags for storage

Information on ice core samples and separation of the inner part of the ice core

Within EPICA, a 2774.15 m long ice core (diameter: 98 mm) was drilled in a fluid filled hole at Kohnen station (Dronning Maud Land (DML), location: 75°00'S, 0°04'E). A 3189.45 m long ice core (diameter: 98 mm) was drilled in a fluid filled hole at EPICA Dome C station (location: 75°06'S, 123°21'E) [1–2]. Samples from Kohnen station are called EDML samples and samples from Dome C station are referred to as EDC samples. 9 samples from the EDML ice core and 11 samples from the EDC ice core were chosen for REE analysis. All samples originate from glacial times. Samples from Kohnen station cover the period from 16.6 kyr before present (b.p., where present is defined as 1950) to 48.7 kyr b.p. [3]. The top of the youngest Dome C ice core sample was 14.2 kyr old and the bottom of the oldest ice core was 21.5 kyr old [4].

A section from the inner part of the ice core was available for REE analysis. From the top of each ice-core sample a 30 cm long section was cut using a band saw, stored in a cold room at –20°C at the Laboratoire de Glaciologie et Geophysique de l'Environnement (Grenoble, France) and used for further sample preparation steps. The sample surface was decontaminated in a first step by sawing 1 cm off the surface with a band saw. The 30 cm long section was divided into three 10 cm long parts. Each part was rinsed with 1 to 2 L ultrapure water three times. In consequence of this procedure the weight of each part was reduced by 50%. The three parts of each section were placed in pre-cleaned high density polyethylene (HDPE) bottles and melted at room temperature. Samples were dispersed by pivoting; aliquots were filled in polystyrene (PS) vials and finally stored at -20°C.

Reference

- [1] EPICA Community Members, *Nature*, 444 (2006) 195.
- [2] EPICA Community Members, *Nature*, 429 (2004) 623.
- [3] U. Ruth, J.M. Barnola, J. Beer, M. Bigler, T. Blunier, E. Castellano, H. Fischer, F. Fundel, P. Huybrechts, P. Kaufmann, S. Kipfstuhl, A. Lambrecht, A. Morganti, H. Oerter, F. Parrenin, O. Rybak, M. Severi, R. Udisti, F. Wilhelms, E. Wolff, *Clim. Past*, 3 (2007) 475.
- [4] L. Augustin, J. Jouzel, PANGAEA, doi:10.1594/PANGAEA.198743, http://store.pangaea.de/Projects/EPICA/EDC_desc.pdf (2004).

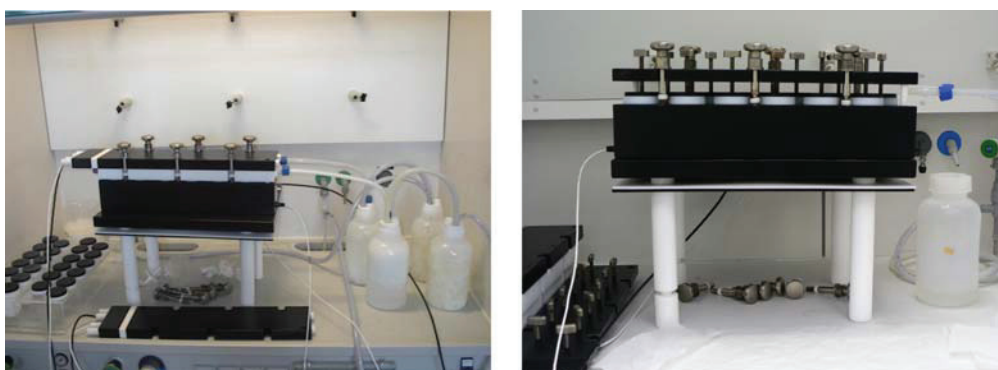


Figure S1: *Left: Experimental setup for concentration of liquid samples before the addition of acids and after acid digestion. Right: Experimental setup for the acid digestion of Antarctic ice core samples.*

Table S1: Digestion programme of Antarctic ice core samples.*Concentration of samples before digestion*

Programme	heating plate	time (hours)	command	Temperature (°C)
concentration	bottom plate	2	heat up to	160
		1.12'	keep constant on	160
	upper plate	1.20'	cool down to	110
		1.30'	keep constant on	110
		1	keep constant on	90

Digestion

(with 2 mL sub-boiled HNO₃ (distilled 65 %, p.a., Merck), 1 mL sub-boiled HF (40 %, suprapure, Merck) and 2 mL H₂O₂ (30 %, suprapure, Merck))

Programme	heating plate	time (hours)	command	Temperature (°C)
digestion	bottom plate	1	heat up to	100
		5	keep constant on	100
		1	heat up to	120
		2	keep constant on	120
		1	heat up to	140
		2	keep constant on	140
		1	heat up to	160
		2	keep constant on	160
		1	heat up to	180
		4	keep constant on	180
		2	heat up to	210
		7	keep constant on	210
		2	keep constant on	170
		2	keep constant on	160
		1.30'	keep constant on	140

Concentration of samples after digestion

Programme	heating plate	time (hours)	command	Temperature (°C)
concentration	bottom plate	2	heat up to	160
		0.32'	keep constant on	160
	upper plate	1.20'	heat up to	110
		1.30'	keep constant on	110
		1	keep constant on	90

Table S2: *Analysed isotopes with natural abundances and potential interference species, which are taken into account for evaluating ICP-TOF-MS data.*

Isotope	Analyte		Potential Interferences	
	Abundance (%)	Species	Abundance (%) ^a	
¹³⁹ La	99.91			
¹⁴⁰ Ce	88.48			
¹⁴¹ Pr	100			
¹⁴² Nd	27.13	¹⁴² Ce	11.08	
¹⁴³ Nd	12.18			
¹⁴⁴ Nd	23.8	¹⁴⁴ Sm	3.1	
¹⁴⁵ Nd	8.3			
¹⁴⁶ Nd	17.19			
¹⁴⁷ Sm	15			
¹⁴⁹ Sm	13.8			
¹⁵² Sm	26.7			
¹⁵¹ Eu	47.8			
¹⁵³ Eu	52.2			
¹⁵⁵ Gd	14.8	¹³⁹ La ¹⁶ O	99.67	
¹⁵⁶ Gd	20.47	¹⁴⁰ Ce ¹⁶ O	88.26	
¹⁵⁷ Gd	15.65	¹⁴¹ Pr ¹⁶ O	99.76	
¹⁵⁸ Gd	24.84	¹⁴² Nd ¹⁶ O	27.09	
		¹⁴² Ce ¹⁶ O	11.05	
¹⁵⁹ Tb	100	¹⁴³ Nd ¹⁶ O	12.15	
¹⁶¹ Dy	18.9	¹⁴⁵ Nd ¹⁶ O	8.28	
¹⁶³ Dy	24.9	¹⁴⁷ Sm ¹⁶ O	14.96	
¹⁶⁴ Dy	28.2	¹⁴⁸ Sm ¹⁶ O	11.27	
		¹⁴⁸ Nd ¹⁶ O	5.75	
		¹⁶⁴ Er	1.61	
¹⁶⁵ Ho	100	¹⁴⁹ Sm ¹⁶ O	13.77	
¹⁶⁶ Er	33.6	¹⁵⁰ Nd ¹⁶ O	5.63	
¹⁶⁷ Er	22.95	¹⁵¹ Eu ¹⁶ O	47.69	
¹⁶⁸ Er	26.8	¹⁵² Sm ¹⁶ O	26.64	
¹⁶⁹ Tm	100	¹⁵³ Eu ¹⁶ O	52.07	
¹⁷¹ Yb	14.3	¹⁵⁵ Gd ¹⁶ O	14.76	
¹⁷² Yb	21.9	¹⁵⁶ Gd ¹⁶ O	20.42	
¹⁷³ Yb	16.12	¹⁵⁷ Gd ¹⁶ O	15.61	
¹⁷⁴ Yb	31.8	¹⁵⁸ Gd ¹⁶ O	24.78	
¹⁷⁵ Lu	100	¹⁵⁹ Tb ¹⁶ O	99.76	

^a For polyatomic species calculated as the product of the natural abundance of each isotope divided by 100.

Table S3: REE concentrations with SD in ng L⁻¹ of molten EDML and EDC ice core samples analysed by ICP-TOF-MS, ICP-Q-MS and ICP-SF-MS as shown in Figure 1. Attention: Values shown in this table represent concentrations after applying the concentration factor of about 4 and subtracting blank concentrations. Concentrations exceeding the calibration limits are not listed.

EDML depth * (m)	age [23] (kyr b.p.)	La ± SD	Ce ± SD	Pr ± SD	Nd ± SD	Sm ± SD	Eu ± SD	Gd ± SD	Tb ± SD	Dy ± SD	Ho ± SD	Er ± SD	Tm ± SD	Yb ± SD	Lu ± SD
872	TOF	7.7 ± 0.1	14.5 ± 0.2	1.2 ± 0.0	5.6 ± 0.2	1.4 ± 0.1	0.5 ± 0.1	1.1 ± 0.1	0.2 ± 0.02	1.2 ± 0.1	0.2 ± 0.04	0.7 ± 0.1	0.2 ± 0.04	0.8 ± 0.1	0.2 ± 0.04
	Q	8.2 ± 0.2	20.2 ± 5.7	2.6 ± 0.4	8.8 ± 1.0	1.9 ± 0.2	0.4 ± 0.1	1.7 ± 0.2	0.3 ± 0.02	1.6 ± 0.1	0.3 ± 0.02	0.8 ± 0.03	0.2 ± 0.02	0.9 ± 0.1	0.1 ± 0.02
904	SF	8.9 ± 0.5	22.4 ± 1.2	2.5 ± 0.1	8.1 ± 0.4	1.9 ± 0.1	0.5 ± 0.03	1.6 ± 0.1	0.2 ± 0.01	1.4 ± 0.1	0.3 ± 0.01	0.8 ± 0.02	0.1 ± 0.01	0.8 ± 0.0	0.1 ± 0.01
	TOF	92.5 ± 2.5	102.5 ± 3.9	10.6 ± 0.1	54.4 ± 2.8	9.9 ± 0.1	3.5 ± 0.1	7.3 ± 0.3	2.0 ± 0.04	7.1 ± 0.04	2.2 ± 0.1	4.5 ± 0.1	1.5 ± 0.05	4.6 ± 0.1	1.5 ± 0.05
Q	Q	42.3 ± 1.6	97.3 ± 27.6	12.3 ± 1.8	43.7 ± 5.2	9.9 ± 1.1	3.4 ± 0.7	8.4 ± 0.8	2.3 ± 0.1	7.7 ± 0.4	2.4 ± 0.1	4.8 ± 0.2	1.8 ± 0.3	4.9 ± 0.6	1.5 ± 0.2
	SF	50.1 ± 6.3	115.1 ± 9.9	14.4 ± 1.1	43.2 ± 2.7	10.6 ± 0.7	3.7 ± 0.2	8.9 ± 0.5	2.4 ± 0.1	8.3 ± 0.6	2.6 ± 0.1	5.3 ± 0.3	1.8 ± 0.1	5.2 ± 0.3	1.7 ± 0.1
953	TOF	110.2 ± 0.4	229.1 ± 1.7	22.0 ± 0.3	206.0 ± 0.6	5.4 ± 0.3	15.5 ± 0.6	2.7 ± 0.3	14.2 ± 0.3	3.1 ± 0.2	7.7 ± 0.3	1.4 ± 0.3	8.5 ± 0.3	8.5 ± 0.3	1.5 ± 0.2
	Q	86.1 ± 1.3	224.0 ± 62.8	25.2 ± 3.6	96.7 ± 11.0	19.9 ± 2.0	4.6 ± 0.9	16.3 ± 1.6	2.5 ± 0.1	15.5 ± 0.6	3.0 ± 0.2	8.4 ± 0.4	1.3 ± 0.1	8.9 ± 1.1	1.3 ± 0.2
1002	SF	98.6 ± 5.5	247.4 ± 14.3	27.4 ± 1.4	89.8 ± 5.1	20.4 ± 1.2	5.0 ± 0.3	16.9 ± 0.9	2.6 ± 0.1	15.3 ± 0.8	3.1 ± 0.2	8.7 ± 0.3	1.3 ± 0.1	8.7 ± 0.4	1.3 ± 0.1
	TOF	60.2 ± 0.4	134.2 ± 0.9	14.4 ± 0.1	72.6 ± 6.8	13.1 ± 0.1	4.6 ± 0.1	10.8 ± 0.2	2.9 ± 0.1	9.5 ± 0.02	3.1 ± 0.1	5.7 ± 0.2	2.2 ± 0.05	6.1 ± 0.1	2.3 ± 0.1
Q	Q	52.4 ± 0.6	132.7 ± 37.2	14.8 ± 2.1	57.4 ± 6.5	11.1 ± 1.1	2.6 ± 0.5	9.5 ± 0.9	1.5 ± 0.1	9.1 ± 0.4	1.8 ± 0.1	5.2 ± 0.2	0.7 ± 0.1	5.0 ± 0.6	0.8 ± 0.1
	SF	65.6 ± 7.3	151.8 ± 10.4	16.5 ± 0.8	53.9 ± 4.7	12.2 ± 0.7	2.9 ± 0.2	10.2 ± 0.6	1.5 ± 0.1	9.1 ± 0.5	1.8 ± 0.1	5.2 ± 0.1	0.7 ± 0.04	5.0 ± 0.3	0.7 ± 0.04
1102	TOF	115.4 ± 0.8	24.8 ± 0.2	24.8 ± 0.2	22.2 ± 0.1	22.2 ± 0.1	5.5 ± 0.2	16.6 ± 0.1	2.6 ± 0.1	15.1 ± 0.3	3.1 ± 0.1	8.1 ± 0.2	1.4 ± 0.05	8.4 ± 0.2	1.3 ± 0.1
	Q	94.6 ± 1.1	258.3 ± 72.5	28.3 ± 4.0	107.4 ± 12.3	20.9 ± 2.1	5.0 ± 0.9	17.3 ± 1.7	2.5 ± 0.1	15.4 ± 0.7	3.0 ± 0.2	8.5 ± 0.3	1.3 ± 0.1	9.0 ± 1.1	1.2 ± 0.2
1202	SF	140.2 ± 13.8	138.7 ± 13.2	58.9 ± 6.6	184.8 ± 21.4	40.2 ± 4.3	10.4 ± 0.9	32.6 ± 3.4	5.1 ± 0.5	30.2 ± 2.7	5.9 ± 0.7	16.6 ± 1.5	2.5 ± 0.3	16.4 ± 1.8	2.4 ± 0.3
	TOF	38.3 ± 2.1	50.1 ± 1.4	6.4 ± 0.02	26.0 ± 2.0	5.1 ± 0.2	1.5 ± 0.1	3.6 ± 0.2	0.5 ± 0.03	3.3 ± 0.1	0.7 ± 0.1	1.9 ± 0.1	0.4 ± 0.03	2.1 ± 0.1	0.4 ± 0.04
Q	Q	18.9 ± 0.5	45.1 ± 12.7	5.0 ± 0.7	20.5 ± 2.4	4.1 ± 0.4	0.9 ± 0.2	3.4 ± 0.3	0.5 ± 0.03	3.1 ± 0.2	0.6 ± 0.04	1.9 ± 0.2	0.3 ± 0.03	1.9 ± 0.2	0.3 ± 0.04
	SF	21.4 ± 1.1	49.2 ± 3.0	5.6 ± 0.3	18.6 ± 1.1	4.2 ± 0.3	1.0 ± 0.1	3.5 ± 0.2	0.6 ± 0.03	3.3 ± 0.2	0.6 ± 0.04	1.9 ± 0.1	0.3 ± 0.02	1.9 ± 0.1	0.3 ± 0.01
1302	TOF	14.0 ± 0.1	15.7 ± 0.3	1.7 ± 0.1	5.3 ± 0.2	1.4 ± 0.1	0.5 ± 0.1	1.1 ± 0.1	0.2 ± 0.02	0.9 ± 0.1	0.2 ± 0.04	0.6 ± 0.04	0.1 ± 0.03	0.8 ± 0.04	0.1 ± 0.04
	Q	8.0 ± 1.0	16.6 ± 4.7	3.1 ± 0.9	9.5 ± 1.1	2.6 ± 0.3	1.8 ± 0.8	2.3 ± 0.5	0.7 ± 0.3	1.8 ± 0.2	0.7 ± 0.3	0.9 ± 0.1	0.5 ± 0.2	1.0 ± 0.2	0.7 ± 0.2
SF	SF	9.2 ± 0.5	21.6 ± 1.2	2.4 ± 0.1	8.0 ± 0.5	1.9 ± 0.1	0.5 ± 0.0	1.5 ± 0.1	0.2 ± 0.01	1.3 ± 0.1	0.3 ± 0.02	0.8 ± 0.04	0.1 ± 0.01	0.8 ± 0.1	0.1 ± 0.01
	TOF	6.9 ± 0.1	16.9 ± 0.2	1.9 ± 0.03	6.8 ± 0.1	1.6 ± 0.1	0.5 ± 0.1	1.2 ± 0.1	0.2 ± 0.03	1.1 ± 0.0	0.2 ± 0.04	0.8 ± 0.04	0.2 ± 0.03	0.8 ± 0.04	0.1 ± 0.04
Q	Q	10.2 ± 0.7	24.1 ± 6.8	2.6 ± 0.4	10.4 ± 1.2	2.1 ± 0.2	0.5 ± 0.1	1.9 ± 0.2	0.3 ± 0.02	1.6 ± 0.1	0.3 ± 0.02	0.9 ± 0.03	0.2 ± 0.02	1.0 ± 0.1	0.1 ± 0.02
	SF	10.2 ± 0.6	24.1 ± 1.3	2.7 ± 0.1	9.1 ± 0.6	2.1 ± 0.1	0.5 ± 0.0	1.8 ± 0.1	0.2 ± 0.02	1.6 ± 0.1	0.3 ± 0.02	0.9 ± 0.03	0.1 ± 0.01	0.9 ± 0.04	0.1 ± 0.01
1502	TOF	17.2 ± 0.2	38.5 ± 0.3	4.7 ± 0.1	16.2 ± 0.3	3.8 ± 0.1	1.1 ± 0.1	3.5 ± 0.3	0.6 ± 0.04	3.3 ± 0.1	0.7 ± 0.04	2.1 ± 0.1	0.4 ± 0.03	2.1 ± 0.03	0.4 ± 0.05
	Q	17.3 ± 0.2	40.2 ± 11.3	4.6 ± 0.7	18.7 ± 2.1	3.9 ± 0.4	0.9 ± 0.2	3.9 ± 0.4	0.5 ± 0.02	3.6 ± 0.2	0.7 ± 0.04	2.0 ± 0.1	0.3 ± 0.04	2.2 ± 0.3	0.3 ± 0.05
SF	26.3 ± 2.5	61.8 ± 6.3	6.9 ± 0.6	23.0 ± 2.0	5.6 ± 0.5	1.4 ± 0.1	5.0 ± 0.4	0.8 ± 0.1	4.9 ± 0.4	1.0 ± 0.1	2.9 ± 0.2	0.4 ± 0.03	2.9 ± 0.2	0.4 ± 0.03	

* top of the ice core bag

Table S 3: continued

EDC depth * (m)	age [24] (kyr b.p.)	La ± SD	Ce ± SD	Pr ± SD	Nd ± SD	Sm ± SD	Eu ± SD	Gd ± SD	Tb ± SD	Dy ± SD	Ho ± SD	Er ± SD	Tm ± SD	Yb ± SD	Lu ± SD
405.9	14.2	TOF													
		Q	14.0 ± 0.2	45.5 ± 12.8	5.6 ± 0.2	18.6 ± 0.4	2.3 ± 0.1	3.0 ± 0.1	0.8 ± 0.1	2.8 ± 0.1	0.8 ± 0.1	2.3 ± 0.1	0.6 ± 0.1	2.1 ± 0.1	0.6 ± 0.1
		SF	14.6 ± 1.2	38.5 ± 2.9	3.9 ± 0.3	11.0 ± 0.9	0.8 ± 0.2	2.3 ± 0.3	0.6 ± 0.1	2.8 ± 0.1	0.7 ± 0.04	1.9 ± 0.1	0.5 ± 0.1	2.0 ± 0.2	0.5 ± 0.1
411.4	14.5	TOF													
		Q	6.4 ± 0.1	15.4 ± 4.3	1.8 ± 0.3	5.7 ± 0.7	0.8 ± 0.1	0.9 ± 0.1	0.3 ± 0.1	0.7 ± 0.1	0.3 ± 0.02	0.6 ± 0.02	0.3 ± 0.03	0.6 ± 0.1	0.2 ± 0.04
		SF	6.3 ± 0.5	12.9 ± 0.8	1.6 ± 0.1	4.7 ± 0.3	0.9 ± 0.1	0.4 ± 0.03	0.3 ± 0.02	0.8 ± 0.04	0.3 ± 0.02	0.5 ± 0.02	0.2 ± 0.01	0.5 ± 0.04	0.2 ± 0.01
422.4	15.1	TOF													
		Q	10.2 ± 0.1	20.5 ± 5.8	2.7 ± 0.2	8.6 ± 0.4	7.6 ± 0.2	14.5 ± 1.0	1.6 ± 0.1	1.6 ± 0.1	0.6 ± 0.1	1.4 ± 0.2	0.5 ± 0.1	1.6 ± 0.1	0.4 ± 0.1
		SF	8.9 ± 0.6		2.3 ± 0.2	6.3 ± 0.5	1.8 ± 0.1	1.5 ± 0.1	0.5 ± 0.03	1.3 ± 0.1	0.4 ± 0.03	0.8 ± 0.1	0.2 ± 0.02	0.8 ± 0.1	0.2 ± 0.02
442.2	16.2	TOF													
		Q	15.3 ± 2.7	35.9 ± 10.5	5.9 ± 3.1	14.1 ± 3.5	3.7 ± 3.4	4.7 ± 2.7	2.9 ± 2.6	4.4 ± 2.5	2.9 ± 2.5	3.1 ± 2.1	2.7 ± 2.5	3.6 ± 2.5	2.7 ± 2.5
		SF	11.5 ± 0.8	27.3 ± 1.9	2.7 ± 0.2	8.8 ± 0.7	1.9 ± 0.1	1.7 ± 0.1	0.2 ± 0.02	1.6 ± 0.2	0.3 ± 0.03	1.0 ± 0.1	0.1 ± 0.01	1.0 ± 0.1	0.1 ± 0.01
451.6	16.7	TOF													
		Q	27.0 ± 2.5	36.0 ± 11.1	25.9 ± 3.8	34.3 ± 3.9	28.5 ± 2.9	24.2 ± 2.8	22.7 ± 1.3	25.7 ± 1.3	22.6 ± 1.6	23.6 ± 1.7	22.0 ± 2.3	27.4 ± 3.6	22.5 ± 3.5
		SF	27.1 ± 1.9	33.9 ± 2.7	22.3 ± 1.4	25.8 ± 1.7	21.6 ± 1.5	21.0 ± 1.6	20.3 ± 1.5	19.9 ± 1.2	19.2 ± 1.4	19.8 ± 0.8	18.6 ± 1.3	19.3 ± 1.1	19.1 ± 1.2
460.9	17.4	TOF													
		Q	9.5 ± 0.2	18.0 ± 0.3	2.4 ± 0.1	7.4 ± 0.3	2.2 ± 0.2	1.4 ± 0.1	0.3 ± 0.1	1.1 ± 0.1	0.4 ± 0.1	0.9 ± 0.1	0.2 ± 0.1	0.8 ± 0.1	0.2 ± 0.1
		SF	7.0 ± 0.1	17.5 ± 4.9	2.0 ± 0.3	8.1 ± 0.9	1.7 ± 0.2	1.6 ± 0.2	0.3 ± 0.03	1.5 ± 0.1	0.3 ± 0.04	1.0 ± 0.0	0.2 ± 0.03	0.8 ± 0.1	0.2 ± 0.04
470.3	18.1	TOF													
		Q	9.0 ± 1.4	26.4 ± 8.1	5.6 ± 2.2	13.8 ± 2.0	3.0 ± 0.5	3.3 ± 1.2	0.5 ± 0.1	2.3 ± 0.3	0.4 ± 0.03	1.6 ± 0.3	0.3 ± 0.03	1.4 ± 0.2	0.3 ± 0.05
		SF	12.8 ± 1.1	27.2 ± 2.6	3.7 ± 0.2	12.6 ± 0.9	3.1 ± 0.3	2.7 ± 0.2	0.5 ± 0.04	2.4 ± 0.2	0.5 ± 0.04	1.4 ± 0.1	0.2 ± 0.02	1.4 ± 0.1	0.2 ± 0.02
481.8	19.1	TOF													
		Q	16.6 ± 0.3	41.3 ± 11.6	4.8 ± 0.7	18.3 ± 2.1	3.9 ± 0.4	3.6 ± 0.4	0.6 ± 0.04	3.7 ± 0.3	0.7 ± 0.04	2.1 ± 0.1	0.3 ± 0.04	1.9 ± 0.2	0.4 ± 0.05
		SF	18.9 ± 1.3	37.4 ± 2.6	5.1 ± 0.4	17.3 ± 1.3	4.5 ± 0.3	4.4 ± 0.3	0.7 ± 0.1	4.1 ± 0.3	0.9 ± 0.1	2.4 ± 0.1	0.4 ± 0.02	2.2 ± 0.2	0.4 ± 0.02
490.6	18.5	TOF													
		Q	18.9 ± 0.4	48.5 ± 13.6	5.4 ± 0.8	21.4 ± 2.4	4.2 ± 0.4	3.4 ± 0.3	0.5 ± 0.05	3.4 ± 0.1	0.7 ± 0.04	1.9 ± 0.1	0.3 ± 0.03	1.9 ± 0.2	0.3 ± 0.1
		SF	21.3 ± 1.5	43.0 ± 3.3	5.7 ± 0.4	20.0 ± 1.6	4.8 ± 0.3	4.1 ± 0.4	0.7 ± 0.05	3.8 ± 0.3	0.8 ± 0.04	2.1 ± 0.1	0.3 ± 0.02	2.0 ± 0.2	0.3 ± 0.02
502.7	20.9	TOF													
		Q	16.9 ± 1.0	44.5 ± 12.7	4.8 ± 0.7	18.9 ± 2.2	4.0 ± 0.5	3.7 ± 0.5	0.5 ± 0.05	2.9 ± 0.2	0.6 ± 0.03	1.9 ± 0.1	0.3 ± 0.03	1.8 ± 0.2	0.3 ± 0.04
		SF	22.1 ± 1.5	46.5 ± 3.2	6.1 ± 0.4	20.3 ± 1.4	5.0 ± 0.4	4.3 ± 0.3	0.7 ± 0.05	3.7 ± 0.3	0.8 ± 0.1	2.2 ± 0.1	0.3 ± 0.02	2.2 ± 0.2	0.3 ± 0.02
510.4	21.5	TOF													
		Q	13.5 ± 0.2	37.4 ± 10.5	3.9 ± 0.6	15.4 ± 1.7	2.9 ± 0.3	2.6 ± 0.2	0.4 ± 0.02	2.6 ± 0.1	0.5 ± 0.03	1.4 ± 0.1	0.2 ± 0.02	1.5 ± 0.2	0.2 ± 0.03
		SF	16.0 ± 0.9	33.9 ± 2.0	4.5 ± 0.2	15.2 ± 0.9	3.7 ± 0.2	3.2 ± 0.2	0.5 ± 0.03	2.9 ± 0.2	0.6 ± 0.04	1.7 ± 0.1	0.2 ± 0.01	1.6 ± 0.1	0.2 ± 0.01

* top of the ice core bag

Acknowledgement

I am grateful to Prof Dr. Heinrich Miller and Dr. Michael Kriews for the opportunity to do my own research in the laboratories of the Alfred Wegener Institute for Polar and Marine Research in Bremerhaven.

Thanks to Prof. Dr. Heinrich Miller and PD Dr. Sabine Kasten for assessing my thesis.

All discussions during the last years with my co-authors and colleagues – especially Michael, Heiko, Rolf, Frank, Urs, Paolo, Doris, Tom, Eva and Philipp lead to improved data interpretation and presentation. Thanks!

Special thanks to Michael, Ilse and Frank: You always managed to cheer me up if problems with the laboratories, the ICP-TOF-MS or any private matter lead to bad mood. Ilse, I thank you a lot for your support in the laboratory!

Without the help from Berlin and Jena, the ICP-TOF-MS system would have been at a stand still much longer: Thank you Christian Lüdke, Erwin Hoffmann, Jörg Wollbrandt, Jochen Skole and Eike Thamm!

I would also like to thank Christian Lüdke once more: Thank you very much for your patience and time you spent in reading my manuscripts, my dissertation and your introduction to the interpretation of statistical results from analytical data.

Much help to construct spare parts for the LA-ICP-TOF-MS system was provided by Erich Dunker, Matthias Littmann and all other people from our “Wissenschaftliche Werkstatt”. Thanks! Everything concerning the installation of the laser ablation system in the clean room laboratories was only possible with the help of Wilfried Ruhe and Ingo Beninga (Fa. Impres). Thank you two!

Thanks to all unnamed colleagues who were interested in my work during the last years.

Without my friends from my “Heimat” (Westerwald) and my new “Zuhause” (Bremerhaven) the last years would have been much more difficult. Thanks for all your support and all the Sushi and “Doppelkopf” evenings we had together.

I would also like to thank my now “extended family”. Thanks to Barbara for your daily jokes you sent during the last 5 months. Christian, I would like to thank you for providing me your knowledge of the schematics of generator systems. Special thanks to my parents Christa and Peter for all your support and for the wonderful former “nuclear family”.

At last I thank my new “nuclear family”. Dear Frank, thanks for all your support during the last years and for being one another!

Appendix

A1 Utility Model

Vorrichtung zum mechanischen Abtragen der obersten Schicht einer Festkörperprobe

D. Dick, M. Kriews, H. Reinhardt, E. Dunker, M. Littmann

Gebrauchsmuster DE 20 2004 010 599 U1.



(19)
Bundesrepublik Deutschland
Deutsches Patent- und Markenamt

(10) DE 20 2004 010 599 U1 2004.12.09

(12)

Gebrauchsmusterschrift

(22) Anmeldetag: **02.07.2004**
(47) Eintragungstag: **04.11.2004**
(43) Bekanntmachung im Patentblatt: **09.12.2004**

(51) Int Cl.: **G01N 1/06**
G01N 1/04, B26D 5/02, B26D 1/18,
B26D 7/26

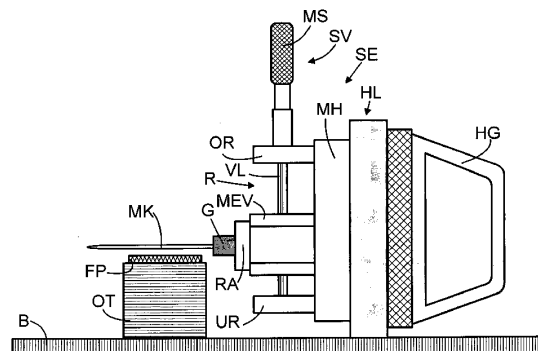
(66) Innere Priorität:
103 40 890.8 31.08.2003

(71) Name und Wohnsitz des Inhabers:
Stiftung Alfred-Wegener-Institut für Polar- und
Meeresforschung, 27568 Bremerhaven, DE

Die folgenden Angaben sind den vom Anmelder eingereichten Unterlagen entnommen

(54) Bezeichnung: **Vorrichtung zum mechanischen Abtragen der obersten Schicht einer Festkörperprobe**

(57) Hauptanspruch: Vorrichtung zum mechanischen Abtragen der obersten Schicht einer Festkörperprobe mit einer Basis, einem Objektträger, einer einen Messerhalter, der auf einer horizontalen Linearführung verschiebbar angeordnet ist, mit zumindest einer Messereinspannvorrichtung zur Aufnahme einer biegesteifen Messerklinge aufweisenden Schneideinrichtung und einer Schnitthöhenverstellereinrichtung, dadurch gekennzeichnet, dass der Objektträger (OT) auf der Basis (B) fixiert ist, der Messerhalter (MH) aus einem Rahmen (R) mit einer vertikalen Linearführung (VL) besteht, auf der die Messereinspannvorrichtung (MEV) verschiebbar angeordnet ist, dass die Messerklinge (MK) abriebfest oder aus einem festkörperprobenfremden Material ausgebildet und zumindest einseitig in der Messereinspannvorrichtung (MEV) eingespannt ist, und dass die Schnitthöhenverstellereinrichtung (SV) von einer an dem Rahmen (R) des verschiebbaren Messerhalters (MH) fixierten, die Messereinspannvorrichtung (MEV) auf der vertikalen Linearführung (VL) stufenlos verstellenden Feineinstellvorrichtung (MS) gebildet ist.



DE 20 2004 010 599 U1 2004.12.09

Beschreibung

[0001] Die vorliegende Neuerung bezieht sich auf eine Vorrichtung zum mechanischen Abtragen der obersten Schicht einer Festkörperprobe mit einer Basis, einem Objektträger, einer Messerhalter, der auf einer horizontalen Linearführung verschiebbar angeordnet ist, mit zumindest einer Messereinspannvorrichtung zur Aufnahme einer biegesteifen Messerklinge aufweisenden Schneideinrichtung und einer Schnitthöhenverstelleinrichtung.

[0002] Verschiedene Untersuchungsmethoden an Materialproben erfordern eine ebene und glatte, einige auch eine von Kontaminationen mit Fremdmaterial freie Oberfläche der Probe. Es können dies bildgebende Verfahren sein, bei denen eine Probenoberfläche fotografiert und der Bildinhalt ausgewertet wird. Diese Methode wird häufig auf organische Proben angewendet, um mit Hilfe von computererzeugten dreidimensionalen Abbildungen die räumliche Struktur anatomischer Präparate zu untersuchen oder für Lehrzwecke bereitzustellen. Es können aber auch erodierende Verfahren sein, bei denen kleinste Mengen Oberflächenmaterial herausgelöst und einer Spurenelement-Analyse zugeführt werden. Wenn es dabei um weiche und nicht formstabile Materialien geht, ist das Einfrieren eine bekannte Vorgehensweise. Organisches Material kann dazu zuvor z.B. in Paraffin eingebettet werden. Andere Materialproben liegen schon in ihrer Ausgangsform gefroren vor. Hierzu zählt z.B. Eis aus in den Dauerfrostgebieten der Erde gewonnenen Bohrkernen. Die sehr empfindlichen Spektrometer zur Spurenelementanalyse erfordern eine extrem saubere, von Kontaminationen freie Oberfläche. Die Präparation der Oberflächen vor und nach deren Untersuchungen muss schnell gehen und verlangt Dicken der Abtragung bis in den Millimeter-Bereich. Die Abtragung kann zerspanend erfolgen. Die abgetragene Schicht kann für andere Untersuchungen der Probe weiterverwendet werden.

[0003] In der deutschen Gebrauchsmusterschrift G 92 11 155.6 U1 (Einrichtung zum sukzessiven Abtragen der obersten Schicht gefrorener Gewebestücke) wird eine Vorrichtung vorgestellt, die von einer Festkörperprobe eine Schicht von bis zu 5 mm in einem einzigen Arbeitsgang zerspanend abtragen kann. Dabei handelt es sich um eine als Rotations-Kryomikrotom bezeichnete Vorrichtung. Auf einer Basis kann ein Objektträger manuell oder automatisch in einer vorgegebenen Richtung bewegt werden. Eine festmontierte Schneideinrichtung ist mit einer schnell rotierenden, horizontal zur Oberfläche der Festkörperprobe ausgerichteten Welle als Messerhalter mit einem Fräskopf als Messereinspannvorrichtung mit zwei auswechselbaren, auf ganzer Länge eingespannten Frässhneiden als Messerklingen ausgeführt. Eine Einstellung der Neigung der Messerklingen gegen die Oberfläche der Festkörperprobe ist

nicht vorgesehen, die Messerklingen sind im Fräskopf fixiert. Mit der Schnitthöhenverstelleinrichtung kann der Objektträger stufenlos in der Höhe zur Wahl der Dicke der abzutragenden Schicht eingestellt werden. Zum Abtragen der obersten Schicht der Festkörperprobe wird der Objektträger auf seiner Führung gegen die Messerklingen des Fräskopfs bewegt. Eine schnell arbeitende Fräse kann zwar die Bearbeitungsdauer für das Abtragen von Schichten in Millimeterstärke entscheidend herabsetzen, bietet aber hinsichtlich einer Kontamination der Probenoberfläche keinen Schutz, da die für die eingesetzten einfachen Messerklingen verwendeten Materialien auch essentiell in den meisten Proben enthalten sind.

[0004] Mikrotome sind weithin bekannte Geräte zur Herstellung von Dünnschnitten verschiedener Materialien zur Betrachtung unter dem Mikroskop. Eine Vielzahl von Veröffentlichungen befasst sich mit der Weiterentwicklung einzelner Aspekte wie Messermaterial und -form, automatisiertem Betrieb, Anpassung an spezifische Probenmaterialien und die sichere Handhabung der extrem dünnen Schnitte (bis hinab zu 50 nm) usw. Bei gefrorenen Proben wird auch von der Kryomikrotomie gesprochen.

[0005] In der österreichischen Patentschrift AT 374 282 (Mikrotour) wird ein Mikrotour vorgestellt, das auf einer vertikal ausgerichteten Basis einen mittels Getriebe und Kurbel manuell vertikal verschiebbaren Objektträger und eine fest angeordnete, mittels einer Schnitthöhenverstelleinrichtung stufenlos einstellbare Schneideinrichtung mit einer einstellbaren Messerklinge vorsieht. Es hebt Schichtdicken im Mikrometerbereich ab, sodass eine neue Oberflächenpräparation für die weiter oben beschriebenen Untersuchungsmethoden mit der Notwendigkeit zum Abtragen großer Schichtdicken sehr lange (mehrere Minuten) dauern kann.

[0006] In der deutschen Patentschrift DE 24 49 622 C3 wird ein Kno-Mikrotour vorgestellt, das in der Lage ist, auch bei sehr großen (bis 400 × 150 mm) Festkörperproben dünne Schichten (bis herunter zu 2 µm) mit konstanter Dicke abzuheben. Dazu wird hier auf einer waagrecht angeordneten Basis ein Objektträger horizontal verschiebbar angeordnet. Die Schneideinrichtung ist in einem massiven Rahmen angeordnet, der fest mit der Basis verbunden ist. Der obere Teil des Rahmens mit Messerhalter, Messereinspannvorrichtung ist zur Schnitthöhenverstellung über eine Schraubspindel mit Schnecke verschiebbar mit dem unteren Teil verbunden. Die Einstellung kann manuell oder automatisch gesteuert erfolgen. Die auf ganzer Länge eingespannte Messerklinge ist starr gehalten.

[0007] Der Einsatz von unterschiedlichen Materialien für die Messerklingen hat verschiedene Gründe. Stahl ist preiswert und hat eine mittlere Standzeit bei

DE 20 2004 010 599 U1 2004.12.09

hoher zulässiger Schneidkraft, ist aber nicht frei von Abrieb, der außerdem aus verschiedenen Stoffzusammensetzungen besteht. Glas ist billig, aber empfindlich und hat nur eine geringe Standzeit. Es muss nach wenigen Schnitten durch den Anwender neu zu gerichtet werden. Glas ist für extreme Dünnschnitte geeignet, es kann aber aufgrund der Herstellmethode Markierungen auf der Oberfläche hinterlassen. Saphir ist hart und scharf, hat aber eine geringe Standzeit bei kleiner zulässiger Schneidkraft. In der US-Patenschrift US 49 39 195 wird darüber hinaus z.B. eine mit einer Diamantschicht überzogene Messerklinge vorgestellt, die eine hohe Standzeit, hohe Schneidkraft und antikorrosive Eigenschaften aufweist. Dazu wird die Messerklinge einem plasmainduzierten chemischen Abscheideverfahren aus der Gasphase eines kohlenstoffhaltigen Gasgemischs mit anschließender Temperaturbehandlung bis 1300 °C unterzogen. Die Messerklinge kann aus beliebigem Material sein. Einzige Voraussetzung ist, dass sie der Wärmebehandlung standhält.

[0008] In dem deutschen Gebrauchsmuster G 89 10 071 U1 wird ein Schlittenmikrotom vorgestellt, das über einen in einer Horizontalführung verschiebbaren Schlitten mit Messerhalterung verfügt. Der Objektträger ist vertikal über nicht näher beschriebene Elemente verstellbar, die Schlittenbewegung erfolgt motorisch. Die Messerklinge ist verstellbar eingespannt, die Einspannung erfolgt über eine große Strecke, damit die Klinge die Schneidkraft sicher aufnehmen kann ohne sich zu verstellen. Gegen Schwingungen des Messers ist die Klinge besonders breit und stabil ausgelegt. Ein Abdeckband soll vor Verunreinigungen der Horizontalführungen schützen.

[0009] Die deutsche Offenlegungsschrift DE 196 06 969 A1, von der die vorliegende Neuerung als nächstliegendem Stand der Technik ausgeht, beschreibt ebenfalls ein Schlittenmikrotom, das über einen in einer Horizontalführung verschiebbaren Schlitten mit Messerhalterung verfügt. Der Objektträger ist vertikal über ein mehrstufiges Verstellgetriebe motorisch stufig verstellbar, die Schlittenbewegung erfolgt mit Hilfe eines Handgriffs. Die Messerklinge ist verstellbar einseitig eingespannt, ein Vibrationsschutz ist nicht vorgesehen. Auch hier soll eine Bandabdeckung die Horizontalführung vor Verschmutzungen schützen. Die Gewinnung von ebenen Probenoberflächen für andere Untersuchungsverfahren durch zerpannende Methoden kann aufgrund der Konstruktion der dafür eingesetzten Vorrichtungen als ein Spezialgebiet der Mikrotomie bezeichnet werden. Bei einer speziellen physikalischen Untersuchungsmethode wird die durch das Mikrotom gewonnene ebene Probenoberfläche nach einem bestimmten Abtragungsmuster mit Hilfe eines Lasers hochortsaufgelöst ablatiert und einem Massenspektrometer zugeführt. Damit eine gleichmäßige Abtragung des Probenmaterials erfolgt, ist eine ebene Probenoberfläche Voraus-

setzung. Nach dem Laserbeschuss der Probe kann es erforderlich sein, eine Wiederholmessung durchzuführen. Daher ist es nötig, vor der nächsten Untersuchung Probenmaterial in der durch die Eindringtiefe des Lasers bestimmte Dicke abzutragen. Wegen der extremen Empfindlichkeit des Massenspektrometers muss bei jedem Abtragen der Oberfläche eine Verunreinigung der Probe mit von der Vorrichtung oder dem abtragenden Messer stammenden Fremdpartikeln vermieden werden. Ein Standard-Mikrotom kann diese Aufgaben nicht erfüllen. Die Abtragung der erforderlichen Schichtdicken dauert zu lange, und eine Kontamination der Oberfläche der Festkörperprobe durch das Material der Messerklinge ist nur durch den Einsatz teurer Spezialmesser vermeidbar.

[0010] Keine der zuvor beschriebenen Vorrichtungen kann aufgrund der verwendeten Materialien der Messer und der beweglichen Bauteile Abrieb und damit eine Kontamination der Oberfläche der Festkörperprobe vermeiden, die sich verfälschend auf das Untersuchungsergebnis der Materialzusammensetzung auswirkt.

[0011] Es ist daher die Aufgabe der vorliegenden Neuerung, eine Vorrichtung zum mechanischen Abtragen der obersten Schicht einer Festkörperprobe mit einer Basis, einem Objektträger, einer einen Messerhalter, der auf einer horizontalen Linearführung verschiebbar angeordnet ist, mit zumindest einer Messereinspannvorrichtung zur Aufnahme einer Messerklinge aufweisenden Schneideinrichtung und einer Schnitthöhenverstelleinrichtung derart weiterzubilden, dass damit einfach und schnell eine glatte Oberfläche einer gefrorenen Probe durch Abtragen einer Schicht mit einer Dicke im Bereich von bis zu einigen zehntel Millimetern unter Vermeidung von zumindest nicht als solche erkennbarer Kontamination mit Fremdpartikeln herstellbar ist.

[0012] Als Lösung ist bei der neuerungsgemäßen Vorrichtung der gattungsgemäßen Art vorgesehen, dass der Objektträger auf der Basis fixiert ist, der Messerhalter aus einem Rahmen mit einer vertikalen Linearführung besteht, auf der die Messereinspannvorrichtung verschiebbar angeordnet ist, dass die Messerklinge abriebfest oder aus einem festkörperprobenfremden Material ausgebildet und zumindest einseitig in der Messereinspannvorrichtung eingespannt ist, und dass die Schnitthöhenverstelleinrichtung von einer an dem Rahmen des verschiebbaren Messerhalters fixierten, die Messereinspannvorrichtung auf der vertikalen Linearführung stufenlos stellenden Feineinstellvorrichtung gebildet ist.

[0013] Bei der Verwendung nicht abriebfreier Messerklingen ist eine auftretende Kontamination immer dann zuverlässig erkenn- und identifizierbar, wenn ein Vorkommen der gleichen Substanz in der Materialprobe definitiv ausgeschlossen werden kann. Nur

in diesem Fall kann eine Kontamination toleriert werden, grundsätzlich sicherer ist es aber, jedwede Kontamination auszuschließen. Zur Vermeidung von durch mechanische Konstruktionen bedingten nicht erkennbaren Kontaminationen einerseits und zur beschleunigten Bearbeitung der Probe andererseits ist mit der neuerungsgemäßen Vorrichtung ein allen Anforderungen genügender Kompromiss zwischen einem Standard-Mikrotom und einer abtragenden Oberflächen-Fräse gefunden. Die einfache Konstruktion vermeidet motorische Antriebe und komplizierte Verstellvorrichtungen. Zur Erzeugung ebener Oberflächen reicht bereits eine einseitige Einspannung der Messerklinge im Messerhalter aus. Um jedoch eine zum Objektträger planparallele Oberfläche erhalten und um Schwingungen der Messerklinge zu vermeiden, ist es nach einer Ausgestaltung der Neuerungen vorteilhaft, wenn die Messerklinge beidseitig in der Messereinspannvorrichtung eingespannt ist. Dadurch verdoppeln sich zwar die entsprechenden haltenden Elemente in der Messereinspannvorrichtung, aber der Vorteil der schwingungsfrei und dabei reibungsarm geführten Messerklinge ist bedeutsam.

[0014] Zur unter allen Bedingungen einfachen, reibungsfreien und parallel zur Probenoberflächen ausführbaren Bewegung des Messerhalters ist in einer vorteilhaften Fortführung des neuerungsgemäßen Mikrotoms vorgesehen, dass der Messerhalter mittels Kugelbuchsen auf der horizontalen Linearführung läuft. Dadurch kann trotz der häufigen und in schnellem Rhythmus erfolgenden Hinundherbewegung beim Abtragungsvorgang auf eine die Kontaminierung der Probe begünstigende Schmierverzicht werden. Darüber hinaus kann dadurch die neuerungsgemäße Vorrichtung, die über keine eigene Probenkühleinrichtung verfügt, als Ganzes in einem Kältelabor eingesetzt werden, weil die Bewegung nicht durch ein zähes oder gefrorenes Schmiermittel behindert wird. Weiterhin ist vorteilhaft vorgesehen, dass der Messerhalter mittels eines Handgriffs auf der horizontalen Lineartührung verschiebbar ist. Die Verwendung eines Handgriffs zur Betätigung vermeidet einen teuren Motor und gestattet so die Verwendung der Vorrichtung auch ohne Hilfsspannungsquelle.

[0015] Eine vorteilhafte Fortführung der neuerungsgemäßen Vorrichtung sieht vor, dass die Messerklinge bei einseitiger Einspannung mit einem Griff eine Einheit bildet und diese als handelsübliches Haushaltsmesser ausgebildet ist, bei dem die Klinge als Keramik Klinge ausgebildet ist. Die Verwendung eines handelsüblichen Haushaltsmessers trägt dem Umstand Rechnung, dass ein Feinschnitt nicht erforderlich und die Herstellung einer glatten Oberfläche mit einer gut geschärften Klinge ohne Weiteres möglich ist. Dabei ist ein solches Messer deutlich billiger als eine professionelle Mikrotom-Messerklinge. Keramikklingen haben verschiedene Vorteile gegenüber

standardmäßigen metallischen Klängen. Zum einen haben sie bei gleichen äußeren Abmessungen und gleicher Schärfe eine deutlich höhere Standzeit und zum anderen geht von ihnen kein Abrieb aus, das heißt, der abtragende Schnitt erfolgt völlig frei von jeglicher Kontaminationen der Probenoberfläche. Gegenüber Messerklingen mit einem Diamantüberzug ist darüber hinaus eine Keramik Klinge deutlich preiswerter und einfacher herstellbar. Bei der Verwendung einer nicht kontaminierenden Messerklinge ist der Anwender auf jeden Fall auf der sicheren Seite, insbesondere dann, wenn nicht hundertprozentig ein Vorkommen des Materials der Messerklinge in der zu untersuchenden Festkörperprobe ausgeschlossen werden kann. Andererseits gibt es aber bestimmte Festkörperproben, bei denen ein solcher Ausschluss mit vollständiger Sicherheit vorgenommen werden kann. Aufgrund ihrer speziellen Herkunft zählen insbesondere Eisproben zu diesen Festkörperproben. Deshalb kann bei der Neuerungen gemäß einer nächsten vorteilhaften Fortführung auch vorgesehen sein, dass die Messerklinge aus einem hochreinem Metallblech, insbesondere Molybdänblech, besteht, wobei nur solche Metalle verwendet werden, die bekanntermaßen nicht in der zu untersuchenden Festkörperprobe vorkommen. Molybdänblech ist zwar wie alle Metalle nicht abriebfest, allerdings wird durch die hohe Reinheit des Materials bei der Auswertung durch das Massenspektrometer ein einzelner, eindeutig dem Molybdän zuordenbarer Peak erzeugt, der als exakt definierte Kontamination aus der Betrachtung ohne Weiteres ausgeblendet werden kann. Die Messung verfälschendes Fremdmaterial kommt in dem hochreinen Molybdänblech nicht vor. Um auch bei einem erhöhten Kraftaufwand bedingenden, stärkeren Abtragungen eine ebene Probenoberfläche sicherzustellen, kann ein Versteifungsblech auf die Messerklinge aus Metallblech aufgebracht werden. Es kann zur Vermeidung von Verunreinigungen ebenfalls insbesondere aus einem hochreinen Molybdänblech bestehen und mit üblichen Verfahren, z.B. Kleben, auf der Messerklinge befestigt werden. Beide Bleche werden, wiederum bei einseitiger Einspannung, gemeinsam in einem Griff gefasst, der in die Messereinspannvorrichtung eingespannt werden kann.

[0016] Um allen Erfordernissen des Probenmaterials gerecht zu werden, sieht eine weitere vorteilhafte Fortführung der neuerungsgemäßen Vorrichtung vor, dass der Neigungswinkel der Messerklinge um deren Längsachse gegenüber der abzutragenden Oberfläche der Festkörperprobe einstellbar ist. Eine weitere Fortführung sieht vor, dass die Messereinspannvorrichtung zumindest ein von zumindest einer ersten Feststellschraube in seiner Winkellage fixierbares rohrförmiges Aufnahmestück mit zumindest zwei weiteren Feststellschrauben zur Fixierung des Griffs der Messerklinge aufweist. Mit den weiteren Feststellschrauben wird die Messerklinge oder der jewei-

DE 20 2004 010 599 U1 2004.12.09

lige Griff sicher innerhalb des jeweiligen Aufnahmestücks eingeklemmt und gegen Verrutschen und Verdrehen gesichert. Das jeweilige Aufnahmestück wird seinerseits in einer jeweiligen zylindrischen Bohrung mit einem dem Außendurchmesser des Aufnahmestücks entsprechenden Innendurchmesser der Messereinspannvorrichtung angeordnet und dort in einer stufenlos wählbaren Winkellage zum Abgleich der Messerstellung zur Probenoberfläche durch die erste Feststellschraube fixiert. Durch die Notwendigkeit der Fixierung im Falle der Verwendung eines Hausmessers mit seinem ergonomisch geformten und zwischen den Fabrikaten abweichend gestalteten Handgriff in der gewünschten Winkellage der Messerklinge zur Festkörperprobe bei einseitiger Einspannung in der Messereinspannvorrichtung ist es erforderlich, den die Messereinspannvorrichtung aufnehmenden Messerhalter bewegbar und den Objektträger fix zu gestalten anstelle der sonst üblicherweise umgekehrten Vorgehensweise. Ein feststehendes Messer mit derart unterschiedlich möglicher Gestaltung würde einen sehr komplizierten Verstell- und Bewegungsmechanismus des Objektträgers zur Folge haben. Die genannten Maßnahmen können bei einer beidseitigen Einspannung der Messerklinge in der Messereinspannvorrichtung entfallen.

[0017] Eine weitere vorteilhafte Fortführung der neuerungsgemäßen Vorrichtung wird dadurch erreicht, dass die Basis und der Objektträger aus Polyoxymethylen (POM) gebildet sind. Dieser Kunststoff mit der Strukturformel $[-(\text{CH}_2)\text{-O}]_n$ ist ein technischer Thermoplast mit einer ganzen Reihe guter Eigenschaften, die ihn für die angegebenen Verwendungen geeignet machen. Für den direkten Einsatz im Kältelabor ist POM äußerst formstabil und hat auch bei tiefen Temperaturen eine gute Kerbschlagzähigkeit, das heißt, es tritt kein Verspröden ein. Für die genaue Probenhaltung lässt es sich gut bearbeiten und ist auch bei kleinen Toleranzen sehr maßhaltig. Gegen unerwünschte Kontaminationen der Probenoberfläche ist es extrem verschleiß- und abriebfest mit besonderen Gleiteigenschaften und resistent gegen die meisten Lösungsmittel. POM steht in vielen Grundabmessungen als Halbzeug zur Verfügung.

[0018] Ferner ist vorteilhaft vorgesehen, dass die Feineinstellvorrichtung der Schnitthöhenverstelleinrichtung als Mikrometerschraube ausgebildet ist. Die Schnitthöhenverstelleinrichtung wird auch am Messerhalter realisiert, indem die eigentliche Messereinspannvorrichtung mit dem Messdorn einer Mikrometerschraube derart verbunden ist, dass das am Einstellrad der Mikrometerschraube ablesbare Maß dem Höhenmaß über der Oberkante des Probenhalters entspricht und die Messereinspannvorrichtung mit den Drehungen am Einstellrad um das dort angezeigte Maß in seiner vertikalen Linearführung angehoben oder gesenkt wird. Damit ist eine stufenlose Verstellung der Schnittdicke nach den Erfordernissen der

Probe realisiert.

[0019] Eine weitere vorteilhafte Fortführung sieht vor, dass der Objektträger höhenverstellbar ausgebildet ist. Zur Überbrückung größerer Höhendifferenzen kann der Objektträger durch definierte Zwischenlagen in eine für die Feineinstellung der Höhenverstelleinrichtung günstige Ausgangshöhe gebracht werden. Für das Handling des Probenmaterials ist schließlich vorteilhaft vorgesehen, dass der Objektträger an seiner Oberfläche in Verlängerung der eingesetzten Festkörperprobe Griffmulden aufweist.

[0020] Ausbildungsformen der beanspruchten Vorrichtung zum mechanischen Abtragen der obersten Schicht einer Festkörperprobe werden nachfolgend anhand der schematischen Figuren näher erläutert. Dabei zeigt

[0021] Fig. 1 eine Vorrichtung für eine einseitige Einspannung der Messerklinge in der Seitenansicht und

[0022] Fig. 2 eine Vorrichtung für beidseitige Einspannung der Messerklinge in der Seitenansicht.

[0023] Die Fig. 1 zeigt eine Seitenansicht der beanspruchten Vorrichtung für eine einseitige Einspannung. Auf der die Basis B bildenden Platte ist der Objektträger OT, beide aus Polyoxymethylen (POM), mit der in den Objektträger OT eingelassenen Festkörperprobe FP fixiert. Ebenfalls auf der Basis B fixiert ist die Schneideinrichtung SE. Sie besteht aus dem fest montierten Tragrahmen TR und der darin angeordneten horizontalen Linearführung HL aus zwei metallischen Rundstangen. Darauf läuft in Kugellagern der Messerhalter MH, der über den Handgriff HG in horizontaler Richtung hin und her bewegt werden kann. Der Messerhalter MH besteht seinerseits aus dem Rahmen R und der vertikalen Linearführung VL. Der Rahmen R besteht aus der (nicht sichtbaren) Rahmenplatte RP, dem oberen Riegel OR und dem unteren Riegel UR, die die vertikale Linearführung VL aus zwei metallischen Rundstangen tragen, und dem mittleren Riegel MR, der seinerseits die Messereinspannvorrichtung MEV trägt. Diese wird von einem rohrförmigen Aufnahmestück RA gebildet, das in einer Bohrung mit hinterem Anschlag frei drehbar angeordnet ist und von einer ersten Feststellschraube EF in beliebiger Winkelposition fixiert werden kann. In dem rohrförmigen Aufnahmestück RA wird z.B. die Messerklinge MK mit Griff G mit den weiteren Feststellschrauben WF eingeklemmt. Die Höhenposition der Messerklinge MK wird mit der Schnitthöhenverstelleinrichtung SV eingestellt. Dazu kann der mittlere Riegel MR zusammen mit der Messereinspannvorrichtung MEV auf der vertikalen Linearführung VL auf und ab bewegt werden, indem die Mikrometerschraube MS sich auf dem oberen Riegel OR abstützt und ihr Messdorn mit dem mittleren Rie-

DE 20 2004 010 599 U1 2004.12.09

gel MR verbunden ist. Mit der beschriebenen Konstruktion kann die Probenoberfläche PO mit der Messerklinge MK in einstellbarer Winkellage und einstellbarer Schnitthöhe bedarfsgerecht bearbeitet werden. Gut sichtbar ist in dieser Ansicht der Handgriff HG zur Betätigung der Schneideinrichtung SE.

[0024] Fig. 2 zeigt eine Seitenansicht der beanspruchten Vorrichtung mit einer beidseitigen Einspannung der Messerklinge MK in einem entsprechend beidseitig ausgeführten Messereinspannvorrichtung MEV. Es ist erkennbar, dass alle Elemente der horizontalen Linearführung HL und des Messerhalters MH doppelt ausgeführt sind. Die Basis B einerseits und der gemeinsame obere Riegel OR der Rahmen R der Messerhalter MH andererseits bilden die mechanische Klammer zur beidseitigen Einspannung der Messerklinge MK. Die gemeinsame Schnitthöhenverstelleinrichtung SV wirkt mit der einzigen Mikrometerschraube MS auf den gemeinsamen mittleren Riegel MR und stützt sich auf dem gemeinsamen oberen Riegel OR ab. Die Schneideinrichtung SE wird insgesamt über die beiden Handgriffe HG betätigt.

Bezugszeichenliste

B	Basis
OT	Objektträger
SE	Schneideinrichtung
TR	Tragrahmen
SV	Schnitthöhenverstelleinrichtung
FP	Festkörperprobe
PO	Probenoberfläche
HL	horizontale Linearführung

Bezugszeichenliste

HG	Handgriff
MH	Messerhalter
R	Rahmen
MEV	Messereinspannvorrichtung
MK	Messerklinge
G	Griff
MS	Mikrometerschraube
EF	erste Feststellschraube
WF	weitere Feststellschraube
RA	rohrförmiges Aufnahmestück
RP	Rahmenplatte
OR	oberer Riegel
MR	mittlerer Riegel
UR	unterer Riegel
VL	vertikale Linearführung
VB	Versteifungsblech

Schutzansprüche

1. Vorrichtung zum mechanischen Abtragen der obersten Schicht einer Festkörperprobe mit einer Basis, einem Objektträger, einer einen Messerhalter,

der auf einer horizontalen Linearführung verschiebbar angeordnet ist, mit zumindest einer Messereinspannvorrichtung zur Aufnahme einer biegesteifen Messerklinge aufweisenden Schneideinrichtung und einer Schnitthöhenverstelleinrichtung, **dadurch gekennzeichnet**, dass der Objektträger (OT) auf der Basis (B) fixiert ist, der Messerhalter (MH) aus einem Rahmen (R) mit einer vertikalen Linearführung (VL) besteht, auf der die Messereinspannvorrichtung (MEV) verschiebbar angeordnet ist, dass die Messerklinge (MK) abriebfest oder aus einem festkörperprobenfremden Material ausgebildet und zumindest einseitig in der Messereinspannvorrichtung (MEV) eingespannt ist, und dass die Schnitthöhenverstelleinrichtung (SV) von einer an dem Rahmen (R) des verschiebbaren Messerhalters (MH) fixierten, die Messereinspannvorrichtung (MEV) auf der vertikalen Linearführung (VL) stufenlos verstellenden Feinverstellvorrichtung (MS) gebildet ist.

2. Vorrichtung nach Anspruch 1, dadurch gekennzeichnet, dass die Messerklinge (MK) beidseitig in der Messereinspannvorrichtung (MEV) eingespannt ist.

3. Vorrichtung nach Anspruch 1 oder 2, dadurch gekennzeichnet, dass der Messerhalter (MH) mittels Kugelbuchsen auf der horizontalen Linearführung (HL) läuft.

4. Vorrichtung nach einem der Ansprüche 1 bis 3, dadurch gekennzeichnet, dass der Messerhalter (MH) mittels zumindest eines Handgriffs (HG) auf der horizontalen Linearführung (HL) verschiebbar ist.

5. Vorrichtung nach einem der Ansprüche 1 bis 4, dadurch gekennzeichnet, dass die Messerklinge (MK) bei einseitiger Einspannung mit einem Griff (G) eine Einheit bildet und diese als handelsübliches Haushaltsmesser ausgebildet ist, bei dem die Klinge als Keramik Klinge ausgebildet ist.

6. Vorrichtung nach einem der Ansprüche 1 bis 5, dadurch gekennzeichnet, dass die Messerklinge (MK) aus einem hochreinem Metallblech, insbesondere Molybdänblech, besteht, wobei nur solche Metalle verwendet werden, die bekanntermaßen nicht in der zu untersuchenden Festkörperprobe (FP) vorkommen.

7. Vorrichtung nach einem der Ansprüche 5 oder 6, dadurch gekennzeichnet, dass der Neigungswinkel der Messerklinge (MK) um deren Längsachse gegenüber der abzutragenden Oberfläche der Festkörperprobe (FP) einstellbar ist.

8. Vorrichtung nach einem der Ansprüche 1 bis 7, dadurch gekennzeichnet, dass die Messereinspannvorrichtung (MEV) zumindest ein von zumindest einer ersten Feststellschraube (EF) in seiner Winkella-

DE 20 2004 010 599 U1 2004.12.09

ge fixierbares rohrförmiges Aufnahmestück (RA) mit zumindest zwei weiteren Feststellschrauben (WF) zur Fixierung des Griffs (G) der Messerklinge (MK) aufweist.

9. Vorrichtung nach einem der Ansprüche 1 bis 8, dadurch gekennzeichnet, dass die Basis (B) und der Objektträger (OT) aus Polyoxymethylen gebildet sind.

10. Vorrichtung nach einem der Ansprüche 1 bis 9, dadurch gekennzeichnet, dass die Feineinstellvorrichtung der Schnitthöhenverstelleinrichtung (SV) als Mikrometerschraube (MS) ausgebildet ist.

11. Vorrichtung nach einem der Ansprüche 1 bis 10, dadurch gekennzeichnet, dass der Objektträger (OT) höhenverstellbar ausgebildet ist.

12. Vorrichtung nach einem der Ansprüche 1 bis 11, dadurch gekennzeichnet, dass der Objektträger (OT) an seiner Oberfläche in Verlängerung der eingesetzten Festkörperprobe (FP) Griffmulden aufweist.

Es folgt ein Blatt Zeichnungen

DE 20 2004 010 599 U1 2004.12.09

Anhängende Zeichnungen

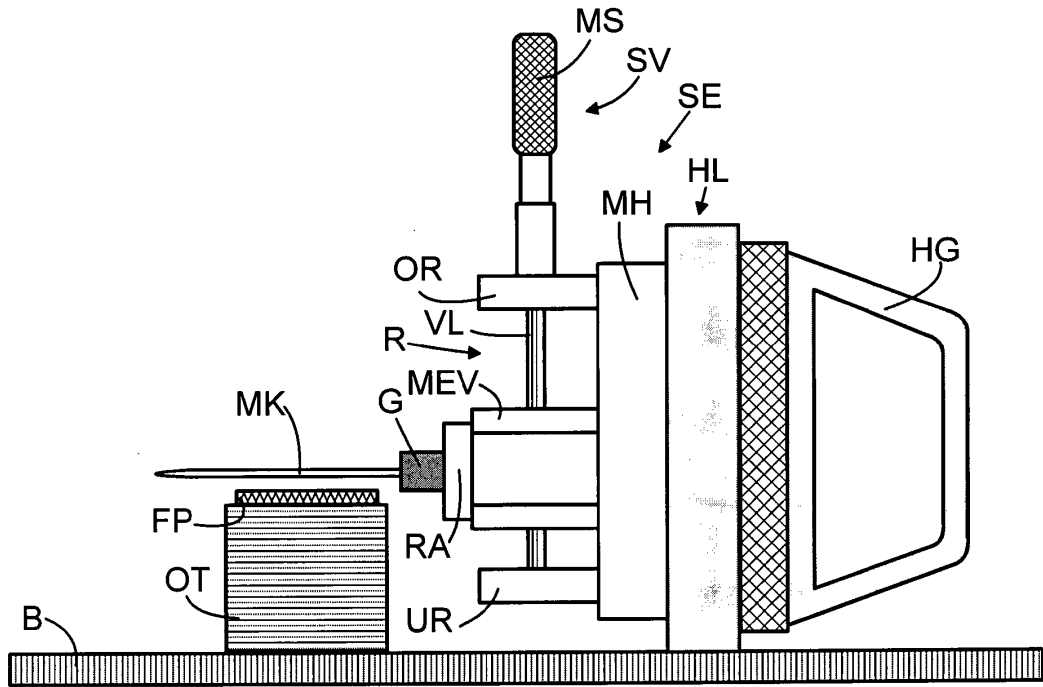


Fig.1

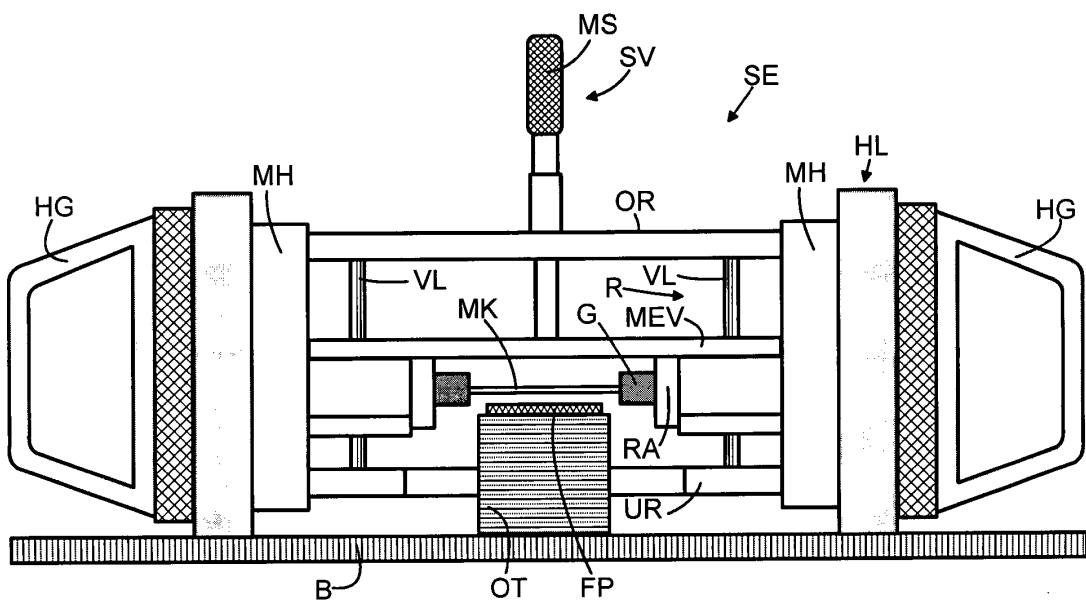


Fig.2

A2 Publication Bunsen Magazin

**Hochaufgelöste Detektion von Spurenelementen in Eisbohrkernen
mit einem neuen Laserablations-ICP-MS Verfahren**

M. Kriews, D. Dick, H. Reinhardt

Bunsen Magazin, 2005, No.6, 167-171.

Michael Kriews, Dorothee Dick und Heiko Reinhardt

Physikalische Chemie in der Polarforschung

- Hochaufgelöste Detektion von Spurenelementen in Eisbohrkernen mit einem neuen Laserablations-ICP-MS-Verfahren -

DAS ALFRED-WEGENER-INSTITUT FÜR POLAR- UND MEERESFORSCHUNG

Polar- und Meeresforschung sind zentrale Themen der Erdsystem- und globalen Umweltforschung. Die Stiftung Alfred-Wegener-Institut führt wissenschaftliche Projekte in der Arktis, Antarktis und den gemäßigten Breiten durch. Sie koordiniert die Polarforschung in Deutschland und stellt die für Polarexpeditionen erforderliche Ausrüstung und Logistik zur Verfügung.

1980 wurde das Institut in Bremerhaven als Stiftung des öffentlichen Rechts gegründet. Die Stiftung Alfred-Wegener-Institut für Polar- und Meeresforschung umfasst das Alfred-Wegener-Institut für Polar- und Meeresforschung in Bremerhaven, die Forschungsstelle Potsdam, die Biologische Anstalt Helgoland und die Wattenmeerstation Sylt. Sie ist Mitglied der Hermann von Helmholtz-Gemeinschaft Deutscher Forschungszentren (HGF) und beschäftigt rund 780 Mitarbeiterinnen und Mitarbeiter.

Ziel der wissenschaftlichen Arbeit ist ein besseres Verständnis der Beziehungen zwischen Ozean, Eis und Atmosphäre, der Tier- und Pflanzenwelt der Arktis und Antarktis sowie der Entwicklungsgeschichte der polaren Kontinente und Meere. Die Polargebiete der Erde zeichnen sich durch starke saisonale und kurz- bis langfristige Veränderungen der Umweltbedingungen aus. Diese wirken über die Atmosphäre, die Ozeane und die Vereisung intensiv auf die Entwicklung des weltweiten Klimas und auf die speziellen Ökosysteme im Meer und an Land ein. Die moderne Polar- und Meeresforschung trägt dazu bei globale Zusammenhänge aufzuklären und Informationen über unsere Umwelt zu liefern. Wissenschaftler verschiedener Disziplinen arbeiten am AWI gemeinsam und fachübergreifend an der Erforschung von Klima-, Bio- und Geosystemen, um das Gesamtsystem Erde besser zu verstehen.

Einer der Forschungsbereiche des Instituts ist der Fachbereich Geosystem, in dem die Prozesse unserer Erde erfasst und untersucht werden, die die Entwicklung des Klimas prägen. Diese spiegeln sich im Sedimentaufbau der Ozeane, in terrestrischen Ablagerungen und in den polaren Eiskappen wider. Letztere werden im Fachbereich Geowissenschaften von Wissenschaftlern der Sektion Glaziologie untersucht. Ein Teil der dort durchgeführten Arbeiten mit physikalisch-chemischen Hintergrund wird im Folgenden dargestellt.

DAS EIS DER POLARGEBIETE ALS KLIMAARCHIV

Das Eis der Polarregionen enthält Informationen über das Paläoklima und bietet für die Untersuchung der natürlichen Klimavariabilität eine wichtige Datenbasis. Die Untersuchung von Eisbohrkernen aus

M. Kriews, D. Dick, H. Reinhardt,
Alfred-Wegener-Institut für Polar- und Meeresforschung,
Am Handelshafen 12, 27570 Bremerhaven
Tel. 0471 / 48 31-14 20, Fax 0471 / 48 31-11 49
mkriews@awi-bremerhaven.de

polaren Eisschilden ermöglicht eine Rekonstruktion des Erdklimas von bis zu 850000 Jahre zurück in die Vergangenheit. Die atmosphärischen Spurenstoffe, die zusammen mit dem Niederschlag Jahr für Jahr auf den Eisschilden deponiert werden, unterliegen starken natürlichen Schwankungen sowohl auf großen (Wechsel zwischen einer Warm- und Kaltzeit), als auch auf kleinen Zeitskalen von Jahrzehnten bis hin zu saisonalen Variationen. Umweltbedingte Veränderungen können als chemische und physikalische Parameter in Eiskernen detektiert werden. Unter den chemischen Parametern interessieren auch die Spurenelemente. Die Analyse ihrer Signaturen im Eis geben Hinweise über Quellstärke und Transportmechanismen von Aerosolen der Paläoatmosphäre sowie über den Paläovulkanismus (Legrand und Delmas 1994, Boutron et al. 1994). Die Analysen aus den Eisbohrkernen liefern einen wichtigen Beitrag zum Verständnis der natürlichen Klimavariabilität.

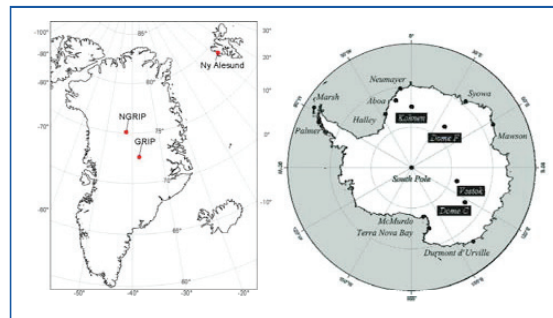


Abbildung 1: Einige Tiefbohrungen von Eiskernen auf Grönland und in der Antarktis in den Polarregionen.

Je nach zu untersuchendem Spurenstoff, Anion, Kation oder Molekül wird eine bestimmte Analysenmethode angewendet. Allen Methoden ist gemein, dass vor der eigentlichen Analyse hohe Ansprüche an die Probennahme, Probenvorbereitung und schließlich an die Analysetechnik gestellt werden. Durch die besondere geographische und meteorologische Lage der Polargebiete, ist der Einfluss durch luftgetragene Stäube und biogene Emissionen aus Böden und Pflanzen von den Kontinenten her stark vermindert. Die zu erwarteten Konzentrationen sind daher gering.

Die bisher bekannten Verfahren mit chemisch-physikalischen Methoden zur elementanalytischen Untersuchung liefern keine ausreichend hohe Auflösung der Messwerte, die den Erfordernissen der sehr dünnen Schichten im Eis großer Tiefen, wo die Jahresschichten aufgrund des hohen Drucks nur wenige Millimeter oder weniger dick sind, gerecht werden. Die Proben müssen in aufwändigen Präparationsverfahren aufgeschmolzen, angereichert und mit Chemikalien versetzt werden, um sie zu analysieren. Durch die relativ großen Volumina, die zur Analyse benötigt werden, verringert sich die Ortsauflösung und damit auch die

Zeitauflösung (Jahresschichten) der detektierten Spurenelemente in einer Eisprobe. Daneben ist eine auftretende Probe n e r s c h m u t z u n g durch Kontakt mit unterschiedlichen Flüssigkeiten, Gefäßen und Verfahrensvorrichtungen nicht auszuschließen.

Bisher mussten für eine Analyse etwa fünf Gramm Eis geschmolzen werden. Mit einem von uns neu entwickelten Eisanalyse-Verfahren (LA-ICP-MS = Laserablation induktiv gekoppelte Plasma-Massenspektrometrie) können geringste Elementgehalte (Ultrapurenbereich) in Eisbohrkernproben mit einer bisher nicht erreichten räumlichen und damit zeitlichen Auflösung gemessen werden. Auch in tiefen Eisschichten werden nur 1,5 mg gefrorene Probe benötigt, dies entspricht einer räumlichen Auflösung von ca. 150 µm.

GRUNDLAGEN

Die LA-ICP-MS ist eine vielseitig einsetzbare Methode für die Analyse von Feststoffen aus den unterschiedlichsten Bereichen, wie z.B. geologische, archäologische und biologische Proben. Die Vorteile der LA-ICP-MS gegenüber der Lösungsanalytik liegen in der erreichbaren räumlichen Auflösung und der reduzierten Kontaminationsgefahr sowie dem Wegfall einer Probenvorbereitung, wie sie für die Analyse vieler Probenlösungen notwendig ist, z.B. ein oxidativer Vollaufschluss. Einen Übersichtsartikel über die Feststoffanalyse mit LA-ICP-MS liefern Günther et al. (1999). Hoffmann et al. (1994) beschreiben die Untersuchung von Eichen, deren Jahresringe Informationen über verschiedene saisonale Wachstumsphasen und veränderte Umweltbedingungen enthalten.

EXPERIMENTELLES

Bei dem von uns entwickelten Analyseverfahren (Reinhardt et al. 2001) wird ein Laserablationssystem (Abb. 3) in Kombination mit einem Quadrupol-ICP-MS ELAN 6000 (PE-Sciex) oder einem Time-of Flight-ICP-MS (Analytik Jena) eingesetzt. Die Wellenlänge des Laserlichts, wie es mit einem Nd-YAG Laser (Indi 10-Spectra Physics) erzeugt wird, liegt im infraroten Bereich (1064 nm). Dort wird ein um 2-3 Größenordnungen höherer Absorptionskoeffizient gegenüber den UV-Wellenlängen, wie sie vielfach für die Analysen geologischer und biologischer Proben eingesetzt wird, erreicht (Abb. 2).

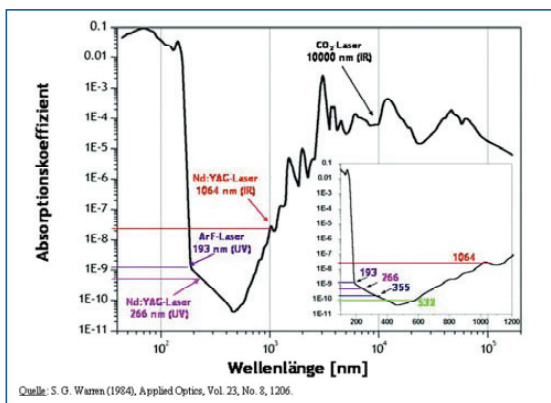


Abbildung 2: Absorptionskoeffizienten verschiedener Wellenlängen in Eis.

Zur Untersuchung der entlang der Kernachse geschnittenen und anschließend dekontaminierten gefrorenen Eisbohrkernstücke (Abb. 3), die eine Länge von bis zu 10 cm und eine Breite von 5 cm haben können, wird eine von uns entwickelte und patentierte, auf -45°C kühlbare Probenkammer (Abb. 4) eingesetzt (Kriewes et al. 2001). Abbildung 5 zeigt ein Foto der Laserablationseinheit zusammen mit der neu entwickelten Kryo-Probenkammer (Cryolac™).

Das Bearbeiten der Eisproben erfolgt in einem Kaltlabor bei -25°C unter einer Reinraumwerkbank mit speziellen Werkzeugen, die die Probe nicht kontaminieren. Die nachfolgenden Analysen werden in einem Reinraumlabor durchgeführt, um keine Verunreinigungen aus der Umgebungsluft in die Proben einzutragen.



Abbildung 3: Ein Eiskern wird dem Kernrohr nach der Bohrung entnommen. Der Durchmesser des Kerns ist ca. 10 cm und hat eine Länge von ca. 1-2 m.

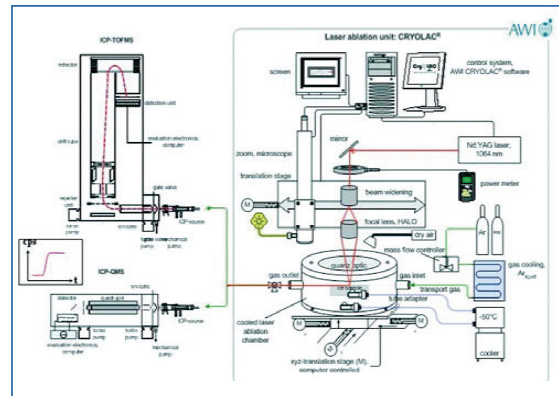


Abbildung 4: Experimenteller Aufbau zur Untersuchung von Spurenelementen in Eisproben mit der Laserablations-ICP-MS. In der Kryo-Probenkammer bleibt der feste Aggregatzustand des Eises während der Analyse erhalten.

Unter den optimierten Bedingungen für den Laser wurde ein Materialabtrag von 28µg/Puls ermittelt. Die Kalibration erfolgte nach einem speziellen Präparationsweg mittels eingefrorener, kommerziell erhältlicher Multielementlösungen. Durch dieses spezielle Verfahren (Reinhardt 2002) gelang es bei 6-fach Wiederholmessungen relative Standardabweichungen im Bereich von 3-6% zu erreichen. Es wurden umfangreiche Kalibrationsstudien

im Bereich von 10 ppt-100 ppb durchgeführt. Dabei konnten für die meisten untersuchten Elemente Korrelationskoeffizienten im Bereich von 0,9-1,0 erreicht werden (Abb. 7). Mit den hergestellten Eisstandards konnten erfolgreich quantitative Analysen für 62 relevante Isotope direkt aus dem Feststoff durchgeführt werden. Die erreichten Nachweisgrenzen liegen im Bereich von Nanogramm pro Kilogramm für die Elemente Na, Mg, Al, Zn, Cd, Pb, Seltene Erden, Th, U und von Mikrogramm pro Kilogramm für die Elemente Ca und Fe. Ein anschaulicher Vergleich, um welches Konzentrationslevel es hier geht, ist beispielsweise der Anstieg der Natriumkonzentration in einem 50-m-Schwimmbad bereits um 1 pg/g (ppt) Natrium, wenn nur ein einziges Salzkörnchen von 1 mm Kantenlänge hineingelangt. Selbstverständlich nach vollständiger Verteilung des aufgelösten Körnchens im gesamten Becken.

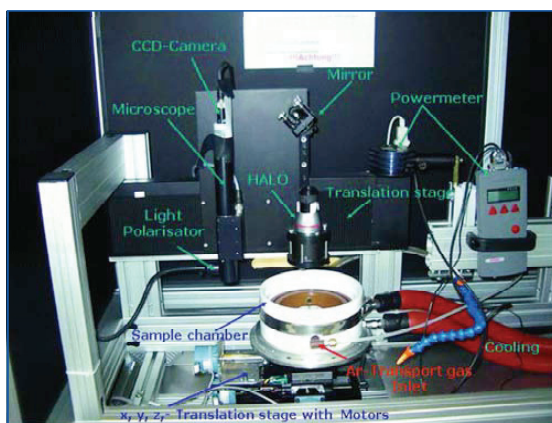


Abbildung 5: Anordnung der am AWI neu entwickelten und patentierten Kryo-Probenkammer in der Laserablationseinheit.

Um Variationen im Materialabtrag und deren Einfluß auf die Reproduzierbarkeit zu minimieren, wurden die Analyseergebnisse auf das Isotop ^{17}OH als ein Hauptbestandteil des Eises normiert. Die Validierung der Methode erfolgte durch die Analyse von gefrorenen Standardreferenzmaterialien, deren zertifizierte Werte mit $\pm 10\%$ wiedergefunden wurden (Reinhardt et al. 2003). Die räumliche und damit verbunden auch zeitliche Auflösung der von uns eingesetzten Methode ist neben der Art des eingesetzten ICP-MS-Geräts, begrenzt durch den Durchmesser des Laser-Einschusskraters. Dieser lag bei ca. 300 μm , wie Aufnahmen mit einem Kryo-Elektronenrastermikroskop zeigen. Die Struktur und Ausdehnung eines Lasereinschusskraters auf der Eisoberfläche sind in Abbildung 6 dargestellt. Mittlerweile ist es uns durch Modifikationen an der Laseroptik gelungen, den Strahldurchmesser auf ca. 150 μm zu reduzieren. Mit dieser neuen Laseroptik in Kombination mit der Polarisations-Mikroskop-Einheit soll in Zukunft neben der Zeitreihenanalyse auch untersucht werden wo im Eiskristallgitter deponierte Spurenstoffe angereichert und aufkonzentriert werden.

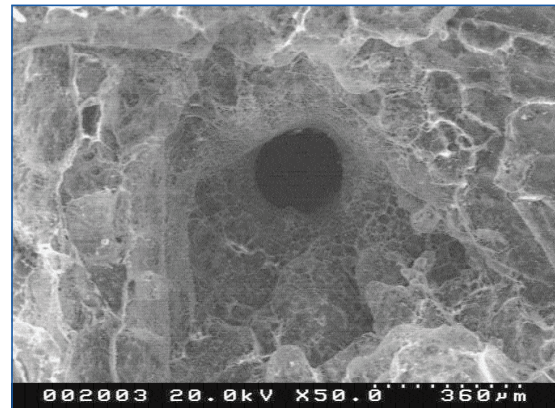


Abbildung 6: Kryo-Rasterelektronenmikroskopie-Aufnahme eines Laser-Einschusskraters auf einer Eisoberfläche nach einem Beschuss mit 50 Laserpulsen und einer Laserenergie von 306 mJ je Puls.

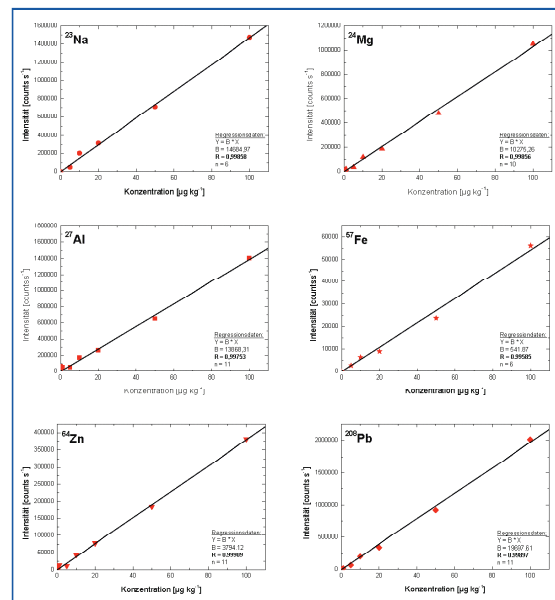


Abbildung 7: Beispiele zur Kalibration der LA-ICP-MS mit Eisstandards. Für viele Elemente werden lineare Kalibrationsgeraden in einem Konzentrationsbereich von 0-100 $\mu\text{g kg}^{-1}$ erhalten.

ANWENDUNGEN

1. ARKTIS-GRÖNLAND

Als ein Anwendungsbeispiel zur quantitativen Analyse, mit der von uns entwickelten Methode, zeigt Abb. 8 exemplarisch hochaufgelöste Signaturen für ausgewählte Elemente in einer

Eisprobe des grönländischen NGRIP-Eisbohrkerns aus einer Tiefe von 1826 m, aus der Zeit des letzten glazialen Maximums 24200 Jahre vor heute. Der NGRIP-Eisbohrkern wurde in der Mitte des grönländischen Festlandeis auf der Position 75,1° N, 42,3° W, auf einer Höhe von etwa 3000 m NN (über Meeresspiegel) gebohrt.

Aluminium ist bei unseren Untersuchungen ein Element, das für den Eintrag von Mineralstaub in das Inlandeis charakteristisch ist. Andere Elemente wie Natrium und Magnesium dienen als Indikatoren für den Eintrag von Seesalz aus marinen Quellen. Anthropogene Quellen für Schneehaltstoffe und Kontaminationen während des Bohrvorgangs lassen sich durch Elemente wie Blei, Cadmium und Zink charakterisieren. Durch die Möglichkeit mit dieser neuen Methode hochaufgelöste Multiementanalysen durchzuführen, können zeitlich hochaufgelöste Informationen über die chemische Zusammensetzung des Eises gewonnen werden. Aus den Konzentrationsverhältnissen verschiedener Elemente lassen sich zusätzlich Informationen über Quellgebiete und Quellstärke atmosphärischer Aerosole in der Paläoumwelt ermitteln.

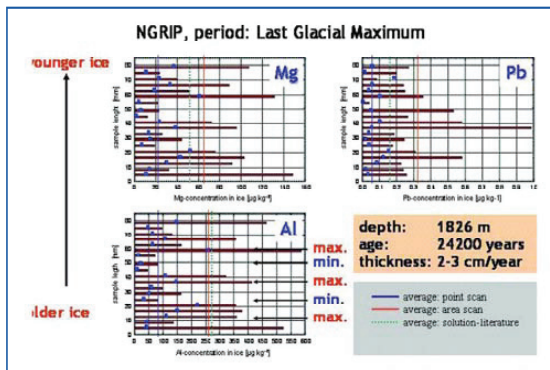


Abbildung 8: Raster für die Analyse der NGRIP-Probe aus dem letzten glazialen Maximum mit Punkt- und Flächenscans, sowie die gemessenen Konzentrationen für Al, Mg und Pb; die erreichte Ortsauflösung auf der Probenoberfläche beträgt 4 mm.

Bei dem in Abb.8 dargestellten Punktskan wird mit dem Laser nur auf einen Punkt des Eises geschossen und dort die Elementkonzentration gemessen. Da die chemische Zusammensetzung des Eises nicht homogen ist, bekommt man über das Verfahren des Flächenscans verlässlichere Aussagen über die mittlere Elementkonzentration im Eis entlang der Tiefen-/Zeitachse.

Die beobachteten Konzentrationsschwankungen entlang der Tiefen- / Zeitachse (Kernachse) können ein Hinweis auf saisonale Variationen des Aerosolgehalts in der Paläoatmosphäre sein. Wie in Abb.8 anhand der Minima und Maxima zu erkennen ist, lassen sich in der Tiefe von 1826 m noch einzelne Jahresschichten problemlos auflösen. Der Mittelwert über alle abgescannten Flächen ergibt einen Konzentrationswert, der recht gut mit dem Wert übereinstimmt, der traditionell nach Aufschmelzen der gesamten Probe mit der Lösungs-ICP-MS und der GF-AAS (Graphitrohr-Atomabsorptionsspektrometrie) sowie der Ionenchromatographie gemessen wurde (The Greenland Summit Ice Cores CD-ROM 1997).

2. ANTARKTIS-KOHNEN STATION

Ein weiteres Anwendungsbeispiel zeigt exemplarisch Ergebnisse der Untersuchung eines Eiskerns aus der Antarktis von der Kohnen Station. Sie befindet sich im Dronning Maud Land (DML) (Position: 75° 0.10' S, 0° 4.07' E) und ist eine von zwei Bohrlokalationen des EPICA-Projektes (European Project for Ice Coring in Antarctica). Sie befindet sich im atlantischen Sektor der Antarktis. Der an dieser Stelle gebohrte Kern wird bei Erreichen des Grundgesteins eine Länge von 2882 m haben und die Klimageschichte der ca. letzten 300000 Jahre widerspiegeln. Das hier untersuchte Kernstück (EDML 270) stammt aus 269 bis 270 m Tiefe (Dick 2003). Aufgrund eines Partikelhorizonts war dieser Kern sehr interessant. Er befand sich in 269,6 m Tiefe und hatte eine Ausdehnung von ca. 3 mm (Abb. 9). Das Alter wurde bisher nur über das Dielectric Profiling (DEP) ermittelt. Demnach hat das Eis in der Tiefe 269,6 m ein Alter von ca. 3500 Jahren. Untersuchungen dieses Kernabschnittes mit Hilfe der Ionenchromatographie (IC) und Messungen der elektrische Leitfähigkeit (ECM = Electric Conductivity Measurement) lieferten keine charakteristischen Messsignale in dieser Schicht.

Um das 1 m lange Kernstück analysieren zu können, musste es an die Dimensionen der Probenkammer angepasst werden. Dazu wurde es in 13 Stücke gesägt. Auf jeder Probe wurde alle 4 mm eine Linie abgelasert, auf der Probe im Bereich des Staubhorizonts sogar alle 3 mm. Das ergibt eine Gesamtzahl von 233 abgescannten Linien, auf denen jeweils 62 Isotope analysiert wurden.

Exemplarisch sind in Abbildung 10 die Konzentrationsverläufe für die Elemente Na, Al, S, Ni und Pt dargestellt. Deutlich ist die Variabilität der Konzentrationen der Elemente innerhalb des untersuchten Zeitraums von ca. 15 Jahren zu sehen. Ein besonders deutlicher Anstieg der Elementkonzentrationen innerhalb des Staubhorizonts bei 269,6 m ist zu erkennen. Über die Konzentrationsverhältnisse verschiedener Elemente soll in der weiteren Auswertung versucht werden herauszufinden, ob es sich um eine vulkanische oder andere Quelle für den Staubhorizont handelt.

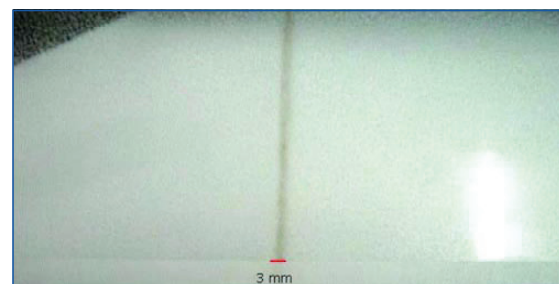


Abbildung 9: Partikelhorizont in der Eiskernprobe EDML 270. Tiefe: 269.6 m, Alter: ca. 3500 Jahre

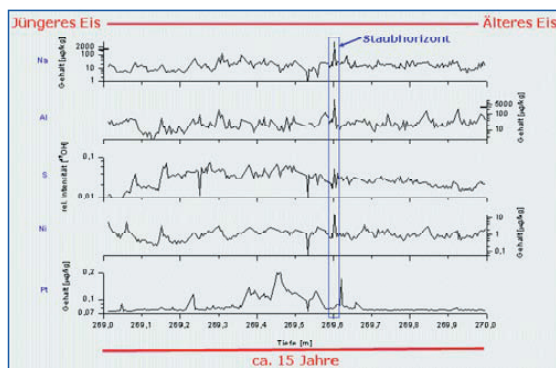


Abbildung 10: Elementkonzentrationen (Na, Al, S, Ni, Pt) entlang eines 1 m langen Kernsegments in der Eiskernprobe EDML 270. Tiefe: 269-270 m, Alter: ca. 3500 Jahre

ZUSAMMENFASSUNG

Im Rahmen der Arbeiten zum Forschungs- und Entwicklungsprogramm des Instituts sind interdisziplinären Arbeiten erforderlich. In einem Teilaspekt zur Untersuchung der Klimavariabilität der Paläoatmosphäre kommen auch physikalisch-chemische Methoden zum Einsatz. Die Entwicklung eines neuen Analyseverfahrens und seine Anwendung zur Untersuchung von Spurenelementen in Eisbohrkernen wurde vorgestellt. Es konnte im Verlauf der Entwicklungsarbeiten gezeigt werden, dass Vorteile der neuen Methode gegenüber der Lösungsanalytik erreicht werden konnten. Diese sind z.B. ein reduziertes Kontaminationsrisiko, weniger Probenvorbereitungsschritte sowie eine höhere räumlich/zeitliche Auflösung der Verteilung der chemischen Elemente im Eis. Das nicht ablatierte Probenmaterial wird während der Analyse nicht zerstört und ist weiteren Analysemethoden zugänglich.

Mit dieser neuen, sehr nachweisstarken und hochauflösenden Methode sind von uns inzwischen auch schon Untersuchungen an tiefgefrorenen biologischen Materialien durchgeführt worden, um die räumliche Verteilung von Spurenelementen in Gewebeproben zu charakterisieren. Diese Fragestellung spielt eine entscheidende Rolle in der Tumorforschung sowie im Bereich des Materialabriebs bei Implantationen künstlicher Gelenke. Ein weiteres Anwendungsgebiet konnte ebenfalls erfolgreich bearbeitet werden. Hierbei handelte es sich um die Untersuchung von Spurenelementen in gefrorenen Sedimentkernen des Sakrower Sees bei Potsdam.

EPILOG

Die Physikalische Chemie ist ein Fachgebiet, welches wesentliche Beiträge zum besseren Verständnis komplexer Systeme, wie z.B. die Beziehungen zwischen Ozean, Eis und Atmosphäre, der Tier- und Pflanzenwelt der Arktis und Antarktis sowie der Entwicklungsgeschichte der polaren Kontinente und Meere liefert.

LITERATUR

Boutron C. F., Candelone J.-P., Hong S. (1994): *Past and recent changes in the large-scale tropospheric cycles of lead and other heavy metals as documented in Antarctic and Greenland snow and ice: A review*, *Geochim. Cosmochim. Ac.*, 58, 15, 3217-3225.

Dick D. (2003): *Hochauflösende Analyse der chemischen Zusammensetzung des antarktischen Eisbohrkerns EDML 270 und Charakterisierung des eingeschlossenen Partikelhorizonts mittels Laserablations-ICP-MS und Kryo-Rasterelektronenmikroskopie*, Diplomarbeit der Europa Fachhochschule Fresenius in Idstein-Taunus.

Günther D., Jackson S. E., Longerich H. P. (1999): *Laser ablation and arc/spark solid sample introduction into inductively coupled plasma mass spectrometers*, *Spectrochim. Acta B*, 54, 381-409.

Hoffmann E., Lüdke C., Scholze H., Stephanowitz H. (1994): *Analytical investigations of tree rings by laser ablation ICP-MS*, *Fresen. J. Anal. Chem.*, 350, 253-259.

Kriews M., Reinhardt H., Dunker E., Beninga I., Hoffmann E., Lüdke C. (2001): *Elementanalyseverfahren zur Detektion von Spurenelementen und Anordnung zu seiner Durchführung*, Deutsches Patent- und Markenamt, DE 199 34 561 A1, München.

Legrand M., Delmas, R. (1994): *Ice core chemistry: implications for the past atmosphere*, In: *European Research Course on Atmospheres, Topics in Atmospheric and Interstellar Physics and Chemistry*, C.F. Boutron (Hrsg.), Les Editions de Physique, Les Ulis, France.

Reinhardt H., Kriews M., Miller H., Schrems O., Lüdke C., Hoffmann E., Skole J. (2001): *Laser ablation inductively coupled plasma mass spectrometry: a new tool for trace element analysis in ice cores*, *Fresen. J. Anal. Chem.*, 370, 5, 629-636.

Reinhardt H. (2002): *Entwicklung und Anwendung eines Laserablations-ICP-MS-Verfahrens zur Multielementanalyse von atmosphärischen Einträgen in Eisbohrkernen*, Reports on Polar Research 414, Alfred Wegener Institut for Polar and Marine Research, Bremerhaven.

Reinhardt H., Kriews M., Miller H., Lüdke C., Hoffmann E., Skole J. (2003): *Application of LA-ICP-MS in polar ice core studies*, *Anal. Bioanal. Chem.*, 375, 1265-1275.

The Greenland Summit ice cores CD-ROM (1997): *File name: gripion.dat*, Available from the National Snow And Ice Data Center, University of Colorado at Boulder, and the world data center-A for paleoclimatology, National Geophysical Data Center, Boulder, Colorado.

A3 Element concentrations along EDML meter 270

Table A 1: Element concentration with SD in $\mu\text{g kg}^{-1}$ in EDML meter 270 (269–270 m depth) obtained by LA-ICP-Q-MS. Only values exceeding the DL and the lowest concentrated standard are shown.

depth/m	Na	SD	Mg	SD	Al	SD	K	SD	Mn	SD	Fe	SD	Co	SD	Ni	SD	Zn	SD	Sr	SD	Cd	SD	Ba	SD	La	SD	Ce	SD	Pb	SD	Bi	SD
269.008	33.4	16.2	57.6	4.9	90.0	21.0	1.11	1.04	0.917	0.262	17.0	2.6	0.024	0.007	1.321	0.840	0.119	0.119	0.025	0.009			0.119	0.119			0.006	0.003	0.438	0.013	0.026	0.013
269.012	38.5	13.4	42.2	7.8	48.6	23.9	0.77	0.20	0.187	0.131	5.52	0.80	0.021	0.010	0.704	0.470	0.076	0.030					0.076	0.030			0.006	0.004	0.482	0.133	0.019	0.133
269.016	15.6	10.4	33.8	3.8	39.6	2.4	0.65	0.23	0.277	0.057	4.38	1.65	0.012	0.004	0.535	0.153	0.043	0.015					0.043	0.015			0.006	0.004	0.340	0.004	0.012	0.004
269.02	14.2	5.77	17.1	1.7	28.3	6.4			0.111	0.037	2.41	0.80	0.009	0.001	0.332	0.083	0.068	0.005					0.068	0.005					0.231	0.003	0.006	0.003
269.024	7.95	3.21	13.8	2.3	17.9	1.8			0.077	0.062	1.25	1.24	0.009	0.001	0.267	0.095	0.038	0.028					0.038	0.028			0.006	0.004	0.090	0.003	0.153	0.001
269.028	5.70	1.62	12.8	16.7	14.6	30.1			0.091	0.131	2.15	0.98	0.009	0.014	0.202	0.173	0.014	0.009					0.014	0.009			0.005	0.000	0.075	0.000	0.075	0.000
269.032	4.42	1.01	10.6	1.6	15.3	27.5			0.155	0.082	1.58	0.53	0.009	0.014	0.187	0.202	0.012	0.016					0.012	0.016			0.005	0.002	0.175	0.001	0.175	0.001
269.036	4.63	2.55	9.77	2.35	27.2	14.0			0.099	0.058	1.19	0.26	0.017	0.021	0.183	0.233	0.019	0.009					0.019	0.009			0.006	0.011	0.204	0.001	0.204	0.001
269.04	4.22	1.27	7.70	2.25	19.6	3.5			0.080	0.050	1.79	0.56	0.007	0.010	0.355	0.120	0.016	0.004					0.016	0.004			0.006	0.011	0.204	0.001	0.204	0.001
269.044	2.69	0.64	4.12	1.09	7.05	1.08	17.4	6.6	0.078	0.009	1.27	1.13	0.007	0.013	0.259	0.138	0.044	0.017					0.044	0.017			0.006	0.006	0.173	0.001	0.173	0.001
269.048	4.12	1.09	7.05	1.08	17.4	6.6			0.102	0.180	1.55	1.01	0.009	0.008	0.529	0.115	0.017	0.003					0.017	0.003			0.005	0.002	0.175	0.001	0.175	0.001
269.052	4.65	1.65	6.03	2.70	16.5	9.1			0.156	0.041	2.45	0.56	0.009	0.008	0.998	0.526	0.028	0.002					0.028	0.002			0.005	0.002	0.232	0.001	0.232	0.001
269.056	3.54	0.98	5.73	1.11	24.6	18.4			0.117	0.011	2.18	0.92	0.007	0.010	0.355	0.120	0.023	0.015					0.023	0.015			0.010	0.006	0.807	0.002	0.807	0.002
269.06	3.09	0.71	4.35	0.96	18.0	11.9			0.158	0.195	3.86	1.35	0.023	0.015	0.813	0.741	0.044	0.017					0.044	0.017			0.010	0.006	0.170	0.001	0.170	0.001
269.064	1.84	0.27	3.90	0.70	14.6	5.4			0.099	0.009	0.58	0.19	0.009	0.005	0.289	0.124	0.066	0.013					0.066	0.013			0.006	0.001	0.463	0.000	0.463	0.000
269.07	6.70	1.60	3.97	1.22	15.8	5.6	1.23	0.37	0.092	0.032	0.65	0.28	0.010	0.005	0.257	0.333	0.062	0.010					0.062	0.010			0.006	0.001	0.986	0.001	0.986	0.001
269.084	8.00	0.94	3.05	0.34	7.13	1.86	0.83	0.06	0.087	0.032	0.60	0.43	0.007	0.004	0.242	0.091	0.062	0.010					0.062	0.010			0.009	0.001	0.616	0.001	0.616	0.001
269.091	8.00	0.94	3.05	0.34	7.13	1.86	0.83	0.06	0.087	0.032	0.60	0.43	0.007	0.004	0.242	0.091	0.062	0.010					0.062	0.010			0.009	0.001	0.616	0.001	0.616	0.001
269.095	8.67	1.33	3.17	0.63	4.70	3.58	0.89	0.17	0.109	0.032	0.62	0.33	0.011	0.003	0.281	0.080	0.060	0.025					0.060	0.025			0.007	0.003	0.536	0.001	0.536	0.001
269.099	11.3	0.3	2.79	0.43	4.65	0.73	1.51	0.19	0.109	0.032	0.62	0.33	0.011	0.003	0.281	0.080	0.060	0.025					0.060	0.025			0.007	0.003	0.536	0.001	0.536	0.001
269.103	9.76	0.35	3.14	0.66	3.79	1.04	1.03	0.09	0.109	0.032	0.62	0.33	0.011	0.003	0.281	0.080	0.060	0.025					0.060	0.025			0.012	0.006	0.439	0.000	0.439	0.000
269.107	6.70	1.60	3.97	1.22	15.8	5.6	1.23	0.37	0.092	0.032	0.65	0.28	0.010	0.005	0.257	0.333	0.062	0.010					0.062	0.010			0.006	0.001	0.364	0.001	0.364	0.001
269.111	7.95	2.24	1.59	0.58	3.19	2.51	0.92	0.21	0.078	0.019	0.43	0.06	0.007	0.004	0.242	0.091	0.043	0.006					0.043	0.006			0.004	0.001	0.249	0.000	0.249	0.000
269.115	2.87	0.87	0.90	0.18	3.39	0.97	0.64	0.17	0.115	0.095	0.54	0.05	0.008	0.007	0.179	0.040	0.87	0.22					0.087	0.22			0.012	0.006	0.142	0.000	0.142	0.000
269.119	3.34	0.48	0.83	0.13	4.42	2.08	0.58	0.12	0.115	0.095	0.54	0.05	0.008	0.007	0.179	0.040	0.87	0.22					0.087	0.22			0.012	0.006	0.142	0.000	0.142	0.000
269.123	4.08	1.44	0.81	0.36	3.07	1.46	0.62	0.17	0.115	0.095	0.54	0.05	0.008	0.007	0.179	0.040	0.87	0.22					0.087	0.22			0.012	0.006	0.142	0.000	0.142	0.000
269.127	3.40	0.69	0.81	0.36	2.31	0.66	0.58	0.12	0.115	0.095	0.54	0.05	0.008	0.007	0.179	0.040	0.87	0.22					0.087	0.22			0.012	0.006	0.142	0.000	0.142	0.000
269.131	3.81	0.54	0.93	0.32	3.32	0.32	0.62	0.17	0.115	0.095	0.54	0.05	0.008	0.007	0.179	0.040	0.87	0.22					0.087	0.22			0.012	0.006	0.142	0.000	0.142	0.000
269.135	4.52	1.06	1.14	0.37	2.45	1.71	0.64	0.17	0.115	0.095	0.54	0.05	0.008	0.007	0.179	0.040	0.87	0.22					0.087	0.22			0.012	0.006	0.142	0.000	0.142	0.000
269.139	3.22	0.87	0.96	0.27	2.81	1.13	0.58	0.11	0.115	0.095	0.54	0.05	0.008	0.007	0.179	0.040	0.87	0.22					0.087	0.22			0.012	0.006	0.142	0.000	0.142	0.000
269.143	3.84	1.27	1.49	0.91	1.98	0.57	0.58	0.11	0.115	0.095	0.54	0.05	0.008	0.007	0.179	0.040	0.87	0.22					0.087	0.22			0.012	0.006	0.142	0.000	0.142	0.000
269.161	5.81	2.42	3.06	1.32	9.63	1.50	0.58	0.11	0.077	0.017	1.86	1.00	0.008	0.011	0.248	0.078	0.046	0.018					0.046	0.018			0.010	0.004	0.125	0.001	0.125	0.001
269.165	10.5	0.9	4.34	1.40	10.1	2.2	1.01	0.28	0.179	0.138	5.01	1.45	0.014	0.005	0.328	0.124	0.091	0.042					0.091	0.042			0.010	0.004	0.118	0.000	0.118	0.000
269.169	5.43	0.89	1.07	0.23	6.70	1.75	0.98	0.23	0.179	0.138	5.01	1.45	0.014	0.005	0.328	0.124	0.091	0.042					0.091	0.042			0.010	0.004	0.118	0.000	0.118	0.000
269.173	2.74	0.75	0.50	0.13	3.02	1.17	0.62	0.17	0.179	0.138	3.96	1.31	0.012	0.007	0.118	0.030	0.042	0.021					0.042	0.021			0.012	0.006	0.094	0.001	0.094	0.001
269.177	2.54	0.17	0.59	0.29	3.10	0.69	0.98	0.23	0.179	0.138	3.96	1.31	0.012	0.007	0.118	0.030	0.042	0.021					0.042	0.021			0.012	0.006	0.094	0.001	0.094	0.001
269.181	3.66	1.30	1.22	0.25	3.34	0.86	0.62	0.17	0.179	0.138	1.13	0.60	0.008	0.005	0.144	0.127	0.065	0.034					0.065	0.034			0.009	0.001	0.093	0.001	0.093	0.001
269.185	2.62	0.54	0.62	0.16	4.86	1.76	0.62	0.17	0.179	0.138	1.13	0.60	0.008	0.005	0.144	0.127	0.065	0.034					0.065	0.034			0.009	0.001	0.093	0.001	0.093	0.001
269.189	3.35	0.66	1.04	0.46	2.64	1.21	0.62	0.17	0.179	0.138	1.13	0.60	0.008	0.005	0.144	0.127	0.065	0.034					0.065	0.034			0.009	0.001	0.093	0.001	0.093	0.001
269.193	1.90	0.40	0.75	0.13	2.63	1.07	0.97	0.19	0.179	0.138	0.97	0.19	0.019	0.019	0.193	0.061	0.042	0.026					0.042	0.026			0.019	0.001	0.168	0.001	0.168	0.001
269.197	2.62	1.47	1.00	0.38	3.80	1.29	0.57	0.22	0.179	0.138	1.27	0.53	0.009	0.003	0.093	0.053	0.059	0.027					0.059	0.027			0.019	0.001	0.219	0.001	0.219	0.001
269.201	3.16	1.52	1.02	0.24	4.43	2.18	0.57	0.22	0.179	0.138	1.11	0.38	0.007	0.003	0.155																	

Table A 1: Element concentration with SD in $\mu\text{g kg}^{-1}$ in EDM meter 270 (269–270 m depth) obtained by LA-ICP-Q-MS. Only values exceeding the DL and the lowest concentrated standard are shown (continued).

depth/m	Na	Mg	Al	K	Mn	Fe	Co	Ni	Zn	Sr	Cd	Ba	La	Ce	Pb	Bi	SD
269.258	12.2	3.20	8.39	1.13	0.078	2.74	1.04	0.018	0.154	0.029	0.031	0.111	0.048	0.004	0.339	0.001	
269.262	13.2	4.26	14.4	1.41	0.103	3.13	0.95	0.014	0.196	0.039	0.031	0.114	0.046	0.005	0.366	0.001	
269.266	11.9	1.7	9.20	1.75	0.114	2.54	1.35	0.020	0.153	0.077	0.031	0.018	0.092	0.011	0.378	0.001	
269.27	14.9	3.3	2.92	0.97	0.137	4.83	0.34	0.013	0.135	0.021	0.034	0.043	0.165	0.004	0.383	0.001	
269.274	12.1	1.3	4.15	2.06	0.134	3.05	1.09	0.016	0.206	0.032	0.036	0.009	0.138	0.016	0.416	0.003	
269.278	14.4	0.9	4.97	2.61	0.185	5.24	1.00	0.021	0.342	0.100	0.060	0.042	0.092	0.039	0.691	0.002	
269.282	12.3	2.4	4.36	0.98	0.144	4.05	1.88	0.026	0.228	0.065	0.047	0.032	0.094	0.045	0.560	0.000	
269.286	12.7	1.7	4.75	0.94	0.210	4.63	0.62	0.034	0.339	0.094	0.067	0.026	0.154	0.074	0.607	0.002	
269.289	21.9	3.3	9.50	2.93	0.243	10.1	0.86	0.042	0.343	0.162	0.060	0.018	0.163	0.039	0.006	0.013	0.716
269.312	5.28	0.92	2.84	0.61	0.113	1.12	0.81	0.043	0.298	0.205	0.047	0.016	0.199	0.040	0.008	0.005	0.699
269.316	4.69	7.21	1.12	0.26	0.093	0.088	0.81	0.009	0.298	0.205	0.047	0.016	0.199	0.040	0.008	0.005	0.699
269.32	6.60	1.63	3.20	2.13			1.61	0.009	0.228	0.065	0.047	0.032	0.094	0.045	0.470	0.002	
269.324	14.6	6.0	1.42	0.44			1.53	0.017	0.130	0.049	0.067	0.026	0.154	0.074	0.367	0.002	
269.328	4.81	1.45	7.80	1.20	0.215	1.17	0.90	0.017	0.130	0.049	0.067	0.026	0.154	0.074	0.367	0.002	
269.332	3.29	6.00	1.04	0.28			0.48	0.007	0.178	0.057	0.081	0.004	0.043	0.146	0.006	0.002	0.728
269.336	5.19	0.95	2.35	3.53			0.94	0.038	0.208	0.030	0.034	0.012	0.447	0.235	0.005	0.005	0.596
269.34	6.96	1.63	3.74	2.53			0.12	0.017	0.154	0.026	0.036	0.008	0.381	0.120	0.005	0.002	0.349
269.344	6.50	0.90	3.14	4.36			1.01	0.016	0.178	0.057	0.081	0.004	0.043	0.146	0.006	0.001	0.613
269.348	8.38	1.86	4.02	3.40	0.093	0.028	1.25	0.035	0.178	0.057	0.081	0.004	0.043	0.146	0.006	0.001	0.613
269.352	9.34	6.17	5.56	4.32	0.23	0.23	1.15	0.035	0.208	0.030	0.034	0.012	0.447	0.235	0.005	0.002	0.349
269.356	13.3	1.3	5.47	1.72	0.05	0.63	0.88	0.024	0.247	0.053	0.078	0.030	0.344	0.016	0.015	0.007	0.857
269.385	25.5	14.0	7.24	1.10	0.108	0.028	1.35	0.035	0.279	0.021	0.074	0.017	0.039	0.045	0.007	0.003	1.202
269.387	40.6	10.5	23.4	3.38	0.126	0.174	7.75	0.044	0.227	0.069	0.083	0.018	0.065	0.017	0.008	0.002	1.290
269.395	14.5	5.1	14.9	1.14	0.124	5.23	1.12	0.044	0.304	0.095	0.092	0.032	0.304	0.028	0.005	0.003	1.230
269.395	13.5	1.8	9.69	2.47	0.079	10.1	0.91	0.019	0.300	0.095	0.061	0.019	0.044	0.077	0.006	0.010	1.462
269.395	13.5	1.8	8.84	5.46	0.101	0.067	4.00	0.047	0.247	0.137	0.074	0.017	0.052	0.012	0.007	0.003	1.814
269.395	15.3	6.5	13.2	4.1	0.090	0.023	3.54	0.039	0.176	0.141	0.051	0.009	0.047	0.039	0.008	0.003	1.396
269.403	8.21	7.50	6.26	0.83	0.126	0.150	2.43	0.037	0.353	0.435	0.095	0.026	0.028	0.034	0.008	0.030	1.347
269.407	8.43	2.22	4.49	4.40	0.080	0.139	1.54	0.035	0.401	0.135	0.084	0.038	0.047	0.016	0.011	0.004	1.944
269.411	8.86	1.25	5.43	14.6	0.17	1.17	2.47	0.017	0.237	0.101	0.049	0.024	0.024	0.449	0.007	0.003	2.544
269.415	8.49	2.26	10.7	4.5	0.125	0.130	2.56	0.048	0.191	0.176	0.073	0.024	0.034	0.031	0.010	0.003	2.693
269.419	10.5	7.5	5.38	9.25	0.15	0.177	2.41	0.024	0.198	0.131	0.101	0.038	0.047	0.035	0.008	0.009	2.001
269.423	12.3	6.2	13.0	3.09	0.077	0.079	2.80	0.058	0.214	0.086	0.084	0.029	0.034	0.006	0.008	0.002	1.345
269.425	7.79	0.95	1.08	0.58	0.139	1.54	1.92	0.037	0.166	0.080	0.038	0.006	0.034	0.201	0.007	0.001	1.324
269.431	9.11	1.87	10.6	9.1	0.093	1.348	1.50	0.037	0.188	0.042	0.067	0.016	0.044	0.018	0.005	0.003	1.246
269.435	12.9	1.0	4.55	5.51	0.093	0.056	2.09	0.021	0.206	0.107	0.066	0.022	0.039	0.010	0.009	0.011	1.301
269.439	15.3	5.0	15.2	18.6	0.126	0.139	4.39	0.055	0.167	0.157	0.054	0.020	0.052	0.020	0.007	0.004	1.301
269.453	58.0	9.8	180.6	40.6	0.437	2.04	1.8	0.096	0.456	0.072	0.184	0.071	0.127	0.025	0.052	0.012	1.840
269.457	17.0	5.4	32.3	19.2	0.152	0.111	6.66	0.040	0.212	0.044	0.066	0.017	0.047	0.028	0.013	0.201	0.834
269.461	18.6	3.1	16.2	4.4	0.183	0.144	5.59	0.017	0.243	0.060	0.063	0.010	0.078	0.023	0.012	0.107	1.057
269.465	16.8	7.0	13.9	4.0	0.118	0.043	5.79	0.015	0.169	0.009	0.056	0.010	0.101	0.021	0.009	0.005	0.695
269.469	14.2	1.9	31.4	29.3	0.125	0.064	6.95	0.027	0.121	0.037	0.052	0.013	0.096	0.052	0.010	0.004	0.581
269.473	6.18	1.10	4.78	18.3	0.27	2.66	1.42	0.010	0.126	0.064	0.039	0.015	0.034	0.024	0.007	0.004	0.462
269.475	7.78	3.54	1.77	1.29	0.085	0.56	3.70	0.011	0.189	0.052	0.037	0.010	0.054	0.025	0.007	0.000	0.674
269.481	11.7	8.5	2.46	0.86	0.113	1.15	1.29	0.018	0.189	0.052	0.037	0.010	0.054	0.025	0.006	0.001	0.657
269.485	7.89	2.02	11.3	20.2	0.081	0.078	2.18	0.013	0.198	0.056	0.030	0.010	0.028	0.011	0.005	0.001	0.818
269.489	6.54	0.87	2.35	0.56	0.148	0.112	3.96	0.017	0.143	0.067	0.039	0.013	0.067	0.024	0.006	0.004	0.365
269.493	6.31	2.78	2.03	4.11	0.22	1.73	2.26	0.015	0.119	0.048	0.036	0.006	0.036	0.006	0.005	0.002	0.775
269.497	10.9	5.2	4.06	0.78	0.083	0.100	2.90	0.020	0.219	0.112	0.043	0.004	0.031	0.013	0.005	0.002	0.823
269.501	7.56	1.18	4.00	2.07	0.144	0.062	2.09	0.025	0.203	0.043	0.058	0.017	0.057	0.024	0.007	0.002	0.712
269.505	13.4	2.0	8.03	1.29	0.411	0.134	4.39	0.042	0.314	0.088	0.077	0.013	0.036	0.023	0.012	0.002	1.246
269.509	12.1	11.9	4.98	2.53	0.250	0.087	3.47	0.043	0.242	0.078	0.074	0.024	0.094	0.030	0.008	0.002	1.122
269.513	6.73	8.70	2.23	0.56	0.179	0.184	2.78	0.031	0.224	0.078	0.047	0.009	0.023	0.003	0.008	0.003	0.515

Table A 1: Element concentration with SD in $\mu\text{g kg}^{-1}$ in EDMT meter 270 (269–270 m depth) obtained by LA-ICP-Q-MS. Only values exceeding the DL and the lowest concentrated standard are shown (continued). The particle horizon is grey shaded.

depth/m	Na	Mg	Al	Si	K	Mn	Fe	Co	Ni	Zn	Sr	Cd	Ba	La	Ce	Pb	SD	Bi	SD	
269.536	3.66	1.91	1.07	0.29	1.19	1.7	1.30	0.78	0.008	0.005	0.034	0.006	0.110	0.010	0.004	0.006	0.001	0.677	0.000	
269.54	2.79	0.99	1.27	0.41	11.0	2.8	1.27	1.01	0.031	0.011	0.040	0.014	0.166	0.056	0.006	0.001	0.672	0.001		
269.544	2.63	0.32	1.43	0.47	11.1	1.1	2.04	0.73	0.009	0.002	0.037	0.010	0.115	0.304	0.015	0.002	0.672	0.000		
269.548	4.67	1.83	2.26	0.36	8.64	3.61	1.93	0.84	0.028	0.008	0.040	0.005	0.090	0.023	0.006	0.002	0.672	0.002		
269.552	6.77	1.35	2.34	2.15	9.30	2.42	1.33	0.33	0.025	0.012	0.080	0.007	0.314	0.073	0.006	0.002	1.122	0.000		
269.556	4.76	0.81	2.13	0.67	10.5	6.3	3.36	1.03	0.017	0.022	0.074	0.013	0.161	0.095	0.010	0.002	1.107	0.005	0.004	
269.564	9.62	2.18	4.24	2.42	11.3	7.4	3.74	0.86	0.015	0.023	0.071	0.007	0.272	0.055	0.011	0.005	2.134	0.002		
269.568	10.9	2.1	3.00	2.61	18.4	11.4	2.73	0.92	0.061	0.056	0.101	0.007	0.324	0.434	0.001	0.001	1.687	0.003		
269.5845	11.5	2.3	3.59	0.92	32.1	19.6	1.07	0.43	0.027	0.018	0.059	0.014	0.100	0.016	0.011	0.005	1.642	0.001		
269.5875	10.2	7.8	2.85	0.55	19.4	18.1	1.84	0.75	0.015	0.003	0.044	0.004	0.061	0.010	0.002	0.009	0.007	0.555	0.012	
269.5905	6.01	1.28	2.76	0.47	13.0	1.5	0.96	0.16	0.007	0.004	0.042	0.006	0.043	0.010	0.008	0.002	0.419	0.000		
269.5935	6.08	1.68	2.13	0.26	8.50	13.7	0.85	0.31	0.007	0.004	0.032	0.013	0.060	0.013	0.005	0.002	0.472	0.001		
269.5965	6.02	1.68	2.10	0.67	9.97	3.38	1.61	0.79	0.010	0.003	0.053	0.015	0.101	1.711	0.006	0.003	0.370	0.002		
269.6	79.3	12.8	78.2	5.5	311.4	35.9	48.1	3.7	0.272	0.034	0.459	0.190	0.138	0.017	0.914	0.166	0.026	0.020	0.006	0.006
269.6005	364	61	300	15	1242	58	205	12	1.215	0.084	0.484	0.164	2.729	0.164	0.888	0.004	0.381	0.031	0.554	0.001
269.603	16.0	7.3	8.62	2.80	27.21	5.85	5.20	2.26	0.028	0.012	0.063	0.247	0.117	0.029	0.018	0.003	0.013	0.005	0.674	0.000
269.606	9.21	2.84	2.27	0.92	6.80	0.85	1.08	0.57	0.013	0.002	0.043	0.017	0.074	0.049	0.015	0.012	0.007	0.002	0.623	0.002
269.609	13.2	9.1	5.56	2.57	10.8	3.0	1.26	0.92	0.011	0.017	0.065	0.331	0.133	0.053	0.012	0.015	0.009	0.003	1.003	0.002
269.612	10.4	5.2	2.83	1.66	5.83	2.34	1.05	0.34	0.019	0.011	0.055	0.255	0.160	0.054	0.011	0.005	0.008	0.003	0.984	0.002
269.615	13.3	2.6	3.31	0.82	7.09	0.97	1.57	0.24	0.009	0.007	0.062	0.007	0.147	0.053	0.011	0.005	0.008	0.003	0.984	0.002
269.618	9.78	2.94	3.27	0.22	6.77	2.07	1.21	0.32	0.013	0.003	0.076	0.119	0.266	0.057	0.013	0.003	0.007	0.001	1.030	0.001
269.621	11.0	3.7	3.31	1.36	6.18	0.29	1.10	0.28	0.011	0.006	0.098	0.249	0.115	0.164	0.009	0.002	0.006	0.002	0.909	0.000
269.624	8.82	2.93	2.70	0.63	6.25	1.47	1.25	0.10	0.015	0.026	0.127	0.250	0.147	0.012	0.057	0.005	0.120	0.042	0.891	0.000
269.627	9.42	0.50	3.26	0.67	7.10	2.56	1.02	0.23	0.016	0.010	0.580	0.903	0.174	0.014	0.058	0.005	0.039	0.014	0.909	0.001
269.63	3.76	1.21	1.87	3.23	0.72	5.14	1.17	0.27	0.025	0.008	0.044	0.187	0.144	0.054	0.044	0.012	0.026	0.001	1.31	0.050
269.633	7.18	1.74	1.85	0.35	11.2	2.6	1.22	0.44	0.010	0.006	0.076	0.646	0.204	0.086	0.071	0.036	0.049	0.035	0.117	0.052
269.636	12.1	2.2	4.31	0.33	16.6	5.9	1.58	0.96	0.027	0.005	0.874	1.120	0.541	0.448	0.077	0.042	0.056	0.012	0.131	0.230
269.639	8.85	2.15	3.27	0.41	12.6	3.2	1.52	0.35	0.019	0.005	0.813	0.331	0.197	0.022	0.064	0.017	0.030	0.012	0.105	0.055
269.642	4.92	0.85	2.23	0.35	8.70	0.49	1.59	0.65	0.011	0.008	0.387	0.095	0.122	0.019	0.122	0.019	0.030	0.002	0.068	0.015
269.645	3.76	1.21	1.87	3.23	0.92	3.49	1.34	0.43	0.010	0.002	0.500	0.087	0.053	0.138	0.011	0.002	0.006	0.002	0.471	0.000
269.648	4.08	1.31	1.03	0.48	6.03	2.27	0.56	0.30	0.010	0.016	0.310	0.403	0.053	0.015	0.004	0.003	0.004	0.003	0.448	0.001
269.651	3.10	2.27	1.73	0.42	6.31	1.22	0.62	0.18	0.007	0.004	0.373	0.183	0.074	0.026	0.004	0.001	0.001	0.552	0.001	
269.654	4.99	7.03	1.64	0.34	8.87	0.63	1.03	0.08	0.032	0.022	0.522	0.051	0.093	0.023	0.006	0.003	0.584	0.001		
269.657	3.73	0.49	1.91	1.88	12.5	4.0	1.30	0.72	0.016	0.005	0.520	0.132	0.172	0.073	0.006	0.001	0.694	0.001		
269.678	8.06	1.08	3.71	0.60	16.5	8.0	1.06	0.14	0.039	0.021	1.828	0.351	0.215	0.029	0.057	0.007	0.146	0.028	0.747	0.001
269.682	8.63	0.65	3.18	0.44	11.5	13.4	1.05	0.16	0.023	0.013	1.832	0.424	0.216	0.033	0.056	0.012	0.154	0.051	0.699	0.001
269.686	9.73	2.11	5.07	0.71	25.5	9.2	1.41	0.61	0.026	0.008	2.713	0.951	0.439	0.084	0.091	0.020	0.034	0.009	0.159	0.012
269.69	9.82	5.16	2.05	0.79	7.33	18.1	1.31	0.38	0.023	0.008	1.577	0.637	0.256	0.074	0.053	0.017	0.102	0.043	0.772	0.001
269.694	6.92	2.31	2.63	0.83	7.72	14.4	0.96	0.15	0.018	0.012	1.252	0.661	0.146	0.049	0.048	0.010	0.103	0.052	0.486	0.001
269.698	8.92	1.50	2.40	0.08	6.35	28.3	0.76	0.31	0.014	0.019	1.135	0.589	0.131	0.036	0.046	0.006	0.028	0.015	0.346	0.000
269.702	8.24	1.04	2.74	0.39	8.37	7.98	1.82	0.81	0.020	0.004	0.904	0.160	0.089	0.161	0.005	0.003	0.500	0.000		
269.706	4.96	1.27	2.08	0.82	5.18	4.78	0.58	0.43	0.010	0.038	0.704	0.458	0.065	0.022	0.015	0.003	0.414	0.001		
269.71	4.29	0.24	1.48	0.36	3.49	3.98	0.97	0.37	0.016	0.003	0.653	0.166	0.080	0.085	0.080	0.005	0.348	0.000		
269.718	4.98	1.01	1.40	1.10	4.82	16.1	1.13	0.24	0.009	0.006	0.553	0.612	0.073	0.098	0.073	0.009	0.460	0.001		
269.722	9.75	2.63	6.82	3.21	10.0	5.1	1.11	0.42	0.042	0.048	1.424	1.003	0.381	0.167	0.144	0.031	1.332	0.001		
269.726	6.93	1.20	3.45	3.43	8.15	2.15	1.27	0.38	0.058	0.037	0.657	0.231	0.186	0.163	0.066	0.002	0.787	0.001		
269.73	6.52	5.55	3.03	2.01	7.12	5.85	1.52	0.18	0.018	0.018	0.712	0.306	0.140	0.110	0.008	0.002	1.185	0.000		
269.734	7.37	0.65	3.31	0.32	9.40	12.0	0.48	0.83	0.012	0.010	0.837	0.344	0.140	0.049	0.010	0.004	0.738	0.000		
269.738	6.51	1.78	2.44	0.37	8.55	2.11	1.57	0.31	0.015	0.004	0.700	0.138	0.093	0.021	0.005	0.003	0.571	0.000		
269.742	9.30	1.01	4.67	0.69	10.1	2.9	1.72	1.23	0.023	0.026	1.526	0.297	0.138	0.021	0.013	0.010	0.722	0.000		
269.746	8.06	1.46	5.58	1.66	50.1	23.3	1.18	0.74	0.032	0.012	2.268	1.149	0.194	0.083	0.010	0.004	0.841	0.001		
269.76	7.39	3.06	2.71	0.59	10.8	1.8	2.26	0.47	0.013	0.008	0.688	0.247	0.107	0.041	0.007	0.002	0.620	0.001		

Table A 1: Element concentration with SD in $\mu\text{g kg}^{-1}$ in EDMT meter 270 (269–270 m depth) obtained by LA-ICP-Q-MS. Only values exceeding the DL and the lowest concentrated standard are shown (continued).

depth /m	Na	SD	Mg	SD	Al	SD	K	SD	Mn	SD	Fe	SD	Co	SD	Ni	SD	Zn	SD	Sr	SD	Cd	SD	Ba	SD	La	SD	Ce	SD	Pb	SD	Bi	SD
269764	6.56	2.35	2.76	0.72	10.5	5.1	0.67	0.09	0.090	0.008	1.43	0.27	0.012	0.002	0.598	0.218	0.143	0.054	0.044	0.009	0.044	0.009	0.143	0.054	0.051	0.046	0.089	0.083	0.651	0.000		
269768	5.01	9.4	2.38	2.48	17.6	31.3	0.79	0.83	0.074	0.090	1.65	1.35	0.013	0.014	0.657	0.732	0.135	0.126	0.037	0.034	0.034	0.034	0.100	0.031			0.007	0.004	0.674	0.000		
269772	10.40	1.55	2.00	0.34	7.20	15.1	0.69	0.13	0.081	0.022	1.19	0.53	0.030	0.004	0.582	0.069	0.092	0.023	0.029	0.014	0.029	0.014	0.092	0.023			0.009	0.003	0.465	0.000		
269776	6.39	2.31	2.08	0.91	6.94	14.5	0.63	0.12	0.086	0.033	1.51	0.56	0.016	0.013	0.473	0.150	0.078	0.035	0.040	0.015	0.040	0.015	0.078	0.035			0.009	0.003	0.357	0.000		
26978	8.33	1.77	1.89	1.53	4.45	2.22	0.61	0.21	0.073	0.013	1.22	0.73	0.013	0.045	0.434	0.402	0.109	0.048	0.035	0.009	0.035	0.009	0.109	0.048			0.006	0.003	0.583	0.000		
269784	22.2	5.8	4.34	2.09	5.49	2.25	0.61	0.21	0.080	0.033	1.62	0.25	0.007	0.014	0.390	0.171	0.078	0.144	0.035	0.020	0.035	0.020	0.078	0.144			0.006	0.003	0.319	0.000		
269788	9.22	1.77	3.06	1.64	3.84	5.04					0.58	0.19			0.085	0.478	0.142	0.193				0.142	0.193					0.169	0.000			
269792	3.83	2.98	0.84	0.72	2.47	2.47					1.26	0.21			0.010	0.043	0.063	0.154				0.063	0.154					0.250	0.004			
269796	3.49	1.78	1.08	2.35	2.36	2.62					3.38	1.42			0.030	0.028	0.896	0.630				0.191	0.309					0.599	0.000			
2698	269.8	10.1	13.1	1.91	1.64	7.37	21.2	0.72	0.81	0.06	3.38	1.42			0.014	0.016	0.375	0.642				0.079	0.409					0.517	0.005			
269804	6.99	7.02	3.56	2.90	5.92	5.71	0.74	0.21	0.085	0.038	2.20	1.11			0.016	0.160	0.307	0.222				0.041	0.021					0.006	0.002	0.813	0.000	
269808	6.28	1.96	2.94	0.68	6.21	7.35	0.77	0.70			1.21	0.41			0.064	0.189	0.907	0.631				0.051	0.059					0.009	0.004	0.879	0.002	
269812	7.89	1.67	2.16	1.33	7.20	4.80	0.90	0.66	0.134	0.081	2.50	0.84			0.020	0.013	0.449	0.502				0.091	0.032					0.013	0.005	0.605	0.000	
269816	8.28	2.02	4.14	4.11	6.58	3.89	1.00	0.75	0.074	0.018	2.83	0.97			0.036	0.010	2.682	0.257				0.069	0.039					0.014	0.004	0.586	0.005	
26982	269.82	8.27	0.71	2.89	3.71	9.42	0.78	0.47	0.148	0.148	1.86	0.61			0.027	0.008	1.993	0.313				0.032	0.012					0.011	0.002	0.989	0.000	
269824	7.05	1.97	2.17	2.02	7.23	4.16					1.00	0.29			0.011	0.013	0.547	0.625				0.032	0.012					0.011	0.002	0.677	0.000	
269828	6.66	7.72	3.14	2.37	10.2	8.8	0.66	1.34	0.085	0.046	1.21	0.42			0.010	0.022	0.684	0.192				0.059	0.024					0.011	0.002	0.677	0.000	
269832	9.24	2.18	3.28	1.41	10.0	2.0					1.32	0.60			0.016	0.006	0.410	0.113				0.042	0.037					0.013	0.003	0.690	0.000	
269836	15.6	0.8	12.0	2.1	99.4	20.4	1.51	0.82	0.261	0.050	2.20	1.26			0.036	0.010	2.682	0.257				0.136	0.045					0.013	0.001	1.360	0.006	
269845	8.19	1.85	2.67	2.03	6.17	3.60	1.18	0.27	0.187	0.044	1.86	0.61			0.027	0.008	1.993	0.313				0.093	0.121					0.012	0.005	1.188	0.000	
269849	29.1	9.0	5.79	3.17	36.0	11.6	0.73	0.23	0.400	0.148	0.83	0.69			0.016	0.005	0.406	0.110				0.065	0.017					0.006	0.006	0.641	0.000	
269853	12.4	4.8	4.41	18.15	30.0	8.3	1.91	0.82	0.108	0.097	2.28	1.30			0.027	0.031	1.401	0.772				0.074	0.104					0.011	0.003	1.186	0.002	
269857	9.32	2.06	4.26	0.90	17.9	8.7	1.17	0.70	0.118	0.024	1.93	1.39			0.018	0.008	1.072	0.352				0.063	0.118					0.009	0.004	0.707	0.006	
269861	9.09	2.59	2.90	0.86	16.2	34.2	0.71	0.28	0.088	0.064	1.32	0.60			0.012	0.012	0.696	0.281				0.290	0.041					0.009	0.025	0.615	0.002	
269865	8.19	1.85	2.67	2.03	6.17	3.60	0.73	0.23	0.400	0.148	0.83	0.69			0.016	0.005	0.406	0.110				0.136	0.045					0.006	0.382	0.772	0.000	
269869	6.60	1.58	2.69	2.83	11.0	13.7					0.83	0.69			0.016	0.005	0.406	0.110				0.035	0.010					0.007	0.013	0.631	0.000	
269873	7.85	1.70	4.00	1.60	8.05	3.94	0.60	0.06	0.107	0.121	1.19	0.56			0.009	0.007	0.367	0.131				0.047	0.023					0.005	0.002	0.441	0.000	
269877	5.67	0.91	2.56	1.24	9.71	3.83					1.36	0.73			0.012	0.005	0.316	0.749				0.048	0.013					0.006	0.003	0.872	0.000	
269881	5.77	1.40	2.81	1.06	10.9	2.9	0.73	0.55	0.086	0.091	0.98	0.27			0.010	0.008	0.289	0.261				0.046	0.028					0.004	0.003	0.690	0.002	
269885	6.03	2.94	4.08	1.61	9.71	9.98	0.72	0.75	0.165	0.091	1.51	0.45			0.010	0.009	0.336	0.407				0.076	0.025					0.011	0.087	0.724	0.017	
269889	6.67	1.36	2.72	0.78	8.71	3.40	0.58	0.15	0.165	0.091	0.91	0.96			0.013	0.013	0.594	0.305				0.071	0.051					0.006	0.003	0.664	0.013	
269893	6.66	1.82	1.84	1.80	8.83	4.73	0.64	0.62	0.090	0.069	0.76	0.63			0.021	0.010	0.281	0.145				0.052	0.028					0.006	0.006	0.641	0.000	
269897	4.99	1.21	2.67	0.94	8.13	2.82					1.36	0.73			0.010	0.008	0.289	0.261				0.046	0.028					0.011	0.006	0.751	0.000	
269901	5.23	1.12	2.97	3.98	12.0	19.4					0.85	1.06			0.010	0.008	0.289	0.261				0.046	0.028					0.004	0.003	0.690	0.002	
269905	7.95	1.21	3.74	2.44	11.1	6.0	1.41	0.55	0.106	0.112	1.33	1.01			0.013	0.013	0.594	0.305				0.076	0.025					0.011	0.087	0.724	0.017	
269909	9.63	3.94	4.26	3.67	12.7	16.3	0.69	0.19	0.101	0.037	1.35	0.75			0.025	0.008	0.649	0.233				0.071	0.051					0.006	0.003	0.664	0.013	
269916	9.24	1.59	3.51	2.46	10.1	16.5	1.16	0.18	0.094	0.084	1.01	1.43			0.017	0.010	0.676	0.433				0.086	0.071					0.012	0.005	0.762	0.000	
269934	4.34	0.73	1.73	1.08	18.5	9.6	0.90	0.40	0.122	0.240	1.16	2.01			0.021	0.048	0.414	0.610				0.054	0.037					0.009	0.004	1.674	0.003	
269938	5.66	1.81	3.53	1.41	10.7	16.3	0.58	0.09	0.099	0.069	1.82	0.65			0.012	0.004	0.304	0.285				0.058	0.0356					0.004	0.007	1.408	0.004	
269942	5.44	1.00	1.76	0.54	41.7	20.9					1.62	0.53			0.011	0.006	0.398	0.066				0.057	0.046					0.005	0.022	0.223	0.000	
269946	6.63	1.43	2.44	0.81	6.6	20.5					1.62	0.53			0.011	0.006	0.398	0.066				0.067	0.033					0.020	0.049	0.243	0.000	
26995	2.43	0.75	1.29	0.96	7.6	10.4					1.62	0.53			0.009	0.005	0.653	0.336				0.063	0.018					0.005	0.010	0.338	0.000	
269954	5.54	1.79	2.74	2.11	11.5	4.0	0.61	0.14	0.086	0.036	1.09	0.49			0.014	0.005	0.336	0.178				0.061	0.016					0.004	0.002	0.347	0.002	
269958	5.08	0.70	2.44	0.60	15.7	19.9					1.26	0.36			0.016	0.043	0.441	0.209				0.076	0.033					0.006	0.004	0.545	0.000	
269962	3.71	0.74	2.79	0.79	6.5	15.6					1.15	0.40			0.015	0.005	0.880	0.226				0.058	0.013					0.010	0.017	0.563	0.000	
269966	3.19	1.64	1.63	3.78	9.0	10.4					1.47	0.69			0.013	0.004	0.283	0.213				0.085	0.028					0.004	0.053	0.728	0.000	
269966	3.19	1.64	1.63	3.78	9.0	10.4					0.93	0.83			0.020	0.009	0.273	0														

A4 Element concentrations of subsections of EDML meter 270 obtained by LA-ICP-Q-MS and ICP-Q-MS analysis of acidified and digested samples

Table A 2: Comparison of average element concentrations with SD in ng L^{-1} of EDML meter 270 obtained by LA-ICP-MS analysis and ICP-MS analysis after melting the sample. Average concentrations were calculated for a) all subsections except the subsection including the particle horizon (column 2–4) and b) subsection no. 9 including the particle horizon (column 5–7). Concentrations below the DL were set to DL/2 for average concentration calculations. Concentrations of ICP-MS analysis of digested samples represent the total amount of insoluble and soluble fractions. Values in brackets below the concentration represent recovery rates (in %) in respect to the total element content.

aggregate state	LA-ICP-MS solid	ICP-MS liquid (acidified)	ICP-MS liquid (digested)	LA-ICP-MS solid	ICP-MS liquid (acidified)	ICP-MS liquid (digested)
no. of samples	186	12	12	26	1	1
replicates / sample	5	5	5	5	5	5
	average of subsections 1-8 plus 10-13			subsection no. 9		
Na*	8.5 ± 3.1 (38)	17.2 ± 9.2 (77)	22.4 ± 10.0	24.8 ± 69 (26)	28 ± 1 (29)	94 ± 5
Mg*	4.2 ± 3.7 (105)	4.1 ± 2.6 (105)	4.0 ± 1.7	17.3 ± 58 (44)	6 ± 0.1 (16)	40 ± 6
Sr	50 ± 25 (43)	105 ± 79 (91)	116 ± 66	222 ± 707 (43)	172 ± 2 (34)	512 ± 19
Ba	208 ± 131 (57)	269 ± 179 (74)	362 ± 473	231 ± 517 (36)	170 ± 5.1 (26)	647 ± 33
Al*	13.4 ± 7.5 (90)	9.5 ± 6.7 (64)	14.8 ± 10.0	70 ± 242 (45)	38 ± 1 (24)	155 ± 10
Fe*	2.3 ± 1.3 (31)	7.1 ± 14.0 (97)	7.4 ± 8.4	19 ± 71 (12)	18 ± 1 (11)	155 ± 2
Mn	108 ± 37 (30)	283 ± 216 (78)	364 ± 197	1359 ± 5180 (28)	753 ± 27 (15)	4892 ± 67
Ce	16 ± 19 (217)	4 ± 3 (62)	7 ± 9	26 ± 75 (98)	5 ± 0.2 (20)	27 ± 1
Co	19 ± 9	6 ± 8		71 ± 234 (126)		57 ± 2
Cd	28 ± 14			22 ± 12		
Pb	730 ± 431 (108)	628 ± 563 (93)	674 ± 432	703 ± 220 (103)	359 ± 5 (53)	682 ± 19
Bi	3 ± 1 (100)	3 ± 4 (103)	3 ± 6	2 ± 0 (97)	1 ± 1 (50)	2 ± 0.1

* concentration in $\mu\text{g L}^{-1}$

Average concentrations for LA-ICP-MS (columns 2-4) were calculated as follows:

Average concentrations with SD were calculated for subsections 1-8 plus 10-13. Then average values of subsections were calculated

A5 Relative element intensities in bivalves obtained by LA-ICP-Q-MS analysis

Table A 3: Weighted means of Al, Mn, Fe, Cu, Pb and U normalized to Ca signal (relative intensities) \pm SD (*1000) in annual growth bands of *L. elliptica*. Yearly resolution was obtained until an age of 12. After this age mean values for groups of up to 4 year bands were calculated, due to the spot size of the laser crater. The same weighted value was assigned to each year in a group.

age/yr.	Al	SD	Fe	SD	Mn	SD	Cu	SD	Pb	SD	U	SD
1	0.5992	0.0365	9.3190	0.4632	0.1368	0.0083	1.5238	0.0589	0.0396	0.0025	0.0057	0.0004
2	0.1820	0.0200	1.3390	0.1158	0.0553	0.0025	0.3263	0.0254	0.0121	0.0007	0.0019	0.0002
3	0.0989	0.0095	1.3263	0.0405	0.0269	0.0009	0.3561	0.0274	0.0104	0.0003	0.0011	0.0001
4	0.0747	0.0108	0.9901	0.0526	0.0752	0.0014	0.2883	0.0205	0.0104	0.0006	0.0009	0.0001
5	0.0349	0.0054	0.5760	0.0602	0.0364	0.0013	0.2347	0.0135	0.0089	0.0002	0.0008	0.0001
6	0.0263	0.0038	0.4546	0.0172	0.0194	0.0006	0.0544	0.0027	0.0056	0.0002	0.0005	0.0001
7	0.0233	0.0023	0.3760	0.0159	0.0170	0.0006	0.0761	0.0014	0.0073	0.0002	0.0004	0.0000
8	0.0346	0.0052	0.2935	0.0053	0.0178	0.0008	0.1492	0.0070	0.0071	0.0003	0.0001	0.0000
9	0.0559	0.0022	0.5093	0.0209	0.0177	0.0008	0.1148	0.0048	0.0066	0.0003	0.0002	0.0000
10	0.0497	0.0018	0.4220	0.0049	0.0177	0.0001	0.0987	0.0049	0.0058	0.0002	0.0003	0.0000
11	0.0561	0.0011	0.3193	0.0048	0.0156	0.0007	0.1234	0.0053	0.0073	0.0002	0.0004	0.0000
12	0.0616	0.0007	0.2977	0.0051	0.0254	0.0008	0.1224	0.0044	0.0068	0.0002	0.0004	0.0000
13	0.0533	0.0009	0.6195	0.0034	0.0200	0.0005	0.2596	0.0037	0.0077	0.0002	0.0005	0.0000
14	0.0533	0.0009	0.6195	0.0034	0.0200	0.0005	0.2596	0.0037	0.0077	0.0002	0.0005	0.0000
15	0.0533	0.0004	0.6198	0.0034	0.0227	0.0004	0.2185	0.0032	0.0075	0.0003	0.0004	0.0000
16	0.0533	0.0004	0.6198	0.0034	0.0227	0.0004	0.2185	0.0032	0.0075	0.0003	0.0004	0.0000
17	0.0625	0.0004	0.4571	0.0226	0.0249	0.0004	0.1096	0.0044	0.0065	0.0003	0.0006	0.0000
18	0.0611	0.0033	0.3829	0.0266	0.0208	0.0010	0.1465	0.0043	0.0071	0.0004	0.0006	0.0000
19	0.0611	0.0033	0.3829	0.0266	0.0208	0.0010	0.1465	0.0043	0.0071	0.0004	0.0006	0.0000
20	0.0611	0.0033	0.3829	0.0266	0.0208	0.0010	0.1465	0.0043	0.0071	0.0004	0.0006	0.0000
21	0.0560	0.0068	0.8096	0.1022	0.0191	0.0009	0.1162	0.0067	0.0099	0.0003	0.0007	0.0001
22	0.0560	0.0068	0.8096	0.1022	0.0191	0.0009	0.1162	0.0067	0.0099	0.0003	0.0007	0.0001
23	0.0560	0.0068	0.8096	0.1022	0.0191	0.0009	0.1162	0.0067	0.0099	0.0003	0.0007	0.0001

A6 Program (IDL®) for the evaluation of ICP-TOF-MS data

```

;Data evaluation - continuous mode
;pro program name: RohdatenverarbeitungProben

print,format='(/" *** Rohdatenverarbeitung Proben ***"/)'

;Informationen for interference correction caused by MO+ and M2+

read, 'MO+:',oxide ;MO+*100 = oxide forming rate in %
read, 'M2+:',doubly_charged ;M2+*100 = doubly charged ion rate in %

; *** set and read in of files

data= FILE_SEARCH(filepath\\*',count=a)

print, a ;a = number of data files

line='34002'

matrixno1 = fltarr(a,102)
matrixno2 = fltarr(a,102)

matrixno 3=fltarr(a,12)
matrixno 4=fltarr(a,12)

for i=0, a-1 do begin

    activefile = data(i)

    close,1
    openr,1, activefile
    readf,1,nns
    ns=uindgen(nns)+1
    counts=uintarr(nns)
    ;print,' contains ',nns,' MSA data points'

    nns10=nns/10+1
    ns_ada=uindgen(nns10)*10
    counts_ada=fltarr(nns10)
    ;print,' contains ',nns10,' ADA data points'

    for j=0L,nns-1 do begin
        readf,1,m
        counts(j)=m
    endfor

    for j=0,1 do readf,1,line
    for j=0L,nns10-1 do begin
        readf,1,m_ada
        counts_ada(j)=m_ada
    endfor
endfor

```

endfor

;calculation of integral values, pulse detector

Li7=total(counts[1094:1147])
Na23=total(counts[6043:6117])
Mg24=total(counts[6288:6351])
Mg25=total(counts[6519:6568])
Al27=total(counts[6969:7033])
Si28=total(counts[7204:7266])
Ca43=total(counts[10120:10183])
Ca44=total(counts[10282:10355])
Ca=total(counts[10120:10355])
Ti46=total(counts[10648:10716])
V51=total(counts[11453:11522])
Cr52=total(counts[11617:11692])
Cr53=total(counts[11774:11858])
Fe54=total(counts[11946:12001])
Mn55=total(counts[12091:12162])
Fe56=total(counts[12235:12327])
Fe57=total(counts[12403:12457])
Fe=total(counts[12235:12457])
Co59=total(counts[12698:12773])
Ni60=total(counts[12844:12915])
Ni62=total(counts[13148:13203])
Cu63=total(counts[13285:13386])
Zn64=total(counts[13430:13513])
Cu65=total(counts[13577:13647])
Zn66=total(counts[13717:13795])
Zn67=total(counts[13856:13933])
Ge72=total(counts[14568:14627])
As75=total(counts[14955:15025])
Se76=total(counts[15080:15175])
Rb85=total(counts[16258:16345])
Sr86=total(counts[16368:16455])
Sr88=total(counts[16607:16715])
Sr=Sr86+Sr88
Y89=total(counts[16730:16838])
Rh103=total(counts[18375:18497])
Pd105=total(counts[18618:18720])
Ag107=total(counts[18836:18940])
Ag109=total(counts[19060:19155])
Ag=Ag107+Ag109
Cd111=total(counts[19285:19368])
Cd114=total(counts[19606:19687])
In115=total(counts[19712:19812])
Sn119=total(counts[20150:20225])
Sb121=total(counts[20358:20440])
Ba137=total(counts[21990:22076])
La139=total(counts[22183:22264])
Ce140=total(counts[22281:22363])

Pr141=total(counts[22398:22465])

Nd143=total(counts[22582:22641])

Nd145=total(counts[22770:22850])

Nd146=total(counts[22860:22945])

Sm147=total(counts[22960:23033])

Sm149=total(counts[23152:23218])

Sm152=total(counts[23430:23515])

Sm=Sm147+Sm149+Sm152

Eu151=total(counts[23333:23418])

Eu153=total(counts[23525:23607])

Eu=Eu151+Eu153

Ho165=total(counts[24626:24714])

Hf180=total(counts[25952:26028])

Ir193=total(counts[27040:27135])

Pt194=total(counts[27138:27212])

Pt195=total(counts[27219:27296])

Pt=total(counts[27142:27296])

Au197=total(counts[27381:27467])

Pb204=total(counts[27949:28020])

Tl205=total(counts[28028:28110])

Pb206=total(counts[28117:28189])

Pb207=total(counts[28197:28271])

Pb208=total(counts[28276:28353])

Pb=total(counts[28112:28357])

Bi209=total(counts[28356:28467])

Th232=total(counts[30135:30265])

U238=total(counts[30585:30720])

;isotopes with isobaric or spectral interferences

Ni58=total(counts[12540:12623])-0.1273*Fe57

Nd142=total(counts[22477:22563])-0.1252*Ce140

Nd144=total(counts[22670:22760])-0.2067*Sm147

Gd155=total(counts[23715:23790])-(oxide*0.9976)*La139

Gd157=total(counts[23900:23980])-(oxide*0.9976)*Pr141

Tb159=total(counts[24079:24173])-(oxide*0.7069)*Nd146

Dy161=total(counts[24269:24353])-(oxide*0.4817)*Nd146

Dy163=total(counts[24448:24535])-(oxide*0.9976)*Sm147

Er166=total(counts[24722:24796])-(oxide*0.3273)*Nd146

Er167=total(counts[24810:24894])-(oxide*0.9976)*Eu151

Er168=total(counts[24895:24975])-(oxide*0.9976)*Sm152

Dy164=total(counts[24535:24615])-((oxide*0.7515)*Sm147-((oxide*0.3342)
*Nd146-(0.0479)*Er166

Gd156=total(counts[23802:23890])-(oxide*0.9976)*Ce140-(0.002)*Dy164

Gd158=total(counts[23990:24067])-((oxide*1.5745)*Nd146-((oxide*0.1249)*
Ce140-(0.004)*Dy164

Tm169=total(counts[24982:25071])-(oxide*0.9976)*Eu153

Yb171=total(counts[25165:25246])-((oxide*0.5944)*Gd158

Yb172=total(counts[25253:25340])-((oxide*0.8221)*Gd158
 Yb173=total(counts[25345:25420])-((oxide*0.6285)*Gd158
 Yb174=total(counts[25426:25508])-(oxide*0.9976)*Gd158
 Lu175=total(counts[25514:25602])-(oxide*0.9976)*Tb159
 Ir191=total(counts[26870:26980])-(oxide*0.9976)*Lu175

Nd=Nd142+Nd143+Nd144+Nd145+Nd146
 Gd=Gd155+Gd156+Gd157+Gd158
 Dy=Dy161+Dy163+Dy164
 Er=Er166+Er167
 Yb=Yb171+Yb172+Yb173+Yb174
 Ir=Ir191+Ir193

Ba138=total(counts[22077:22177])-(0.09/99.91)*La139-(0.25/88.48)*Ce140

Ga69=total(counts[14137:14224])-doubly_charged*Ba138

;isotopes analysed

isotopes=['7Li','23Na','24Mg','25Mg','27Al','43Ca','44Ca','Ca','46Ti','51V','\$
 '52Cr','53Cr','55Mn','54Fe','Fe56','57Fe','Fe','59Co','58Ni','60Ni','\$
 '62Ni','63Cu','65Cu','64Zn','66Zn','67Zn','69Ga','72Ge','75As','76Se','\$
 '85Rb','86Sr','88Sr','Sr','89Y','103Rh','105Pd','107Ag','109Ag','Ag','\$
 '111Cd','114Cd','115In','119Sn','121Sb','Ba137','138Ba','139La','\$
 '140Ce','141Pr','142Nd','143Nd','144Nd','145Nd','146Nd','Nd','\$
 '147Sm','149Sm','152Sm','Sm','151Eu','153Eu','Eu','155Gd','156Gd'\$
 ',Gd157','158Gd','Gd','159Tb','161Dy','163Dy','164Dy','Dy','165Ho','\$
 '166Er','167Er','168Er','Er','169Tm','171Yb','172Yb','173Yb','\$
 '174Yb','Yb','175Lu','180Hf','191Ir','193Ir','Ir','194Pt','195Pt','Pt','\$
 '197Au','205Tl','204Pb','206Pb','207Pb','208Pb','Pb','209Bi','232Th','\$
 '238U']

nbars=N_ELEMENTS(isotopes)

x=[Li7,Na23,Mg24,Mg25,Al27,Ca43,Ca44,Ca,Ti46,V51,Cr52,Cr53,Mn55,\$
 Fe54,Fe56,Fe57,Fe,Co59,Ni58,Ni60,Ni62,Cu63,Cu65,Zn64,Zn66,Zn67,\$
 Ga69,Ge72,As75,Se76,Rb85,Sr86,Sr88,Sr,Y89,Rh103,Pd105,Ag107,\$
 Ag109,Ag,Cd111,Cd114,In115,Sn119,Sb121,Ba137,Ba138,La139,Ce140,\$
 Pr141,Nd142,Nd143,Nd144,Nd145,Nd146,Nd,Sm147,Sm149,Sm152,Sm,\$
 Eu151,Eu153,Eu,Gd155,Gd156,Gd157,Gd158,Gd,Tb159,Dy161,Dy163,\$
 Dy164,Dy,Ho165,Er166,Er167,Er168,Er,Tm169,Yb171,Yb172,Yb173,\$
 Yb174,Yb,Lu175,Hf180,Ir191,Ir193,Ir,Pt194,Pt195,Pt,Au197,Tl205,\$
 Pb204,Pb206,Pb207,Pb208,Pb,Bi209,Th232,U238]

matrixno1[i,*]=x

;calculation of integral values, analogue detector

Na23_ada=total(counts_ada[584:590])

Mg24_ada=total(counts_ada[607:613])

Al27_ada=total(counts_ada[674:679])

Ca44_ada=total(counts_ada[994:1002])

V51_ada=total(counts_ada[1107:1117])


```

Cr52_ada=total(counts_ada[1123:1131])
Cr53_ada=total(counts_ada[1139:1146])
Fe56_ada=total(counts_ada[1183:1192])
Cu63_ada=total(counts_ada[1286:1293])
Cu65_ada=total(counts_ada[1314:1320])
Zn64_ada=total(counts_ada[1294:1307])
Zn66_ada=total(counts_ada[1328:1335])
Rh103_ada=total(counts_ada[1780:1789])

isotopes_ada=['Na23','Mg24','Al27','Ca44','V51','Cr52','Cr53','Fe56','Cu63','$
              'Cu65','Zn64','Zn66']

x_ada=[Na23_ada,Mg24_ada,Al27_ada,Ca44_ada,V51_ada,Cr52_ada,$
       Cr53_ada,Fe56_ada,Cu63_ada,Cu65_ada,Zn64_ada,Zn66_ada]

matrixno3[i,*]=x_ada

;***internal normalization by 103Rh
cnorm=1.0*x/(Rh103)
matrixno2[i,*]=cnorm

cnorm_ada=1.0*x_ada/(Rh103_ada)
matrixno4[i,*]=cnorm_ada

close,1

endfor

;Export of evaluated data

close,2
openw,2,'evaluated data.xls', WIDTH=2400

printf,2,'MSAModusRohdaten',isotopes
printf,2, transpose(matrixno 1)
printf,2,'MSAModusinternnormiert',isotopes
printf,2, transpose(matrixno 2)
printf,2,'ADAModusRohdaten',isotopes_ada
printf,2, transpose(matrixno 3)
printf,2,'ADAModusinternnormiert',isotopes_ada
printf,2, transpose(matrixno 4)
printf,2,transpose(data)

close, 2
end

```

A7 Concentration data of reference materials analysed by Aridus II-ICP-TOF-MS

Table A 4: Concentration data with SD in $\mu\text{g L}^{-1}$ of reference material NIST 1640 obtained by Aridus II-ICP-TOF-MS analysis.

Element	certified		Aridus II-ICP-TOF-MS	
	c / $\mu\text{g L}^{-1}$	SD / $\mu\text{g L}^{-1}$	c / $\mu\text{g L}^{-1}$	SD / $\mu\text{g L}^{-1}$
Li	50.7	± 1.4	51.0	± 0.44
Na	29350	± 310	30046	± 407
Mg	5819	± 56	5647	± 23
Al	52	± 1.5	106.3	± 0.83
Ca	7045	± 89	3980	± 49
V	13.0	± 0.37	13.4	± 0.13
Cr	38.6	± 1.6	38.3	± 0.31
Mn	121.5	± 1.1	168	± 1.97
Fe	34.3	± 1.6	36.5	± 0.46
Co	20.3	± 0.31	19.4	± 0.14
Ni	27.4	± 0.8	27.4	± 0.2
Cu	85.2	± 1.2	84.3	± 0.3
Zn	53.2	± 1.1	122.1	± 0.7
As	26.7	± 0.41	26.0	± 0.23
Rb	2	± 0.02	2.31	± 0.05
Sr	124.2	± 0.7	129	± 2.1
Ag	7.62	± 0.25	7.96	± 0.13
Cd	22.79	± 0.96	22.8	± 0.47
Sb	13.79	± 0.42	13.2	± 0.67
Ba	148	± 2.2	150	± 4.20
Pb	27.9	± 0.14	27.9	± 0.22

Table A 5: Concentration data with SD in $\mu\text{g L}^{-1}$ of reference SLRS-4 obtained by Aridus II-ICP-TOF-MS analysis.

Element	certified		Aridus II-ICP-TOF-MS	
	c / $\mu\text{g L}^{-1}$	SD / $\mu\text{g L}^{-1}$	c / $\mu\text{g L}^{-1}$	SD / $\mu\text{g L}^{-1}$
Na	2400	± 200	2567	± 16
Mg	1600	± 100	1521	± 18
Al	54	± 4	56	± 0
Ca	6200	± 200	3360	± 68
V	0.32	± 0.03	0	± 0
Cr	0.3	± 0.02	0.5	± 0.01
Mn	3.37	± 0.18	3.0	± 0.19
Fe	103	± 5	106	± 1.12
Co	0.033	± 0.006	0.4	± 0.01
Ni	0.7	± 0.08	0.8	± 0.03
Cu	1.81	± 0.08	2.21	± 0.02
Zn	0.93	± 0.1	12.1	± 0.1
As	0.68	± 0.06	0.77	± 0.01
Sr	26.3	± 3.20	26.4	± 0.21
Cd	0.012	± 0.002	0.019	± 0.001
Sb	0.23	± 0.04	0	± 0.0
Ba	12.2	± 0.6	12.6	± 0.1
Pb	0.086	± 0.007	0.088	± 0.001
U	0.05	± 0.003	0.05	± 0.00

Table A 6: Concentration data with SD in $\mu\text{g L}^{-1}$ of reference material SPS-SW1 obtained by Aridus II-ICP-TOF-MS analysis.

Element	certified		Aridus II-ICP-TOF-MS	
	c / $\mu\text{g L}^{-1}$	SD / $\mu\text{g L}^{-1}$	c / $\mu\text{g L}^{-1}$	SD / $\mu\text{g L}^{-1}$
Na	2000	± 20	1654	± 12
Mg	400	± 4	456	± 4
Al	50	± 1	54	± 0.4
Ca	2000	± 20	1586	± 37
V	10	± 0.1	10	± 0.2
Cr	2	± 0.02	2	± 0.15
Mn	10	± 0.1	10	± 0.3
Fe	20	± 1	20	± 0.4
Co	2	± 0.02	2	± 0.01
Ni	10	± 0.1	10	± 0.1
Cu	20	± 1	19	± 0.1
Zn	20	± 1	23	± 0.1
As	10	± 0.1	8	± 0.1
Rb	10	± 0.1	10	± 0.0
Sr	50	± 0.5	48	± 0.9
Y	0.5	± 0.01	0.6	± 0.03
Cd	0.5	± 0.01	0.5	± 0.01
Ba	50	± 1	50	± 0.3
La	0.5	± 0.01	0.6	± 0.01
Ce	0.5	± 0.01	0.6	± 0.02
Pr	0.5	± 0.01	0.5	± 0.02
Nd	0.5	± 0.01	0.5	± 0.04
Sm	0.5	± 0.01	0.5	± 0.02
Eu	0.5	± 0.01	0.5	± 0.01
Gd	0.5	± 0.01	0.5	± 0.01
Tb	0.5	± 0.01	0.5	± 0.01
Dy	0.5	± 0.01	0.6	± 0.01
Ho	0.5	± 0.01	0.5	± 0.02
Er	0.5	± 0.01	0.5	± 0.04
Tm	0.5	± 0.01	0.5	± 0.02
Yb	0.5	± 0.01	0.5	± 0.03
Lu	0.5	± 0.01	0.5	± 0.02
Tl	0.5	± 0.01	0.5	± 0.01
Pb	5	± 0.1	5	± 0.0
Th	0.5	± 0.01	0.5	± 0.01
U	0.5	± 0.01	0.5	± 0.00

A8 Concentration data of Intercomparison samples analysed by Aridus II-ICP-TOF-MS

Table A 7: Concentration data with SD in $\mu\text{g L}^{-1}$ of intercomparison samples obtained by Aridus II-ICP-TOF-MS analysis. Only values exceeding the DL and the lowest concentrated standard and values which are lower than the highest concentrated standard are shown.

Probe	Li	SD	Na	SD	Mg	SD	Al	SD	Ca	SD	V	SD	Mn	SD	Fe	SD	Co	SD	Ni	SD	Cu	SD
DM1873	0.016	0.001	19.2	0.6	7.0	0.3			3.91	0.02	0.010	0.001	0.31	0.00	16.4	0.5			0.326	0.002	0.027	0.001
DM1905	0.133	0.011			20.5	0.6			4.02	0.02	0.201	0.004	4.27	0.14	65.7	1.4	0.021	0.000	0.173	0.001	0.054	0.001
DM1954									32.97	0.56							0.069	0.001	0.477	0.003		
DM11003									3.65	0.05	0.264	0.009	4.60	0.06	87.2	2.1	0.014	0.000	0.215	0.002	0.033	0.001
DM11203									22.05	0.23							0.063	0.001	0.401	0.002	0.073	0.001
DM11303											0.061	0.001	3.60	0.16	33.5	1.3	0.008	0.000	0.080	0.001	0.048	0.001
DM11404									7.43	0.05			0.39	0.00	11.8	0.4			0.021	0.001	0.021	0.001
DM11503									3.79	0.03	0.164	0.005	0.48	0.00	13.0	0.7	0.013	0.000	0.045	0.001	0.045	0.001
EDC739									3.61	0.01			4.63	0.09	109.3	2.3	0.114	0.001	3.633	0.090	0.092	0.001
EDC749									5.53	0.03									0.620	0.004		
EDC769									6.34	0.01	0.009	0.001	0.06	0.00	5.9	0.0			0.329	0.002	3.724	0.136
EDC805									2.41	0.02	0.106	0.002	6.54	0.32	4.7	0.0	0.060	0.005	0.963	0.003	6.639	0.281
EDC822									15.95	0.10	0.015	0.001	0.27	0.00	15.9	0.4			0.314	0.002	1.814	0.054
EDC839									3.87	0.02	0.092	0.002	0.04	0.00	24.1	1.0	0.018	0.001	1.191	0.008	3.332	0.095
EDC856									7.16	0.03	0.039	0.001	0.41	0.00	9.0	0.3			0.031	0.001	0.027	0.001
EDC877									3.82	0.03	0.045	0.001	5.63	0.10	14.6	0.4			0.260	0.004	0.246	0.002
EDC893									6.22	0.04	0.045	0.001	5.61	0.18	22.1	1.1			0.038	0.001	0.046	0.001
EDC915									7.36	0.04	0.063	0.001	5.63	0.16	30.5	0.9			0.117	0.002	8.411	0.096
EDC929									7.45	0.03	0.058	0.001	3.92	0.03	24.1	0.6			0.436	0.003	0.030	0.001
									7.35	0.05	0.049	0.001	3.91	0.06	27.7	0.5						

Probe	Zn	SD	As	SD	Rb	SD	Sr	SD	Y	SD	Ag	SD	Cd	SD	In	SD	Sn	SD	Sb	SD	Ba	SD
DM1873			0.021	0.001	0.014	0.000	0.081	0.001	0.004	0.000			0.000	0.000	0.000	0.000			0.004	0.000	0.283	0.005
DM1905			0.079	0.002	0.173	0.004	0.669	0.012	0.041	0.001	0.001	0.000	0.003	0.000	0.001	0.000	0.012	0.000	0.014	0.000	5.277	0.118
DM1954							0.862	0.007			0.001	0.000	0.004	0.000	0.001	0.000	0.032	0.001	0.016	0.000	2.903	0.017
DM11003							0.546	0.005	0.051	0.004	0.003	0.000	0.003	0.000	0.001	0.000	0.028	0.000	0.006	0.000	0.815	0.007
DM11103							0.960	0.004			0.000	0.000	0.004	0.000	0.001	0.000	0.008	0.000	0.021	0.000	2.401	0.019
DM11203							0.392	0.012	0.017	0.000	0.001	0.000	0.001	0.000	0.000	0.000	0.005	0.000	0.006	0.000	4.801	0.164
DM11303		0.3	0.072	0.001	0.064	0.001	0.135	0.002	0.003	0.000	0.000	0.000	0.000	0.000	0.000	0.000	0.002	0.000	0.004	0.000	2.027	0.237
DM11404			0.051	0.001	0.025	0.000	0.148	0.002	0.005	0.000	0.000	0.000	0.001	0.000	0.001	0.000	0.012	0.000	0.007	0.000	0.116	0.005
DM11503		0.5	0.063	0.001	0.061	0.001	0.283	0.007	0.017	0.000	0.004	0.000	0.001	0.000	0.001	0.000	0.013	0.000	0.016	0.001	0.370	0.006
EDC739		0.8	0.102	0.002	0.061	0.001	0.199	0.005	0.012	0.000	0.001	0.000	0.004	0.000	0.013	0.000			0.102	0.001		
EDC749			0.060	0.002	0.000	0.000	0.024	0.001					0.004	0.000	0.001	0.000	0.133	0.002	0.019	0.000		
EDC769			0.113	0.002	0.007	0.000	0.099	0.001	0.003	0.000	0.017	0.000	0.009	0.001	0.001	0.000	0.106	0.005	0.028	0.002	2.230	0.050
EDC805			0.030	0.001	0.010	0.000	0.063	0.001	0.005	0.000	0.002	0.000	0.002	0.000	0.000	0.000	0.017	0.001	0.010	0.001	0.054	0.005
EDC822			0.128	0.003	0.017	0.001	0.105	0.001	0.069	0.006	0.017	0.000	0.009	0.001	0.028	0.002	0.045	0.001	0.026	0.001	0.038	0.004
EDC839			0.022	0.001	0.013	0.000	0.342	0.012	0.004	0.000	0.000	0.000	0.006	0.000	0.000	0.000	0.000	0.000	0.000	0.000	3.962	0.069
EDC856			0.052	0.002	0.031	0.000	0.247	0.005	0.008	0.000	0.001	0.000	0.001	0.000	0.001	0.000	0.066	0.002	0.015	0.001	1.003	0.015
EDC877			0.084	0.001	0.045	0.000	0.405	0.010	0.016	0.000	0.002	0.000	0.003	0.000	0.001	0.000	0.005	0.000	0.009	0.000	7.030	0.208
EDC893		0.3	0.098	0.002	0.068	0.001	0.365	0.007	0.015	0.000			0.002	0.000	0.001	0.000	0.002	0.000	0.001	0.000	0.681	0.005
EDC915		8.8	0.052	0.002	0.053	0.001	0.315	0.007	0.012	0.000			0.001	0.000	0.001	0.000	0.000	0.010	0.000	0.903	0.006	
EDC929			0.022	0.001	0.043	0.000	0.247	0.005	0.010	0.000			0.001	0.000	0.000	0.000	0.000	0.001	0.000	2.688	0.043	

Table A 7: Concentration data with SD in $\mu\text{g L}^{-1}$ of intercomparison samples obtained by Aridis II-ICP-TOF-MS analysis. Only values exceeding the DL and the lowest concentrated standard and values which are lower than the highest concentrated standard are shown.

Probe	La	SD	Ce	SD	Pr	SD	Nd	SD	Sm	SD	Su	SD	Gd	SD	Tb	SD	Dy	SD	Ho	SD
DML873	0.0077	0.0001	0.0145	0.0002	0.0012	0.0000	0.0036	0.0002	0.0014	0.0001	0.0005	0.0001	0.0011	0.0001	0.0002	0.0000	0.0071	0.0001	0.0002	0.0000
DML905	0.0925	0.0025	0.1025	0.0039	0.0106	0.0001	0.0544	0.0028	0.0099	0.0001	0.0035	0.0001	0.0073	0.0003	0.0020	0.0000	0.0071	0.0000	0.0022	0.0001
DML954	0.1102	0.0004	0.2291	0.0017	0.0220	0.0003	0.0726	0.0068	0.0206	0.0006	0.0054	0.0003	0.0155	0.0006	0.0027	0.0003	0.0142	0.0003	0.0031	0.0002
DML1003	0.0602	0.0004	0.1342	0.0009	0.0144	0.0001	0.0726	0.0068	0.0131	0.0001	0.0046	0.0001	0.0108	0.0002	0.0029	0.0001	0.0095	0.0000	0.0031	0.0001
DML1103	0.1154	0.0008			0.0248	0.0002			0.0222	0.0001	0.0055	0.0002	0.0166	0.0001	0.0026	0.0001	0.0151	0.0003	0.0031	0.0001
DML1203	0.0383	0.0021	0.0501	0.0014	0.0064	0.0000	0.0260	0.0020	0.0051	0.0002	0.0015	0.0001	0.0036	0.0002	0.0005	0.0000	0.0033	0.0001	0.0007	0.0001
DML1303	0.0140	0.0001	0.0157	0.0003	0.0017	0.0001	0.0053	0.0002	0.0014	0.0001	0.0005	0.0001	0.0011	0.0001	0.0002	0.0000	0.0009	0.0001	0.0002	0.0000
DML1404	0.0069	0.0001	0.0169	0.0002	0.0019	0.0000	0.0068	0.0001	0.0016	0.0001	0.0005	0.0001	0.0012	0.0001	0.0002	0.0000	0.0011	0.0000	0.0002	0.0000
DML1503	0.0172	0.0002	0.0385	0.0003	0.0047	0.0001	0.0162	0.0003	0.0038	0.0001	0.0011	0.0001	0.0030	0.0001	0.0008	0.0000	0.0028	0.0001	0.0008	0.0001
EDC739					0.0056	0.0002	0.0186	0.0004	0.0053	0.0002	0.0023	0.0001	0.0030	0.0001	0.0008	0.0001	0.0028	0.0001	0.0008	0.0001
EDC749	0.0039	0.0001	0.0131	0.0003	0.0013	0.0001	0.0041	0.0001	0.0006	0.0001	0.0004	0.0001	0.0005	0.0001	0.0003	0.0001	0.0005	0.0001	0.0002	0.0001
EDC769	0.0110	0.0007	0.0295	0.0017	0.0027	0.0002	0.0086	0.0004	0.0031	0.0002	0.0076	0.0002	0.0145	0.0010	0.0016	0.0001	0.0016	0.0001	0.0006	0.0001
EDC805	0.0095	0.0000	0.0277	0.0001	0.0021	0.0000	0.0076	0.0004	0.0013	0.0001	0.0004	0.0001	0.0012	0.0001	0.0001	0.0000	0.0011	0.0000	0.0002	0.0000
EDC822	0.0240	0.0007	0.0349	0.0011	0.0223	0.0012	0.0245	0.0012	0.0206	0.0011	0.0193	0.0011	0.0185	0.0012	0.0181	0.0008	0.0189	0.0009	0.0210	0.0006
EDC839	0.0095	0.0002	0.0180	0.0003	0.0024	0.0001	0.0074	0.0003	0.0022	0.0002	0.0010	0.0002	0.0014	0.0001	0.0003	0.0001	0.0011	0.0001	0.0004	0.0001
EDC856	0.0183	0.0002	0.0273	0.0002	0.0031	0.0000	0.0097	0.0002	0.0027	0.0001	0.0009	0.0001	0.0020	0.0001	0.0004	0.0000	0.0017	0.0000	0.0004	0.0000
EDC877	0.0229	0.0027	0.0485	0.0035	0.0052	0.0001	0.0179	0.0006	0.0050	0.0001	0.0016	0.0002	0.0032	0.0002	0.0007	0.0001	0.0031	0.0001	0.0008	0.0001
EDC893	0.0227	0.0001	0.0462	0.0002	0.0055	0.0001	0.0173	0.0002	0.0040	0.0002	0.0011	0.0001	0.0031	0.0002	0.0006	0.0001	0.0029	0.0001	0.0006	0.0001
EDC915	0.0257	0.0002	0.0502	0.0006	0.0053	0.0001	0.0174	0.0004	0.0038	0.0001	0.0011	0.0001	0.0027	0.0002	0.0004	0.0000	0.0024	0.0001	0.0005	0.0000
EDC929	0.0171	0.0002	0.0380	0.0003	0.0041	0.0001	0.0133	0.0004	0.0034	0.0001	0.0010	0.0001	0.0024	0.0002	0.0003	0.0000	0.0022	0.0001	0.0004	0.0000

Probe	Er	SD	Tm	SD	Yb	SD	Lu	SD	Pt	SD	Au	SD	Pb	SD	Bi	SD	Th	SD	U	SD
DML873	0.0007	0.0001	0.0002	0.0000	0.0008	0.0001	0.0002	0.0000	0.0025	0.0002	0.0007	0.0004	0.031	0.001	0.0015	0.0001	0.0014	0.0001	0.0006	0.0000
DML905	0.0045	0.0001	0.0015	0.0000	0.0046	0.0001	0.0015	0.0000	0.0049	0.0002	0.0027	0.0004	0.031	0.001	0.0015	0.0001	0.0127	0.0007	0.0047	0.0001
DML954	0.0077	0.0003	0.0014	0.0003	0.0085	0.0003	0.0015	0.0002	0.0040	0.0002	0.0035	0.0004	0.029	0.001	0.0079	0.0005	0.0193	0.0014	0.0083	0.0004
DML1003	0.0057	0.0002	0.0022	0.0000	0.0061	0.0001	0.0023	0.0001	0.0014	0.0001	0.0014	0.0001	0.029	0.001	0.0024	0.0001	0.0193	0.0014	0.0063	0.0001
DML1103	0.0081	0.0002	0.0014	0.0000	0.0084	0.0002	0.0013	0.0001	0.0046	0.0002	0.0021	0.0004	0.065	0.001	0.0023	0.0001	0.0052	0.0001	0.0085	0.0001
DML1203	0.0019	0.0001	0.0004	0.0000	0.0021	0.0001	0.0004	0.0000	0.0038	0.0002	0.0032	0.0004	0.014	0.001	0.0006	0.0001	0.0052	0.0001	0.0019	0.0001
DML1303	0.0006	0.0000	0.0001	0.0000	0.0008	0.0000	0.0001	0.0000	0.0018	0.0002	0.0009	0.0004	0.011	0.001	0.0001	0.0001	0.0010	0.0000	0.0004	0.0000
DML1404	0.0008	0.0000	0.0002	0.0000	0.0008	0.0000	0.0001	0.0000	0.0018	0.0002	0.0009	0.0004	0.011	0.001	0.0001	0.0001	0.0015	0.0000	0.0007	0.0001
DML1503	0.0021	0.0001	0.0004	0.0000	0.0021	0.0000	0.0004	0.0000	0.1479	0.0044	0.0037	0.0004	0.018	0.001	0.0017	0.0001	0.0039	0.0001	0.0019	0.0001
EDC739	0.0023	0.0001			0.0021	0.0001			0.157	0.0005	0.0041	0.0005	0.052	0.001	0.0022	0.0001	0.0002	0.0000	0.0049	0.0002
EDC749	0.0005	0.0001	0.0003	0.0001	0.0006	0.0001	0.0002	0.0001	0.0129	0.0005	0.0041	0.0005	0.054	0.001	0.0039	0.0001	0.0002	0.0000	0.0005	0.0001
EDC769	0.0014	0.0002	0.0005	0.0001	0.0016	0.0001	0.0004	0.0001	0.146	0.0004	0.0129	0.0005	0.054	0.001	0.0039	0.0001	0.0002	0.0000	0.0005	0.0001
EDC805	0.0008	0.0001	0.0001	0.0000	0.0009	0.0000	0.0001	0.0000	0.0078	0.0003	0.0149	0.0008	0.008	0.001	0.0299	0.0031	0.0050	0.0000	0.0014	0.0001
EDC822	0.0311	0.0032	0.0203	0.0017	0.0186	0.0011	0.0173	0.0011	0.0049	0.0012	0.0222	0.0023	0.053	0.001	0.0011	0.0001	0.0208	0.0012	0.0305	0.0015
EDC839	0.0009	0.0001	0.0002	0.0001	0.0008	0.0001	0.0002	0.0001	0.0034	0.0002	0.0031	0.0004	0.038	0.001	0.0011	0.0001	0.0007	0.0000	0.0004	0.0001
EDC856	0.0010	0.0001	0.0003	0.0000	0.0012	0.0001	0.0002	0.0000	0.0039	0.0003	0.0029	0.0004	0.007	0.001	0.0012	0.0001	0.0019	0.0001	0.0014	0.0001
EDC877	0.0021	0.0001	0.0004	0.0001	0.0022	0.0001	0.0004	0.0001	0.0066	0.0002	0.0032	0.0004	0.020	0.001	0.0013	0.0001	0.0033	0.0001	0.0020	0.0002
EDC893	0.0017	0.0001	0.0003	0.0000	0.0018	0.0000	0.0004	0.0001	0.0033	0.0002	0.0020	0.0004	0.014	0.001	0.0009	0.0001	0.0048	0.0001	0.0018	0.0001
EDC915	0.0013	0.0000	0.0002	0.0000	0.0014	0.0000	0.0002	0.0000	0.0013	0.0001	0.0020	0.0004	0.081	0.001	0.0020	0.0001	0.0040	0.0000	0.0020	0.0000
EDC929	0.0013	0.0001	0.0002	0.0000	0.0013	0.0000	0.0002	0.0000	0.0012	0.0001	0.0006	0.0001	0.006	0.001	0.0002	0.0001	0.0026	0.0001	0.0013	0.0000

N a m e : Dorothee Wilhelms-Dick..... Datum 21.05.2008.....

Anschrift : Theodor-Heuss-Platz 9, 27568 Bremerhaven.....

E r k l ä r u n g

Hiermit versichere ich, dass ich

1. die Arbeit ohne unerlaubte fremde Hilfe angefertigt habe,
2. keine anderen als die von mir angegebenen Quellen und Hilfsmittel benutzt habe und
3. die den benutzten Werken wörtlich oder inhaltlich entnommenen Stellen als solche kenntlich gemacht habe.

Bremerhaven, den21.05.2008.....

(Unterschrift)